Novel Approaches to Monitor Virus Fate Through Water Treatment Processes

by

Nicole C. Rockey

A dissertation submitted in partial fulfillment
of the requirements for the degree of
Doctor of Philosophy
(Environmental Engineering)
in the University of Michigan
2021

Doctoral Committee:

Professor Lutgarde Raskin, Co-Chair
Associate Professor Krista R. Wigginton, Co-Chair
Dr. Brian Pecson, Trussell Technologies
Associate Professor Christiane E. Wobus

Nicole C. Rockey

nrockey@umich.edu

ORCID iD: 0000-0003-1966-5312

Acknowledgments

This dissertation work is supported by multiple funding sources, including the Water Research Foundation (15-07) and the Paul Busch Award. I am fortunate to have received fellowships and grants that allowed me the flexibility to pursue my research interests. These include the U.S. National Science Foundation Graduate Research Fellowship, the University of Michigan Rackham Predoctoral Research Fellowship, the University of Michigan Rackham Graduate Student Research Grant, and the University of Michigan Rackham Conference Travel Grant.

I would like to acknowledge my co-advisors, Dr. Krista R. Wigginton and Dr. Lutgarde Raskin for their continued guidance, support, investment, and mentorship. I am deeply grateful for their sustained patience and enthusiasm as I developed and pursued my research interests. I thank the members of my dissertation committee, Dr. Christiane Wobus and Dr. Brian Pecson, for playing an integral role in my doctoral research and professional development. Thanks to Dr. Christiane Wobus for opening the Wobus laboratory to me and for help in navigating the human norovirus culture work. Thank you to Dr. Brian Pecson for the insights and guidance related to potable water reuse that rooted my doctoral work. I would also like to thank Dr. Terese Olson for allowing me the opportunity to work with her on research outside of my dissertation, and for her support over the past several years.

This body of work was possible due to the support and dedication of several individuals. I would like to acknowledge Kaitlyn Chin, Kate Harrison, Dr. James B. Henderson, Dr. Tamar Kohn, and Dr. Suzanne Young for their significant contributions to this research. I would also like to thank

current and past members of the Wobus laboratory, especially Dr. Roberto Cieza, Dr. Abimbola Kolawole, Dr. Carmen Mirabelli, and Irene Owusu, for their continued insights and assistance with the human intestinal enteroid cell culture system.

I would like to thank the UM Environmental Biotechnology group for cultivating an incredible and inspiring scientific research environment. The thoughtful scientists in this group were a constant source of support, motivation, and friendship throughout my doctoral studies. Thanks to the Wigginton and Raskin research groups for input on numerous presentations and manuscripts over the years and for helpful research considerations. Thank you to Dr. Nadine Kotlarz for being a wonderful mentor and friend to me as a new doctoral student. I am especially thankful for the friendship of several individuals I have been fortunate enough to meet while at the University of Michigan. To Emily Crossette for being my partner in crime as a member of the Wigginton and Raskin research groups these last several years. To Dr. Raghav Reddy for being an excellent officemate and the most generous person. To Dr. Jeseth Delgado-Vela, Dr. Margaret Reuter, Dr. Caroline Van Steendam, Andrea McFarland and Kate Dowdell for wonderful friendships and thoughtful conversations. To Katie Langenfeld, Enrique Rodriguez, Brett Wagner, and Dr. Yinyin Ye for being my surrogate office mates and great friends (and coffee mates).

Thanks to my parents and siblings for their unwavering love and support. I am grateful to my parents for instilling in me a passion for learning and an understanding of just how powerful education can be. Their efforts have made it possible for me to focus and succeed in my educational endeavors over the years. Lastly, thank you to my husband, David Barron, for being a constant source of support and encouragement through all the setbacks and successes of my PhD.

Table of Contents

List of Tables

List of Figures

List of Appendices

Abstract

As population growth, climate change, and urbanization strain drinking water sources, the increasingly common use of diverse and impacted water supplies necessitates a better understanding of contaminant fate in this setting. Among the human health hazards found in water supplies, viral pathogens are of principal concern, because they can be present in elevated concentrations, are highly infectious, and are difficult to remove due to their small size. Effective viral pathogen removal is of particular importance in direct potable water reuse, in which wastewater is transformed into drinking water. A multibarrier approach to treatment is traditionally used for contaminant removal, where different treatment processes are placed in series and cumulatively reduce virus concentrations to levels that pose no significant public health risk. However, the persistence of several important waterborne viruses (e.g., human norovirus) through treatment processes is not well characterized due to difficulties in virus culturability. This raises questions about whether proposed reuse treatment schemes are sufficient to protect human health. In addition, monitoring strategies used to ensure treatment performance in real-time are not sufficiently sensitive to validate virus reductions, likely resulting in the design of overengineered treatment schemes for virus removal. This dissertation sheds light on alternative molecular and predictive modeling approaches for estimating virus fate through disinfection when traditional methods are not feasible and evaluates flow virometry as a novel approach to accurately validate virus reductions through treatment in real-time.

Results demonstrate that alternative methods to accurately determine virus susceptibility to UV_{254} disinfection treatments can be applied effectively when culture-based approaches are not possible.

Specifically, the UV_{254} sensitivity of human norovirus was established with these alternative approaches and confirmed through use of a novel culture system. The findings show that commonly used approaches to estimate infectious human norovirus levels overestimate norovirus survival through UV_{254} disinfection. Further, flow virometry, a high-throughput method for detecting and enumerating virus particles, was explored as a sensitive method to ensure virus reductions through treatment in real-time. Work revealed that flow virometry could effectively detect large dsDNA virus populations, while smaller RNA and DNA viruses were not reliably measured. Proof-of-concept experiments evaluating virus removal through ultrafiltration indicated that while flow virometry could detect particles in the same size range as viruses, little improvement over currently used monitoring approaches was observed due to limitations in the detection capabilities of current flow cytometers. Taken together, this dissertation research improves our understanding of human norovirus fate through treatment and provides novel methods that can be applied to monitor virus behavior through treatment. Ultimately, this research aids in the development of a regulatory framework that will make direct potable reuse more feasible, economical, and environmentally sustainable while still guaranteeing public health protection.

Chapter 1

Introduction

Viral pathogens pose a significant risk to human health, as evidenced by recent and ongoing pandemics, endemic illnesses, and frequent outbreaks.[1–4] Viruses can spread by various routes, including through food, water, aerosols, fomites, and direct human to human transmission, among others.[1,5,6] The fate of many pathogenic viruses in these settings is not well understood, and questions remain about the most effective ways to monitor and inactivate different viral pathogens for exposure mitigation.

Worldwide, gastrointestinal illnesses are caused largely by viruses, including norovirus, rotavirus, adenovirus, and astrovirus.[7–9] Ingestion of these enteric viral pathogens can lead to viral infection and ultimately gastrointestinal disease. Enteric viruses can be highly infectious, with challenge studies demonstrating that ingestion of small numbers of infectious virus particles can result in disease.[10] These viruses are present in numerous water types, including surface water, drinking water sources, and wastewater.[11–14] The persistence of infectious viruses in water settings necessitates the use of treatment technologies to mitigate viral infection risk. Common water treatment disinfection strategies include the use of UV_{254}, chlorine, chloramine, and ozone. Physical and biological removal processes, such as membrane filtration, granular media filtration, and bioreactors followed by biomass separation steps, are also applied. As regions of the world, including many in the United States, become water-stressed due to the effects of climate change, population growth, water shortage, and urbanization, they seek nontraditional water sources.

Direct potable reuse (DPR), in which wastewater is treated to drinking water standards, is an advanced technology capable of meeting the needs of these communities. Adoption of this technology has not come quickly, however, largely because of several challenges in reuse regulation and implementation. Chief among these difficulties is the assurance of public health, including prevention of the public's exposure to harmful chemical and microbiological contaminants.[16,17] Specifically, microbiological hazards may pose an acute health risk to DPR water consumers if pathogens are not sufficiently removed during treatment. Virus removal is of primary concern in DPR because viruses can be present in elevated concentrations in wastewater[18] and are highly infectious.[10]

To mitigate the microbial risk associated with drinking water, regulations largely focus on keeping the prevalence of illness associated with pathogens in water below a certain threshold.[16,19,20] For example, in the United States, water reuse and drinking water standards include minimum pathogen removal levels created to keep the annual risk of infection at or below 1 person per 10,000.[20–22] To achieve the desired level of pathogen reduction, water systems use a multibarrier approach to treatment, in which unit processes are placed in series and cumulatively provide the total desired amount of removal for a particular pathogen. The removal of pathogens achieved by each unit process is typically determined by research studies at the bench- or pilot-scale. For instance, adenovirus 41 inactivation by UV_{254} has been established in various collimated beam experiments as achieving 4-$\log_{10}$ inactivation at a UV_{254} dose of ~ 186 mJ cm^{-2}.[23]

Additionally, these unit processes must be monitored in real-time to ensure unit processes are inactivating pathogens as intended. The low concentrations of pathogenic viruses required in finished drinking water (e.g., < 2.2 x 10^{-7} viruses/L)[17] makes real-time detection of individual pathogens infeasible at present. Consequently, surrogate virus parameters are monitored in real-

time to validate virus removal. These surrogates vary by unit process, and can include turbidity, conductivity, disinfectant concentration times contact time (Ct), or pressure-decay tests, among others.[16,24,25] When surrogate parameters meet accepted values, $\log_{10}$ pathogen removal credit for the unit process is allotted. Treatment processes may not be effective or may not be applied in instances where virus susceptibility is not well understood or when virus inactivation cannot be validated. In these scenarios, treatment may be overengineered, leading to unsustainable and economically infeasible treatment schemes; on the other hand, underengineered treatment strategies can result in unsafe practices that put the public at increased risk.

Inactivation and removal of important enteric viruses through some unit processes have not been well studied. This is particularly true for emerging or difficult-to-culture viruses. Human norovirus (HuNoV), for example, is an important viral pathogen in water settings because of its large burden of disease as the leading cause of gastrointestinal illness in the United States.[7] To date, our inability to readily culture HuNoV in vitro has limited research focused on infectious HuNoV persistence in the environment and infectivity through water treatment processes. In many cases, surrogate viruses have been used to approximate inactivation of viral pathogens,[26–39] but these viruses may not behave in the same manner as the pathogens they are selected to represent.[40] Viral genome concentrations have also been measured in lieu of culture-based methods,[11,12,41–48] but these measurements provide no information regarding virus infectivity. These approaches are not ideal, because infectious viral pathogen levels may not be accurately estimated with either approach. Alternative methods for assessing virus fate are needed for viruses that cannot be readily cultured or pose an emerging public health threat. To address these needs, I developed innovative methods for estimating virus inactivation through UV_{254} that do not rely on culture systems and applied

these approaches to estimate HuNoV inactivation. I further confirmed the estimated UV_{254} susceptibility of HuNoV using a novel cell culture system.

In addition to better understanding virus fate through water treatment systems, sensitive real-time tools for monitoring virus reductions through unit processes are needed. Surrogates for real-time monitoring are often not as sensitive as necessary to exhibit the same extent of pathogen removal occurring through a particular treatment. In other words, the extent of surrogate removal is often much less than the demonstrated virus removal through the same unit process. This is particularly true for physical and biological removal processes. For example, bench-scale work has established that reverse osmosis can provide over 5-$\log_{10}$ removal of viruses,[49,50] but the surrogates commonly used to validate performance, namely total organic carbon and electrical conductivity, can only ensure 1.5 to 2-$\log_{10}$ removal.[16,24] As a result, only the removal achieved by the surrogate can be allotted. New methods for real-time monitoring of particles in water have the ability to revolutionize the way microbial population reductions are ascertained.

Flow cytometry (FCM), a high-throughput method for real-time particle detection, has been used to rapidly quantify bacteria in water.[51] Virus detection using FCM, coined flow virometry (FVM), may serve as a more sensitive surrogate monitoring approach because, unlike surrogate parameters that measure chemical concentrations or water transparency, FVM measures biological particles of the same size range as viral pathogens of interest. Yet FVM studies in water treatment are limited, and work has not unequivocally determined whether particle counts by flow cytometers indeed measure virus populations.[52–54] Research to further validate the capabilities of FVM for real-time monitoring of viral populations in environmental matrices would be valuable. To this end, I initiated this research by characterizing virus types that can detected using a high sensitivity flow cytometer, and I conducted proof-of-concept experiments to establish the feasibility of FVM

as an accurate real-time surrogate for monitoring the effectiveness of virus removal by membrane processes.

This dissertation introduces novel tools to study the inactivation of viral pathogens through water disinfection strategies and evaluates promising viral monitoring methods. Initial work developed and validated two methods, a genome-wide PCR-based extrapolation approach (Chapter 2) and a predictive modeling approach (Chapter 3), to accurately estimate UV_{254} virus inactivation without relying on traditional culture systems. These alternative approaches were used to determine UV_{254} inactivation of various human viral pathogens, including HuNoV, with no available high-quality inactivation data. HuNoV susceptibility to UV_{254} disinfection was then confirmed using a novel enteroid culture system (Chapter 4). Next, I explored the potential applications of FVM for monitoring virus removal through DPR processes and identified future directions for FVM in this setting (Chapter 5). Information from this work motivated an extensive investigation of FVM methods and ultimately led to proof-of-concept experiments assessing FVM's suitability as a real-time surrogate for virus removal through microfiltration and ultrafiltration (Chapter 6). Ultimately, I summarized the primary findings and implications of this research and presented future research areas (Chapter 7).

1.1 References

(1) de Graaf, M.; van Beek, J.; Koopmans, M. P. G. Human Norovirus Transmission and Evolution in a Changing World. *Nat Rev Micro* **2016**, *14* (7), 421–433.

(2) Jacob, S. T.; Crozier, I.; Fischer, W. A.; Hewlett, A.; Kraft, C. S.; Vega, M.-A. de La; Soka, M. J.; Wahl, V.; Griffiths, A.; Bollinger, L.; Kuhn, J. H. Ebola Virus Disease. *Nat. Rev. Dis. Prim.* **2020**, *6* (1), 13. https://doi.org/10.1038/s41572-020-0147-3.

(3) Morens, D. M.; Fauci, A. S. Emerging Pandemic Diseases: How We Got to COVID-19. *Cell* **2020**, *182* (5), 1077–1092. https://doi.org/https://doi.org/10.1016/j.cell.2020.08.021.

(4) Eisinger, R. W.; Fauci, A. S. Ending the HIV/AIDS Pandemic(1). *Emerg. Infect. Dis.* **2018**, *24* (3), 413–416. https://doi.org/10.3201/eid2403.171797.

(5) Asadi, S.; Gaaloul ben Hnia, N.; Barre, R. S.; Wexler, A. S.; Ristenpart, W. D.; Bouvier, N. M. Influenza A Virus Is Transmissible via Aerosolized Fomites. *Nat. Commun.* **2020**, *11* (1), 4062. https://doi.org/10.1038/s41467-020-17888-w.

(6) Judson, S.; Prescott, J.; Munster, V. Understanding Ebola Virus Transmission. *Viruses* . 2015. https://doi.org/10.3390/v7020511.

(7) Scallan, E.; Hoekstra, R. M.; Angulo, F. J.; Tauxe, R. V; Widdowson, M.-A.; Roy, S. L.; Jones, J. L.; Griffin, P. M. Foodborne Illness Acquired in the United States—Major Pathogens. *Emerg. Infect. Dis.* **2011**, *17* (1), 7–15. https://doi.org/10.3201/eid1701.P11101.

(8) Tate, J. E.; Burton, A. H.; Boschi-Pinto, C.; Steele, A. D.; Duque, J.; Parashar, U. D. 2008 Estimate of Worldwide Rotavirus-Associated Mortality in Children Younger than 5 Years before the Introduction of Universal Rotavirus Vaccination Programmes: A Systematic Review and Meta-Analysis. *Lancet Infect. Dis.* **2012**, *12* (2), 136–141.

https://doi.org/10.1016/S1473-3099(11)70253-5.

(9) Bosch, A.; Pintó, R. M.; Guix, S. Human Astroviruses. *Clin. Microbiol. Rev.* **2014**, *27* (4), 1048 LP – 1074. https://doi.org/10.1128/CMR.00013-14.

(10) F.M., T. P.; L., M. C.; Pengbo, L.; Sara, E. M.; Lisa, L.; S., B. R.; Jacques, L. P.; L., C. R. Norwalk Virus: How Infectious Is It? *J. Med. Virol.* **2008**, *80* (8), 1468–1476. https://doi.org/10.1002/jmv.21237.

(11) Montazeri, N.; Goettert, D.; Achberger, E. C.; Johnson, C. N.; Prinyawiwatkul, W.; Janes, M. E. Pathogenic Enteric Viruses and Microbial Indicators during Secondary Treatment of Municipal Wastewater. *Appl. Environ. Microbiol.* **2015**, *81* (18), 6436–6445. https://doi.org/10.1128/AEM.01218-15.

(12) Campos, C. J. A.; Avant, J.; Lowther, J.; Till, D.; Lees, D. N. Human Norovirus in Untreated Sewage and Effluents from Primary, Secondary and Tertiary Treatment Processes. *Water Res.* **2016**, *103*, 224–232. https://doi.org/http://dx.doi.org/10.1016/j.watres.2016.07.045.

(13) Li, D.; He, M.; Jiang, S. C. Detection of Infectious Adenoviruses in Environmental Waters by Fluorescence-Activated Cell Sorting Assay. *Appl. Environ. Microbiol.* **2010**, *76* (5), 1442–1448. https://doi.org/10.1128/AEM.01937-09.

(14) Chapron, C. D.; Ballester, N. A.; Fontaine, J. H.; Frades, C. N.; Margolin, A. B. Detection of Astroviruses, Enteroviruses, and Adenovirus Types 40 and 41 in Surface Waters Collected and Evaluated by the Information Collection Rule and an Integrated Cell Culture-Nested PCR Procedure. *Appl. Environ. Microbiol.* **2000**, *66* (6), 2520 LP – 2525. https://doi.org/10.1128/AEM.66.6.2520-2525.2000.

(15) Asano, T.; Burton, F.; Leverenz, H.; Tsuchihashi, R.; Tchobanoglous, G. *Water Reuse*

Issues, Technologies, and Applications; McGraw-Hill: New York :, 2007.

(16) World Health Organization. Potable Reuse: Guidance for Producing Safe Drinking-Water. **2017**.

(17) Trussell, R. R.; Salveson, A.; Snyder, S. A.; Trussell, R. S.; Gerrity, D.; Pecson, B. *Potable Reuse: State of the Science Report and Equivalency Criteria for Treatment Trains*; Alexandria, VA, 2013.

(18) Gerba, C. P.; Betancourt, W. Q.; Kitajima, M. How Much Reduction of Virus Is Needed for Recycled Water: A Continuous Changing Need for Assessment? *Water Res.* **2017**, *108*, 25–31. https://doi.org/http://dx.doi.org/10.1016/j.watres.2016.11.020.

(19) EPHC MHNRC and NRMMC. Australian Guidelines for Water Recycling - Augmentation of Drinking Water Supplies. **2008**.

(20) California Department of Public Health. Title 22 and 17 California Code of Regulations. 2015.

(21) Texas Water Development Board. Final Report - Direct Potable Reuse. **2015**.

(22) Macler, B. A.; Regli, S. Use of Microbial Risk Assessment in Setting US Drinking Water Standards. *Int. J. Food Microbiol.* **1993**, *18* (4), 245–256. https://doi.org/http://dx.doi.org/10.1016/0168-1605(93)90148-A.

(23) Hijnen, W. A. M.; Beerendonk, E. F.; Medema, G. J. Inactivation Credit of UV Radiation for Viruses, Bacteria and Protozoan (Oo)Cysts in Water: A Review. *Water Res.* **2006**, *40* (1), 3–22. https://doi.org/https://doi.org/10.1016/j.watres.2005.10.030.

(24) Pype, M.-L.; Lawrence, M. G.; Keller, J.; Gernjak, W. Reverse Osmosis Integrity Monitoring in Water Reuse: The Challenge to Verify Virus Removal – A Review. *Water*

Res. **2016**, *98*, 384–395. https://doi.org/http://dx.doi.org/10.1016/j.watres.2016.04.040.

(25) Pecson, B. M.; Triolo, S. C.; Olivieri, S.; Chen, E. C.; Pisarenko, A. N.; Yang, C.-C.; Olivieri, A.; Haas, C. N.; Trussell, R. S.; Trussell, R. R. Reliability of Pathogen Control in Direct Potable Reuse: Performance Evaluation and QMRA of a Full-Scale 1 MGD Advanced Treatment Train. *Water Res.* **2017**, *122*, 258–268. https://doi.org/https://doi.org/10.1016/j.watres.2017.06.014.

(26) Cannon, J. L.; Papafragkou, E.; Park, G. W.; Osborne, J.; Jaykus, L.-A.; Vinje, J. Surrogates for the Study of Norovirus Stability and Inactivation in the Environment: A Comparison of Murine Norovirus and Feline Calicivirus. *J. Food Prot.* **2006**, *69* (11), 2761–2765. https://doi.org/10.4315/0362-028X-69.11.2761.

(27) Tree, J. A.; Adams, M. R.; Lees, D. N. Disinfection of Feline Calicivirus (a Surrogate for Norovirus) in Wastewaters. *J. Appl. Microbiol.* **2005**, *98* (1), 155–162. https://doi.org/10.1111/j.1365-2672.2004.02442.x.

(28) Beck, S. E.; Rodriguez, R. A.; Hawkins, M. A.; Hargy, T. M.; Larason, T. C.; Linden, K. G. Comparison of UV-Induced Inactivation and RNA Damage in MS2 Phage across the Germicidal UV Spectrum. *Appl. Environ. Microbiol.* **2016**, *82* (5), 1468–1474.

(29) Lin, K.; Marr, L. C. Aerosolization of Ebola Virus Surrogates in Wastewater Systems. *Environ. Sci. Technol.* **2017**, *51* (5), 2669–2675. https://doi.org/10.1021/acs.est.6b04846.

(30) Ye, Y.; Chang, P. H.; Hartert, J.; Wigginton, K. R. Reactivity of Enveloped Virus Genome, Proteins, and Lipids with Free Chlorine and UV254. *Environ. Sci. Technol.* **2018**, *52* (14), 7698–7708. https://doi.org/10.1021/acs.est.8b00824.

(31) Cromeans, T.; Park, G. W.; Costantini, V.; Lee, D.; Wang, Q.; Farkas, T.; Lee, A.; Vinjé, J.

Comprehensive Comparison of Cultivable Norovirus Surrogates in Response to Different Inactivation and Disinfection Treatments. *Appl. Environ. Microbiol.* **2014**, *80* (18), 5743 LP – 5751.

(32) Thurston-Enriquez, J. A.; Haas, C. N.; Jacangelo, J.; Riley, K.; Gerba, C. P. Inactivation of Feline Calicivirus and Adenovirus Type 40 by UV Radiation. *Appl. Environ. Microbiol.* **2003**, *69* (1), 577–582.

(33) Bae, J.; Schwab, K. J. Evaluation of Murine Norovirus, Feline Calicivirus, Poliovirus, and MS2 as Surrogates for Human Norovirus in a Model of Viral Persistence in Surface Water and Groundwater. *Appl. Environ. Microbiol.* **2008**, *74* (2), 477 LP – 484.

(34) Dunkin, N.; Weng, S.; Coulter, C. G.; Jacangelo, J. G.; Schwab, K. Reduction of Human Norovirus GI, GII, and Surrogates by Peracetic Acid and Monochloramine in Municipal Secondary Wastewater Effluent. *Environ. Sci. Technol.* **2017**. https://doi.org/10.1021/acs.est.7b02954.

(35) Park, G. W.; Linden, K. G.; Sobsey, M. D. Inactivation of Murine Norovirus, Feline Calicivirus and Echovirus 12 as Surrogates for Human Norovirus (NoV) and Coliphage (F+) MS2 by Ultraviolet Light (254 Nm) and the Effect of Cell Association on UV Inactivation. *Lett. Appl. Microbiol.* **2011**, *52* (2), 162–167. https://doi.org/10.1111/j.1472-765X.2010.02982.x.

(36) Kampf, G.; Todt, D.; Pfaender, S.; Steinmann, E. Persistence of Coronaviruses on Inanimate Surfaces and Their Inactivation with Biocidal Agents. *J. Hosp. Infect.* **2020**, *104* (3), 246–251. https://doi.org/10.1016/j.jhin.2020.01.022.

(37) Ludwig-Begall, L. F.; Wielick, C.; Dams, L.; Nauwynck, H.; Demeuldre, P.-F.; Napp, A.;

Laperre, J.; Haubruge, E.; Thiry, E. The Use of Germicidal Ultraviolet Light, Vaporised Hydrogen Peroxide and Dry Heat to Decontaminate Face Masks and Filtering Respirators Contaminated with a SARS-CoV-2 Surrogate Virus. *J. Hosp. Infect.* **2020**, S0195-6701(20)30413-8. https://doi.org/10.1016/j.jhin.2020.08.025.

(38) Hirneisen, K. A.; Kniel, K. E. Comparing Human Norovirus Surrogates: Murine Norovirus and Tulane Virus. *J. Food Prot.* **2013**, *76* (1), 139–143. https://doi.org/10.4315/0362-028X.JFP-12-216.

(39) Prussin, A. J.; Schwake, D. O.; Lin, K.; Gallagher, D. L.; Buttling, L.; Marr, L. C. Survival of the Enveloped Virus Phi6 in Droplets as a Function of Relative Humidity, Absolute Humidity, and Temperature. *Appl. Environ. Microbiol.* **2018**, *84* (12), e00551-18. https://doi.org/10.1128/AEM.00551-18.

(40) Richards, G. P. Critical Review of Norovirus Surrogates in Food Safety Research: Rationale for Considering Volunteer Studies. *Food Environ. Virol.* **2012**, *4* (1), 6–13. https://doi.org/10.1007/s12560-011-9072-7.

(41) Barrett, M.; Fitzhenry, K.; O'Flaherty, V.; Dore, W.; Keaveney, S.; Cormican, M.; Rowan, N.; Clifford, E. Detection, Fate and Inactivation of Pathogenic Norovirus Employing Settlement and UV Treatment in Wastewater Treatment Facilities. *Sci. Total Environ.* **2016**, *568*, 1026–1036. https://doi.org/http://dx.doi.org/10.1016/j.scitotenv.2016.06.067.

(42) Flannery, J.; Keaveney, S.; Rajko-Nenow, P.; O'Flaherty, V.; Doré, W. Concentration of Norovirus during Wastewater Treatment and Its Impact on Oyster Contamination. *Appl. Environ. Microbiol.* **2012**, *78* (9), 3400–3406. https://doi.org/10.1128/AEM.07569-11.

(43) He, J.-W.; Jiang, S. Quantification of Enterococci and Human Adenoviruses in

Environmental Samples by Real-Time PCR. *Appl. Environ. Microbiol.* **2005**, *71* (5), 2250–2255.

(44) da Silva, A. K.; Le Saux, J.-C.; Parnaudeau, S.; Pommepuy, M.; Elimelech, M.; Le Guyader, F. S. Evaluation of Removal of Noroviruses during Wastewater Treatment, Using Real-Time Reverse Transcription-PCR: Different Behaviors of Genogroups I and II. *Appl. Environ. Microbiol.* **2007**, *73* (24), 7891–7897. https://doi.org/10.1128/AEM.01428-07.

(45) Farkas, K.; Marshall, M.; Cooper, D.; McDonald, J. E.; Malham, S. K.; Peters, D. E.; Maloney, J. D.; Jones, D. L. Seasonal and Diurnal Surveillance of Treated and Untreated Wastewater for Human Enteric Viruses. *Environ. Sci. Pollut. Res. Int.* **2018**. https://doi.org/10.1007/s11356-018-3261-y.

(46) Medema, G.; Heijnen, L.; Elsinga, G.; Italiaander, R.; Brouwer, A. Presence of SARS-Coronavirus-2 RNA in Sewage and Correlation with Reported COVID-19 Prevalence in the Early Stage of the Epidemic in The Netherlands. *Environ. Sci. Technol. Lett.* **2020**, *7* (7), 511–516. https://doi.org/10.1021/acs.estlett.0c00357.

(47) Chia, P. Y.; Coleman, K. K.; Tan, Y. K.; Ong, S. W. X.; Gum, M.; Lau, S. K.; Lim, X. F.; Lim, A. S.; Sutjipto, S.; Lee, P. H.; Son, T. T.; Young, B. E.; Milton, D. K.; Gray, G. C.; Schuster, S.; Barkham, T.; De, P. P.; Vasoo, S.; Chan, M.; Ang, B. S. P.; Tan, B. H.; Leo, Y.-S.; Ng, O.-T.; Wong, M. S. Y.; Marimuthu, K.; Lye, D. C.; Lim, P. L.; Lee, C. C.; Ling, L. M.; Lee, L.; Lee, T. H.; Wong, C. S.; Sadarangani, S.; Lin, R. J.; Ng, D. H. L.; Sadasiv, M.; Yeo, T. W.; Choy, C. Y.; Tan, G. S. E.; Dimatatac, F.; Santos, I. F.; Go, C. J.; Chan, Y. K.; Tay, J. Y.; Tan, J. Y.-L.; Pandit, N.; Ho, B. C. H.; Mendis, S.; Chen, Y. Y. C.; Abdad, M. Y.; Moses, D.; Team, for the S. 2019 N. C. O. R. Detection of Air and Surface Contamination by SARS-CoV-2 in Hospital Rooms of Infected Patients. *Nat. Commun.*

2020, *11* (1), 2800. https://doi.org/10.1038/s41467-020-16670-2.

(48) Kenarkoohi, A.; Noorimotlagh, Z.; Falahi, S.; Amarloei, A.; Mirzaee, S. A.; Pakzad, I.; Bastani, E. Hospital Indoor Air Quality Monitoring for the Detection of SARS-CoV-2 (COVID-19) Virus. *Sci. Total Environ.* **2020**, *748*, 141324. https://doi.org/https://doi.org/10.1016/j.scitotenv.2020.141324.

(49) Kitis, M.; Lozier, J. C.; Kim, J.-H.; Mi, B.; Mariñas, B. J. Microbial Removal and Integrity Monitoring of RO and NF Membranes. *J. AWWA* **2003**, *95* (12), 105–119. https://doi.org/10.1002/j.1551-8833.2003.tb10515.x.

(50) Adham, S. S.; Trussell, R. S.; Gagliardo, P. F.; Trussell, R. R. Rejection of MS-2 Virus by RO Membranes. *J. AWWA* **1998**, *90* (9), 130–135. https://doi.org/10.1002/j.1551-8833.1998.tb08505.x.

(51) Besmer, M. D.; Epting, J.; Page, R. M.; Sigrist, J. A.; Huggenberger, P.; Hammes, F. Online Flow Cytometry Reveals Microbial Dynamics Influenced by Concurrent Natural and Operational Events in Groundwater Used for Drinking Water Treatment. *Sci. Rep.* **2016**, *6*, 38462.

(52) Brown, M. R.; Camézuli, S.; Davenport, R. J.; Petelenz-Kurdziel, E.; Øvreås, L.; Curtis, T. P. Flow Cytometric Quantification of Viruses in Activated Sludge. *Water Res.* **2015**, *68*, 414–422. https://doi.org/10.1016/j.watres.2014.10.018.

(53) Huang, X.; Zhao, Z.; Hernandez, D.; Jiang, C. S. Near Real-Time Flow Cytometry Monitoring of Bacterial and Viral Removal Efficiencies during Water Reclamation Processes. *Water*. 2016. https://doi.org/10.3390/w8100464.

(54) Ma, L.; Mao, G.; Liu, J.; Yu, H.; Gao, G.; Wang, Y. Rapid Quantification of Bacteria and

Viruses in Influent, Settled Water, Activated Sludge and Effluent from a Wastewater Treatment Plant Using Flow Cytometry. *Water Sci. Technol.* **2013**, *68* (8), 1763 LP – 1769.

Chapter 2

UV Disinfection of Human Norovirus: Evaluating Infectivity Using a Genome-Wide PCR-Based Approach

Reprinted with permission from: Nicole Rockey, Suzanne Young, Tamar Kohn, Brian Pecson, Christiane E. Wobus, Lutgarde Raskin, and Krista R. Wigginton, UV Disinfection of Human Norovirus: Evaluating Infectivity Using a Genome-Wide PCR-Based Approach, *Environmental Science & Technology*, **2020**, 54 (5), 5077– 5085. DOI: 10.1021/acs.est.9b05747, Copyright (2020) American Chemical Society.

2.1 Abstract

The removal and inactivation of infectious human norovirus is a major focus in water purification, but its fate through disinfection treatment processes is largely unknown owing to the lack of a readily available infectivity assay. In particular, norovirus behavior through unit processes may be over- or underestimated using current approaches for assessing human norovirus infectivity (e.g., surrogates, molecular methods). Here we fill a critical knowledge gap by estimating inactivation data for human norovirus after exposure to UV_{254}, a commonly used disinfection process in the water industry. Specifically, we used a PCR-based approach that accurately tracks positive-sense single-stranded RNA virus inactivation without relying on culturing methods. We first confirmed that the approach is valid with a culturable positive-sense single-stranded RNA human virus, coxsackievirus B5, by applying both qPCR- and culture-based methods to measure inactivation kinetics with UV_{254} treatment. We then applied the qPCR-based method to establish a UV_{254} inactivation curve for human norovirus (inactivation rate constant = 0.27 cm^2 mJ^{-1}). Based on a comparison with previously published data, human norovirus exhibited similar UV_{254}

susceptibility compared with other enteric single-stranded RNA viruses (e.g., Echovirus 12, feline calicivirus), but degraded much faster than MS2 (inactivation rate constant = 0.14 cm^2 mJ^{-1}). In addition to establishing a human norovirus inactivation rate constant, we developed an approach using a single qPCR assay that can be applied to estimate human norovirus inactivation in UV_{254} disinfection systems.

2.2 Introduction

Human norovirus (HuNoV) is a viral pathogen of principal concern in water purification due to its large burden of disease, ubiquitous presence in wastewater, and highly infectious nature. HuNoV is estimated to cause at least 19 million cases of gastroenteritis in the US each year,[1,2] almost 20 times more than any other enteric pathogen.[1] As a result of the high frequency of infection and the high viral titers present in the excreta of infected individuals, HuNoV concentrations in raw wastewater have been measured as high as 3.4×10^9 genome copies/L via reverse transcription quantitative PCR (RT-qPCR).[3] In addition, human challenge studies and subsequent dose-response models have indicated the infectious dose of HuNoV may be as low as one virus particle,[4] although other work suggests the infectious dose may be higher.[5] HuNoV is a particularly important consideration in the planned use of wastewater as a drinking water source (i.e., potable reuse). It is unclear whether the current water reuse guidelines, which are based on other human viruses, are sufficient to meet acceptable HuNoV public health risks.[6,7]

The efficacy of HuNoV inactivation through water treatment processes remains elusive due to the historical lack of a HuNoV culture system. Two systems capable of culturing certain HuNoV strains *in vitro* from HuNoV positive stool samples have been reported in recent years[8–10] but have not been applied to establish inactivation curves. A number of culturable surrogate viruses are commonly employed in challenge tests to approximate HuNoV physical removal or inactivation

in water treatment processes, but questions remain about their ability to mimic HuNoV behavior through these treatments.[11] Likewise, HuNoV genomes are often quantified in samples with RT-qPCR,[12] but these measurements do not provide information on virus infectivity. Pretreatments such as propidium monoazide,[13,14] RNase,[14–16] and platinum or palladium compounds[17] have been suggested to differentiate infectious and noninfectious HuNoV by qPCR; however, these approaches are only successful when noninfectious viruses have compromised protein capsids.[13,18]

Low-pressure UV disinfection (i.e., UV_{254}) primarily targets the viral genome[19–22] and is increasingly employed in drinking water, wastewater, and advanced water treatment for potable reuse. Previous work has noted that the use of traditional qPCR approaches (i.e., targeting amplicons of 100 – 200 base pairs) as a proxy for measuring virus infectivity following UV inactivation overestimates infectious virus levels.[15,23] This is due to the fact that traditional qPCR measures short genome segments, and these segments contain far fewer reactive sites than the entire viral genome. Quantifying intact short genome segments through UV treatment therefore vastly underestimates virus inactivation.[24] Long-range reverse transcription and amplification of larger portions of the genome more closely mirror infectious virus concentrations following treatment.[18,23,25] Measuring entire viral genomes by qPCR before and after UV treatment would be a technically challenging approach to measuring infectious viruses. Virus inactivation has, however, been effectively tracked through disinfection by targeting a large fraction of the genome with qPCR (~50%) and then extrapolating the observed amplicon damage to the damage expected in the full-length genome with Poissonian statistics.[24,26] Originally developed with bacteriophage MS2,[24] the technique has not yet been applied to fill critical knowledge gaps on the inactivation of nonculturable viruses. It should be noted that while this approach works for some virus types, it

may not be applicable for others (e.g., some double-stranded DNA viruses), and in particular those viruses for which host genome repair or genome reactivation may complicate UV_{254} inactivation.

In the current study, we first validate the genome extrapolation approach with a culturable positive-sense single-stranded RNA ((+) ssRNA) human enteric virus, coxsackievirus B5 (CVB5), and then apply the approach to provide UV_{254} inactivation data for HuNoV. We then compare HuNoV UV_{254} inactivation kinetics with those of several other (+) ssRNA viruses, including viruses commonly used as surrogates for HuNoV. Finally, we propose an easy-to-use qPCR tool for measuring HuNoV inactivation through UV_{254} treatment in wastewater, drinking water, and water reuse settings. The inactivation kinetics data and qPCR tool can be applied to current water treatment schemes to assess the log_{10} inactivation of HuNoV achieved by UV_{254} disinfection processes.

2.3 Materials and Methods

2.3.1 Virus stocks and enumeration.

CVB5 (Faulkner strain; ATCC VR-185) was propagated in buffalo green monkey kidney cells (BGMK; kindly provided by the Spiez Laboratory, Switzerland) grown in Minimum Essential Media (MEM; Gibco, Waltham, NY), amended with 1% penicillin and streptomycin, and 2% fetal bovine serum. Cells were incubated at 37°C in 5% CO_2 and 95% humidity and grown to confluence in T25 culture flasks (TPP Techno Plastic Products, Trasadingen, Switzerland).[27] Confluent cells in 96-well plates were infected with concentrated stocks of CVB5 (10^8-10^9 most probable number (mpn)/mL) at a multiplicity of infection equal to 0.1, and cells were checked daily until full cytopathic effect (CPE) was observed.[27] Propagated CVB5 was concentrated with polyethylene glycol, extracted with chloroform, and then filtered and concentrated using 100 kDa molecular

weight cut-off centrifugal filters (Amicon Ultra; Sigma-Aldrich, St. Louis, MO), analogous to a procedure previously described for MS2 coliphage.[28] Infectious CVB5 were enumerated by the mpn method,[27] and infectious virus concentrations are reported in mpn/mL. The CVB5 stocks were stored in virus dilution buffer (VDB; 5 mM NaH_2PO_4, 10 mM NaCl, pH7.4) at 4°C until use. Stock concentrations were measured prior to experiments to confirm initial virus concentrations.

A de-identified human stool sample containing HuNoV GII.4 Sydney was obtained from the Michigan Department of Health and Human Services. Stool suspensions (10%) were generated by spiking the received stool into 1X phosphate buffered saline (PBS; Thermo Fisher Scientific, Waltham, MA) followed by filtration through a 0.22 μm sterile polyethersulfone membrane (CELLTREAT Scientific, Pepperell, MA). The suspensions (approximately 1.5 x 10^7 genome copies/mL) were stored in 260 μL aliquots at -80°C until use. RNase experiments were conducted to assess whether extraviral RNA was present in the HuNoV stool suspensions used for UV inactivation experiments. Details of RNase experiments in stool suspensions are described in the Supporting Information (SI).

Bacteriophage MS2 was used in all CVB5 and HuNoV experiments to confirm that applied UV doses were consistent with expected doses in the literature, and to allow comparison of data between laboratories. Bacteriophage MS2 (ATCC 15597-B1) was propagated in *Escherichia. coli* (ATCC 15597), and concentrated, extracted, and purified, as previously described.[28] Infectious MS2 was enumerated on double agar layer plaque assays using host *E. coli*,[29] and concentrations are reported in plaque forming units (pfu)/mL. The MS2 stocks (~1 x 10^{11} pfu/mL and ~1 x 10^{12} pfu/mL for HuNoV and CVB5 experiments, respectively) were stored at 4°C in VDB.

2.3.2 UV_{254} experiments.

UV_{254} inactivation experiments were carried out with custom-built collimated beam apparatuses. Lamp intensities were measured with potassium iodide chemical actinometry.[30,31]

The CVB5 experiments were conducted in VDB containing both CVB5 (10^6 mpn/mL) and MS2 (10^9 pfu/mL). Experimental solutions (3 mL) were prepared in triplicate in sterile glass beakers, and were optically dilute (> 95% transmittance at 254 nm). The solutions were exposed to 0.15 mW cm^{-2} lamps (Philips, TUV F17T8) under constant mixing and at room temperature for UV_{254} doses ranging from 0 to 150 mJ cm^{-2}. Following UV_{254} exposure, the solutions were aliquoted for MS2 infectivity, CVB5 infectivity, and RNA extraction.

The HuNoV experimental solutions consisted of 1% filtered stool suspensions and MS2 bacteriophage (1 x 10^9 pfu/mL) in PBS. Aliquots of the experimental solutions (220 μL) were placed in a 96-well flat-bottomed plate (Corning, Corning, NY) and continuously mixed at 500 rpm using a 96-well plate mixer (MixMate; Eppendorf, Hamburg, Germany). Samples were exposed to a collimated beam reactor with 0.16 mW cm^{-2} UV_{254} lamps (model G15T8, Philips) at room temperature. The UV_{254} exposures were corrected for average irradiance based on UV_{254} attenuation of the experimental solutions (~40% transmittance at 254 nm) and the sample depth (0.5 cm). The resulting doses ranged from 0 to 152 mJ cm^{-2}. Dark control samples were prepared for each experiment. Following exposure to UV_{254}, samples were divided for MS2 infectivity and RNA extraction. MS2 plaque assays were carried out immediately after all inactivation experiments to verify UV_{254} exposure.[29]

UV_{254} excitation may transform components in HuNoV stool suspensions into reactive species, which may in turn contribute to virus degradation (i.e., indirect photolysis). MS2 experiments were also conducted in buffer solution, which does not contain potential sources of indirect photolysis,

to confirm that inactivation rates determined with stool suspensions did not differ from those in buffer solution. MS2 buffer experiments were conducted in the same manner as the HuNoV stool experiments described above, with the exception that only MS2 bacteriophage (1 x 10^9 pfu/mL) was spiked into PBS. Experimental solutions were optically dilute (>95% transmittance at 254 nm) and therefore correction of the UV_{254} irradiance was not necessary.

Inactivation rate constants k_{inact} (mJ^{-1} cm^2) for MS2 and CVB5 were determined according to the following equation:

$$\ln\left(\frac{C}{C_0}\right) = -k_{inact} \cdot D_{UV_{254}} + constant \quad (1)$$

where C and C_0 are the concentrations of infectious viruses post and prior to UV_{254} exposure, respectively, and D_{UV254} is the UV dose, in mJ cm^{-2}.

2.3.3 RT-qPCR assays.

RNA from CVB5 inactivation experiments was extracted using Viral PureLink RNA Extraction kits (Invitrogen, Waltham, MA), eluted in 50 µL nuclease free water, and stored at -80°C. For HuNoV RNA extractions, 300 µL TRIzol reagent (Invitrogen) was added to 100 µL HuNoV inactivation experiment aliquots and extracted following the Direct-zol RNA MiniPrep Plus kit manufacturer instructions (Zymo Research, Irvine, CA) with no DNase treatment step. The extracted HuNoV RNA was eluted in 50 µL nuclease free water and stored at -80°C.

CVB5 primer sets were developed using Geneious (Version 11.1.4, Biomatters Ltd., Auckland, New Zealand; A.2 Tables

Table). Seven primer sets were selected, covering approximately 49% of the genome. The HuNoV GII.4 Sydney virus genome used in this study was Sanger sequenced using primer walking methods to obtain a nearly complete genome (7,469 bases; NCBI accession number MN703761).

HuNoV primer sets were designed with PrimerSelect (DNASTAR, Madison, WI). Eight sets of primers were selected to cover approximately 50% of the genome (Table).

One-step RT-qPCR of CVB5 extracts was performed using the One Step PrimeScript RT-PCR Kit (Takara Bio, Inc., Kusatsu, Japan) with SYBR Green reagents. 3 µL RNA template and 0.2 µM forward and reverse primers were included in each 15 µL reaction. The same cycling parameters were used for all CVB5 primer sets: initial denaturation at 95°C for 15 s, followed by 40 cycles of denaturation (95°C for 15 s), annealing (60°C for 30 s), and extension (72°C for 20 s), with a final extension step (72°C for 45 s). Each CVB5 run was performed on a magnetic induction cycler qPCR machine (Mic qPCR Cycler, Bio Molecular Systems, Queensland, Australia) with technical replicates (n = 2) and the average concentrations of replicates were used. When neither duplicate amplified, the data point was omitted, and if only one duplicate amplified, that value was used. Each run included a standard curve for all primer sets considered. qPCR standards were produced from extracted CVB5 RNA. The standard curves consisted of five serially diluted standards and a no-template control. The slopes and corresponding efficiencies of each assay are included in Table A.1. R^2 of all standard curves was greater than 0.98.

HuNoV RT-qPCR was carried out using a two-step reaction. cDNA synthesis was conducted for each sample using the iScript cDNA Synthesis kit (Bio-Rad, Hercules, CA) with 5 µL of RNA template in each 20 µL reaction. The qPCR reaction took place with a Mastercycler ep RealPlex 2 system (Eppendorf, Hauppauge, NY) with technical replicates (n = 3) and the average concentration of replicates were included. When the sample concentration was below the limit of quantification (LOQ), the data point was not included in analysis. Each 20 µL reaction consisted of 2 µL of cDNA template, 1X Fast EvaGreen qPCR Master Mix (Biotium, Inc., Fremont, CA), 0.5 µM forward and reverse primers, and 0.625 mg/mL bovine serum albumin (BSA).

Thermocycling conditions included an initial denaturation at 95°C for 5 min, 40 cycles of denaturation (95°C for 20 s), annealing (60°C for 20 s), and extension (72°C for 20 s), and a final extension step (72°C for 1 min). qPCR standards consisted of eight different purified gel products prepared from the GII.4 Sydney stool sample with each primer set. The amplified product was extracted with a QIAquick Gel Extraction kit (Qiagen, Hilden, Germany) and quantified with a Qubit fluorometer (Invitrogen). All standard sequences were confirmed with Sanger sequencing. Each assay contained a standard curve consisting of ≥ five serially diluted standards measured in triplicate and a no-template control. The slopes and corresponding efficiencies of each assay are included in Table A.2. R^2 of all standard curves was greater than 0.99.

RT-qPCR LOQs for each amplicon (Table A.1 and Table A.2) were defined as the threshold cycle (i.e., Ct) associated with the lowest dilution standard that resulted in a relative standard deviation of less than 35%[32] for ten replicates.[33] If after primer design and LOQ determination, a specific amplicon assay was not capable of tracking a sufficient amount of degradation in amplicon concentration before reaching the LOQ, a new primer set was selected and LOQ determination was carried out again. Amplicon degradation could be measured up to at least 0.87-log reduction for all HuNoV sample replicates and assays, based on initial experimental concentrations and assay LOQs. Based on the assay LOQs and starting concentrations of CVB5 amplicons, up to at least 2.7-log reduction was observable.

2.3.4 Extrapolation to the full genome.

The $\log_{10}$ reduction in intact genome concentrations following exposure to UV_{254} was estimated with the following relationship:[24]

$$\log\left(\frac{N}{N_0}\right) = \frac{Genome\ length}{Total\ length\ covered\ by\ n\ amplicons} \cdot log\left(\prod_{i=1}^{n} \frac{x_i}{x_{0,i}}\right) \quad (2)$$

where N_0 and N are the concentrations of intact genomes before and after UV_{254} exposure, respectively, n is the number of amplicons measured with RT-qPCR, i is the amplicon number, and x_0 and x are the concentrations of the intact amplicon measured by RT-qPCR before and after UV_{254} inactivation, respectively. Decay rate constants for each amplicon, k_i (mJ^{-1} cm^2), were determined according to the following equation:

$$\ln\left(\frac{x_i}{x_{0,i}}\right) = -k_i \cdot D_{UV_{254}} + constant \quad (3)$$

The amplicons used were not identical in length (Table A.1 and Table A.2). Because larger nucleotide sequences have more potential UV_{254} reaction sites than smaller sequences, amplicon decay rate constants cannot be directly compared to identify differential amplicon reactivity. To account for differences in amplicon size, k_i was normalized by the respective amplicon length (i.e., each amplicon decay rate constant was divided by the number of nucleotides in the amplicon), yielding the normalized amplicon decay rate constant $k_{i,\,norm}$ (mJ^{-1} cm^2 $base^{-1}$).

The decay rate constant for the full genome, k_{genome} (mJ^{-1} cm^2), is described by the following equation:

$$\ln\left(\frac{N}{N_0}\right) = -k_{genome} \cdot D_{UV_{254}} + constant \quad (4)$$

2.3.5 Statistical analyses.

All statistical comparisons and experimental data regression analyses were conducted in Prism version 7.0b (GraphPad, La Jolla, CA). Each rate constant (i.e., k_i and k_{inact}) was determined by conducting a single linear regression analysis on all experimental data (i.e., $\ln(x_i/x_{i,0})$ or $\ln(C/C_0)$ values at all UV doses). The full genome decay rate constant (i.e., k_{genome}) was determined by extrapolating amplicon degradation of each data point to the full genome using Equation 2 and

conducting a linear regression analysis on all the resulting genome degradation values. The error provided for each rate constant represents the 95% confidence interval (CI) of the linear regression slope.

In some cases, inactivation curves and genome degradation curves exhibited tailing at high UV_{254} doses; this effect may be due to the pyrimidine dimer reactions reaching photostationary states.[34–36] In these cases, only the linear portion of the curve was included in determination of k_{inact}, k_i, or k_{genome}. The linear portion of the curve was identified as the region for which the inclusion of increasing doses did not reduce the R^2 value. An Analysis of Covariance was employed to assess whether two linear regression slopes were significantly different from each other.

2.4 Results and Discussion

This study was undertaken to determine the inactivation of HuNoV through UV_{254} disinfection using a genome-wide PCR-based approach originally developed with bacteriophage MS2 inactivation by UV_{254}.[24] To confirm that the framework accurately estimates the UV_{254} inactivation kinetics of other (+) ssRNA viruses, we first tested the approach on CVB5, a culturable virus, so that infectivity through UV_{254} inactivation could be compared to genome extrapolation results.

2.4.1 Framework validation using CVB5.

UV_{254} doses for CVB5 experiments were verified with MS2, which was inactivated at similar rates (k_{inact} = 0.14 ± 0.01 cm^2 mJ^{-1}; mean ± 95% CI; Figure A.1) to those described in the literature (average k_{inact} = 0.13 cm^2 mJ^{-1}).[37] The values of $k_{i,\ norm}$ for the seven amplicons of the CVB5 genome measured with RT-qPCR ranged from 3.4 x 10^{-5} to 6.1 x 10^{-5} cm^2 mJ^{-1} $base^{-1}$ (Figure A.2). These rate constants are similar to the range of values (1.6 x 10^{-5} to 4.8 x 10^{-5} cm^2 mJ^{-1} $base^{-1}$) detected for other (+) ssRNA virus amplicons when normalized by amplicon length.[28,34]

Extrapolation of the data from the seven CVB5 amplicons to the entire genome resulted in a CVB5 genome decay rate of 0.35 ± 0.07 cm^2 mJ^{-1} (Figure 2.1). Amplicon coverage of 49% of the genome was chosen for extrapolation because it alleviates variability in amplicon degradation that arises when extrapolating inactivation with a reduced number of amplicons.[24] The estimated inactivation rate was similar to the inactivation rate constant determined with infectivity assays (k_{inact} = 0.33 ± 0.03 cm^2 mJ^{-1}; Figure 2.1). Our CVB5 results provide further evidence that the qPCR extrapolation method, which was originally verified with MS2, is effective at estimating the infectivity of (+) ssRNA viruses through UV_{254} treatment. It is therefore reasonable to assume that this method can also be applied to predict the inactivation kinetics of (+) ssRNA viruses that are difficult or not yet possible to culture.

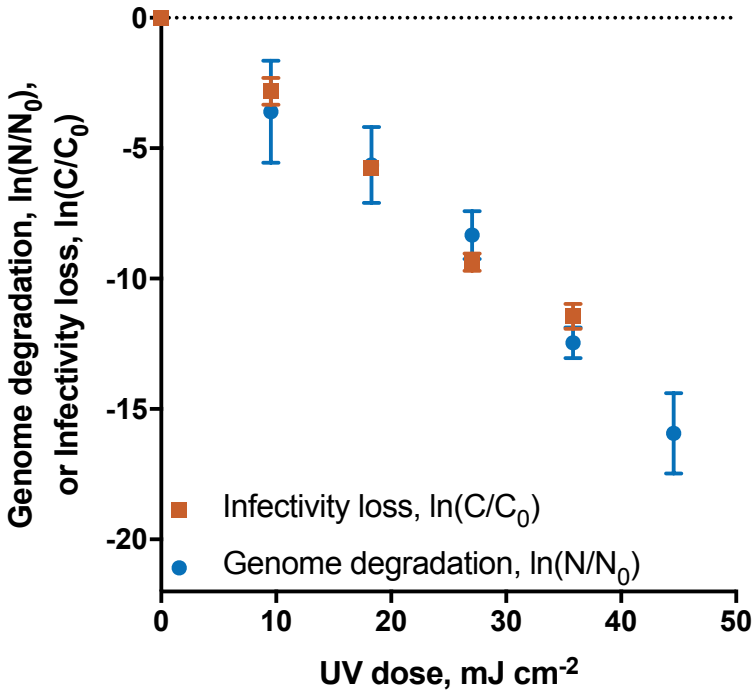

Figure 2.1. Degradation of CVB5 genome and loss of infectivity following UV_{254} exposure. Error bars depict standard error of the mean of three independent replicates (N = 3). CVB5 was spiked into VDB at a final concentration of 10^6 mpn/mL. Error bars are present for each symbol but in some cases are smaller than the symbol. Data re-used by permission from Springer Nature: Food and Environmental Virology,

Relationship Between Inactivation and Genome Damage of Human Enteroviruses Upon Treatment by UV254, Free Chlorine, and Ozone. Young, S., Torrey, J., Bachmann, V., Kohn, T.38 Copyright © 2019, Springer Science Business Media, LLC, part of Springer Nature, advance online publication, 29. October 2019 (doi: 10.1007/s12560-019-09411-2).

2.4.2 Estimation of HuNoV UV_{254} inactivation.

Next, we applied this approach to predict the inactivation kinetics of HuNoV. In these experiments, MS2 was used to verify the UV_{254} dose applied to viruses in suspension. The MS2 inactivation rate (k_{inact} = 0.14 ± 0.02 cm^2 mJ^{-1}; Figure A.3) was similar to values reported in the literature (average k_{inact} = 0.13 cm^2 mJ^{-1}),[37] thus confirming the UV_{254} doses experienced by HuNoV during experimentation. The MS2 kinetics also corresponded with those measured in the CVB5/MS2 experiments discussed above, indicating that the experimental conditions were similar for all of the viruses studied. The HuNoV genome concentrations were similar in RNase-treated and untreated HuNoV suspensions used for inactivation experiments (Figure A.4), revealing that there was minimal extraviral RNA in the suspensions.

Constituents of HuNoV stool suspensions may react with photons during UV_{254} inactivation and generate reactive species that result in indirect photolysis of viruses. To ensure that indirect photolysis did not occur during UV_{254} inactivation, MS2 inactivation in PBS (i.e., a photosensitizer-free solution) was compared to MS2 inactivation in the stool suspension. Rates of MS2 inactivation in buffer (k_{inact} = 0.14 ± 0.02 cm^2 mJ^{-1}; Figure A.5) were the same as those in stool suspensions (k_{inact} = 0.14 ± 0.02 cm^2 mJ^{-1}). The similar rates of MS2 inactivation between buffer solution and stool suspensions suggest that indirect photolysis did not contribute to the inactivation rates observed in HuNoV experiments.

HuNoV UV_{254} inactivation resulted in normalized decay rate constants $k_{i,\ norm}$ for the eight measured regions in the HuNoV genome ranging from 2.1 x 10^{-5} to 4.9 x 10^{-5} cm^2 mJ^{-1} $base^{-1}$ (Figure 2.2a). These values are comparable to the rate constants measured for the CVB5 genome regions, as well as to RNA rate constants reported in the literature.[28,34] The range of observed HuNoV amplicon reactivities after accounting for amplicon length is consistent with previous studies that have reported varying UV_{254} reaction kinetics across the genomes of other ssRNA viruses.[28,34] Individual RNA nucleotides and specific RNA sequences have unique UV reactivities.[39] Specifically, pyrimidine bases are more photoreactive than purine bases, forming both pyrimidine hydrates and pyrimidine dimers. Indeed, the fastest reacting amplicon (i.e., Amplicon 1) contained 257 pyrimidines, whereas the slowest reacting amplicon (i.e., Amplicon 4) contained 222 pyrimidines. RNA secondary structure can also impact the photoreactivity of nucleic acids.[40] Consequently, amplifying only a small region of the genome and extrapolating damage to the whole genome may under- or over-predict genome reactivity;[24] incorporating the reactivities of several amplicons covering different portions of the genome seeks to avoid this potential bias.

The reactivities of the eight HuNoV genome regions were used to construct an inactivation curve for the entire HuNoV genome (Figure 2.2b). Fitted to equation 2, the resulting inactivation rate constant k_{genome} for HuNoV was 0.27 ± 0.03 cm^2 mJ^{-1}. As mentioned above, HuNoV UV_{254} inactivation curves generated from infectivity assays are not available due to the lack of a reliable and quantitative culture-based infectivity assay. Based on the inactivation rate constant determined from our extrapolated genome data, a 4-log inactivation of GII HuNoV would be expected following a UV_{254} dose of approximately 34 mJ cm^{-2}.

This finding is a significant departure from previous reports of 0- to 1.5-log inactivation at treatment plants and in lab-scale studies after UV_{254} doses as high as 300 mJ cm^{-2}. [3,15,41] These studies also relied on qPCR, but used short regions of the genome (~100 bases) to determine virus inactivation.[3,15,41] The discrepancy between our HuNoV inactivation results and those reported in previous studies lies in the fact that their results represent the reactivity of a small portion (i.e., <1%) of the genome, whereas our results represent the reactivity of the entire genome. Such discrepancies have been reported for culturable viruses,[18,23,25,42] but not for HuNoV.

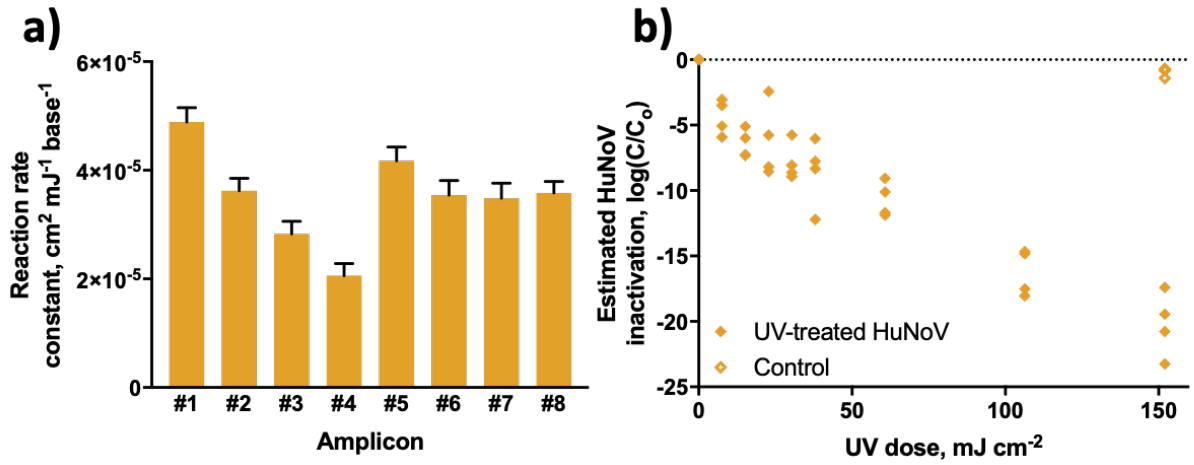

Figure 2.2 Reactivity of HuNoV following UV_{254} exposure. Reaction rate constants for HuNoV amplicons, normalized by number of bases in each amplicon (a), and estimated HuNoV inactivation using extrapolation of genome degradation data from all eight amplicons, following equation 2 (b). Experiments were performed in replicate (N = 4) and error bars depict standard error of the mean of four independent replicates. HuNoV was spiked into PBS at a final concentrations of 1.5 x 10^6 gene copies/mL.

2.4.3 Comparison of HuNoV and other (+) ssRNA viruses.

The availability of a HuNoV inactivation rate constant provides an opportunity to compare the susceptibility of HuNoV to culturable viruses, especially those commonly used as HuNoV surrogates. Feline calicivirus (FCV) and murine norovirus (MNV), for example, are both members of the *Caliciviridae* family and share many traits with HuNoV, including RNA genome

organization[43,44] and capsids with similar diameters and icosahedral shapes.[45] Despite these structural similarities, the usefulness of these viruses as surrogates for HuNoV has been debated.[11,46] A comparison of our HuNoV UV_{254} inactivation kinetics and published inactivation kinetics of FCV and MNV confirms that they are appropriate surrogates for HuNoV in UV_{254} disinfection processes (Figure 2.3). Likewise, the enteroviruses CVB5 and echovirus 12, which are also (+) ssRNA viruses, have similar inactivation rates. Compared to HuNoV and the other ssRNA viruses presented in Figure 2.3, bacteriophage MS2 is not inactivated as quickly by UV_{254}. This is likely because MS2 has a smaller genome than the other viruses (3.6 kb versus approximately 7.5 kb), thus containing fewer UV_{254} targets (Table A.3). Our results suggest that the HuNoV genome is not more resistant to UV_{254} than other (+) ssRNA viruses with similarly-sized genomes, as measured with RT-qPCR. Therefore, culturable (+) ssRNA enteric viruses appear to be effective surrogates for tracking HuNoV inactivation with UV_{254}.

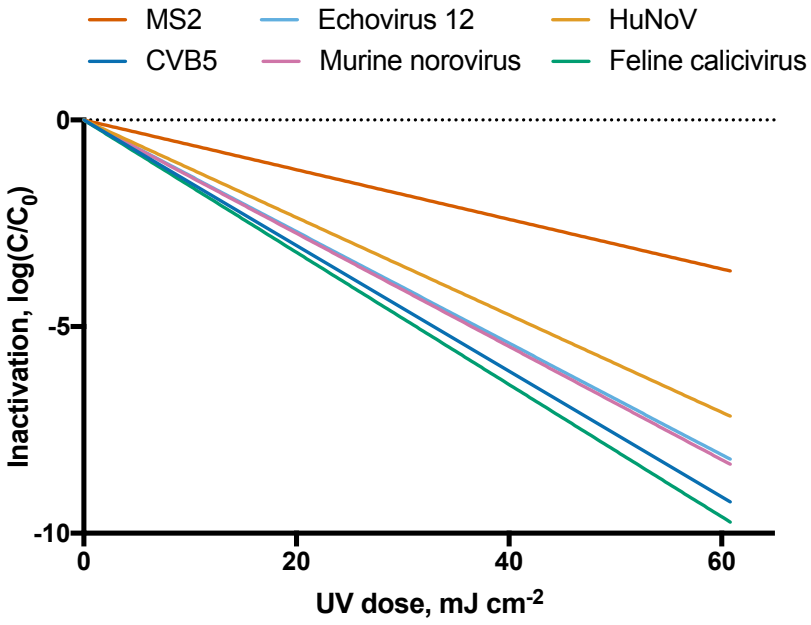

Figure 2.3 HuNoV inactivation curve based on amplicon extrapolation approach and inactivation curves of other (+) ssRNA viruses (MS2, CVB5, MNV, echovirus 12, and FCV). First-order reaction rate constants obtained from Park et al.[47] and this study (Table A.3).

2.4.4 HuNoV inactivation monitoring in water treatment settings.

We used eight primer sets spanning the HuNoV GII.4 Sydney genome to approximate the reaction kinetics of the entire genome. This same approach cannot be applied to measure the inactivation of environmental HuNoV strains in UV treatment processes because the eight primer sets were designed specifically for the HuNoV GII.4 Sydney strain used in our experiments. The large sequence diversity in HuNoV genomes does not allow for the design of primers spanning the entire HuNoV genome, while also targeting a large portion of known HuNoV strains.

To evaluate UV_{254} inactivation of environmental HuNoV, we selected a generic GII HuNoV primer set, namely G2SK,[48] from the conserved region of the GII HuNoV genome for monitoring the UV_{254} inactivation of environmental GII HuNoV. We note that we cannot assume that the reactivity of the 344 base genome region captured with primer set G2SK is representative of the reactivity of the entire genome; instead, we can develop a relationship to link the reactivity of the G2SK region to the reactivity of the HuNoV genome. Specifically, we measured the UV_{254} reaction kinetics of the G2SK amplicon (Figure A.6) in the same samples used to measure the eight primer sets and correlated the resulting data with the HuNoV inactivation kinetics obtained with our extrapolation approach (Figure 2.4). The resulting relationship can be applied by others to assess the UV_{254} inactivation of environmental HuNoV strains using only G2SK amplicon measurements:

$$log_{10}\left(\frac{N}{N_0}\right) = Slope \cdot log_{10}\left(\frac{x}{x_0}\right) \quad (5)$$

where, $\log_{10}(x/x_0)$ refers to the lognormal degradation of the G2SK amplicon through UV_{254} treatment, $\log_{10}(N/N_0)$ refers to the lognormal HuNoV inactivation through UV_{254} treatment, and Slope is equal to 17.6. This approach does not extrapolate the G2SK amplicon results, but rather

applies the relationship between the degradation of the G2SK amplicon and the degradation of the entire genome. For example, if a 0.5-log removal of the G2SK amplicon is measured through UV_{254} treatment, then the overall GII HuNoV inactivation of 8.8-log (i.e., 17.6 · 0.5) has been achieved. It is worth mentioning that this relationship was obtained using estimated UV_{254} inactivation data for a GII.4 Sydney HuNoV strain. While we would expect that other GII strains behave similarly through UV_{254} treatment, it is possible that other environmental GII strains may deviate slightly from this relationship. Additionally, use of this tool can only monitor HuNoV inactivation at levels of 1-log or more, because the G2SK degradation must be sufficient to detect a reduction in concentration with qPCR (details and results of a G2SK qPCR sensitivity analysis are provided in Appendix A and Figure A.7).

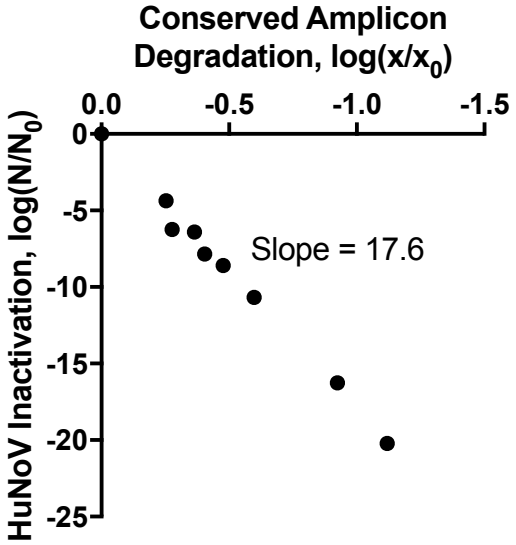

Figure 2.4 Relationship between HuNoV inactivation through UV_{254} treatment and degradation of the conserved amplicon G2SK. The slope of the best-fit linear regression is 17.6 and R^2 is 0.99.

2.4.5 Environmental implications.

This study provides a critical HuNoV inactivation rate constant for UV_{254} disinfection and determined that the rate of HuNoV inactivation was much faster than reported in previous studies

that used traditional qPCR approaches. Our work underscores the importance of accounting for the entire genome when evaluating UV_{254} inactivation rates and highlights the limitations of measuring only a small portion of the genome. Although other approaches for estimating infectivity with molecular methods (e.g., sample pre-treatment before qPCR, near full-genome amplification) have improved inactivation approximations in the absence of infectivity assays, they suffer from multiple sample preparation steps, considerable assay optimization, and the inability to accurately track UV_{254} inactivation.[13,18] The correlation developed here between short amplicon decay and genome inactivation will be a useful tool for rapidly assessing UV_{254} inactivation in real world scenarios.

One important factor enabling the success of this approach is that UV_{254} irradiation's primary mode of action is damage to nucleic acid, which is the explicit target of the RT-qPCR assay. While the method used in this study could also be adapted for use with other disinfectants, such application would need to account for the different inactivation mechanisms of these disinfectants.[34,49,50] The method would also need to be adapted for the inactivation of dsDNA viruses that undergo DNA repair in their host cells.

Our results suggest that HuNoV behaves similarly to other enteric (+) ssRNA viruses through UV_{254} inactivation, though bacteriophage MS2 is more resistant due to its shorter genome length. This is an important finding because MS2 is commonly used to assess the degree of virus inactivation through UV_{254} systems;[51] these findings provide confidence that MS2 inactivation can be used as a conservative estimator of HuNoV removal. Our findings further suggest that surrogates such as FCV and MNV are more appropriate for assessing HuNoV inactivation through UV_{254} treatment. Whether these surrogates are also suitable for estimating HuNoV infectivity through other disinfecting treatments (e.g., ozone, chlorine, advanced oxidation) remains to be

determined. Ongoing work towards quantitative HuNoV *in vitro* culture systems[8,10] will ultimately facilitate measurement of HuNoV disinfection kinetics, which is critical to the water treatment field.

2.5 References

(1) Scallan, E.; Hoekstra, R. M.; Angulo, F. J.; Tauxe, R. V; Widdowson, M.-A.; Roy, S. L.; Jones, J. L.; Griffin, P. M. Foodborne Illness Acquired in the United States—Major Pathogens. *Emerg. Infect. Dis.* **2011**, *17* (1), 7–15.

(2) Hall, A. J.; Lopman, B. A.; Payne, D. C.; Patel, M. M.; Gastañaduy, P. A.; Vinjé, J.; Parashar, U. D. Norovirus Disease in the United States. *Emerg. Infect. Dis.* **2013**, *19* (8), 1198–1205.

(3) Campos, C. J. A.; Avant, J.; Lowther, J.; Till, D.; Lees, D. N. Human Norovirus in Untreated Sewage and Effluents from Primary, Secondary and Tertiary Treatment Processes. *Water Res.* **2016**, *103*, 224–232.

(4) Teunis, P. F. M.; Moe, C. L.; Liu, P.; Miller, S. E.; Lindesmith, L.; Baric, R. S.; Le Pendu, J.; Calderon, R. L. Norwalk Virus: How Infectious Is It? *J. Med. Virol.* **2008**, *80* (8), 1468–1476.

(5) Schmidt, P. J. Norovirus Dose–Response: Are Currently Available Data Informative Enough to Determine How Susceptible Humans Are to Infection from a Single Virus? *Risk Anal.* **2014**, *35* (7), 1364–1383.

(6) Gerba, C. P.; Betancourt, W. Q.; Kitajima, M. How Much Reduction of Virus Is Needed for Recycled Water: A Continuous Changing Need for Assessment? *Water Res.* **2017**, *108*, 25–31.

(7) Soller, J. A.; Eftim, S. E.; Warren, I.; Nappier, S. P. Evaluation of Microbiological Risks Associated with Direct Potable Reuse. *Microb. Risk Anal.* **2016**, *5*, 3–14.

(8) Ettayebi, K.; Crawford, S. E.; Murakami, K.; Broughman, J. R.; Karandikar, U.; Tenge, V. R.; Neill, F. H.; Blutt, S. E.; Zeng, X.-L.; Qu, L.; Kou, B.; Opekun, A. R.; Burrin, D.; Graham, D. Y.; Ramani, S.; Atmar, R. L.; Estes, M. K. Replication of Human Noroviruses in Stem Cell–Derived Human Enteroids. *Science* **2016**, *353* (6306), 1387–1393.

(9) Jones, M. K.; Watanabe, M.; Zhu, S.; Graves, C. L.; Keyes, L. R.; Grau, K. R.; Gonzalez-Hernandez, M. B.; Iovine, N. M.; Wobus, C. E.; Vinjé, J.; Tibbetts, S. A.; Wallet, S. M.; Karst, S. M. Enteric Bacteria Promote Human and Mouse Norovirus Infection of B Cells. *Science* **2014**, *346* (6210), 755–759.

(10) Costantini, V.; Morantz, E. K.; Browne, H.; Ettayebi, K.; Zeng, X.-L.; Atmar, R. L.; Estes, M. K.; Vinjé, J. Human Norovirus Replication in Human Intestinal Enteroids as Model to Evaluate Virus Inactivation. *Emerg. Infect. Dis. J.* **2018**, *24* (8), 1453–1464.

(11) Richards, G. P. Critical Review of Norovirus Surrogates in Food Safety Research: Rationale for Considering Volunteer Studies. *Food Environ. Virol.* **2012**, *4* (1), 6–13.

(12) Knight, A.; Li, D.; Uyttendaele, M.; Jaykus, L.-A. A Critical Review of Methods for Detecting Human Noroviruses and Predicting Their Infectivity. *Crit. Rev. Microbiol.* **2013**, *39* (3), 295–309.

(13) Karim, M. R.; Fout, G. S.; Johnson, C. H.; White, K. M.; Parshionikar, S. U. Propidium Monoazide Reverse Transcriptase PCR and RT-QPCR for Detecting Infectious Enterovirus and Norovirus. *J. Virol. Methods* **2015**, *219*, 51–61.

(14) Oristo, S.; Lee, H.-J.; Maunula, L. Performance of Pre-RT-QPCR Treatments to Discriminate Infectious Human Rotaviruses and Noroviruses from Heat-Inactivated Viruses: Applications of PMA/PMAxx, Benzonase and RNase. *J. Appl. Microbiol.* **2018**,

124 (4), 1008–1016.

(15) Rönnqvist, M.; Mikkelä, A.; Tuominen, P.; Salo, S.; Maunula, L. Ultraviolet Light Inactivation of Murine Norovirus and Human Norovirus GII: PCR May Overestimate the Persistence of Noroviruses Even When Combined with Pre-PCR Treatments. *Food Environ. Virol.* **2014**, *6* (1), 48–57.

(16) Topping, J. R.; Schnerr, H.; Haines, J.; Scott, M.; Carter, M. J.; Willcocks, M. M.; Bellamy, K.; Brown, D. W.; Gray, J. J.; Gallimore, C. I.; Knight, A. I. Temperature Inactivation of Feline Calicivirus Vaccine Strain FCV F-9 in Comparison with Human Noroviruses Using an RNA Exposure Assay and Reverse Transcribed Quantitative Real-Time Polymerase Chain Reaction—A Novel Method for Predicting Virus Infectivity. *J. Virol. Methods* **2009**, *156* (1), 89–95.

(17) Fraisse, A.; Niveau, F.; Hennechart-Collette, C.; Coudray-Meunier, C.; Martin-Latil, S.; Perelle, S. Discrimination of Infectious and Heat-Treated Norovirus by Combining Platinum Compounds and Real-Time RT-PCR. *Int. J. Food Microbiol.* **2018**, *269*, 64–74.

(18) Ho, J.; Seidel, M.; Niessner, R.; Eggers, J.; Tiehm, A. Long Amplicon (LA)-QPCR for the Discrimination of Infectious and Noninfectious Phix174 Bacteriophages after UV Inactivation. *Water Res.* **2016**, *103*, 141–148.

(19) Miller, R. L.; Plagemann, P. G. W. Effect of Ultraviolet Light on Mengovirus: Formation of Uracil Dimers, Instability and Degradation of Capsid, and Covalent Linkage of Protein to Viral RNA. *J. Virol.* **1974**, *13* (3), 729 LP – 739.

(20) Miller, N.; Cerutti, P. Structure of the Photohydration Products of Cytidine and Uridine. *Proc. Natl. Acad. Sci. U. S. A.* **1968**, *59* (1), 34–38.

(21) Singer, B. Chemical Modification of Viral Ribonucleic Acid: IX. The Effect of Ultraviolet Irradiation on TMV-RNA and Other Polynucleotides. *Virology* **1971**, *45* (1), 101–107.

(22) Wurtmann, E. J.; Wolin, S. L. RNA under Attack: Cellular Handling of RNA Damage. *Crit. Rev. Biochem. Mol. Biol.* **2009**, *44* (1), 34–49.

(23) Simonet, J.; Gantzer, C. Inactivation of Poliovirus 1 and F-Specific RNA Phages and Degradation of Their Genomes by UV Irradiation at 254 Nanometers. *Appl. Environ. Microbiol.* **2006**, *72* (12), 7671 LP – 7677.

(24) Pecson, B. M.; Ackermann, M.; Kohn, T. Framework for Using Quantitative PCR as a Nonculture Based Method To Estimate Virus Infectivity. *Environ. Sci. Technol.* **2011**, *45* (6), 2257–2263.

(25) Wolf, S.; Rivera-Aban, M.; Greening, G. E. Long-Range Reverse Transcription as a Useful Tool to Assess the Genomic Integrity of Norovirus. *Food Environ. Virol.* **2009**, *1* (3), 129.

(26) Calgua, B.; Carratalà, A.; Guerrero-Latorre, L.; de Abreu Corrêa, A.; Kohn, T.; Sommer, R.; Girones, R. UVC Inactivation of DsDNA and SsRNA Viruses in Water: UV Fluences and a QPCR-Based Approach to Evaluate Decay on Viral Infectivity. *Food Environ. Virol.* **2014**, *6* (4), 260–268.

(27) Meister, S.; Verbyla, M. E.; Klinger, M.; Kohn, T. Variability in Disinfection Resistance between Currently Circulating Enterovirus B Serotypes and Strains. *Environ. Sci. Technol.* **2018**, *52* (6), 3696–3705.

(28) Pecson, B. M.; Martin, L. V.; Kohn, T. Quantitative PCR for Determining the Infectivity of Bacteriophage MS2 upon Inactivation by Heat, UV-B Radiation, and Singlet Oxygen: Advantages and Limitations of an Enzymatic Treatment To Reduce False-Positive Results.

Appl. Environ. Microbiol. **2009**, *75* (17), 5544–5554.

(29) United States Environmental Protection Agency. *Method 1601: Male-Specific (F+) and Somatic Coliphage in Water by Two-Step Enrichment Procedure*; Washington, D.C., 2001.

(30) Rahn, R. O. Potassium Iodide as a Chemical Actinometer for 254 Nm Radiation: Use of Lodate as an Electron Scavenger. *Photochem. Photobiol.* **1997**, *66* (4), 450–455.

(31) Rahn, R. O.; Bolton, J.; Stefan, M. I. The Lodide/Lodate Actinometer in UV Disinfection: Determination of the Fluence Rate Distribution in UV Reactors. *Photochem. Photobiol.* **2006**, *82* (2), 611–615.

(32) Forootan, A.; Sjöback, R.; Björkman, J.; Sjögreen, B.; Linz, L.; Kubista, M. Methods to Determine Limit of Detection and Limit of Quantification in Quantitative Real-Time PCR (QPCR). *Biomol. Detect. Quantif.* **2017**, *12*, 1–6.

(33) Hougs, L.; Gatto, F.; Goerlich, O.; Grohmann, L.; Lieske, K.; Mazzara, M.; Narendja, F.; Ovesna, J.; Papazova, N.; Scholtens, I.; Zel, J. *Verification of Analytical Methods for GMO Testing When Implementing Interlaboratory Validated Methods*; 2017.

(34) Qiao, Z.; Ye, Y.; Chang, P. H.; Thirunarayanan, D.; Wigginton, K. R. Nucleic Acid Photolysis by UV254 and the Impact of Virus Encapsidation. *Environ. Sci. Technol.* **2018**, *52* (18), 10408–10415.

(35) Helleiner, C. W.; Pearson, M. L.; Johns, H. E. The Ultraviolet Photochemistry of Deoxyuridylyl (3′→ 5′) Deoxyuridine. *Proc. Natl. Acad. Sci. U. S. A.* **1963**, *50* (4), 761–767.

(36) Johns, H. E.; Pearson, M. L.; LeBlanc, J. C.; Helleiner, C. W. The Ultraviolet Photochemistry of Thymidylyl-(3′→5′)-Thymidine. *J. Mol. Biol.* **1964**, *9* (2), 503-IN1.

(37) Hijnen, W. A. M.; Beerendonk, E. F.; Medema, G. J. Inactivation Credit of UV Radiation for Viruses, Bacteria and Protozoan (Oo)Cysts in Water: A Review. *Water Res.* **2006**, *40* (1), 3–22.

(38) Young, S.; Torrey, J.; Bachmann, V.; Kohn, T. Relationship Between Inactivation and Genome Damage of Human Enteroviruses Upon Treatment by UV_{254}, Free Chlorine, and Ozone. *Food Environ. Virol.* **2019**.

(39) Smith, K. C.; Hanawalt, P. C. Photochemistry of the Nucleic Acids. In *Molecular Photobiology: Inactivation and Recovery*; Horecker, B., Kaplan, N. O., Marmur, J., Eds.; Academic Press, 1969; pp 57–84.

(40) Pearson, M.; Johns, H. E. Suppression of Hydrate and Dimer Formation in Ultraviolet-Irradiated Poly (A + U) Relative to Poly U. *J. Mol. Biol.* **1966**, *20* (2), 215–229.

(41) Qiu, Y.; Lee, B. E.; Neumann, N.; Ashbolt, N.; Craik, S.; Maal-Bared, R.; Pang, X. L. Assessment of Human Virus Removal during Municipal Wastewater Treatment in Edmonton, Canada. *J. Appl. Microbiol.* **2015**, *119* (6), 1729–1739.

(42) Tanaka, T.; Nogariya, O.; Shionoiri, N.; Maeda, Y.; Arakaki, A. Integrated Molecular Analysis of the Inactivation of a Non-Enveloped Virus, Feline Calicivirus, by UV-C Radiation. *J. Biosci. Bioeng.* **2018**, *126* (1), 63–68.

(43) Wobus, C. E.; Thackray, L. B.; Virgin, H. W. Murine Norovirus: A Model System To Study Norovirus Biology and Pathogenesis. *J. Virol.* **2006**, *80* (11), 5104 LP – 5112.

(44) Radford, A. D.; Coyne, K. P.; Dawson, S.; Porter, C. J.; Gaskell, R. M. Feline Calicivirus. *Vet. Res.* **2007**, *38* (2), 319–335.

(45) Bhella, D.; Gatherer, D.; Chaudhry, Y.; Pink, R.; Goodfellow, I. G. Structural Insights into

Calicivirus Attachment and Uncoating. *J. Virol.* **2008**, *82* (16), 8051 LP – 8058.

(46) Cannon, J. L.; Papafragkou, E.; Park, G. W.; Osborne, J.; Jaykus, L.-A.; Vinje, J. Surrogates for the Study of Norovirus Stability and Inactivation in the Environment: A Comparison of Murine Norovirus and Feline Calicivirus. *J. Food Prot.* **2006**, *69* (11), 2761–2765.

(47) Park, G. W.; Linden, K. G.; Sobsey, M. D. Inactivation of Murine Norovirus, Feline Calicivirus and Echovirus 12 as Surrogates for Human Norovirus (NoV) and Coliphage (F+) MS2 by Ultraviolet Light (254 Nm) and the Effect of Cell Association on UV Inactivation. *Lett. Appl. Microbiol.* **2011**, *52* (2), 162–167.

(48) Kojima, S.; Kageyama, T.; Fukushi, S.; Hoshino, F. B.; Shinohara, M.; Uchida, K.; Natori, K.; Takeda, N.; Katayama, K. Genogroup-Specific PCR Primers for Detection of Norwalk-like Viruses. *J. Virol. Methods* **2002**, *100* (1), 107–114.

(49) Torrey, J.; von Gunten, U.; Kohn, T. Differences in Viral Disinfection Mechanisms as Revealed by Quantitative Transfection of Echovirus 11 Genomes. *Appl. Environ. Microbiol.* **2019**, *85* (14).

(50) Wigginton, K. R.; Pecson, B. M.; Sigstam, T.; Bosshard, F.; Kohn, T. Virus Inactivation Mechanisms: Impact of Disinfectants on Virus Function and Structural Integrity. *Environ. Sci. Technol.* **2012**, *46* (21), 12069–12078.

(51) National Water Research Institute. *Ultraviolet Disinfection: Guidelines for Drinking Water and Water Reuse*; 2012.

Chapter 3

Predictive Modeling of Virus Inactivation by UV

3.1 Abstract

UV_{254} disinfection strategies are commonly applied to inactivate pathogenic viruses in water, food, air, and on surfaces. There is a need for methods that rapidly predict the kinetics of virus inactivation by UV_{254}, particularly for emerging and difficult-to-culture viruses. We conducted a systematic literature review of inactivation rate constants for a wide range of viruses. Using these data and virus characteristics, we developed and evaluated linear and non-linear models for predicting inactivation rate constants. Multiple linear regressions performed best for predicting the inactivation kinetics of (+) ssRNA and dsDNA viruses, with cross-validated root mean squared relative prediction errors similar to those associated with experimental rate constants. We tested the models by predicting and measuring inactivation rate constants of a (+) ssRNA mouse coronavirus and a dsDNA marine bacteriophage; the predicted rate constants were within 7% and 71% of the experimental rate constants, respectively, indicating that the prediction was more accurate for the (+) ssRNA virus than the dsDNA virus. Finally, we applied our models to predict the UV_{254} rate constants of several viruses for which high-quality UV_{254} inactivation data are not

available. Our models will be valuable for predicting inactivation kinetics of emerging or difficult-to-culture viruses.

3.2 Introduction

Viruses can cause diverse and costly illnesses in humans and other animals.[1] A variety of approaches have therefore been developed to decontaminate food, water, air, and surfaces that may contain infective viruses.[2–7] UV_{254} treatment, in particular, is gaining popularity as an alternative to more traditional chemical disinfection strategies.[8–10] Viruses can have highly variable UV_{254} susceptibilities.[11,12] For example, two dsDNA viruses, adenovirus type 40 and bacteriophage T6, are inactivated by UV_{254} at the widely varying rates of ~ 0.06 cm^2 mJ^{-1}.[13–18] and ~ 5.4 cm^2 mJ^{-1},[19] respectively.

Viruses have diverse genome types, including double-stranded RNA (dsRNA), single-stranded RNA (ssRNA), double-stranded DNA (dsDNA), and single-stranded DNA (ssDNA). UV_{254} inactivates by primarily targeting viral genetic material, and the different biochemical structures associated with these viral genome types result in distinct sensitivities to UV_{254}.[20] Nucleic acid primary structure, or nucleotide base sequence, also affects UV_{254} genome reactivity – pyrimidine bases, for instance, are about an order of magnitude more reactive with UV_{254} than purine bases.[21,22] The replication modes of viruses differ, and an enzyme of one virus may stall at a UV_{254} lesion that does not affect the replication enzyme of another virus. For example, the reverse transcriptase enzymes involved in the generation of retrovirus mRNA may have different sensitivities to photochemical modifications in nucleic acid compared to the RNA dependent RNA polymerase enzymes used by other RNA viruses to synthesize mRNA.[23] Additional differences in viral infection cycles impact virus sensitivity to UV_{254}.[24] dsDNA virus genomes, for example, can undergo nucleic acid repair once inside host cells.[24–26] This means that a virus may be inactivated

by UV_{254} treatment through base modification, only to be repaired and thus rendered infectious again when such repair mechanisms are available. We note these differences in virus genome type and mode of mRNA generation are utilized in the Baltimore virus classification system (e.g., Group 1: dsDNA viruses, Group IV: (+) ssRNA viruses).[1,27]

Virus disinfection methods are evaluated by enumerating infective viruses before and after treatment, typically with virus culture systems. Relying on culture-based approaches to evaluate inactivation kinetics is often challenging. Most notably, many human viruses that are spread through the environment are not readily culturable. For highly pathogenic viruses that are culturable, disinfection experiments are complicated by biosafety restrictions. Disinfection experiments with severe acute respiratory syndrome (SARS) coronaviruses (SARS-CoV-1 and SARS-CoV-2), for example, are limited to biosafety level 3 laboratories and work with ebolaviruses require biosafety level 4 facilities. Alternative approaches for determining virus inactivation kinetics would be valuable, especially for difficult-to-culture and emerging viruses. Earlier studies have worked towards a predictive manner of evaluating UV_{254} virus inactivation based on virus attributes.[28,29] Recently developed modeling strategies, an improved understanding of virus UV_{254} inactivation mechanisms, and additional high-quality inactivation data published in recent years provide the necessary tools and information to expand upon these initial predictive approaches.

In this study, we develop models to predict rate constants for virus inactivation with UV_{254} treatment in aqueous suspension using variables that are expected to play a role in inactivation, such as genome sequence composition and genome repair information. We conducted a systematic review to gather high quality virus inactivation data from the literature and used the resulting data set to train and validate the predictive performance of four different models (i.e., multiple linear

regression, elastic net regularization, boosted trees, and random forests). The models developed in this research will facilitate rapid evaluation of UV_{254} inactivation rate constants for a broad class of virus types based solely on virus genome sequence and genome repair information.

3.3 Materials and Methods

3.3.1 Systematic review of UV_{254} virus inactivation data.

We conducted a systematic literature review to capture high quality UV_{254} virus inactivation data using the PRISMA guidelines.[30] Data were extracted from studies if they adhered to all of the following criteria: the UV_{254} lamp fluences were measured and reported; sources emitted UV irradiation principally at wavelengths of 253, 253.7, 254, or 255 nm; viruses were irradiated in a liquid suspension; infective viruses were enumerated with quantitative culture-based approaches (e.g., plaque assay); attenuation through the sample solution was taken into account, or negligible UV_{254} attenuation was reported (transmittance > 95%) or could be assumed based on the reported viral stock purification techniques and matrix solution composition; stirring was reported when attenuation was significant (transmittance < 95%); first-order kinetics were reported or could be confirmed with reported data points for at least two UV_{254} fluences; the first-order inactivation rate constant or log-removal dose (e.g., D_{99}) was provided or could be determined with data presented in a plot or table. For publications that contained valuable data, but for which not all criteria could be evaluated, corresponding authors were contacted when possible to inquire about the criteria. For studies that reported multiple UV_{254} inactivation experiments for the same virus (e.g., in different solutions, with multiple UV_{254} sources), we combined all data to determine a single inactivation rate constant with linear regression analysis. All data were re-extracted by a second reviewer and discrepancies were addressed. Additional details of our systematic review process are included in Appendix B.

3.3.2 Final data set used in modeling.

An inactivation rate constant collected in the systematic review was included in the modeling work if the virus' genome sequence was available through NCBI and if the error associated with the inactivation rate constant was available. Information on NCBI sequence selection is provided in Appendix B. For viruses with three or more inactivation rate constants obtained from the systematic review, outlier rate constants (i.e., values lying >1.5 times the interquartile range above the third quartile or below the first quartile) were not included in model development. We calculated the inverse variance weighted mean inactivation rate constant for each virus using the following equation:

$$\bar{k}_v = \frac{\sum_{i=1}^{n} k_i \cdot w_i}{\sum_{i=1}^{n} w_i} \quad (1)$$

where $\bar{k}_v$ is the inverse variance weighted mean for the virus, n is the number of experimental rate constants for the virus, k_i is the inactivation rate constant for experiment i, and w_i is the weight for experiment i, defined as:

$$w_i = \frac{1}{SE_i^2} \quad (2)$$

where $SE_{,i}$ is the standard error of the inactivation rate constant for experiment i. The standard error of the inverse variance weighted mean, SE_v, was evaluated for each virus as:

$$SE_v = \sqrt{\frac{1}{\sum_{i=1}^{n} w_i}} \quad (3)$$

We estimated the inter-experimental error for viruses with more than one experimental rate constant in the literature by determining the residual standard deviation from a weighted least squares regression. Virus was the categorical variable in the regression and experimental rate

constant was the dependent variable. Weighting was done using the inverse of the squared experimental standard error normalized by the mean rate constant for that virus.

3.3.3 Predictors.

For model development, we used predictors related to virus structure and behavior that are known or hypothesized to affect UV_{254} inactivation. The specific predictors incorporated included structure of nucleic acid strands (i.e., double-stranded or single stranded), genome length, pyrimidine base content in the genome, sequential pyrimidine bases, genome repair mode, and host cell type. Our reasoning for inclusion of predictors and the methods used to determine values for each predictor are included in Appendix B. A list of the exact predictors as well as the values used for each virus are available in Table B.1.

3.3.4 Predictive model optimization.

We used four model classes, namely multiple linear regression, elastic net regularization, boosted trees, and random forests, to predict virus inactivation during UV_{254} disinfection. For each model class, we developed individual models using only (+) ssRNA viruses and only dsDNA viruses. We also generated a single model developed using all viruses included in the collected data set and thus not separated by virus Baltimore classification groups. We assessed model performance using leave-one-virus-out cross-validation. Further details of model training, validation, and prediction performance evaluation are included in Appendix B. Data manipulation, statistical analyses, and modeling work were conducted in R software version 4.0.0.[31] The raw data files and the scripts for model development and prediction are available in Github at https://github.com/nrockey/uv-virus-inactivation-prediction.

3.3.4.1 Multiple linear regression.

Several of the genomic variables are collinear (e.g., numbers of U and UU). We therefore conducted principal component analysis (PCA) on the genomic variables prior to linear modeling to reduce variable dimensionality and eliminate collinearity. The predictors nucleic acid type, genome repair mode, and host cell type were not included in the PCA. We then developed linear regression models containing either the first, first and second, or first, second, and third principal components, as well as the other predictors. Only the first through third principal components were assessed for inclusion in the linear regression models, because they cumulatively explained 97% of the variation in genomic variables. Genomic variables were standardized to unit variance prior to PCA to eliminate dissimilarities in the magnitude of variable values. Linear regression can include one or more predictors that can affect model accuracy. We therefore used best subset selection to evaluate a wide range of potential multiple linear regression models.

3.3.4.2 Elastic net regularization.

As an alternative to best subset selection, we considered linear regression with parameter regularization using L1 ("Lasso") and L2 ("Ridge") penalties, a technique known as the elastic net. We used the 'glmnet' package in R to create models with elastic net regularization. The alpha and lambda hyperparameters, which control the relative contribution and overall scale of the L1 and L2 penalties, respectively, were tuned using a grid search to find the optimal hyperparameters for the data set as determined by leave-one-virus-out cross-validation. Specifically, 11 different values ranging from 0 to 1 with a step of 0.1 were assessed for the hyperparameter alpha, and 100 different lambda values were evaluated for each alpha.

3.3.4.3 Random forests.

To accommodate the use of the modified inverse variance weights, the random forests model was developed in R using the 'xgboost' package with a single round of boosting, and other hyperparameters were set to match defaults from the 'randomForest' package as well as possible.[32]

3.3.4.4 Boosted trees.

Boosted trees modeling was conducted using the 'xgboost' package in R. The number of boosting rounds was selected to minimize the cross-validated error. The hyperparameters for learning rate, tree depth, and minimum terminal node weight were 0.3, 6, and 1, respectively.

3.3.5 Experimental and predicted UV_{254} inactivation of murine hepatitis virus (MHV) and bacteriophage HS2.

To consider how well the models may predict inactivation of a virus not already included in the collected data set, we determined the UV_{254} inactivation rate constant of MHV, a virus in the *Coronaviridae* family and *Betacoronavirus* genus, and of HS2, a marine bacteriophage, and compared experimental inactivation to the model's predicted inactivation. Virus propagation and enumeration details are provided in Appendix B.

3.3.5.1 UV_{254} inactivation of viruses.

All UV_{254} inactivation experiments were conducted with a custom-made collimated beam reactor containing 0.16 mW cm^{-2} lamps (model G15T8, Philips). UV_{254} irradiance was determined using chemical actinometry[33,34] and *Escherichia coli* bacteriophage MS2 (ATCC 15597-B1) was included in all experimental solutions as a biodosimeter to further confirm UV_{254} doses. Infective MS2 was assessed using the double agar overlay approach with host *Escherichia coli* (ATCC 15597).[35] For each UV_{254} exposure, 2 mL of the experimental solution was added to a 10 mL glass

beaker and continuously stirred. Sample solution depth (0.8 cm) and transmittance (~ 47% to 53% for MHV experiments, ~ 79% to 80% for HS2 experiments) were used to determine the average UV_{254} irradiance of the sample according to the Beer-Lambert law.[36] All UV_{254} inactivation experiments were conducted at room temperature (20 to 21°C). Infective viruses were assayed immediately following experiments. Dark controls were conducted with each experiment and consisted of the virus suspended in experimental solution but stored in the dark on ice for the duration of experiments. Three independent replicates were conducted for each inactivation experiment.

For MHV experiments, solutions contained MHV and MS2 diluted in 1X PBS to a final concentration of ~ 10^5 pfu/mL and ~ 10^{10} pfu/mL, respectively. Samples were exposed to UV_{254} for 0 s, 5 s, 15 s, 25 s, and 35 s, which corresponded to UV_{254} doses of approximately 0 mJ cm^{-2}, 0.62 mJ cm^{-2}, 1.2 mJ cm^{-2}, 1.9 mJ cm^{-2}, 3.1 mJ cm^{-2}, and 4.3 mJ cm^{-2}. MS2 infectivity was assayed after larger UV_{254} doses due to its slower inactivation kinetics, namely 37 mJ cm^{-2} and 74 mJ cm^{-2}. For HS2 experiments, solutions contained HS2 and MS2 diluted in 1X PBS to a final concentration of ~ 10^8 pfu/mL and ~ 10^9 pfu/mL, respectively. Samples were irradiated for 0 s, 180 s, 300 s, 480 s, 600 s, and 720 s, which resulted in UV_{254} doses of approximately 0 mJ cm^{-2}, 26 mJ cm^{-2}, 44 mJ cm^{-2}, 70 mJ cm^{-2}, 88 mJ cm^{-2}, and 105 mJ cm^{-2}.

The inactivation rate constant, k_{exp} in $cm^2\ mJ^{-1}$, for MHV, HS2, and MS2 was determined by the following equation:

$$ln\left(\frac{C}{C_0}\right) = k_{exp} \cdot D_{UV254} \quad (4)$$

where C_0 and C are infectious virus concentrations before and after UV_{254} exposure, respectively, in pfu/mL, and D_{UV254} is the average UV_{254} dose, in mJ cm^{-2}.

Experimental inactivation rate constants (i.e., k_{exp}) were determined with linear regression analyses conducted in Prism version 8.4.2 (GraphPad) to obtain experimental inactivation rate constants (i.e., k_{exp}). UV_{254} inactivation curves for some viruses exhibited tailing at high doses. In these situations, only the linear portions of the inactivation curves were included in the linear regression analyses.

3.3.5.2 MHV and HS2 inactivation rate constant prediction.

The UV_{254} inactivation rate constants of MHV and HS2 were predicted using the best-performing inactivation models for (+) ssRNA viruses and dsDNA viruses, respectively. The MHV genome sequence was provided by Dr. Leibowitz (Appendix B Text File 1), and the HS2 genome sequence is available in NCBI (accession no. KF302036).

3.3.6 Predicting UV_{254} inactivation of emerging or difficult-to-culture viruses.

The inactivation rates of several emerging and difficult-to-culture viruses, including SARS-CoV-2, were predicted using the best-performing inactivation model. Sequence data for these viruses were obtained from NCBI and all viruses with sequence information are included in Table B.1.

3.4 Results

3.4.1 Numerous UV_{254} rate constants are available, but only for a limited subset of viruses.

We conducted a systematic review to collect UV_{254} inactivation rate constants and used them for the training and validation of models developed to predict virus inactivation kinetics. Of 2,416 initial studies, 531 underwent full text review, and 103 studies were included in the final data set (Figure B.1). Only data from studies passing a set of experimental criteria were included to ensure collection of high-quality rate constants. These studies produced 224 experimental inactivation

rate constants for 59 viruses (Figure 3.1; Table B.2). Viruses of different strains and types were considered unique.

More than 350 studies from the full text review that reported conducting UV virus inactivation in aqueous suspension were not included in the final data set. Data were excluded most commonly because the article did not address UV_{254} attenuation in the experimental solution and it could not be ruled out based on details in the materials and methods. Nearly 50% of the extracted rate constants represented only five different viruses. For example, there were 62 different experimental inactivation rates for bacteriophage MS2; in contrast, several viruses, including hepatitis E virus, only had one reported inactivation rate constant, and there were many human viruses with no data that met the review criteria (e.g., influenza viruses, ebolaviruses, coronaviruses, herpesviruses). Ultimately 13, 84, 111, 4, and 12 experimental inactivation rate constants were extracted for ssDNA, dsDNA, (+) ssRNA, (-) ssRNA, and dsRNA viruses, respectively, representing 3, 26, 22, 2, and 5 unique viruses (Figure 3.1). No rate constants met the inclusion criteria for retroviral (+) ssRNA viruses, referred to as RT-ssRNA viruses. The inactivation rate constants spanned ~2.5 orders of magnitude (Figure 3.1) and ranged from 0.021 to 7.6 cm^2 mJ^{-1}. The (-) ssRNA viruses had the largest rate constants on average (k = 3.6 cm^2 mJ^{-1}), while dsRNA viruses had the lowest average rate constants (k = 0.15 cm^2 mJ^{-1}). dsDNA virus constants exhibited the widest range of rate constants, spanning from 0.021 to 5.4 cm^2 mJ^{-1} with a mean of 0.55 cm^2 mJ^{-1}. The rate constants collected were associated with the linear portion of the UV_{254} virus inactivation curve and did not incorporate regions of the curve where tailing occurred. Overall, first-order kinetics were observed up to at least 4-log_{10} virus inactivation. This suggests that our models are applicable up to approximately 4-log_{10} virus inactivation. Beyond that point,

our models could overestimate inactivation levels for viruses that exhibit tailing effects during inactivation.

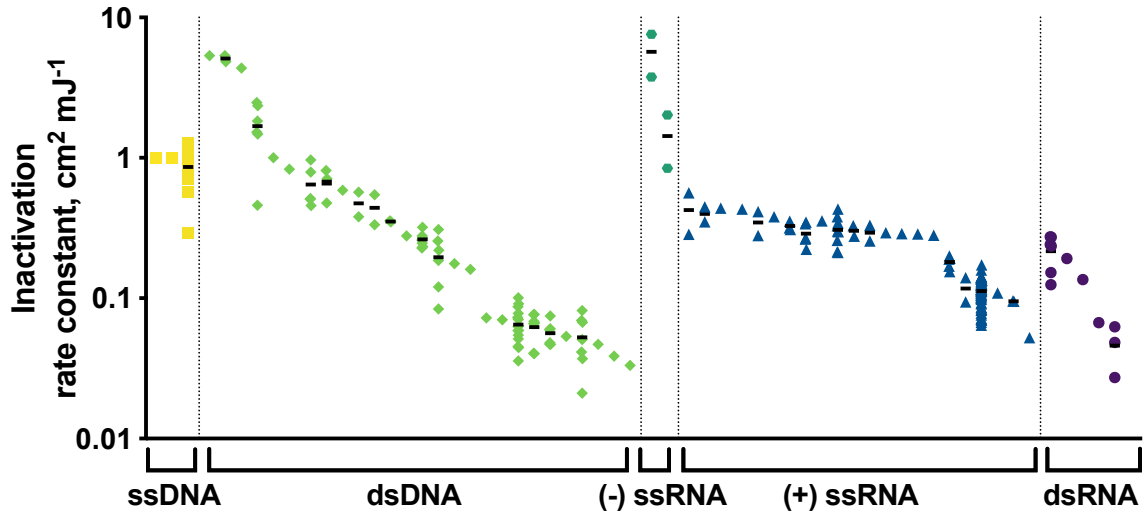

Figure 3.1 Distribution of UV_{254} inactivation rate constants collected from the systematic literature review. Black bars denote arithmetic means of inactivation rate constants for viruses with more than one experimental rate constant. Outliers are not included. ssDNA viruses: three viruses, 13 rate constants; dsDNA viruses: 26 viruses,* 84 rate constants; (-) ssRNA viruses: two viruses, four rate constants; (+) ssRNA viruses: 22 viruses, 107 rate constants (four outlier rate constants removed); dsRNA viruses: five viruses, 12 rate constants. Viruses within each Baltimore classification are ordered from highest to lowest mean rate constant from left to right. Rate constants are reported in Table B.2. *Considers two viruses (i.e., adenovirus 5 and adenovirus 41) assayed in host cells with reduced repair abilities as different from the same viruses assayed in wild-type host cells.

Individual models were developed for the (+) ssRNA and dsDNA virus classes. The limited data sets for viruses in the other Baltimore classifications made it infeasible to develop individual predictive models for the other groups. The data sets used for (+) ssRNA and dsDNA model training and validation included 19 (+) ssRNA viruses with 93 experimental inactivation rate constants and 16 dsDNA viruses with 50 inactivation rate constants, respectively (Table B.2). The model developed with all viruses from the systematic review included 43 viruses with 168 experimental inactivation rate constants.

3.4.2 Rate constants predicted using common modeling approaches.

We used the data collected in the systematic literature review to develop linear regression, elastic net regularization, random forests, and boosted trees models for predicting inactivation rate constants based on several predictors (Table B.1). These model classes were selected to cover a range of different linear and non-linear approaches that are commonly applied in the predictive modeling field.[37]

3.4.2.1 (+) ssRNA virus model.

The cross-validated root mean squared relative prediction errors (RMSrPEs) for the four optimized models varied from 0.22 to 0.95 (Figure 3.2 and Table B.3), with the top performing multiple linear regression resulting in the lowest RMSrPE out of the four optimized model classes. Various subsets of genomic variables were included in multiple linear regression development. Because these genomic variables are highly collinear, we used principal components that incorporated various genomic variable subsets as predictors in the regression models. Ultimately, the multiple linear regression model with one principal component that incorporated the numbers of cytosines (Cs), uracils (Us), uracil doublets (UUs), and uracil triplets (UUUs) resulted in the lowest RMSrPE (0.22 ± 0.23; RMSrPE ± standard error; Table B.3). Other multiple linear regressions performed similarly (Table B.4). The optimized elastic net regularization and boosted trees models resulted in slightly higher RMSrPEs than the top performing multiple linear regression model ($RMSrPE_{elastic\ net} = 0.28 \pm 0.26$, $RMSrPE_{boosted\ trees} = 0.32 \pm 0.28$; Table B.3), and the random forests model had the largest RMSrPE of the (+) ssRNA virus models ($RMSrPE_{random\ forests} = 0.95 \pm 0.48$; Table B.3). Model performance was significantly reduced in the elastic net and random forests models as compared to the multiple linear regression model (Table B.5).

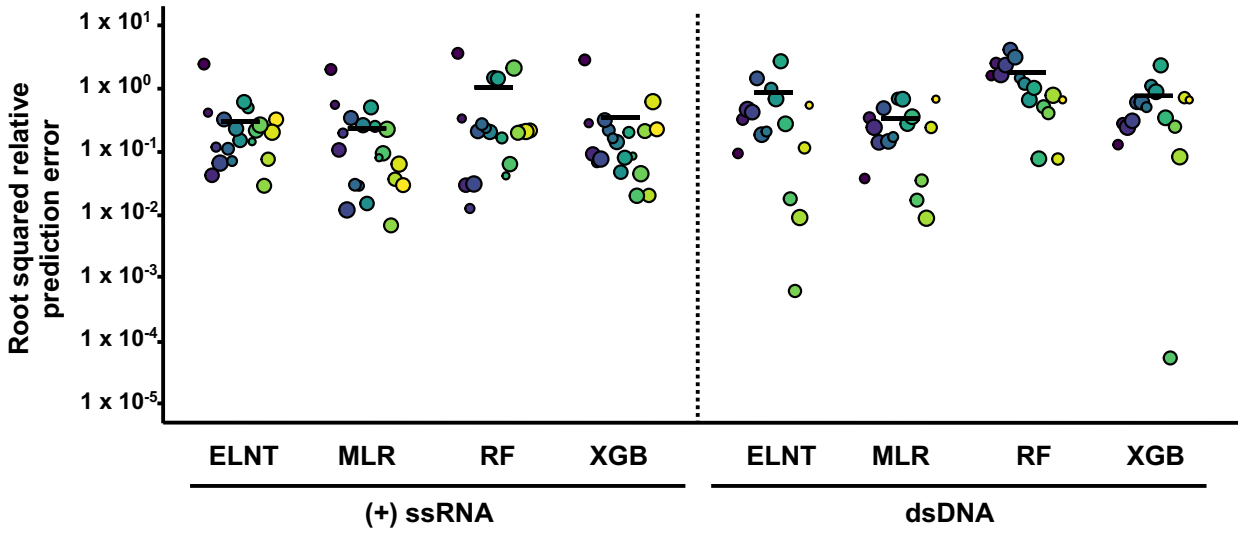

Figure 3.2 Root squared relative prediction error of virus inactivation rate constants using top performing models from each model class developed with only (+) ssRNA viruses (left) or dsDNA viruses (right) in the training and validation set. Individual symbols indicate the root squared relative prediction error of each virus, and the black bar indicates the model's root mean squared relative prediction error. Distinct colors represent different viruses, and the symbol sizes represent the weight of the experimental inactivation rate constant used for inverse variance weighting, where a larger symbol indicates a greater weight. MLR = multiple linear regression, ELNT = elastic net regularization, XGB = boosted trees, RF = random forests.

Predicted (+) ssRNA virus rate constants from the top performing model were within 51% of the mean experimental virus inactivation rate constants obtained from the systematic review, with the exception of the rate constant for Atlantic Halibut Nodavirus (percent error = 182%; Figure B.2a). The RMSrPE from the top performing linear regression model was lower than the estimated relative inter-experimental error of viruses with multiple rate constants in the literature (RMSrPE = 0.22 ± 0.23; relative inter-experimental error = 0.33; Figure 3.3a). In other words, the predicted rate constants for new (+) ssRNA viruses would be at least as accurate as the rate constants determined through experimental studies.

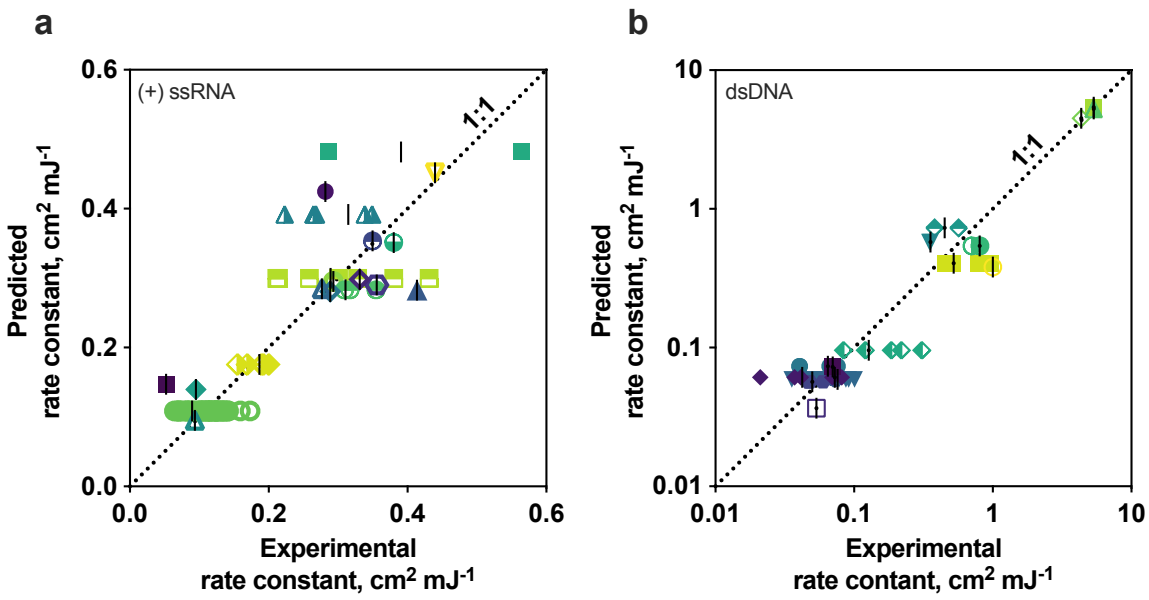

Figure 3.3 Experimental and predicted cross-validated inactivation rate constants for (+) ssRNA viruses (a) and dsDNA viruses (b) present in the training and validation set. Different colors and symbols represent different viruses. Black lines represent the estimated experimental rate constant for each virus. Data included in the models were obtained from the literature with a systematic review, and all predicted and experimental inactivation rate constants are provided in Tables B.1 and B.6.

3.4.2.2 dsDNA virus model.

The genomic variables used in dsDNA model development were equivalent to the (+) ssRNA models, with the exception that thymines (Ts) were substituted for Us (Table B.1). A major distinction of dsDNA viruses is that their genomes can undergo repair in host cells and this impacts their susceptibility to UV_{254}.[24,38–40] Genome repair can be mediated by the host cell or by viral genes,[24] and the varied efficacy of host-mediated dsDNA repair[41–44] impacts virus UV_{254} sensitivity. We included categorical predictors for genome repair mode (i.e., host cell mediated, virus-gene controlled using one repair system, or virus-gene controlled using multiple repair systems) and host cell type (i.e., prokaryotic host, eukaryotic host with wild type repair, or eukaryotic host with reduced repair) in the dsDNA virus inactivation rate constant models.

Genome repair mode and host cell type were assigned based on available information and are described in Appendix B.

The RMSrPE of the four optimized dsDNA model classes ranged from 0.31 to 1.6 (Table B.3), and the optimized multiple linear regression model outperformed the three other optimized model classes (RMSrPE = 0.31 ± 0.28; Figure 3.2 and Table B.3). The optimized elastic net and boosted trees RMSrPEs were slightly higher ($RMSrPE_{elastic\ net}$ = 0.79 ± 0.46, $RMSrPE_{boosted\ trees}$ = 0.70 ± 0.43), though the difference in model performance was not significant (Table B.5), and the random forests model performed significantly worse ($RMSrPE_{random\ forests}$ = 1.6 ± 0.66). The top linear regression model included the genome repair mode and host cell type predictors, as well as one principal component comprising the three genomic variables numbers of thymine doublets (TT), thymine quintuplets (TTTTT), and Cs. As with the top-performing (+) ssRNA model, many of the regressions tested with different genomic variable subsets had similar prediction performance, making it difficult to identify which genomic variables were critical for predicting dsDNA virus rate constants (Table B.4). A point estimate comparison of the regression coefficients for the standardized principal component (β_{PC1} = 0.46), genome repair mode ($\beta_{genome\ repair\ mode}$ = 2.7), and host cell type ($\beta_{host\ cell\ type}$ = -0.37) predictors indicates that the genome repair mode predictor is approximately 5.9 times more important than the principal component predictor ($\beta_{genome\ repair\ mode}/\beta_{PC1}$ = 2.7/0.46). Host cell type was comparable in importance to the genomic variable contribution, collectively represented by the principal component. Prediction performance dropped significantly without genome repair mode as a predictor ($RMSrPE_{opt}$ = 0.31 ± 0.28, $RMSrPE_{no\ repair}$ = 1.0 ± 0.52; Table B.5), further highlighting the importance of genome repair in UV_{254} inactivation.

The multiple linear regression model accurately predicted inactivation rate constants across the wide range of dsDNA virus susceptibilities to UV_{254} (Figure 3.3b). As with the top performing (+) ssRNA model, the predicted error for the top performing dsDNA model was lower than the estimated inter-experimental error for viruses with more than one experimental rate constant (RMSrPE = 0.31 ± 0.28; inter-experimental error of k_{virus} = 0.45). Predictions were poorest for T7M, B40-8, and lambda predicted (percent error = 62%, 63%, and 62%, respectively; Figure B.2b), which are bacteriophages with the same form of genome repair mode. The poor prediction of viruses from this group indicates that some of the rate constants in the training data for viruses with these attributes may be inaccurate, leading to worse performance for bacteriophages with host mediated repair.

3.4.2.3 All-virus model.

Larger data sets generally add predictive power to models, though the increased signal from additional data can be attenuated or negated by increased heterogeneity. We therefore compared the performance of the separate (+) ssRNA and dsDNA virus models with a model that incorporated data from all Baltimore classes. In addition to the genomic variables and repair-related predictors (i.e., genome repair mode and host cell type) included for (+) ssRNA and dsDNA viruses, a categorical predictor for nucleic acid type (i.e., double-stranded or single-stranded) was included. Boosted trees models were the top performing models using all viruses (Table B.3); these performed significantly worse than the models trained using only (+) ssRNA viruses ($RMSrPE_{(+)ssRNA}$ = 0.22 ± 0.23, $RMSrPE_{all}$ = 0.45 ± 0.33; Table B.5) or only dsDNA viruses ($RMSrPE_{dsDNA}$ = 0.31 ± 0.28 vs $RMSrPE_{all}$ = 0.45 ± 0.35; Tables B.3 and B.5). This suggests that using our modeling approach and combining viruses with diverse genome types and infection cycles into one model can negatively impact performance of virus predictions, possibly owing to insufficient data from

less studied classes. Based on these results, we used the separate (+) ssRNA and dsDNA models for subsequent analyses.

3.4.3 Predicted rate constants align with new experimental rate constants.

We applied the optimized (+) ssRNA and dsDNA models to predict the rate constants of one (+) ssRNA virus and one dsDNA virus for which experimental data were not available and then measured the rate constants experimentally. Specifically, we predicted and measured the rate constants for MHV, a (+) ssRNA mouse coronavirus, and HS2, a dsDNA marine bacteriophage. Based on its large genome size (i.e., ~ 270% longer than the largest (+) ssRNA virus genome included in the training and validation set) MHV provided an opportunity to assess the (+) ssRNA model's predictive power using a virus with attributes outside those in the training and validation set (Figure B.3). HS2 bacteriophage has similar genomic attributes to many of the other viruses in the data set (Figure B.3), and genome repair-related predictors are the same as those for most of the phages. Bacteriophage MS2 was included in each experimental solution to confirm UV_{254} doses; the measured MS2 rate constants were in line with those in the literature (0.12 to 0.14 cm^2 mJ^{-1}; Figure B.4 and Table B.2).

The predicted inactivation rate constant for MHV (k_{pred} = 2.05 ± 0.88 cm^2 mJ^{-1}; mean ± 95% margin of error) was not significantly different than the experimental rate constant (k_{exp} = 1.92 ± 0.17 cm^{-2} mJ^{-1}), with a percent error of only 7% (Figure 3.4a). The prediction accuracy the model achieved despite MHV's elevated UV_{254} sensitivity compared with other (+) ssRNA viruses in the data set highlights how linear regression approaches are capable of extrapolating predictions to values distinct from those used in training and validation. In comparison, the MHV inactivation rate constant predicted with the top performing nonlinear approach, boosted trees, was 79% different the experimental value, with a rate constant of 0.40 ± 0.25 cm^2 mJ^{-1}. The accuracy of the

MHV rate constant prediction and the relatively low RMSrPE obtained for the top performing (+) ssRNA virus model provide some confidence that the (+) ssRNA model can effectively predict UV_{254} rate constants for emerging or difficult-to-culture (+) ssRNA viruses; additional out-of-sample validation will be needed, however, to better understand how well the models generalize to new viruses.

The experimental HS2 inactivation kinetics exhibited significant tailing beyond UV_{254} fluences of 50 mJ cm^{-2}; we therefore modeled the first ~5-log_{10} of inactivation to obtain a rate constant from the first-order portion of the curve. The resulting dsDNA HS2 bacteriophage experimental rate constant of $k_{exp} = 0.28 \pm 0.08$ cm^2 mJ^{-1} was 71% lower than the predicted rate constant of $k_{pred} = 0.48 \pm 0.29$ cm^2 mJ^{-1}(Figure 3.4b). Although the error of this dsDNA estimate was larger than that of the (+) ssRNA estimate, the HS2 predicted and experimental constants are not significantly different. This result, in combination with the cross-validation results, suggest that the dsDNA model can effectively predict if a dsDNA virus is particularly resistant to UV_{254} treatment.

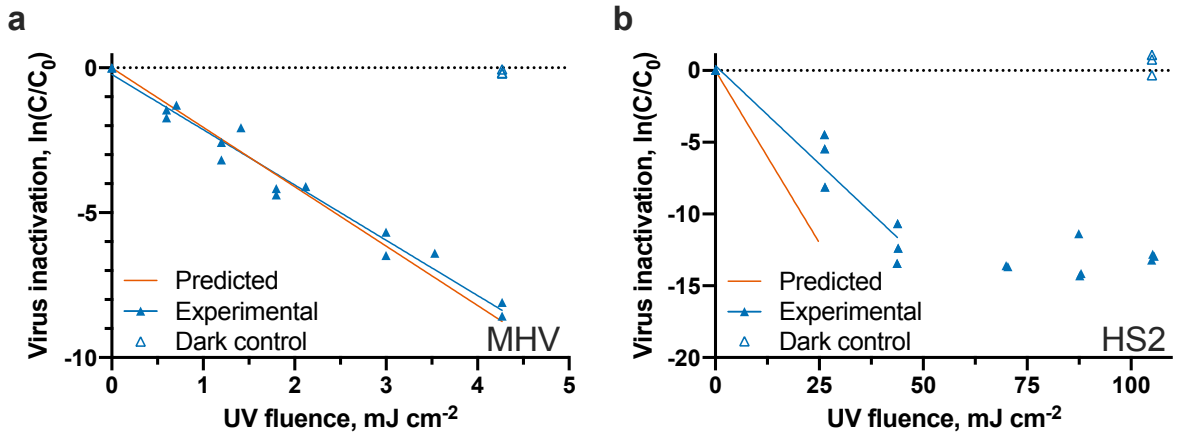

Figure 3.4 Experimental and predicted UV_{254} inactivation of MHV A59 (a) and HS2 bacteriophage (b). All independent replicates (N = 3) from experiments are shown as individual points. The experimental HS2 inactivation rate constant was determined using the first two UV_{254} fluences due to significant tailing beyond UV_{254} fluences of 50 mJ cm^{-2}.

3.4.4 Predictive models estimate inactivation of several emerging and difficult-to-culture viruses.

Our systematic review identified a number of important human viruses that lack published high quality UV_{254} inactivation rate constants in the literature. We therefore applied the (+) ssRNA and dsDNA predictive models to estimate the inactivation rates constants for several viruses, including human norovirus, dengue virus, SARS-CoV-2, and several herpesviruses (Table 3.1). These predictions resulted in a range of inactivation rate constants, from 0.28 for human norovirus to 3.0 $cm^2\ mJ^{-1}$ for human cytomegalovirus. Although these virus rate constants have not been validated with experiments, the performance of our models gives us confidence that the predicted values are good estimates of the actual inactivation rate constants.

Table 3.1 Predicted UV_{254} inactivation rate constants for several viruses without high-quality experimental inactivation rate constants.

Virus	NCBI accession number	Predicted inactivation rate constant, k ($cm^2\ mJ^{-1}$)[a]
(+) ssRNA viruses		
SARS-CoV-1	NC_004718	1.9 ± 0.82
SARS-CoV-2	MN908947	2.0 ± 0.86
Middle eastern respiratory syndrome coronavirus (MERS-CoV)	JX869059	2.1 ± 0.91
Dengue virus	NC_001477	0.38 ± 0.16
Zika virus	NC_035889	0.39 ± 0.17
Human rhinovirus (B14)	K02121	0.34 ± 0.15
Human norovirus (GII.4 Sydney)	JX459908	0.28 ± 0.12
dsDNA viruses		
Herpes simplex virus 1 (strain 17)	NC_001806	1.8 ± 1.1

Epstein-Barr virus	NC_007605	1.9 ± 1.2
Human cytomegalovirus	NC_006273	3.0 ± 1.8
Variola virus (major)	L22579	2.5 ± 1.5

[a]Error shown represents the 95% margin of error of predicted rate constant, as determined by the model's 95% margin of error, estimated as 1.96 times the standard error, where standard error = RMSrPE x virus rate constant.

3.5 Discussion

Through evaluation of a large set of models from four distinct model classes developed with the best currently available data, we identified effective models for predicting UV_{254} inactivation rate constants of (+) ssRNA and dsDNA viruses using simple virus attributes as model predictors. UV_{254} primarily targets viral nucleic acid during irradiation. Pyrimidine bases are more photoreactive than purines,[45] and pyrimidine dimers, in particular, cause a large portion of the UV-induced damage to DNA.[45–51] Limited research centered on ssRNA photolysis suggests pyrimidine hydrates are the primary lesions inducing UV damage.[52] Photochemical damage to nucleic acids can stall or inhibit enzymes required for productive viral infection of host cells.[53–55] Based on this *a priori* knowledge, we included several combinations of pyrimidine bases as predictors in our (+) ssRNA and dsDNA models, namely the numbers of U, UU, UUU, UUUU, UUUUU, C, UC, and CU in (+) ssRNA models and the numbers of T, TT, TTT, TTTT, TTTTT, C, TC, and CT in dsDNA models.

Ultimately, the top performing (+) ssRNA virus model employed one principal component incorporating multiple genomic variables (i.e., numbers of C, U, UU, and UUU), and the top performing dsDNA virus model employed repair mode, host cell type, and one principal component representing three genomic variables (i.e., numbers of C, TT, TTTTT). The relative importance of variables in our top performing predictive models may provide insight into the

mechanisms driving UV_{254} inactivation of viruses. Among the (+) ssRNA models, many of the multiple linear regression models that included distinct subsets of genomic variables performed similarly. This is likely because these genomic variables are so highly correlated that different variable combinations resulted in a similar set of principal components as predictors in modeling, ultimately yielding similar performance among different models. Separating the effects of individual genomic variables was therefore difficult in the (+) ssRNA model. Although the top performing model incorporated multiple genomic variables, several linear regression models using as few as one genomic variable as a predictor resulted in similar model performance. This finding demonstrates that simple aspects of the (+) ssRNA genome provide all the necessary information to accurately predict rate constants for this class of viruses. In the dsDNA model, performance was significantly improved when genome repair predictors were included in addition to principal components incorporating genomic variables. The importance of genome repair was expected. For example, the two dsDNA bacteriophages T2 and T4 have similar genome sizes and composition (Figure B.3b and Table B.1) but dissimilar UV_{254} inactivation rate constants (5.1 cm^{-2} mJ^{-1} for T2 and 1.7 cm^{-2} mJ^{-1} for T4; Table B.2). T4 phage's UV_{254} resistance is due to an additional virus-controlled repair gene in the T4 genome not present in the T2 genome.[56,57] Interestingly, the relative contribution of genomic variables in the dsDNA model was significantly less than the genome repair predictors, which suggests that genome repair is a more important factor in dsDNA UV_{254} inactivation than genomic variables.

Including genome repair as a model predictor presented some limitations. First, the mode and extent of genome repair is not known for many viruses and has not been well-studied across virus families. A single predictor encompassing the contribution of genome repair was therefore not possible. We instead applied multiple categorical predictors. With this approach, only viruses that

shared a particular genome repair mode or host cell type with at least one other virus in the dsDNA data set could be used in cross-validation. Ultimately, the data set used for dsDNA model development and validation lacked numerous forms of dsDNA viruses with distinct repair modes and host cell types, resulting in uncertainty in model performance for certain dsDNA viruses not represented in the training and validation set. To improve future dsDNA virus models, it is critical to have a better understanding of genome repair mechanisms and how they affect UV_{254} inactivation.

Our top performing UV_{254} virus prediction models provide improvements over earlier prediction approaches.[28,29] On average, the (+) ssRNA and dsDNA virus models predicted rate constants to within ~0.2x and ~0.3x of experimental constants, respectively. A previous approach using genome length to determine genome size-normalized sensitivity values for a number of virus families expected uncertainties in predicted values of ~2x.[28] A more recent approach developed predictive models for ssRNA and dsDNA UV_{254} inactivation using genome dimer formation potential, a value that incorporated pyrimidine doublets, genome length, and purines with adjacent pyrimidine doublets.[29] Their reported error as a coefficient of determination (i.e., R^2) was 0.67 for ssRNA viruses compared to 0.74 (adjusted R^2) for our model, and an R^2 value of 0.62 for dsDNA viruses compared to 0.99 (adjusted R^2) for our model. Several factors can be attributed to the improved performance of our models, including extensive curation of data based on quality and the incorporation of genome repair into dsDNA modeling.

In light of the coronavirus disease 2019 (COVID-19) pandemic and the need for effective decontamination strategies, our predictive models provided an opportunity to predict rate constants for a critical group of viruses with very little published inactivation data. Limited data on UV_{254} inactivation for coronaviruses in aqueous suspension are available and the published information

did not pass the inclusion criteria of our systematic review.[10,58–60] This paucity of information on the susceptibility of coronaviruses to UV_{254} is of critical importance for developing effective decontamination strategies. Our predicted rate constants for SARS-CoV-1, SARS-CoV-2, and MERS, and our measured rate constant for the mouse coronavirus MHV, suggest that coronaviruses are much more susceptible to UV_{254} inactivation than other (+) ssRNA viruses. A recent estimate of SARS-CoV-2 UV_{254} susceptibility using the previously developed Lytle and Sagripanti approach[28] is ~ 1.7x greater than our estimate indicates.[61] Discrepancies in new experimental coronavirus data still persist, likely stemming from a lack of checks on UV_{254} attenuation of suspensions.

More robust models are possible with larger data sets that consist of more diverse viruses. Unfortunately, a large portion of UV_{254} inactivation data found during the systematic review did not pass our inclusion criteria. The most common reason for excluding data from our systematic review was a failure to report solution UV_{254} attenuation. An earlier study of SARS-CoV-1 inactivation by UV_{254},[60] for example, did not account for UV_{254} attenuation in the experimental DMEM suspension. The reported inactivation rate constant of 0.003 cm^2 mJ^{-1} was nearly three orders of magnitude lower than our predicted rate constant for SARS-CoV-1 and our measured value for MHV, likely in part due to solution attenuation. We estimate that their rate constant would be closer to 0.35 cm^2 mJ^{-1} after accounting for solution attenuation. This value more closely aligns with our coronavirus values. Similarly, several studies reported UV_{254} inactivation of viruses in blood products without describing how attenuation was considered in their reported doses.[10,62–64] Although these doses are likely representative for these fluids, they cannot be extrapolated to other matrices. More stringent reporting of UV_{254} experimental conditions,[65] including matrix solution transmission at 254 nm, will facilitate future modeling efforts. Our

models predict UV_{254} inactivation rate constants for solutions with 100% transmittance (e.g., purified virus in buffer solution). These rate constants can be adjusted to predict virus inactivation in a solution with significant attenuation using the Beer-Lambert law, which takes into account sample absorbance.[36]

The developed models allow us to predict the effectiveness of current UV_{254} treatment strategies on viral pathogens that are difficult or impossible to culture. For example, human norovirus, which causes gastrointestinal disease, is a major target of UV_{254} disinfection processes in water treatment and food processing. Our (+) ssRNA virus model predicts an inactivation rate constant of 0.28 cm^2 mJ^{-1} for human norovirus GII.4, which is similar to our recently reported rate constant of k = 0.27 cm^2 mJ^{-1} for human norovirus GII.4 Sydney using RT-qPCR data coupled with a full-genome extrapolation approach.[66] This finding indicates that current water treatment guidelines for adequate UV_{254} virus inactivation, which are defined to treat adenovirus 41,[67] are more than sufficient to inactivate human norovirus to acceptable levels. In fact, none of the viruses for which we predicted rate constants had UV_{254} resistance greater than viruses in the *Adenoviridae* family.

The limited and unbalanced data set that we obtained from the systematic review and used in modeling efforts created challenges in our modeling work. Of primary concern, we could not take a commonly used approach to evaluating models, in which a portion of data is held back during model development to assess performance. Holding back the typical 10 – 20% of data would correspond to holding back only two to four viruses from the (+) ssRNA or dsDNA classes for testing. This could result in high variance estimates of prediction performance that would also be highly dependent on the viruses withheld during training. We consequently used leave-one-virus-out cross-validation to more efficiently estimate prediction performance on out of sample data. Another limitation of our models is that they were developed and validated for only (+) ssRNA

and dsDNA viruses. Although many human viruses are in these two classes, many emerging and noteworthy human viruses belong to other classes. In particular, the (-) ssRNA virus class includes several important human pathogens, such as lassa virus, nipah virus, influenza virus, and ebolavirus. Since only two (-) ssRNA viruses were included in our data set, we were unable to assess whether inactivation rate constants for viruses in this group could be accurately predicted with our (+) ssRNA model. More high quality UV_{254} experimental inactivation data for a broader set of viruses would facilitate the holdout approach for validating models and the development of models for other virus Baltimore classification groups.

Additional experimental data could also support an expanded set of predictors beyond the primary genome structure and genome repair parameters included here. Virus attributes, like the secondary structure of single-stranded nucleic acids[22] or nucleic acid interactions with viral proteins,[68] may play a role in virus inactivation by UV_{254}. These structural virus characteristics are not as readily available as genome sequence information and were therefore not considered in the present study. Future research could incorporate these attributes as additional model parameters when more data become available. Another focus of future work could be the expansion of these models to predict the tailing of virus inactivation that is often observed during UV_{254} treatment. Our models focus on the first order portion of the UV_{254} inactivation curve; by understanding the mechanisms that underlie tailing kinetics and including the appropriate predictors, this model could be updated to predict both the first order and tailing regions of the UV_{254} virus inactivation curve.

This research demonstrates the value of predictive models for estimating virus fate in various settings. Using readily available viral genome data, we developed models to predict UV_{254} inactivation of (+) ssRNA and dsDNA viruses. The benefits of predictive models are underlined by the ongoing COVID-19 pandemic: access to the biosafety level 3 laboratories required to work

with SARS-CoV-2 has been limited and, as a result, few experimental inactivation studies have been performed. Our approach can rapidly determine virus susceptibility to UV_{254} using available genomes, but without relying on culture systems that are often unavailable or difficult to access. Other potential applications of our models including identifying outlier UV_{254} data that are published and predicting potential worst-case scenarios for viruses and their susceptibility to UV_{254}. Ultimately, we expect that this predictive modeling approach can be applied to estimate inactivation of microorganisms with other disinfectants and in different settings, such as on surfaces or in air.

3.6 References

(1) Flint, S. J.; Racaniello, V. R.; Rall, G.; Skalka, A. M.; Enquist, L. W. Foundations. In *Principles of Virology, Volume 1: Molecular Biology*; ASM Press: Washington, D.C., 2015; pp 2–23.

(2) Hirneisen, K. A.; Black, E. P.; Cascarino, J. L.; Fino, V. R.; Hoover, D. G.; Kniel, K. E. Viral Inactivation in Foods: A Review of Traditional and Novel Food-Processing Technologies. *Compr. Rev. Food Sci. Food Saf.* **2010**, *9* (1), 3–20. https://doi.org/10.1111/j.1541-4337.2009.00092.x.

(3) Rutala, W. A.; Weber, D. J.; Healthcare Infection Control Practices Adviosry Committee. *Guideline for Disinfection and Sterilization in Healthcare Facilities*; 2008.

(4) Adhikari, A.; Clark, S. Disinfection of Microbial Aerosols. In *Modeling the Transmission and Prevention of Infectious Disease*; Hurst, C. J., Ed.; Springer International Publishing: Cham, 2017; pp 55–71. https://doi.org/10.1007/978-3-319-60616-3_3.

(5) Benjamin, M. M.; Lawler, D. F. *Water Quality Engineering*; Wiley: Hoboken, N.J, 2013.

(6) Metcalf; Eddy; Tchobanoglous, G.; Stensel, H. D.; Tsuchihashi, R.; Burton, F. L.; Abu-Orf, M.; Bowden, G.; Pfrang, W. *Wastewater Engineering : Treatment and Resource Recovery*, 5th ed.; McGraw-Hill Education: New York, 2014.

(7) Gunter-Ward, D. M.; Patras, A.; S. Bhullar, M.; Kilonzo-Nthenge, A.; Pokharel, B.; Sasges, M. Efficacy of Ultraviolet (UV-C) Light in Reducing Foodborne Pathogens and Model Viruses in Skim Milk. *J. Food Process. Preserv.* **2018**, *42* (2), e13485. https://doi.org/10.1111/jfpp.13485.

(8) Pavia, M.; Simpser, E.; Becker, M.; Mainquist, W. K.; Velez, K. A. The Effect of Ultraviolet-C Technology on Viral Infection Incidence in a Pediatric Long-Term Care Facility. *Am. J. Infect. Control* **2018**, *46* (6), 720–722. https://doi.org/https://doi.org/10.1016/j.ajic.2018.01.014.

(9) Ward, D. M.; Patras, A.; Kilonzo-Nthenge, A.; Yannam, S. K.; Pan, C.; Xiao, H.; Sasges, M. UV-C Treatment on the Safety of Skim Milk: Effect on Microbial Inactivation and Cytotoxicity Evaluation. *J. Food Process Eng.* **2019**, *42* (4), e12944. https://doi.org/10.1111/jfpe.12944.

(10) Eickmann, M.; Gravemann, U.; Handke, W.; Tolksdorf, F.; Reichenberg, S.; Müller, T. H.; Seltsam, A. Inactivation of Ebola Virus and Middle East Respiratory Syndrome Coronavirus in Platelet Concentrates and Plasma by Ultraviolet C Light and Methylene Blue plus Visible Light, Respectively. *Transfusion* **2018**, *58* (9), 2202–2207. https://doi.org/10.1111/trf.14652.

(11) Hijnen, W. A. M.; Beerendonk, E. F.; Medema, G. J. Inactivation Credit of UV Radiation for Viruses, Bacteria and Protozoan (Oo)Cysts in Water: A Review. *Water Res.* **2006**, *40* (1), 3–22. https://doi.org/https://doi.org/10.1016/j.watres.2005.10.030.

(12) Shimizu, A.; Shimizu, N.; Tanaka, A.; Jinno-Oue, A.; Roy, B. B.; Shinagawa, M.; Ishikawa, O.; Hoshino, H. Human T-Cell Leukaemia Virus Type I Is Highly Sensitive to UV-C Light. *J. Gen. Virol.* **2004**, *85* (8), 2397–2406.

(13) Jacangelo, J. G.; Loughran, P.; Petrik, B.; Simpson, D.; McIlroy, C. Removal of Enteric Viruses and Selected Microbial Indicators by UV Irradiation of Secondary Effluent. *Water Sci. Technol.* **2003**, *47* (9), 193–198. https://doi.org/10.2166/wst.2003.0522.

(14) Linden, K. G.; Thurston, J.; Schaefer, R.; Malley, J. P. Enhanced UV Inactivation of Adenoviruses under Polychromatic UV Lamps. *Appl. Environ. Microbiol.* **2007**, *73* (23), 7571 LP – 7574. https://doi.org/10.1128/AEM.01587-07.

(15) Guo, H.; Chu, X.; Hu, J. Effect of Host Cells on Low- and Medium-Pressure UV Inactivation of Adenoviruses. *Appl. Environ. Microbiol.* **2010**, *76* (21), 7068 LP – 7075. https://doi.org/10.1128/AEM.00185-10.

(16) Thurston-Enriquez, J. A.; Haas, C. N.; Jacangelo, J.; Riley, K.; Gerba, C. P. Inactivation of Feline Calicivirus and Adenovirus Type 40 by UV Radiation. *Appl. Environ. Microbiol.* **2003**, *69* (1), 577–582.

(17) Meng, Q. S.; Gerba, C. P. Comparative Inactivation of Enteric Adenoviruses, Poliovirus and Coliphages by Ultraviolet Irradiation. *Water Res.* **1996**, *30* (11), 2665–2668. https://doi.org/https://doi.org/10.1016/S0043-1354(96)00179-0.

(18) Malley, J.; Linden, K.; Mofidi, A.; Bolton, J.; Crozes, G.; Cushing, B.; Mackey, E.; Laine, J. M.; Janex, M.-L. *Inactivation of Pathogens with Innovative UV Technologies*; American Water Works Association Research Foundation, 2004; Vol. 1.

(19) Luria, S. E.; Dulbecco, R. Genetic Recombinations Leading to Production of Active Bacteriophage from Ultraviolet Inactivated Bacteriophage Particles. *Genetics* **1949**, *34* (2), 93–125.

(20) Qiao, Z.; Ye, Y.; Chang, P. H.; Thirunarayanan, D.; Wigginton, K. R. Nucleic Acid Photolysis by UV254 and the Impact of Virus Encapsidation. *Environ. Sci. Technol.* **2018**. https://doi.org/10.1021/acs.est.8b02308.

(21) Smith, K. C.; Hanawalt, P. C. Photochemistry of the Nucleic Acids. In *Molecular Photobiology: Inactivation and Recovery*; Horecker, B., Kaplan, N. O., Marmur, J., Eds.; Academic Press, 1969; pp 57–84. https://doi.org/https://doi.org/10.1016/B978-1-4831-9742-5.50009-2.

(22) Pearson, M.; Johns, H. E. Suppression of Hydrate and Dimer Formation in Ultraviolet-Irradiated Poly (A + U) Relative to Poly U. *J. Mol. Biol.* **1966**, *20* (2), 215–229. https://doi.org/https://doi.org/10.1016/0022-2836(66)90061-1.

(23) Henderson, E. E.; Tudor, G.; Yang, J.-Y. Inactivation of the Human Immunodeficiency Virus Type 1 (HIV-1) by Ultraviolet and X Irradiation. *Radiat. Res.* **1992**, *131* (2), 169–176. https://doi.org/10.2307/3578438.

(24) Harm, W. *Biological Effects of Ultraviolet Radiation*; IUPAB biophysics series. 1; Cambridge University Press: Cambridge, Eng. ; New York :, 1980.

(25) Harm, W. Gene-Controlled Reactivation of Ultraviolet-Inactivated Bacteriophage. *J. Cell. Comp. Physiol.* **1961**, *58* (S1), 69–77. https://doi.org/10.1002/jcp.1030580408.

(26) Day III, R. S. Cellular Reactivation of Ultraviolet-Irradiated Human Adenovirus 2 in Normal and Xeroderma Pigmentosum Fibroblasts. *Photochem. Photobiol.* **1974**, *19* (1), 9–13. https://doi.org/10.1111/j.1751-1097.1974.tb06467.x.

(27) Baltimore, D. Expression of Animal Virus Genomes. *Bacteriol. Rev.* **1971**, *35* (3), 235–241.

(28) Lytle, C. D.; Sagripanti, J.-L. Predicted Inactivation of Viruses of Relevance to Biodefense by Solar Radiation. *J. Virol.* **2005**, *79* (22), 14244–14252. https://doi.org/10.1128/JVI.79.22.14244-14252.2005.

(29) Kowalski, W. J.; Bahnfleth, W. P.; Hernandez, M. T. A Genomic Model for Predicting the Ultraviolet Susceptibility of Viruses. *IUVA News* **2009**, *11* (2), 15–28.

(30) Moher, D.; Liberati, A.; Tetzlaff, J.; Altman, D. G.; Group, T. P. Preferred Reporting Items for Systematic Reviews and Meta-Analyses: The PRISMA Statement. *PLOS Med.* **2009**, *6* (7), e1000097.

(31) R Core Team. R: A Language and Environment for Statistical Computing. Vienna, Austria 2020.

(32) xgboost developers. Random Forests in XGBoost https://xgboost.readthedocs.io/en/latest/tutorials/rf.html.

(33) Rahn, R. O.; Bolton, J.; Stefan, M. I. The Lodide/Lodate Actinometer in UV Disinfection: Determination of the Fluence Rate Distribution in UV Reactors. *Photochem. Photobiol.* **2006**, *82* (2), 611–615. https://doi.org/10.1562/2005-06-10-RN-570.

(34) Rahn, R. O. Potassium Iodide as a Chemical Actinometer for 254 Nm Radiation: Use of Lodate as an Electron Scavenger. *Photochem. Photobiol.* **1997**, *66* (4), 450–455. https://doi.org/10.1111/j.1751-1097.1997.tb03172.x.

(35) United States Environmental Protection Agency. *Method 1601: Male-Specific (F+) and Somatic Coliphage in Water by Two-Step Enrichment Procedure*; Washington, D.C., 2001.

(36) Morowitz, H. J. Absorption Effects in Volume Irradiation of Microorganisms. *Science (80-.).* **1950**, *111* (2879), 229–230.

(37) Kuhn, M.; Johnson, K. Applied Predictive Modeling. Springer New York: New York 2013. https://doi.org/10.1007/978-1-4614-6849-3.

(38) Harm, W. On the Relationship between Host-Cell Reactivation and UV-Reactivation in UV-Inactivated Phages. *Z. Vererbungsl.* **1963**, *94* (1), 67–79. https://doi.org/10.1007/BF00895157.

(39) Rupert, C. S.; Harm, W. Reactivation After Photobiological Damage. In *Advances in Radiation Biology*; AUGENSTEIN, L. G., MASON, R., ZELLE, M. A. X. B. T.-A. in R. B., Eds.; Elsevier, 1966; Vol. 2, pp 1–81. https://doi.org/https://doi.org/10.1016/B978-1-4832-3121-1.50006-2.

(40) Day, R. S. Studies on Repair of Adenovirus 2 by Human Fibroblasts Using Normal, Xeroderma Pigmentosum, and Xeroderma Pigmentosum Heterozygous Strains. *Cancer Res.* **1974**, *34* (8), 1965 LP – 1970.

(41) Rainbow, A. J. Defective Repair of UV-Damaged DNA in Human Tumor and SV40-Transformed Human Cells but Not in Adenovirus-Transformed Human Cells. *Carcinogenesis* **1989**, *10* (6), 1073–1077. https://doi.org/10.1093/carcin/10.6.1073.

(42) MacRae, S. L.; Croken, M. M.; Calder, R. B.; Aliper, A.; Milholland, B.; White, R. R.; Zhavoronkov, A.; Gladyshev, V. N.; Seluanov, A.; Gorbunova, V.; Zhang, Z. D.; Vijg, J. DNA Repair in Species with Extreme Lifespan Differences. *Aging (Albany. NY).* **2015**, *7* (12), 1171–1184. https://doi.org/10.18632/aging.100866.

(43) Henderson, E. E. Host Cell Reactivation of Epstein-Barr Virus in Normal and Repairdefective Leukocytes. *Cancer Res.* **1978**, *38* (10), 3256 LP – 3263.

(44) Lytle, C. D.; Aaronson, S. A.; Harvey, E. Host-Cell Reactivation in Mammalian Cells. *Int. J. Radiat. Biol. Relat. Stud. Physics, Chem. Med.* **1972**, *22* (2), 159–165. https://doi.org/10.1080/rab.22.2.159.165.

(45) Smith, K. C. Physical and Chemical Changes Induced in Nucleic Acids by Ultraviolet Light. *Radiat. Res. Suppl.* **1966**, *6*, 54–79. https://doi.org/10.2307/3583551.

(46) Schreier, W. J.; Schrader, T. E.; Koller, F. O.; Gilch, P.; Crespo-Hernández, C. E.; Swaminathan, V. N.; Carell, T.; Zinth, W.; Kohler, B. Thymine Dimerization in DNA Is an Ultrafast Photoreaction. *Science (80-.).* **2007**, *315* (5812), 625 LP – 629. https://doi.org/10.1126/science.1135428.

(47) Meistrich, M. L. Contribution of Thymine Dimers to the Ultraviolet Light Inactivation of Mutants of Bacteriophage T4. *J. Mol. Biol.* **1972**, *66* (1), 97–106. https://doi.org/https://doi.org/10.1016/S0022-2836(72)80008-1.

(48) Law, Y. K.; Forties, R. A.; Liu, X.; Poirier, M. G.; Kohler, B. Sequence-Dependent Thymine Dimer Formation and Photoreversal Rates in Double-Stranded DNA. *Photochem. Photobiol. Sci.* **2013**, *12* (8), 1431–1439. https://doi.org/10.1039/C3PP50078K.

(49) Becker, M. M.; Wang, Z. Origin of Ultraviolet Damage in DNA. *J. Mol. Biol.* **1989**, *210* (3), 429–438. https://doi.org/https://doi.org/10.1016/0022-2836(89)90120-4.

(50) Kundu, L. M.; Linne, U.; Marahiel, M.; Carell, T. RNA Is More UV Resistant than DNA: The Formation of UV-Induced DNA Lesions Is Strongly Sequence and Conformation Dependent. *Chem. – A Eur. J.* **2004**, *10* (22), 5697–5705. https://doi.org/10.1002/chem.200305731.

(51) Setlow, R. B.; Carrier, W. L. The Disappearance of Thymine Dimers from DNA: An Error-Correcting Mechanism. *Proc. Natl. Acad. Sci. U. S. A.* **1964**, *51* (2), 226–231. https://doi.org/10.1073/pnas.51.2.226.

(52) Small, G. D.; Tao, M.; Gordon, M. P. Pyrimidine Hydrates and Dimers in Ultraviolet-Irradiated Tobacco Mosaic Virus Ribonucleic Acid. *J. Mol. Biol.* **1968**, *38* (1), 75–87. https://doi.org/https://doi.org/10.1016/0022-2836(68)90129-0.

(53) Sinha, R. P.; Häder, D.-P. UV-Induced DNA Damage and Repair: A Review. *Photochem. Photobiol. Sci.* **2002**, *1* (4), 225–236. https://doi.org/10.1039/B201230H.

(54) Eglin, R. P.; Gugerli, P.; Wildy, P. Ultraviolet Irradiation of Herpes Simplex Virus (Type 1): Delayed Transcription and Comparative Sensitivities of Virus Functions. *J. Gen. Virol.* **1980**, *49* (1), 23–31. https://doi.org/https://doi.org/10.1099/0022-1317-49-1-23.

(55) Yuan, F.; Zhang, Y.; Rajpal, D. K.; Wu, X.; Guo, D.; Wang, M.; Taylor, J.-S.; Wang, Z. Specificity of DNA Lesion Bypass by the Yeast DNA Polymerase η. *J. Biol. Chem.* **2000**, *275* (11), 8233–8239.

(56) Streisinger, G. The Genetic Control of Ultraviolet Sensitivity Levels in Bacteriophages T2 and T4. *Virology* **1956**, *2* (1), 1–12. https://doi.org/https://doi.org/10.1016/0042-6822(56)90072-1.

(57) Harm, W. Mutants of Phage T4 with Increased Sensitivity to Ultraviolet. *Virology* **1963**, *19* (1), 66–71. https://doi.org/https://doi.org/10.1016/0042-6822(63)90025-4.

(58) Pratelli, A. Canine Coronavirus Inactivation with Physical and Chemical Agents. *Vet. J.* **2008**, *177* (1), 71–79. https://doi.org/https://doi.org/10.1016/j.tvjl.2007.03.019.

(59) Darnell, M. E. R.; Taylor, D. R. Evaluation of Inactivation Methods for Severe Acute Respiratory Syndrome Coronavirus in Noncellular Blood Products. *Transfusion* **2006**, *46* (10), 1770–1777. https://doi.org/10.1111/j.1537-2995.2006.00976.x.

(60) Darnell, M. E. R.; Subbarao, K.; Feinstone, S. M.; Taylor, D. R. Inactivation of the Coronavirus That Induces Severe Acute Respiratory Syndrome, SARS-CoV. *J. Virol. Methods* **2004**, *121* (1), 85–91. https://doi.org/https://doi.org/10.1016/j.jviromet.2004.06.006.

(61) Sagripanti, J.-L.; Lytle, C. D. Estimated Inactivation of Coronaviruses by Solar Radiation With Special Reference to COVID-19. *Photochem. Photobiol.* **2020**, *96* (4), 731–737. https://doi.org/10.1111/php.13293.

(62) Faddy, H. M.; Fryk, J. J.; Prow, N. A.; Watterson, D.; Young, P. R.; Hall, R. A.; Tolksdorf, F.; Sumian, C.; Gravemann, U.; Seltsam, A.; Marks, D. C. Inactivation of Dengue, Chikungunya, and Ross River Viruses in Platelet Concentrates after Treatment with Ultraviolet C Light. *Transfusion* **2016**, *56* (6pt2), 1548–1555. https://doi.org/10.1111/trf.13519.

(63) Blázquez, E.; Rodríguez, C.; Ródenas, J.; Navarro, N.; Riquelme, C.; Rosell, R.; Campbell, J.; Crenshaw, J.; Segalés, J.; Pujols, J.; Polo, J. Evaluation of the Effectiveness of the SurePure Turbulator Ultraviolet-C Irradiation Equipment on Inactivation of Different Enveloped and Non-Enveloped Viruses Inoculated in Commercially Collected Liquid Animal Plasma. *PLoS One* **2019**, *14* (2). https://doi.org/http://dx.doi.org/10.1371/journal.pone.0212332.

(64) Mohr, H.; Steil, L.; Gravemann, U.; Thiele, T.; Hammer, E.; Greinacher, A.; Mueller, T. H.; Voelker, U. A Novel Approach to Pathogen Reduction in Platelet Concentrates Using Short-Wave Ultraviolet Light. *Transfusion* **2009**, *49* (12), 2612–2624. https://doi.org/10.1111/j.1537-2995.2009.02334.x.

(65) Bolton, J. R.; Linden, K. G. Standardization of Methods for Fluence (UV Dose) Determination in Bench-Scale UV Experiments. *J. Environ. Eng.* **2003**, *129* (3), 209–215. https://doi.org/10.1061/(ASCE)0733-9372(2003)129:3(209).

(66) Rockey, N.; Young, S.; Kohn, T.; Pecson, B.; Wobus, C. E.; Raskin, L.; Wigginton, K. R. UV Disinfection of Human Norovirus: Evaluating Infectivity Using a Genome-Wide PCR-Based Approach. *Environ. Sci. Technol.* **2020**, *54* (5), 2851–2858. https://doi.org/10.1021/acs.est.9b05747.

(67) U.S. Environmental Protection Agency. *National Primary Drinking Water Regulations: The Long Term 2 Enhanced Surface Water Treatment Rule. EPA-HQ-*; 2006.

(68) Wigginton, K. R.; Menin, L.; Sigstam, T.; Gannon, G.; Cascella, M.; Hamidane, H. Ben; Tsybin, Y. O.; Waridel, P.; Kohn, T. UV Radiation Induces Genome-Mediated, Site-Specific Cleavage in Viral Proteins. *ChemBioChem* **2012**, *13* (6), 837–845. https://doi.org/10.1002/cbic.201100601.

Chapter 4

Quantification of Infectious Human Norovirus Levels Through UV_{254} Disinfection Using a Novel Enteroid Culture System

Nicole C. Rockey,[1] Tamar Kohn,[2] Brian Pecson,[3] Lutgarde Raskin,[1] Christiane E. Wobus,[4] Krista R. Wigginton*,[1]

[1]Department of Civil & Environmental Engineering, University of Michigan, Ann Arbor, MI
[2]Laboratory of Environmental Chemistry, School of Architecture, Civil & Environmental Engineering (ENAC), École Polytechnique Fédérale de Lausanne, Lausanne, Switzerland
[3]Trussell Technologies, Inc., Oakland, CA
[4]Department of Microbiology & Immunology, University of Michigan, Ann Arbor, MI

4.1 Abstract

Human norovirus is a leading cause of enteric disease worldwide, yet the lack of a readily available cell culture system has severely limited our understanding of norovirus fate in the environment and through inactivating treatments. Here, we developed an approach to quantify infectious human norovirus levels using a novel human intestinal enteroid cell culture system and most probable number calculations. We applied the quantitative method to characterize the extent of human norovirus inactivation with UV_{254} disinfection. Our preliminary UV_{254} inactivation results indicate that human norovirus has similar UV_{254} susceptibility compared with other common enteric (+) ssRNA viruses, requiring approximately 27 mJ cm^{-2} for 4-log_{10} inactivation. These findings will inform effective mitigation strategies for water and food industries, where human norovirus is a major concern. The quantitative infectivity method we developed shows promise for future

research focused on investigating the persistence of infectious human norovirus in environmental settings.

4.2 Introduction

Human norovirus (HuNoV) is estimated as the leading cause of gastrointestinal illness in the United States and worldwide,[1,2] frequently causing vomiting and diarrhea in infected individuals.[3] Possible sources of HuNoV exposure include ingestion of contaminated food or liquids, as well as direct human-to-human contact.[4–11] HuNoV can be highly infectious, with challenge studies revealing that as little as one viral particle may result in infection.[12] However, culturing HuNoV in vitro has proven difficult since the virus' discovery in 1968. Numerous attempts to culture the virus using distinct cell culture systems have not been effective.[13–16] Recent work using novel culture systems have been more promising.[17–19] Although culturing HuNoV in some of these systems has been difficult to reproduce,[18] the human intestinal enteroid (HIE) system[17] has been successfully applied in various laboratories.[20–23] Drawbacks of the new HuNoV culture system include its technical complexities and costliness; consequently, it is not currently available in most laboratories. In addition, the propagation of infectious HuNoV from this culture systems is not yet achievable. As a result, researchers must rely on stool samples with high titer HuNoV from infected individuals. And with only a fraction of HuNoV positive stool samples resulting in productive infection in HIEs,[20] research with the HIE HuNoV culture system is limited by the lack of readily available virus stocks.

These challenges have severely limited research focused on evaluating the presence and fate of infectious HuNoV in the environment. As a result, little is currently known about the fate of infectious HuNoV in environmental matrices, including through water and wastewater treatment. Often, studies use other approaches, such as reverse transcription quantitative polymerase chain

reaction (RT-qPCR), to detect HuNoV in samples.[24–30] These methods, however, only quantify a small portion of the virus particle and therefore likely vastly overestimate infectious virus concentrations in a sample.

A better understanding of HuNoV infectivity through unit processes would inform effective strategies for mitigating HuNoV risk in various food and environmental settings. In particular, the field of direct potable water reuse (DPR), in which wastewater is treated to drinking water standards,[31] would benefit from an improved understanding of HuNoV infectivity through water treatment processes. HuNoV is of principal concern in water reuse, because the starting source water in reuse can contain elevated levels of this enteric pathogen (~ 1 – 10^6 viruses/L).[32,33] However, some DPR risk assessments do not consider HuNoV because of a lack of infectivity data[34] or rely on assumptions about HuNoV persistence to model exposure risk in finished water.[35,36] This means that proposed or established reuse schemes may currently be under or overengineered for HuNoV treatment.

In this study, we applied the recently developed HIE culture system to study infectious HuNoV through UV_{254} disinfection. We first developed a quantitative infectivity assay using a most probable number (MPN) approach,[37] and then used the approach to quantify the infectious HuNoV before and after exposure to UV_{254}. Our resulting HuNoV inactivation data will inform future risk assessments focused on UV_{254} disinfection to limit enteric viral pathogen exposure. In addition, our quantitative approach for tracking HuNoV infectivity will be a valuable research tool for future studies on the fate of infectious HuNoV in various environmental settings.

4.3 Materials and Methods

4.3.1 Virus stocks.

A stool sample containing HuNoV GII.4 was obtained from New York (18-20942 NY). The sample was diluted 1:100 in sterile 1X phosphate buffer saline (PBS) solution (Cat. No. 10010023, Invitrogen) and filtered through a 0.2 µm polyethersulfone membrane (Cat. No. 229747, CELLTreat Scientific). Aliquots of the diluted, filtered stock solution were stored at -80°C until use.

4.3.2 Human intestinal enteroids (HIEs).

Fetal ileum cells (FI 124) were kindly provided by Dr. J. Spence and the Translational Tissue Modeling Laboratory (University of Michigan). HIE maintenance and monolayer preparation were conducted as previously described with slight modifications.[17,20,38,39] Briefly, 3D HIEs were kept in Matrigel basement membrane matrix (Cat. Nos. 354234 and 354623, Corning) and passaged every six to seven days. Passaging was conducted by adding 1 mL ice cold $CMGF^-$ (Table C.1) to each well of a 6-well plate (Cat. No. CC7682-7506, USA Scientific) containing 3D HIEs. Cells were dislodged by vigorously pipetting the gel and media solution five or more times, and a 25G x 5/8" needle syringe (Cat. No. 26403, Exel International) was used to further break up and collect the cells from each well. Wells were rinsed with an additional 1 mL of 1X PBS to collect residual cells. Cells were centrifuged at 80 x g for five minutes at 4°C, and the supernatant was removed and replaced with Matrigel. 3D HIEs were generated by placing 20 10 µL droplets of Matrigel containing cells in each well of a 6-well plate. After allowing Matrigel to solidify, $CMGF^+$ (Table C.1) was added. Cells were incubated at 37°C and 5% CO_2, and media was replaced every 48 hours.

HIE monolayers were generated from 3D HIEs. Medium on 3D HIEs was replaced with 1 mL of 0.5 mM ethylenediaminetetraacetic acid (EDTA; Cat. No. 51201, Lonza) in 1X PBS. Cells were dislodged, collected, and centrifuged for five minutes at 200 x g and 4°C. The pellet was suspended in 0.05% trypsin-EDTA (Cat. No. 25300-054, Gibco) and the solution was incubated for five minutes at 37°C. $CMGF^-$ medium containing 10% fetal bovine serum (Cat. No. SH30396.03, Thermo Scientific) was added to inactivate the trypsin. Cells were gently pipetted at least 50x, and the solution was applied to a pre-rinsed 40 µm strainer (Cat. No. 22-363-547, Fisher Scientific). The resulting cell suspension was centrifuged at 400 x g for five minutes at 4°C and resuspended in $CMGF^+$ medium containing 10 µM Y27632 (Cat. No. 1254, R&D Systems). The cell suspension was seeded at a density of 1 to 2 x 10^5 cells/well into collagen-treated wells in a 96-well flat-bottomed plate (Cat. No. 353072, Corning). For collagen pre-treatment, 100 µL of 33 µg/mL collagen IV (Cat. No. C8919, Sigma-Aldrich) in cold sterile water was added to wells, and the 96-well plate was incubated at 37°C for at least two hours prior to replacement with HIE cell suspension. $CMGF^+$ medium was replaced every 48 hours until HIE monolayers were confluent. $CMGF^+$ medium on confluent monolayers was then replaced with differentiation medium (Table C.1). Five to six days after differentiation was initiated, we used monolayers in HuNoV infections.

4.3.3 HuNoV infectivity assay.

We used an integrated cell culture RT-qPCR (ICC-RT-qPCR) method to confirm HuNoV infection of cells.

4.3.3.1 HuNoV infection of HIEs.

Medium on HIE monolayers was replaced with differentiation medium supplemented with 500 µM sodium glycochenodeoxycholic acid (GCDCA; Cat. No. G0759, Sigma) and 10 µM

ruxolitinib (Cat No. 11609, Cayman Chemical Company) at least 24 hours before infection. Prior to infection, HIE monolayers were washed once with CMGF-. Each HuNoV sample was diluted 1:20 in $CMGF^-$ supplemented with 500 µM GCDCA and 10 µM ruxolitinib. HuNoV samples in $CMGF^-$ solution were applied to HIE monolayers using 100 µL of inoculum in each well. Infected HIE monolayers were incubated for one hour at 37°C, and HIEs were then washed twice with $CMGF^-$. 100 µL differentiation medium with GCDCA and ruxolitinib was added to all wells. The HIEs were then incubated at 37°C and frozen at -80°C 3 days post infection (dpi). During each infection, a subset of HIEs were infected with the original HuNoV sample, incubated, and washed as described for the 3 dpi samples. Immediately following washing and replacement with differentiation medium, the material from these wells was harvested to confirm the initial concentration of HuNoV in the HIE wells at 0 dpi.

4.3.3.2 RNA extraction.

Samples were thawed at room temperature, and 300 µL of TRIzol reagent (Cat. No. 15596026, Invitrogen) was mixed with the contents of each well. The RNA MiniPrep Plus (Cat. No. R2072, Directzol) was used to extract RNA as per manufacturer instructions. No DNase I treatment was conducted. Extracts were suspended in 50 µL nuclease free water and stored at -80°C or immediately quantified.

4.3.3.3 RT-qPCR.

One-step RT-qPCR was carried out using a Mastercycler ep RealPlex 2 system (Eppendorf). Each 20 µL reaction consisted of 5 µL RNA template, 0.3 µL probe (QNIFS; Table C.2),[40] 1 µL each of forward and reverse primers (QNIF2d/COG2R; Table C.2),[40,41] 0.5 µL iScript advanced RT (Cat. No. 172-5141, BioRad), 2.2 µL nuclease-free water, and 10 µL iTaq Universal Probes One-

Step Reaction Mix (Cat. No. 172-5141, BioRad). Cycling conditions included cDNA synthesis at 50°C for 10 min, initial denaturation at 95°C for 3 min, followed by 40 cycles of denaturation at 95°C for 20 s, annealing at 60°C for 20 s, and extension at 72°C for 20 s. A purified gel product prepared from a GII.4 Sydney stool sample was used for the qPCR standard. Each qPCR assay included a standard curve with at least 4 serially diluted standards and a no-template control. All samples and standards were run in duplicate.

4.3.4 Quantitative MPN approach.

An MPN approach[37] was taken to quantify infectious HuNoV levels in samples. Four to six replicates of each HuNoV sample dilution were applied to the HIE wells. Specific dilutions of the untreated samples included 10x, 50x, and 100x and dilutions of the UV_{254}-treated samples included no dilution, 5x, and 10x.

4.3.4.1 MPN Calculation.

A sample was considered HuNoV positive when the 3 dpi HuNoV genome copy concentration amplified in both RT-qPCR replicates conducted. Any samples with a 3 dpi HuNoV genome copy concentration below detection were considered HuNoV negative. The concentration of infectious HuNoV in the original HuNoV sample, in MPN/mL, was then calculated using the MPN calculator developed by the U.S. Environmental Protection Agency (USEPA).[42]

4.3.5 UV_{254} irradiation.

A HuNoV sample was exposed to UV_{254} using a custom-built collimated beam apparatus. We confirmed the lamp's UV_{254} irradiance, 0.16 mW cm^{-2}, using potassium iodide chemical actinometry.[43,44] For the UV_{254} irradiation experiment, MS2 bacteriophage was added to the 1:100 filtered HuNoV stock (~10^7 gene copies/mL) at a final concentration of ~10^9 plaque forming units

(pfu)/mL. The average solution irradiance was determined by the Beer-Lambert law, considering sample absorbance at 254 nm (0.26) and sample depth (0.5 cm). 220 µL of the solution was added to one well of a 96-well plate for each irradiation time point. During UV_{254} treatment, the plate was shaken using a 96-well plate shaker. The irradiated sample was immediately collected and stored on ice until being diluted and applied to HIEs. Two irradiation time points were carried out in a single experiment and included an unirradiated sample and an irradiated sample. The sample was irradiated for 0 s and 60 s, resulting in average UV_{254} fluences of 0 mJ cm^{-2} and ~ 8.2 mJ cm^{-2}, respectively. One experiment was conducted. MS2 bacteriophage inactivation was evaluated immediately following irradiation to confirm the UV_{254} fluence applied to viruses in the sample.

4.4 Results and Discussion

4.4.1 Quantitative HuNoV infectivity assay.

Initially, we intended to measure the UV_{254} inactivation kinetics for HuNoV by measuring the HuNoV RNA signal at 3 dpi in both the untreated and UV_{254}-treated HuNoV samples. For this to work, the HuNoV RNA signal at 3 dpi would need to scale with the amount of infectious HuNoV that was inoculated in the cells. Control experiments, however, demonstrated that the HuNoV RNA signal at 3 dpi did not correlate 1:1 with the amount of infectious HuNoV applied to the HIE well (Figure 4.1). For dilutions where all replicates had a measurable HuNoV RNA signal at 3 dpi, the signal varied by up to 1-log_{10} among replicates. In certain cases, some replicates of the same dilution did not have a detectable HuNoV RNA signal at 3 dpi. This suggests the quantity of RNA transcribed over the course of an infection is not representative of how much infectious HuNoV is applied to HIEs. This may be due in part to the fact that the time-course of infection varies between HuNoV samples and between dilutions of the same HuNoV sample.[20] Consequently, halting each infection at 3 dpi may not capture RNA copies that are comparable from one sample to another or

from one dilution to another. It is worth noting that other work with the HIE assay has used the fold change in HuNoV RNA signal from 3 to 0 dpi to quantify the extent of HIE infection by HuNoV.[17] However, at the sample dilutions used in our work, most 0 dpi samples were below detection by RT-qPCR. We therefore relied only on the HuNoV RNA signal at 3 dpi.

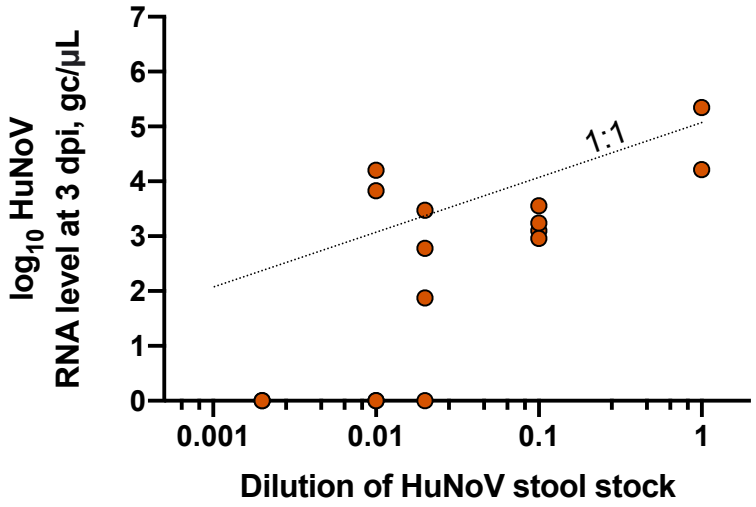

Figure 4.1 Log_{10} HuNoV RNA signal at 3 dpi for the same HuNoV positive stool sample at dilutions of 1x, 10x, 50x, 100x, and 500x. Technical replicates vary between 2 and 4, depending on the dilution. Samples below detection are shown at a HuNoV RNA signal of 0.

Due to the issues with using the HuNoV RNA signal at 3 dpi to infer the concentration of infectious viruses in a sample, we considered the MPN method as an alternative. The MPN method, which relies on Poisson statistics to define the most likely quantity of an organism in a sample, has been successfully applied to measure the concentrations of other viruses.[45–51] This approach assumes that (1) the microorganism is evenly and randomly distributed throughout the sample, and (2) microbial growth will result if one or more microorganisms is inoculated with the host.[37] To effectively determine the MPN, multiple dilutions of the sample and multiple replicates of each dilution must be cultured separately such that some replicates will be negative and others will be positive. We used various 2x, 5x, or 10x dilutions of each sample and four, five, or six replicates

of each dilution to determine which combination of dilutions and replicates was optimal for reliably determining the MPN of infectious HuNoV in samples.

Overall, we found that regardless of the number of replicates and dilutions used, the MPN estimate was consistent within the same experiment (Figure 4.2). As the number of replicates increased, the margin of error was slightly reduced (Figure 4.2a). This is in line with MPN theory, because as additional replicates are included for each dilution, confidence in capturing the true ratio of positive and negative samples at a particular dilution increases.[37] Expanding the range of sample dilutions by an additional 2x to 10x did not greatly affect the MPN estimate or margin of error for two different samples (Figure 4.2b). This may be because the additional tested dilutions did not provide meaningful information beyond the information provided with the initial dilutions. Use of dilutions covering a smaller range than what was tested (e.g., 2-fold, 3-fold) would likely lead to improved MPN calculations. For our purposes, the slight increase in confidence observed from added dilutions was not as important as obtaining the true MPN concentration. We concluded that the confidence intervals achieved by the MPN assay using three dilutions and six replicates each was sufficient to move forward with the UV_{254} inactivation experiments.

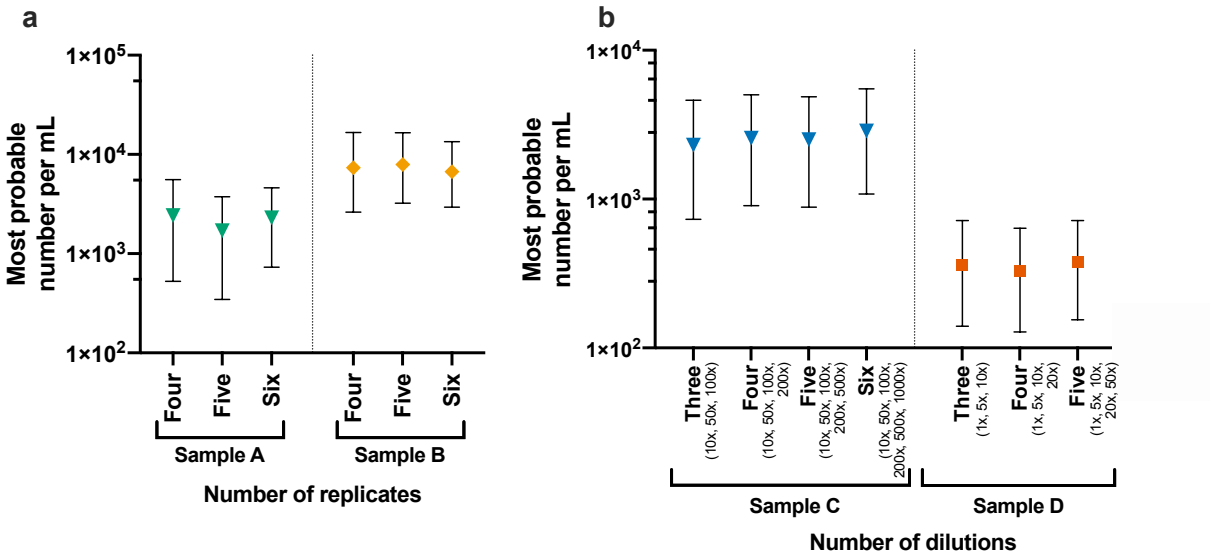

Figure 4.2 MPN concentrations and 95% margins of error resulting from experiments conducted using three dilutions (i.e., 10x, 50x, and 100x) with four, five or six replicates of each dilution (a) and using three, four, five, or six dilutions with six replicates of each dilution (b). Error bars indicate margin of upper and lower 95% confidence. Dilutions used in (b) are indicated in parentheses beside the number of dilutions used.

4.4.2 Inactivation of HuNoV by UV_{254}.

UV_{254} disinfection was conducted at a single UV_{254} dose, ~ 8.2 mJ cm^{-2}. Only one irradiated sample and one unirradiated sample were included in the same UV_{254} experiment so the number of HIE wells needed for a given experiment was not excessive. The UV_{254} dose of ~ 8.2 mJ cm^{-2} was selected because it was anticipated to result in approximately 1-log_{10} inactivation of HuNoV based on previous estimates of UV_{254} HuNoV susceptibility.[52,53] Log_{10} inactivation greater than 1-log_{10} was avoided to ensure that infectious HuNoV in irradiated samples was not below detection limits of the MPN HIE assay.

Because only UV_{254} at one dose was used, we assumed first-order virus inactivation kinetics. Bacteriophage MS2 inactivation was used to confirm the UV_{254} dose delivered to viruses in the sample during irradiation and resulted in a rate constant of 0.17 cm^2 mJ^{-2}, in line with previously reported constants.[52] HuNoV inactivation with UV_{254} resulted in a rate constant of 0.34 ± 0.18 cm^2 mJ^{-1} (mean ± 95% margin of error; Figure 4.3), showing that a UV_{254} dose of ~ 27 mJ cm^{-2} is required for 4-log_{10} inactivation of HuNoV. It is important to note that these findings are preliminary, as only one experiment was conducted. Difficulties with HIE culturing prevented the inclusion of additional HuNoV UV_{254} inactivation data, although work continues to verify the results of this initial experiment. These results suggest HuNoV is similarly susceptible to UV_{254} compared with other (+) ssRNA enteric human viruses.[52] For example, various human enteroviruses, including poliovirus 1, echovirus 11, and coxsackievirus B5, have reported rate

constants ranging from 0.21 to 0.43 cm^{-2} mJ^{-1}.[52] The common surrogate bacteriophage MS2 is significantly more resistant to UV_{254} inactivation than HuNoV based on our results. HuNoV surrogates murine norovirus (MNV) and feline calicivirus (FCV) have been widely used in studies of environmental HuNoV fate because they are in the *Caliciviridae* family, like HuNoV, and share many structural and genomic similarities with HuNoV.[54,55] MNV and FCV have UV_{254} rate constants of ~ 0.33 mJ cm^{-2} and ~ 0.29 mJ cm^{-2},[52] respectively, which are in line with HuNoV inactivation. Although these preliminary UV_{254} findings must be confirmed with additional replicates to be certain, MNV and FCV are likely accurate HuNoV surrogates through UV_{254}. Beyond UV_{254} inactivation, use of the culture system work should be conducted to assess HuNoV infectivity through other disinfection strategies, such as chlorine or ozone, to confirm that MNV and FCV also behave similarly to HuNoV through other treatments.

Past studies looking at HuNoV levels through UV_{254} treatment have identified much greater HuNoV resistance to UV_{254} disinfection than we found with the in vitro assay, indicating as little as 0 to 1.5-log_{10} HuNov inactivation with as high a UV_{254} dose as 300 mJ cm^{-2}.[24,56,57] This is likely because RT-qPCR methods were applied. Traditional molecular approaches for measuring HuNoV gene copies measure only a small portion of the genome, which do not accurately track infectious virus particles. Research with various (+) ssRNA viruses has shown that molecular approaches using longer regions of the viral genome demonstrate inactivation more similar to that of the infectious virus;[58,59] however short of amplifying the entire genome or using an alternative extrapolation approach, discrepancies remain.

We recently reported on two alternative approaches to estimate HuNoV inactivation by UV_{254} in the absence of a readily available infectivity assay. The first approach, which detected UV_{254} damage to multiple regions of the HuNoV genome using RT-qPCR and extrapolated that damage

to the full-length genome, resulted in a rate constant of 0.27 ± 0.03 cm^2 mJ^{-1}.[53] The second approach applied a linear regression model to predict inactivation using genome sequence information and resulted in a rate constant of k_{pred} = 0.28 ± 0.12 cm^2 mJ^{-1}.[52] Both of these approaches yielded similar HuNoV UV_{254} susceptibility (k = 0.34 ± 0.18 cm^2 mJ^{-1}) to the infectivity analysis conducted here. The preliminary culture-based results obtained here offer additional confidence that using a non-traditional qPCR extrapolation approach[53,60] or a predictive modeling approach[52] can accurately predict UV_{254} inactivation of (+) ssRNA viruses.

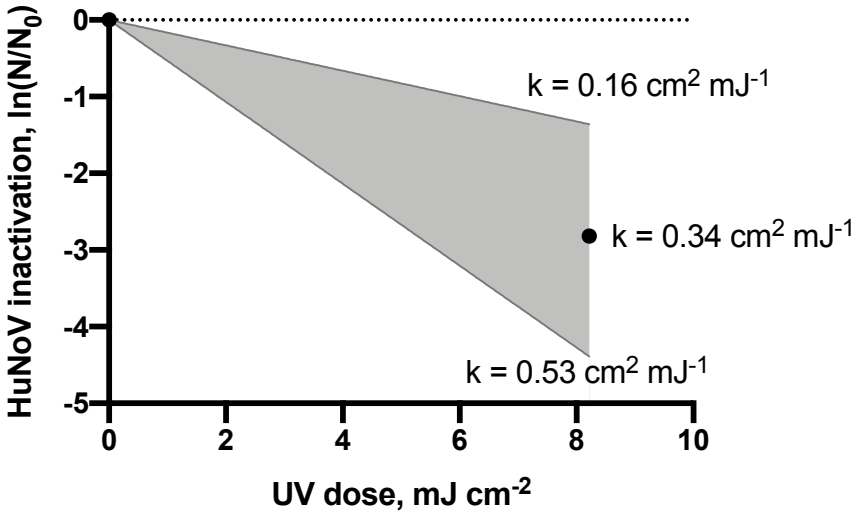

Figure 4.3 Inactivation of HuNoV as a function of UV_{254} dose, in mJ cm^{-2}. One independent replicate is shown. Shading indicates the 95% confidence interval of the linear regression. The estimated inactivation rate constant, defined as the slope of the linear regression, is displayed, along with the values associated with the 95% confidence interval of the rate constant.

4.4.3 Freeze-thaw of HuNoV samples.

Experiments to determine fate and behavior of HuNoV may require a large quantity and high concentration of HuNoV positive stool sample that can replicate in the HIEs. Ensuring the retention of infectious HuNoV in a sample between freeze-thaws was therefore critical. We investigated the effect of freeze-thaw on HuNoV infectivity of HIEs. Results indicate that the same

stool sample before a freeze-thaw yielded significantly higher RNA gene copy levels at 3 dpi as opposed to the same sample that had undergone one additional freeze-thaw from -80°C to room temperature (Figure 4.4). This suggests that levels of HuNoV capable of effectively infecting and replicating in HIEs are significantly reduced through freeze-thaw cycles of HuNoV positive samples. Past work with HuNoV GII.4 stability through freeze-thaws observed negligible degradation of the RNA genome, as measured by RT-qPCR, and capsid proteins, as measured by capsid binding to magnetic beads, after as many as 14 freeze-thaws.[61] While the study did not observe degradation of these two components of the HuNoV particle, infectivity was not evaluated. Our findings clearly establish a large reduction in HuNoV infectivity following as little as one freeze-thaw. This suggests that HuNoV inactivation is indeed occurring in some form through freeze-thaw, although that inactivation may not be detected using assays targeting specific components of the virus capsid or genome. Future work should work to determine which specific components of the virus particle are degraded through freeze-thaw.

It is important to note that the sample evaluated in our experiments was a fecal sample that had been diluted 1:100 in 1X PBS and filtered through a 0.2 μm PES membrane prior to freezing. This dilution and filtration might have impacted HuNoV persistence through the freeze-thaw process and HuNoV in raw stool samples may be more or less stable. To date, the mechanism of HuNoV inactivation through the freeze-thaw process is not known. A previous report of infectious virus degradation through freeze-thaws focused on enveloped viruses.[62] In general, more research is needed to determine the stability of viruses in stool samples and in purified forms through storage and freeze-thaw processes.

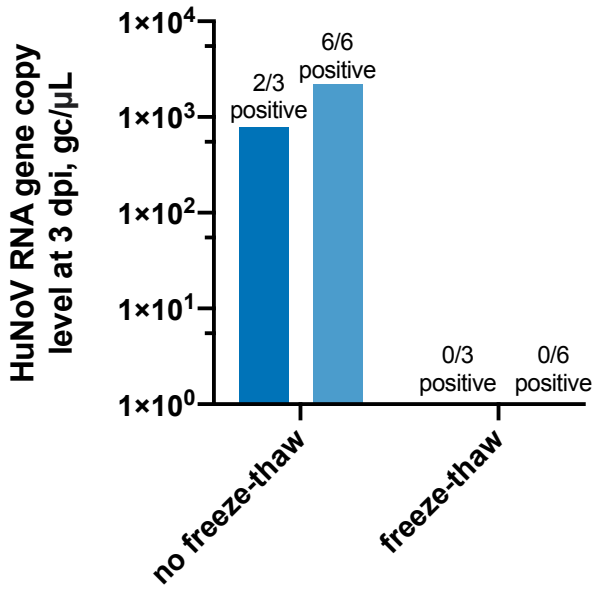

Figure 4.4 3 dpi HuNoV RNA gene copy levels of the same sample diluted 10x before and after an additional freeze-thaw. Three or six technical replicates of the same sample dilution were conducted for two independent experiments. The number of positive technical replicates are shown for each independent experiment.

4.4.4 Implications.

To date, the lack of a reliable HuNoV cell culture system has hindered studies of infectious HuNoV persistence in the environment and through water treatments processes. Here, we provide preliminary UV_{254} inactivation data for HuNoV determined with an in vitro culture system. These findings suggest that HuNoV behaves similarly to many other (+) ssRNA viruses through UV_{254} disinfection. Adenovirus 41, an enteric dsDNA virus that is highly resistant to UV_{254} inactivation, is almost an order of magnitude more resistant to UV_{254} than HuNoV. UV_{254} treatments intended to inactivate adenovirus 41 by 4-$\log_{10}$ will inactivate HuNoV by > 20-$\log_{10}$ assuming first order kinetics is maintained to these levels of inactivation. Additional work will be needed to confirm the HuNoV UV_{254} susceptibility observed here and establish that first order inactivation kinetics are exhibited by HuNoV in this UV_{254} treatment range.

For this work, we used a high-titer GII.4 HuNoV sample that we knew could productively infect the HIEs based on past experiments. An important limitation of this cell culture assay for use in the environmental setting is its inability to support growth of certain circulating noroviruses. Previous work screened over 80 fecal samples containing 12 different genogroups of HuNoV for infection in the enteroids, including 65 samples with GII HuNoV, and determined that roughly only 20% resulted in productive infection.[20] Our preliminary screening of HuNoV stool samples revealed a similar inability of certain HuNoV positive stool samples to produce measurable increases in viral RNA after 3 days of viral infection. Even in samples that could productively infect HIEs, titers had to be sufficiently high to evaluate inactivation and apply the dilutions necessary for the MPN approach. Without the ability to propagate HuNoV in vitro, obtaining and finding suitable HuNoV positive stool samples for environmental fate studies using HIEs will continue to present a major barrier for the field. We do not yet understand what differences from sample to sample cause the disparities in productive HIE infection, although strain-specific differences likely play a role.[17] It has also been suggested that certain cofactors, such as the bile GCDCA, can support or enhance HIE infection, depending on the strain.[17] It is important to note that in this work, bile was always added to HIEs before and during infection, so this parameter was eliminated in our study. Some research has indicated that stool samples with elevated norovirus gene copy concentrations and that come from young patients more commonly infect HIEs successfully,[20] while more recent work suggests samples from adults are just as capable of productive HIE infection.[21] These results have important implications for the environmental virology field, because this tool cannot yet reliably be used for monitoring native infectious HuNoV in environmental matrices.

Several other viruses, including astrovirus or rotavirus, can produce high RNA titers after inoculation in HIEs.[39,63] Environmental samples such as primary wastewater likely contain a variety of different enteric viral pathogens. The HIEs, which are not a specific host for HuNoV, would therefore support growth of many different viruses that can grow rapidly in human intestinal cell lines. In these cases, it is possible that although HuNoV is present in the sample, no increase in viral RNA is measured because other viruses more effectively infect the HIEs and use host cell machinery. Future work in the virology field to distinguish methods for selective growth of HuNoV could facilitate the use of this tool for monitoring purposes and for better understanding the environmental fate of HuNoV.

4.5 References

(1) Scallan, E.; Hoekstra, R. M.; Angulo, F. J.; Tauxe, R. V; Widdowson, M.-A.; Roy, S. L.; Jones, J. L.; Griffin, P. M. Foodborne Illness Acquired in the United States—Major Pathogens. *Emerg. Infect. Dis.* **2011**, *17* (1), 7–15. https://doi.org/10.3201/eid1701.P11101.

(2) Pires, S. M.; Fischer-Walker, C. L.; Lanata, C. F.; Devleesschauwer, B.; Hall, A. J.; Kirk, M. D.; Duarte, A. S. R.; Black, R. E.; Angulo, F. J. Aetiology-Specific Estimates of the Global and Regional Incidence and Mortality of Diarrhoeal Diseases Commonly Transmitted through Food. *PLoS One* **2015**, *10* (12), e0142927.

(3) Dolin, R.; Blacklow, N. R.; DuPont, H.; Buscho, R. F.; Wyatt, R. G.; Kasel, J. A.; Hornick, R.; Chanock, R. M. Biological Properties of Norwalk Agent of Acute Infectious Nonbacterial Gastroenteritis. *Proc. Soc. Exp. Biol. Med.* **1972**, *140* (2), 578–583. https://doi.org/10.3181/00379727-140-36508.

(4) Saupe, A. A.; Rounds, J.; Sorenson, A.; Hedeen, N.; Bagstad, E.; Reinberg, R.; Wagley, A. G.; Cebelinski, E.; Smith, K. Outbreak of Norovirus Gastroenteritis Associated With Ice Cream Contaminated by Frozen Raspberries From China—Minnesota, United States, 2016. *Clin. Infect. Dis.* **2020**. https://doi.org/10.1093/cid/ciaa821.

(5) Verhoef, L.; Hewitt, J.; Barclay, L.; Ahmed, S. M.; Lake, R.; Hall, A. J.; Lopman, B.; Kroneman, A.; Vennema, H.; Vinjé, J.; Koopmans, M. Norovirus Genotype Profiles Associated with Foodborne Transmission, 1999-2012. *Emerg. Infect. Dis.* **2015**, *21* (4), 592–599. https://doi.org/10.3201/eid2104.141073.

(6) Daniels, N. A.; Bergmire-Sweat, D. A.; Schwab, K. J.; Hendricks, K. A.; Reddy, S.; Rowe, S. M.; Fankhauser, R. L.; Monroe, S. S.; Atmar, R. L.; Glass, R. I.; Mead, P. A Foodborne

Outbreak of Gastroenteritis Associated with Norwalk-like Viruses: First Molecular Traceback to Deli Sandwiches Contaminated during Preparation. *J. Infect. Dis.* **2000**, *181* (4), 1467–1470. https://doi.org/10.1086/315365.

(7) Blanco, A.; Guix, S.; Fuster, N.; Fuentes, C.; Bartolomé, R.; Cornejo, T.; Pintó, R. M.; Bosch, A. Norovirus in Bottled Water Associated with Gastroenteritis Outbreak, Spain, 2016. *Emerg. Infect. Dis. J.* **2017**, *23* (9), 1531. https://doi.org/10.3201/eid2309.161489.

(8) ter Waarbeek, H. L. G.; Dukers-Muijrers, N. H. T. M.; Vennema, H.; Hoebe, C. J. P. A. Waterborne Gastroenteritis Outbreak at a Scouting Camp Caused by Two Norovirus Genogroups: GI and GII. *J. Clin. Virol.* **2010**, *47* (3), 268–272. https://doi.org/https://doi.org/10.1016/j.jcv.2009.12.002.

(9) Maunula, L.; Miettinen, I. T.; von Bonsdorff, C.-H. Norovirus Outbreaks from Drinking Water. *Emerg. Infect. Dis.* **2005**, *11* (11), 1716–1721. https://doi.org/10.3201/eid1111.050487.

(10) Li, J.; Gao, X.; Ye, Y.-L.; Wan, T.; Zang, H.; Mo, P.-H.; Song, C.-L. An Acute Gastroenteritis Outbreak Associated with Person-to-Person Transmission in a Primary School in Shanghai: First Report of a GI.5 Norovirus Outbreak in China. *BMC Infect. Dis.* **2018**, *18* (1), 316. https://doi.org/10.1186/s12879-018-3224-4.

(11) Wilkswo, M. E.; Hall, A. J. Outbreaks of Acute Gastroenteritis Transmitted by Person-to-Person Contact--United States, 2009-2010. *Am. J. Public Health* **2014**, *104* (11), e13–e14. https://doi.org/10.2105/AJPH.2014.10411e13.

(12) F.M., T. P.; L., M. C.; Pengbo, L.; Sara, E. M.; Lisa, L.; S., B. R.; Jacques, L. P.; L., C. R. Norwalk Virus: How Infectious Is It? *J. Med. Virol.* **2008**, *80* (8), 1468–1476. https://doi.org/10.1002/jmv.21237.

(13) Duizer, E.; Schwab, K. J.; Neill, F. H.; Atmar, R. L.; Koopmans, M. P. G.; Estes, M. K. Laboratory Efforts to Cultivate Noroviruses. *J. Gen. Virol.* **2004**, *85* (1), 79–87.

(14) Straub, T. M.; Bartholomew, R. A.; Valdez, C. O.; Valentine, N. B.; Dohnalkova, A.; Ozanich, R. M.; Bruckner-Lea, C. J.; Call, D. R. Human Norovirus Infection of Caco-2 Cells Grown as a 3-Dimensional Tissue Structure. *J. Water Health* **2011**, *9* (2), 225–240.

(15) Straub, T. M.; Höner zu Bentrup, K.; Coghlan, P. O.; Dohnalkova, A.; Mayer, B. K.; Bartholomew, R. A.; Valdez, C. O.; Bruckner-Lea, C. J.; Gerba, C. P.; Abbaszadegan, M. A.; Nickerson, C. A. In Vitro Cell Culture Infectivity Assay for Human Noroviruses. *Emerg. Infect. Dis.* **2007**, *13* (3), 396–403. https://doi.org/10.3201/eid1303.060549.

(16) Papafragkou, E.; Hewitt, J.; Park, G. W.; Greening, G.; Vinjé, J. Challenges of Culturing Human Norovirus in Three-Dimensional Organoid Intestinal Cell Culture Models. *PLoS One* **2013**, *8* (6), e63485.

(17) Ettayebi, K.; Crawford, S. E.; Murakami, K.; Broughman, J. R.; Karandikar, U.; Tenge, V. R.; Neill, F. H.; Blutt, S. E.; Zeng, X.-L.; Qu, L.; Kou, B.; Opekun, A. R.; Burrin, D.; Graham, D. Y.; Ramani, S.; Atmar, R. L.; Estes, M. K. Replication of Human Noroviruses in Stem Cell–Derived Human Enteroids. *Science (80-.).* **2016**.

(18) Jones, M. K.; Grau, K. R.; Costantini, V.; Kolawole, A. O.; de Graaf, M.; Freiden, P.; Graves, C. L.; Koopmans, M.; Wallet, S. M.; Tibbetts, S. A.; Schultz-Cherry, S.; Wobus, C. E.; Vinjé, J.; Karst, S. M. Human Norovirus Culture in B Cells. *Nat. Protoc.* **2015**, *10* (12), 1939–1947. https://doi.org/10.1038/nprot.2015.121.

(19) Van Dycke, J.; Ny, A.; Conceição-Neto, N.; Maes, J.; Hosmillo, M.; Cuvry, A.; Goodfellow, I.; Nogueira, T. C.; Verbeken, E.; Matthijnssens, J.; de Witte, P.; Neyts, J.; Rocha-

Pereira, J. A Robust Human Norovirus Replication Model in Zebrafish Larvae. *PLOS Pathog.* **2019**, *15* (9), e1008009.

(20) Costantini, V.; Morantz, E. K.; Browne, H.; Ettayebi, K.; Zeng, X.-L.; Atmar, R. L.; Estes, M. K.; Vinjé, J. Human Norovirus Replication in Human Intestinal Enteroids as Model to Evaluate Virus Inactivation. *Emerg. Infect. Dis. J.* **2018**, *24* (8). https://doi.org/10.3201/eid2408.180126.

(21) Chan, M. C.-W.; Cheung, S. K. C.; Mohammad, K. N.; Chan, J. C. M.; Estes, M. K.; Chan, P. K. S. Use of Human Intestinal Enteroids to Detect Human Norovirus Infectivity. *Emerg. Infect. Dis.* **2019**, *25* (9), 1730–1735. https://doi.org/10.3201/eid2509.190205.

(22) Haga, K.; Ettayebi, K.; Tenge, V. R.; Karandikar, U. C.; Lewis, M. A.; Lin, S.-C.; Neill, F. H.; Ayyar, B. V; Zeng, X.-L.; Larson, G.; Ramani, S.; Atmar, R. L.; Estesa, M. K. Genetic Manipulation of Human Intestinal Enteroids Demonstrates the Necessity of a Functional Fucosyltransferase 2 Gene for Secretor-Dependent Human Norovirus Infection. *MBio* **2020**, *11* (2). https://doi.org/10.1128/mBio.00251-20.

(23) Hosmillo, M.; Chaudhry, Y.; Nayak, K.; Sorgeloos, F.; Koo, B.-K.; Merenda, A.; Lillestol, R.; Drumright, L.; Zilbauer, M.; Goodfellow, I. Norovirus Replication in Human Intestinal Epithelial Cells Is Restricted by the Interferon-Induced JAK/STAT Signaling Pathway and Rna Polymerase Ii-Mediated Transcriptional Responses. *MBio* **2020**, *11* (2). https://doi.org/10.1128/mBio.00215-20.

(24) Campos, C. J. A.; Avant, J.; Lowther, J.; Till, D.; Lees, D. N. Human Norovirus in Untreated Sewage and Effluents from Primary, Secondary and Tertiary Treatment Processes. *Water Res.* **2016**, *103*, 224–232. https://doi.org/http://dx.doi.org/10.1016/j.watres.2016.07.045.

(25) Montazeri, N.; Goettert, D.; Achberger, E. C.; Johnson, C. N.; Prinyawiwatkul, W.; Janes, M. E. Pathogenic Enteric Viruses and Microbial Indicators during Secondary Treatment of Municipal Wastewater. *Appl. Environ. Microbiol.* **2015**, *81* (18), 6436–6445. https://doi.org/10.1128/AEM.01218-15.

(26) Flannery, J.; Keaveney, S.; Rajko-Nenow, P.; O'Flaherty, V.; Doré, W. Concentration of Norovirus during Wastewater Treatment and Its Impact on Oyster Contamination. *Appl. Environ. Microbiol.* **2012**, *78* (9), 3400–3406. https://doi.org/10.1128/AEM.07569-11.

(27) Katayama, H.; Haramoto, E.; Oguma, K.; Yamashita, H.; Tajima, A.; Nakajima, H.; Ohgaki, S. One-Year Monthly Quantitative Survey of Noroviruses, Enteroviruses, and Adenoviruses in Wastewater Collected from Six Plants in Japan. *Water Res.* **2008**, *42* (6), 1441–1448. https://doi.org/https://doi.org/10.1016/j.watres.2007.10.029.

(28) Francy, D. S.; Stelzer, E. A.; Bushon, R. N.; Brady, A. M. G.; Williston, A. G.; Riddell, K. R.; Borchardt, M. A.; Spencer, S. K.; Gellner, T. M. Comparative Effectiveness of Membrane Bioreactors, Conventional Secondary Treatment, and Chlorine and UV Disinfection to Remove Microorganisms from Municipal Wastewaters. *Water Res.* **2012**, *46* (13), 4164–4178. https://doi.org/https://doi.org/10.1016/j.watres.2012.04.044.

(29) Farkas, K.; Marshall, M.; Cooper, D.; McDonald, J. E.; Malham, S. K.; Peters, D. E.; Maloney, J. D.; Jones, D. L. Seasonal and Diurnal Surveillance of Treated and Untreated Wastewater for Human Enteric Viruses. *Environ. Sci. Pollut. Res. Int.* **2018**. https://doi.org/10.1007/s11356-018-3261-y.

(30) da Silva, A. K.; Le Saux, J.-C.; Parnaudeau, S.; Pommepuy, M.; Elimelech, M.; Le Guyader, F. S. Evaluation of Removal of Noroviruses during Wastewater Treatment, Using Real-

Time Reverse Transcription-PCR: Different Behaviors of Genogroups I and II. *Appl. Environ. Microbiol.* **2007**, *73* (24), 7891–7897. https://doi.org/10.1128/AEM.01428-07.

(31) Asano, T.; Burton, F.; Leverenz, H.; Tsuchihashi, R.; Tchobanoglous, G. *Water Reuse Issues, Technologies, and Applications*; McGraw-Hill: New York :, 2007.

(32) Pouillot, R.; Van Doren, J. M.; Woods, J.; Plante, D.; Smith, M.; Goblick, G.; Roberts, C.; Locas, A.; Hajen, W.; Stobo, J.; White, J.; Holtzman, J.; Buenaventura, E.; Burkhardt, W.; Catford, A.; Edwards, R.; DePaola, A.; Calci, K. R. Meta-Analysis of the Reduction of Norovirus and Male-Specific Coliphage Concentrations in Wastewater Treatment Plants. *Appl. Environ. Microbiol.* **2015**, *81* (14), 4669–4681.

(33) N.Haas, C.; B.Rose, J.; P.Gerba, C. Quantitative Microbial Risk Assessment. **2014**.

(34) Texas Water Development Board. Final Report - Direct Potable Reuse. **2015**.

(35) Soller, J. A.; Eftim, S. E.; Warren, I.; Nappier, S. P. Evaluation of Microbiological Risks Associated with Direct Potable Reuse. *Microb. Risk Anal.* **2016**. https://doi.org/http://dx.doi.org/10.1016/j.mran.2016.08.003.

(36) World Health Organization. Potable Reuse: Guidance for Producing Safe Drinking-Water. **2017**.

(37) Cochran, W. G. Estimation of Bacterial Densities by Means of the "Most Probable Number." *Biometrics* **1950**, *6* (2), 105–116. https://doi.org/10.2307/3001491.

(38) Zou, W. Y.; Blutt, S. E.; Crawford, S. E.; Ettayebi, K.; Zeng, X.-L.; Saxena, K.; Ramani, S.; Karandikar, U. C.; Zachos, N. C.; Estes, M. K. Human Intestinal Enteroids: New Models to Study Gastrointestinal Virus Infections; Humana Press: Totowa, NJ, 2017; pp 1–19. https://doi.org/10.1007/7651_2017_1.

(39) Kolawole, A. O.; Mirabelli, C.; Hill, D. R.; Svoboda, S. A.; Janowski, A. B.; Passalacqua, K. D.; Rodriguez, B. N.; Dame, M. K.; Freiden, P.; Berger, R. P.; Vu, D.; Hosmillo, M.; O'Riordan, M. X. D.; Schultz-Cherry, S.; Guix, S.; Spence, J. R.; Wang, D.; Wobus, C. E. Astrovirus Replication in Human Intestinal Enteroids Reveals Multi-Cellular Tropism and an Intricate Host Innate Immune Landscape. *PLOS Pathog.* **2019**, *15* (10), e1008057.

(40) Loisy, F.; Atmar, R. L.; Guillon, P.; Le Cann, P.; Pommepuy, M.; Le Guyader, F. S. Real-Time RT-PCR for Norovirus Screening in Shellfish. *J. Virol. Methods* **2005**, *123* (1), 1–7. https://doi.org/https://doi.org/10.1016/j.jviromet.2004.08.023.

(41) Kageyama, T.; Kojima, S.; Shinohara, M.; Uchida, K.; Fukushi, S.; Hoshino, F. B.; Takeda, N.; Katayama, K. Broadly Reactive and Highly Sensitive Assay for Norwalk-Like Viruses Based on Real-Time Quantitative Reverse Transcription-PCR. *J. Clin. Microbiol.* **2003**, *41* (4), 1548–1557. https://doi.org/10.1128/JCM.41.4.1548-1557.2003.

(42) U.S. Environmental Protection Agency. Most Probable Number (MPN) Calculator.

(43) Rahn, R. O.; Bolton, J.; Stefan, M. I. The Lodide/Lodate Actinometer in UV Disinfection: Determination of the Fluence Rate Distribution in UV Reactors. *Photochem. Photobiol.* **2006**, *82* (2), 611–615. https://doi.org/10.1562/2005-06-10-RN-570.

(44) Rahn, R. O. Potassium Iodide as a Chemical Actinometer for 254 Nm Radiation: Use of Lodate as an Electron Scavenger. *Photochem. Photobiol.* **1997**, *66* (4), 450–455. https://doi.org/10.1111/j.1751-1097.1997.tb03172.x.

(45) Chang, S. L.; Berg, G.; Busch, K. A.; Stevenson, R. E.; Clarke, N. A.; Kabler, P. W. Application of the "Most Probable Number" Method for Estimating Concentrations of Animal

Viruses by the Tissue Culture Technique. *Virology* **1958**, *6* (1), 27–42. https://doi.org/https://doi.org/10.1016/0042-6822(58)90057-6.

(46) Thurston-Enriquez, J. A.; Haas, C. N.; Jacangelo, J.; Riley, K.; Gerba, C. P. Inactivation of Feline Calicivirus and Adenovirus Type 40 by UV Radiation. *Appl. Environ. Microbiol.* **2003**, *69* (1), 577–582.

(47) Zhong, Q.; Carratala, A.; Ossola, R.; Bachmann, V.; Kohn, T. Cross-Resistance of UV- or Chlorine Dioxide-Resistant Echovirus 11 to Other Disinfectants. *Front. Microbiol.* **2017**, *8*. https://doi.org/10.3389/fmicb.2017.01928.

(48) Abad, F. X.; Pinto, R. M.; Bosch, A. Flow Cytometry Detection of Infectious Rotaviruses in Environmental and Clinical Samples. *Appl. Environ. Microbiol.* **1998**, *64* (7), 2392–2396.

(49) Gerba, C. P.; Gramos, D. M.; Nwachuku, N. Comparative Inactivation of Enteroviruses and Adenovirus 2 by UV Light. *Appl. Environ. Microbiol.* **2002**, *68* (10), 5167 LP – 5169. https://doi.org/10.1128/AEM.68.10.5167-5169.2002.

(50) Kott, Y. Estimation of Low Numbers of Escherichia Coli Bacteriophage by Use of the Most Probable Number Method. *Appl. Microbiol.* **1966**, *14* (2), 141–144.

(51) Meister, S.; Verbyla, M. E.; Klinger, M.; Kohn, T. Variability in Disinfection Resistance between Currently Circulating Enterovirus B Serotypes and Strains. *Environ. Sci. Technol.* **2018**, *52* (6), 3696–3705. https://doi.org/10.1021/acs.est.8b00851.

(52) Rockey, N. C.; Henderson, J. B.; Chin, K.; Raskin, L.; Wigginton, K. R. Predictive Modeling of Virus Inactivation by UV. **2020**.

(53) Rockey, N.; Young, S.; Kohn, T.; Pecson, B.; Wobus, C. E.; Raskin, L.; Wigginton, K. R. UV Disinfection of Human Norovirus: Evaluating Infectivity Using a Genome-Wide PCR-Based

Approach. *Environ. Sci. Technol.* **2020**, *54* (5), 2851–2858. https://doi.org/10.1021/acs.est.9b05747.

(54) Green, K. Y.; Ando, T.; Balayan, M. S.; Berke, T.; Clarke, I. N.; Estes, M. K.; Matson, D. O.; Nakata, S.; Neill, J. D.; Studdert, M. J.; Thiel, H.-J. Taxonomy of the Caliciviruses. *J. Infect. Dis.* **2000**, *181* (Supplement_2), S322–S330. https://doi.org/10.1086/315591.

(55) Wobus, C. E.; Thackray, L. B.; Virgin, H. W. Murine Norovirus: A Model System To Study Norovirus Biology and Pathogenesis. *J. Virol.* **2006**, *80* (11), 5104 LP – 5112. https://doi.org/10.1128/JVI.02346-05.

(56) Rönnqvist, M.; Mikkelä, A.; Tuominen, P.; Salo, S.; Maunula, L. Ultraviolet Light Inactivation of Murine Norovirus and Human Norovirus GII: PCR May Overestimate the Persistence of Noroviruses Even When Combined with Pre-PCR Treatments. *Food Environ. Virol.* **2014**, *6* (1), 48–57. https://doi.org/10.1007/s12560-013-9128-y.

(57) Qiu, Y.; Lee, B. E.; Neumann, N.; Ashbolt, N.; Craik, S.; Maal-Bared, R.; Pang, X. L. Assessment of Human Virus Removal during Municipal Wastewater Treatment in Edmonton, Canada. *J. Appl. Microbiol.* **2015**, *119* (6), 1729–1739. https://doi.org/10.1111/jam.12971.

(58) Ho, J.; Seidel, M.; Niessner, R.; Eggers, J.; Tiehm, A. Long Amplicon (LA)-QPCR for the Discrimination of Infectious and Noninfectious Phix174 Bacteriophages after UV Inactivation. *Water Res.* **2016**, *103*, 141–148. https://doi.org/https://doi.org/10.1016/j.watres.2016.07.032.

(59) Simonet, J.; Gantzer, C. Inactivation of Poliovirus 1 and F-Specific RNA Phages and Degradation of Their Genomes by UV Irradiation at 254 Nanometers. *Appl. Environ. Microbiol.* **2006**, *72* (12), 7671 LP – 7677. https://doi.org/10.1128/AEM.01106-06.

(60) Pecson, B. M.; Ackermann, M.; Kohn, T. Framework for Using Quantitative PCR as a Nonculture Based Method To Estimate Virus Infectivity. *Environ. Sci. Technol.* **2011**, *45* (6), 2257–2263. https://doi.org/10.1021/es103488e.

(61) Richards, G. P.; Watson, M. A.; Meade, G. K.; Hovan, G. L.; Kingsley, D. H. Resilience of Norovirus GII.4 to Freezing and Thawing: Implications for Virus Infectivity. *Food Environ. Virol.* **2012**, *4* (4), 192–197. https://doi.org/10.1007/s12560-012-9089-6.

(62) Wallis, C.; Melnick, J. L. Stabilization of Enveloped Viruses by Dimethyl Sulfoxide. *J. Virol.* **1968**, *2* (9), 953–954. https://doi.org/10.1128/JVI.2.9.953-954.1968.

(63) Saxena, K.; Blutt, S. E.; Ettayebi, K.; Zeng, X.-L.; Broughman, J. R.; Crawford, S. E.; Karandikar, U. C.; Sastri, N. P.; Conner, M. E.; Opekun, A. R.; Graham, D. Y.; Qureshi, W.; Sherman, V.; Foulke-Abel, J.; In, J.; Kovbasnjuk, O.; Zachos, N. C.; Donowitz, M.; Estes, M. K. Human Intestinal Enteroids: A New Model To Study Human Rotavirus Infection, Host Restriction, and Pathophysiology. *J. Virol.* **2016**, *90* (1), 43–56. https://doi.org/10.1128/JVI.01930-15.

Chapter 5

The Utility of Flow Cytometry for Potable Reuse

Reprinted with permission from: Nicole Rockey, Heather N. Bischel, Tamar Kohn, Brian Pecson, Krista R. Wigginton, The utility of flow cytometry for potable reuse, *Current Opinion in Biotechnology* 2019, *57*, 42 – 49. DOI: 10.1016/j.copbio.2018.12.009, Copyright (2018) Elsiever Ltd.

5.1 Abstract

Protecting public health from pathogens is critical when treating wastewater to drinking water standards (i.e., planned water reuse). Viruses are a principal concern, yet real-time monitoring strategies do not currently measure virus removal through reuse processes. Flow cytometry (FCM) has enabled rapid and sensitive bacteria monitoring in water treatment applications, but methods for virus and protozoa monitoring remain immature. We discuss recent advances in the FCM field and FCM applications for quantifying microorganisms in water. We focus on flow virometry (FVM) developments, as virus enumeration methods show promise for water reuse applications. Ultimately, we propose FVM for near real-time monitoring across treatment to more accurately validate virus particle removal and for pilot studies to characterize removal through understudied unit processes.

5.2 Introduction

Wastewater is increasingly used as an alternative water source to meet potable needs,[1–3] giving rise to new challenges in assuring public health. Pathogenic microorganisms are of principal

concern in wastewater reuse due to the acute health risks they pose to consumers. Virus removal, in particular, is a major driver in the regulation and design of planned potable water reuse because they are present in high concentrations in wastewater,[1,4–6] and their small size (20 nm to over 200 nm) makes them difficult to remove.[7] Depending on the intended application and project location, reuse regulations and guidelines for virus removal range from 8- to 13-logs or more from raw or treated wastewater to finished water.[4,5,8]

Ideally, pathogens would be monitored directly in finished drinking water to demonstrate the water is safe; however, this is infeasible due to the extremely low pathogen concentrations in safe finished water (e.g., 10^{-7} enteric viruses/L ^{1}). Instead, individual unit processes in the treatment train are allotted log removal credits for groups of pathogens, and the credits are summed across the treatment train. To maintain removal credits, the proper functioning of a unit process is ensured in real- or near real-time by monitoring an easy-to-measure surrogate parameter, such as turbidity or electrical conductivity. These surrogate parameters often underestimate actual microorganism removal. Virus removal credits, in particular, are very conservative. Consequently, potable water reuse treatment trains may be over-engineered for pathogen removal because utilities cannot demonstrate the actual log reductions for common unit processes (e.g., biofiltration, ultrafiltration, reverse osmosis).

The water treatment field in general, and the wastewater reuse field in particular, would greatly benefit from technologies that accurately depict microorganism concentrations in real- or near real-time and demonstrate their reductions through specific unit processes. We believe flow cytometry (FCM), a high-throughput technique that uses light scattering and fluorescence for particle detection,[9] can fill some of these needs for microbe monitoring and will be increasingly applied for wastewater reuse monitoring. The main advantage of FCM over currently used surrogate

parameters is that it directly detects microorganisms. The main advantages of FCM for reuse applications over other microbial detection techniques are that it is high-throughput, reproducible, and can concurrently enumerate different microorganism groups based on size and fluorescence properties. In this perspective, we review recent applications and advances in FCM for environmental monitoring. We discuss the three main pathogen groups but focus on virus detection using FCM, coined flow virometry (FVM), as we see this as an area ripe for advancement in coming years. Based on demonstrated capabilities of FCM and FVM, we propose three specific applications in potable water reuse.

5.3 Recent applications and advances in the use of FCM for bacteria and protozoa monitoring.

Bacteria enumeration via FCM is far more advanced than protozoa or virus monitoring in terms of experience, automation, and proof-of-concept research.[10,11] Bacteria in drinking and surface water matrices can effectively be monitored in real-time[12–14] using flow cytometers with automated modules that routinely sample, stain, and enumerate bacteria with fifteen-minute resolution.[15] Online bacteria monitoring via FCM in full-scale water treatment systems offers improved resolution, reproducibility, and statistical power over traditional bacteria monitoring methods such as heterotrophic plate counts.[11] Bacteria staining techniques aimed at assessing viability are now commonly applied to distinguish intact from membrane compromised bacteria [10]. Total and viable bacteria levels have been enumerated via FCM in various water types (Table 5.1). Total bacteria reductions of about 2-logs have been reported across conventional wastewater treatment,[16,17] whereas a microfiltration unit process in a water reclamation facility can remove over 5-logs.[18]

Table 5.1 Microorganism concentrations measured by FCM/FVM in water samples that are relevant for potable reuse.

Sample type	Bacteria		Viruses (counts/ml)
	Total (counts/ml)	Viable (counts/ml)	
Surface water	~10^6 [12,50]	~10^6 [51]	No data
Groundwater	1 x 10^3 to 5 x 10^6 [12,14,52,53]	~10^5 [54]	No data
Raw wastewater	1.74 to 2 x 10^8 [16,17]	8.4 x 10^7 [17]	3.72 x 10^8 [16]
Primary treated wastewater	~10^8 [16–18]	8.4 x 10^7 [17]	~10^8 [16,18]
Activated sludge	2.24 to 3.3 x 10^9 [16,17]	1.24 to 2.3 x 10^9 [16,17,55]	10^8 to 7.33 x 10^9 [16,41]
Secondary treated wastewater	2.2 x 10^6 to 3.87 x 10^8 [16–18]	1.7 x 10^6 to ~10^8 [16,17]	~10^8 [16,18]
Tertiary treated wastewater (disinfected)	~10^6 [16,18]	~10^6 [16]	~10^8 [16,18]
Microfiltration effluent	≤ 10^2 [18]	No data	7.3 x 10^6 [42]
Reverse osmosis effluent	≤ 10^2 [18]	No data	≤ 10^4 [18]
Finished drinking water	~10^5 [56]	~10^5 [51]	No data

Unlike bacteria monitoring with FCM, measuring total protozoa populations has not been a focused area of research. This may be due to the presence of algae or other detrital material of similar size or fluorescent intensity[19,20] Instead, protozoa FCM research has centered on

quantifying the pathogens *Cryptosporidium spp.* and *Giardia spp.* in water because of their health and regulatory relevance. Depending on the sample matrix, significant concentration steps are required prior to FCM analysis to detect them.[21,22] Future work to address these limitations would help make protozoa monitoring using FCM more realistic as a real-time reuse monitoring strategy.

5.4 Recent applications and advances in the use of FVM for virus detection

5.4.1 Advances in FVM.

Improvements in sample preparation and FVM instrumentation are enabling quantification of total virus populations as well as specific viral strains. Most flow cytometers are unable to differentiate biological particles below approximately 300 nm from the background signal (i.e., noise) of the instrument based solely on light scattering properties[23,24] As a result, virus particles are commonly tagged with fluorescent dyes via antibodies, fluorescent proteins, or nucleic acid stains to facilitate detection. Even when stained or tagged, however, virus particle signals are at or near the background signals of some flow cytometers. The background signal arises from the optical, fluidic, and electronic components of the flow cytometer. Increased laser wattage, use of photomultiplier tubes (PMTs) or digital focusing systems (DFS) in place of photodiode detectors, filtration of sheath fluid used during sample analysis, decreased internal chamber size, and continual instrument cleaning are all strategies to help reduce background signals for improved nanoparticle detection.[25,26] The difficult in distinguishing a single virus particle from multiple virus particles in one FVM event[27] can be addressed via sample dilution [28], slower flow rates (< 1000 events per second),[29] or smaller internal chamber size [25]. Building on these advances, the field of medical virology has conclusively demonstrated the utility of FVM to detect specific virus particles, including HIV-1,[30,31] T4 and lambda phage,[32] HSV-1,[33] Junin virus,[34] and filoviruses.[35]

These studies have used specialized flow cytometers with stringent controls to ensure accuracy in distinguishing viral populations.

5.4.2 Application of FVM to environmental samples.

Applications of FVM in medical virology tend to concentrate on the detection and characterization of targeted virus species. Antibody-based fluorescent tagging therefore provides advantages in these applications due to its specificity. Environmental FVM studies, on the other hand, have typically focused on the enumeration of total virus particles. Here, nucleic acid staining is more applicable than antibody tagging because it theoretically targets all viruses in the sample. In reality, FVM fluorescence signals observed following nucleic acid staining are not consistent among viruses with variable genome types, genome sizes, and capsid structures.

In terms of environmental measurement, FVM has been used most extensively in marine biology for the enumeration of native marine virus populations stained with nucleic acid dyes.[28,36–38] FVM research in the marine biology setting has almost exclusively relied on dyes from the SYBR family. These are newer dyes with lower intrinsic fluorescence and improved nucleic acid signals compared to older dyes (e.g., DAPI; Table 5.2). SYTO, TOTO, and YOYO dyes, also newer dyes commonly employed by the medical virology field, are avoided in marine biology because they lose their binding affinity in samples with high ionic strength.[39,40] These dyes have yet to be explored with viruses in freshwater samples. Prior to analysis, marine virus samples are often pretreated with fixation, heat, and flash-freezing to improve virus particle fluorescence signals.

Table 5.2 Properties of nucleic acid stains and reference FCM studies that have used the specified stains for different analyses.

Fluorescence Dye	Quantum Yield	Fluorescence absorption/emission maxima (nm)	Examples of use in FCM
Traditional dyes			
Ethidium Bromide (EB)	0.14 (DNA)[57]	518/605[58]	Bacteria viability & enumeration[59]
4′,6-diamidino-2-phenylindole (DAPI)	0.34 (DNA)[58]	358/461[58]	Bacteria enumeration[60]
Hoechst Family			
Hoechst 33342	0.38 (DNA)[58]	350/461[58]	Bacteria enumeration[60]
Enhanced dyes			
PicoGreen	0.53 (dsDNA), 0.42 (RNA)[61]	500/523[61]	Virus enumeration[39]
SYBR Family			
SYBR Gold	0.7 (DNA, RNA)[62]	495/537[62]	Virus enumeration[37] Virus/bacteria enumeration[18]
SYBR Green I (SGI)	0.8 (DNA), 0.4 (RNA)[40]	494/521[40]	Virus enumeration[28,63] Bacteria viability & enumeration[17,55,64] Virus/bacteria enumeration[16]
SYBR Green II (SGII)	0.36 (DNA), 0.54 (RNA)[40]	494/521[40]	Virus enumeration[41]
SYTO Family			
SYTO 9	0.60 (DNA), 0.2 (RNA)[40]	480/500[40]	Bacteria sorting[65] Bacteria viability[66]
SYTO 13	0.4 (DNA), 0.4 (RNA)[40]	488-491/509-514[40]	Bacteria sorting[65,67] Virus sorting[33,68]
TOTO Family			
TOTO-1	0.34 (DNA)[58]	514/531[58]	Bacteria diversity[69]
YOYO Family			

YOYO-1	0.52 (DNA)[58]	491/509[58]	Virus sorting[34] Virus enumeration[39]

5.4.3 FVM for water quality monitoring.

Water quality and water treatment researchers have drawn from procedures used in marine biology to enumerate total virus populations in wastewater and reclaimed water samples.[16,18,41,42] Overall, various combinations of SYBR Gold, SYBR Green I, and SYBR Green II have been employed, and pretreatments include sample flash-freezing, heating and incubation, and fixation.[16,41,42] In complex samples like wastewater, an additional virus disaggregation step, such as Tween 80 and sodium pyrophosphate pretreatment can improve virus enumeration.[41] An ultrasonication pretreatment step did not improve enumeration in activated sludge samples[16,41] but did improve virus particle counts in settled wastewater samples.[16]

FVM has been used to measure virus concentrations and removal rates for a range of treatment technologies in wastewater and water reuse systems (Table 5.1). No significant reduction in virus concentrations were observed through traditional wastewater processes via FVM.[16,18] Of note, total detectable virus concentrations were reduced by over 4-logs through the microfiltration process of a reclamation facility in a recent study employing FVM.[18] Reductions through the subsequent reverse osmosis unit processes were not measurable because the detection limit of the method had been reached.[18] In the same study, over 4-logs of total detectable virus particles were removed through a membrane bioreactor process. At this point, infective and non-infective viral fractions have not been differentiated with FVM.

5.4.4 Methodological challenges in FVM for water quality monitoring.

A number of challenges must be addressed before the utilization of FVM for water quality monitoring can be fully realized. One primary challenge is in confirming that all or most virus particles are actually being measured by FVM (i.e., avoiding false negatives). This is particularly difficult when enumerating virus particles with small genomes or single stranded genomes (e.g., ssRNA or ssDNA), which tend to emit smaller fluorescence signals. Studies often use transmission electron microscopy and/or epifluorescence microscopy to confirm total virus particle counts obtained by FVM.[16,41,42] Spike additions of pure virus stocks into sample matrices are also critical to verify that the FVM method can effectively quantify the virus populations of interest. For example, Brown et al.[41] measured total virus particle counts in samples with and without spike additions of T4 coliphage to assess recovery in activated sludge samples. Realizing the diversity of potential virus targets, we propose future studies spike virus cocktails, consisting of several different viruses, into samples to more accurately characterize the impacts of genome and structure type and size on recoveries.

Another significant challenge is minimizing false positives. These can be caused by cytometer background noise,[28] particles that autofluoresce (e.g., colloids),[43] and biological particles that fluoresce when stained (e.g., microvesicles, gene transfer agents, or extracellular DNA).[44] To address background noise of the machine, filtered and autoclaved samples are typically run through the cytometer and subtracted from stained samples.[41,42] Measuring the same sample before and after staining can help identify particles that are not virus particles. For biological samples, DNAse treatments have been used with limited success to reduce the likelihood of detecting free DNA.[41] Chloroform treatment of samples prior to the addition of DNAse could also prove

beneficial by releasing membrane-associated nucleic acids from biological particles that may otherwise results in false positives (e.g., microvesicles, gene-transfer agents).

5.5 Our vision of FCM in wastewater reuse applications

Based on previous work in FCM for water monitoring, we envision at least three major applications of flow cytometry in the water reuse setting (Figure 5.1). First, we believe FCM will become an important near-real time surrogate measurement for validating log reduction values through physical treatment processes (e.g., filtration, sedimentation). Specifically, reductions of groups of particles with certain fluorescence properties could be used to represent the removal of microorganisms with the same FCM properties. For example, if flow cytometer measurements show a 99% reduction in detectable virus-like particles across a unit process, then 2-log virus reduction will be granted for enteric viruses. Before this is feasible, research will need to establish whether reductions measured with FCM correlate with actual virus removal. As an example of our proposed approach, the 4-log total virus removal measured by Huang et al.[18] through microfiltration with FVM is similar to virus removal that has been achieved through microfiltration,[45] although microfiltration virus removal has been highly variable (i.e., 0 to >5-log removal[46]). Where this approach can be applied in the reuse scheme will depend on detection methods for the particular cytometer and native virus particle concentrations. A wide range of FVM detection limits has been reported in various matrices, from 80 to 10^4 particles/ml.[16,18,31] Beyond viruses, we imagine similar approaches could be made for bacteria and protozoa reductions across unit processes.

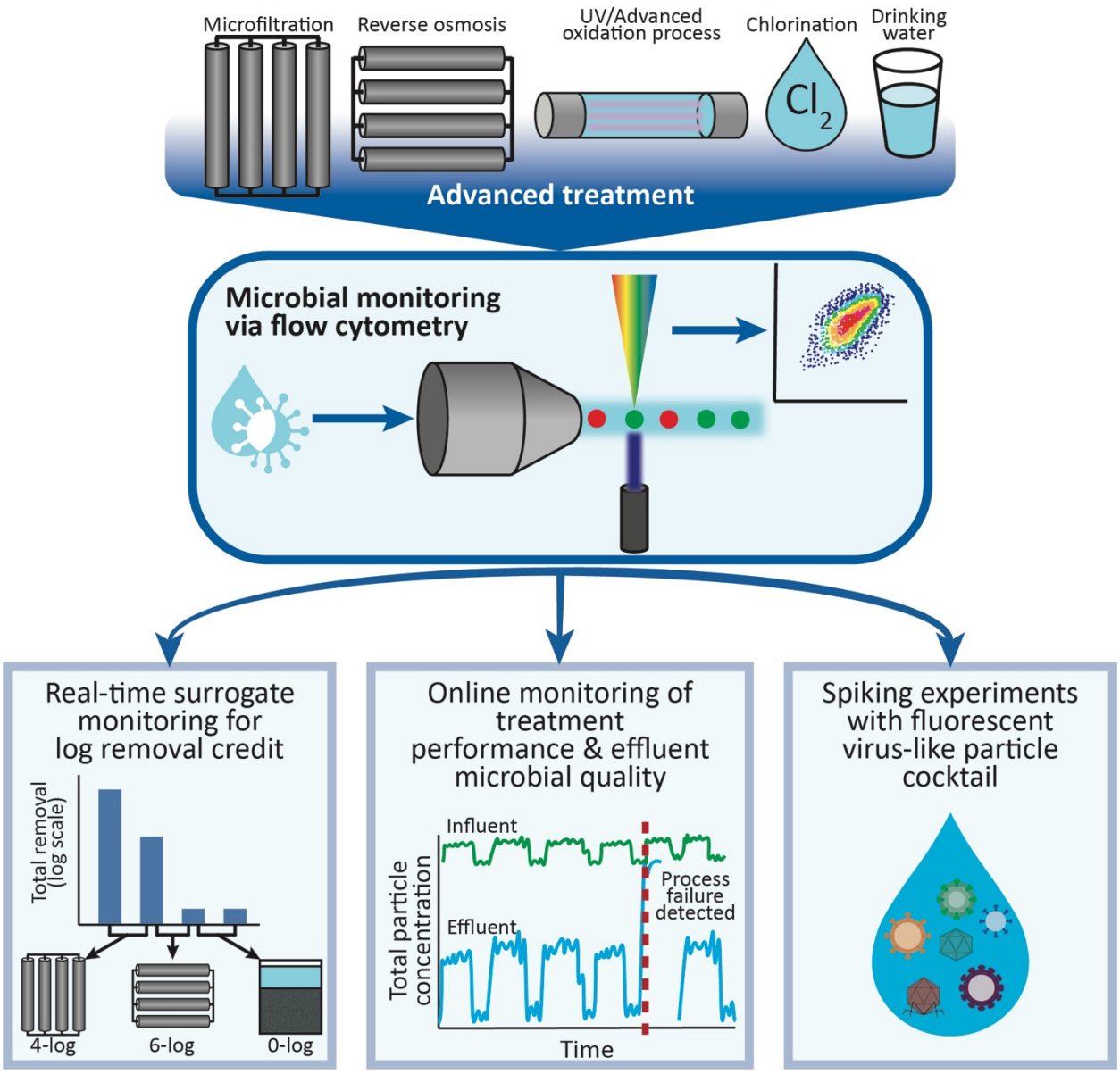

Figure 5.1 Three potential applications of FCM in an example advanced water treatment scheme. In the first application, log removal credits are maintained through unit processes by real-time particle monitoring. In the second application, online influent and effluent FCM monitoring detects aberrations in water quality and system performance. In the third application, cocktails of noninfective fluorescent viruses are added to water samples before unit processes to characterize virus removal.

We also envision using FCM to continuously monitor particles of a certain size or fluorescence to help inform operators of changes in treatment plant influent or effluent quality. For example, potable reuse effluent could be continuously measured with FCM and trends in particle size

distributions, fluorescence characteristics, or particle concentrations could be correlated with overall system performance. Aberrations in the FCM data would thus serve as an immediate warning for failures in the treatment train. This is similar to using turbidity measurements to detect changes in water quality, but FCM would provide more relevant and extensive information related to microbial water quality. Future research at actual plants should study how variations in FCM "fingerprints" correlate with other indices used to assess influent water quality or overall treatment train performance.

Finally, we see FCM as a powerful tool for improved virus removal studies at the bench- and pilot-scale level. Currently, bench-scale and pilot-scale assessments of unit processes involve spiking in one or two surrogate viruses and measuring removal with culture-based methods. These studies are not only time consuming, but the selected surrogate viruses do not represent the behavior of all viruses of interest in water.[47] An alternative approach measures the reduction in spiked fluorescent latex bead concentrations,[46] but these particles have little in common with virus particles. Instead, we propose using cocktails of bacteriophages of various sizes and genome types with stained nucleic acids that are readily detected by FVM for bench-scale and pilot-scale assessment. Alternatively, lab-synthesized virus-like particles identical to a variety of human pathogens in structure but containing nontoxic fluorescent tags instead of nucleic acids can be used as a cocktail for spiking experiments.[48] In either manner, the virus cocktails could be utilized to directly and rapidly measure virus log removals in pilot scale systems with FVM. An exciting application of the virus-like particle spike cocktail is in assessing pathogenic virus reductions through biological treatment processes, which often also involve physical particle removal. Biological treatment likely propagates bacteriophage and thus increases total virus concentrations in treated water while pathogenic virus concentrations are concurrently decreasing. Therefore,

measuring background total virus concentrations before and after biological processes by FVM would not provide an accurate assessment of pathogenic virus removal. Adding fluorescent virus particles that do not replicate could alleviate these issues and enable the accurate measurement of physical virus removal in unit processes where virus propagation occurs.

5.6 Conclusions and future implications

We envision that FCM will revolutionize how microbial monitoring is conducted through potable reuse, especially for virus detection. To bring this vision towards reality, research should compare instrument performance with different virus particle sizes of variable genome types (i.e., ssDNA, dsDNA, ssRNA, dsRNA) and assess fluorescence stains already employed in other applications. This research should be conducted in real waters with a range of characteristics, spanning from untreated municipal wastewater to finished reclaimed drinking water. Techniques should be developed that differentiate infective and noninfective virus particles with FVM, particularly as virus particles are inactivated through disinfection unit processes. A potential method for distinguishing infective virus particles could include the use of enzymatic pretreatment[49] to eliminate fluorescence from virus particles with degraded capsids. Research is also necessary to establish relationships between total particle concentrations measured with FCM and pathogenic microorganism concentrations. Finally, FVM monitoring should be studied through bench-scale unit processes, followed by testing at the pilot-scale, and should ultimately be applied in full-scale systems with automated monitoring.

5.7 References

(1) Trussell, R. R.; Salveson, A.; Snyder, S. A.; Trussell, R. S.; Gerrity, D.; Pecson, B. *Potable Reuse: State of the Science Report and Equivalency Criteria for Treatment Trains*; Alexandria, VA, 2013.

(2) Gerrity, D.; Gamage, S.; Jones, D.; Korshin, G. V; Lee, Y.; Pisarenko, A.; Trenholm, R. A.; von Gunten, U.; Wert, E. C.; Snyder, S. A. Development of Surrogate Correlation Models to Predict Trace Organic Contaminant Oxidation and Microbial Inactivation during Ozonation. *Water Res.* **2012**, *46* (19), 6257–6272. https://doi.org/http://dx.doi.org/10.1016/j.watres.2012.08.037.

(3) National Research Council. *Water Reuse: Potential for Expanding the Nation's Water Supply Through Reuse of Municipal Wastewater*; 2012.

(4) California Department of Public Health. Title 22 and 17 California Code of Regulations. 2015.

(5) Texas Water Development Board. Final Report - Direct Potable Reuse. **2015**.

(6) EPHC MHNRC and NRMMC. Australian Guidelines for Water Recycling - Augmentation of Drinking Water Supplies. **2008**.

(7) Pype, M.-L.; Lawrence, M. G.; Keller, J.; Gernjak, W. Reverse Osmosis Integrity Monitoring in Water Reuse: The Challenge to Verify Virus Removal – A Review. *Water Res.* **2016**, *98*, 384–395. https://doi.org/http://dx.doi.org/10.1016/j.watres.2016.04.040.

(8) World Health Organization. Potable Reuse: Guidance for Producing Safe Drinking-Water. **2017**.

(9) Shapiro, H. M. *Practical Flow Cytometry*, Fourth Edi.; Joh Wiley & Sons, Inc.: Hoboken, New Jersey, 2003.

(10) Wang, Y.; Hammes, F.; De Roy, K.; Verstraete, W.; Boon, N. Past, Present and Future Applications of Flow Cytometry in Aquatic Microbiology. *Trends Biotechnol.* **2010**, *28* (8), 416–424. https://doi.org/10.1016/j.tibtech.2010.04.006.

(11) Van Nevel, S.; Koetzsch, S.; Proctor, C. R.; Besmer, M. D.; Prest, E. I.; Vrouwenvelder, J. S.; Knezev, A.; Boon, N.; Hammes, F. Flow Cytometric Bacterial Cell Counts Challenge Conventional Heterotrophic Plate Counts for Routine Microbiological Drinking Water Monitoring. *Water Res.* **2017**, *113*, 191–206. https://doi.org/https://doi.org/10.1016/j.watres.2017.01.065.

(12) Hammes, F.; Broger, T.; Weilenmann, H.-U.; Vital, M.; Helbing, J.; Bosshart, U.; Huber, P.; Peter Odermatt, R.; Sonnleitner, B. Development and Laboratory-Scale Testing of a Fully Automated Online Flow Cytometer for Drinking Water Analysis. *Cytom. Part A* **2012**, *81A* (6), 508–516. https://doi.org/10.1002/cyto.a.22048.

(13) Brognaux, A.; Han, S.; Sørensen, S. J.; Lebeau, F.; Thonart, P.; Delvigne, F. A Low-Cost, Multiplexable, Automated Flow Cytometry Procedure for the Characterization of Microbial Stress Dynamics in Bioreactors. *Microb. Cell Fact.* **2013**, *12* (OCTOBER 2013), 100. https://doi.org/10.1186/1475-2859-12-100.

(14) Besmer, M. D.; Hammes, F. Short-Term Microbial Dynamics in a Drinking Water Plant Treating Groundwater with Occasional High Microbial Loads. *Water Res.* **2016**, *107*, 11–18. https://doi.org/https://doi.org/10.1016/j.watres.2016.10.041.

(15) Besmer, M. D.; Epting, J.; Page, R. M.; Sigrist, J. A.; Huggenberger, P.; Hammes, F. Online

Flow Cytometry Reveals Microbial Dynamics Influenced by Concurrent Natural and Operational Events in Groundwater Used for Drinking Water Treatment. *Sci. Rep.* **2016**, *6*, 38462.

(16) Ma, L.; Mao, G.; Liu, J.; Yu, H.; Gao, G.; Wang, Y. Rapid Quantification of Bacteria and Viruses in Influent, Settled Water, Activated Sludge and Effluent from a Wastewater Treatment Plant Using Flow Cytometry. *Water Sci. Technol.* **2013**, *68* (8), 1763 LP – 1769.

(17) Foladori, P.; Bruni, L.; Tamburini, S.; Ziglio, G. Direct Quantification of Bacterial Biomass in Influent, Effluent and Activated Sludge of Wastewater Treatment Plants by Using Flow Cytometry. *Water Res.* **2010**, *44* (13), 3807–3818. https://doi.org/http://dx.doi.org/10.1016/j.watres.2010.04.027.

(18) Huang, X.; Zhao, Z.; Hernandez, D.; Jiang, C. S. Near Real-Time Flow Cytometry Monitoring of Bacterial and Viral Removal Efficiencies during Water Reclamation Processes. *Water*. 2016. https://doi.org/10.3390/w8100464.

(19) Keserue, H.-A.; Füchslin, H. P.; Wittwer, M.; Nguyen-Viet, H.; Nguyen, T. T.; Surinkul, N.; Koottatep, T.; Schürch, N.; Egli, T. Comparison of Rapid Methods for Detection of Giardia Spp. and Cryptosporidium Spp. (Oo)Cysts Using Transportable Instrumentation in a Field Deployment. *Environ. Sci. Technol.* **2012**, *46* (16), 8952–8959. https://doi.org/10.1021/es301974m.

(20) Keserue, H.-A.; Füchslin, H. P.; Egli, T. Rapid Detection and Enumeration of Giardia Lamblia Cysts in Water Samples by Immunomagnetic Separation and Flow Cytometric Analysis. *Appl. Environ. Microbiol.* **2011**, *77* (15), 5420–5427. https://doi.org/10.1128/AEM.00416-11.

(21) Vesey, G.; Hutton, P.; Champion, A.; Ashbolt, N.; Williams, K. L.; Warton, A.; Veal, D. Application of Flow Cytometric Methods for the Routine Detection of Cryptosporidium and Giardia in Water. *Cytometry* **1994**, *16* (1), 1–6. https://doi.org/10.1002/cyto.990160102.

(22) Ferrari, B. C.; Veal, D. Analysis-Only Detection of Giardia by Combining Immunomagnetic Separation and Two-Color Flow Cytometry. *Cytometry. A* **2003**, *51* (2), 79–86. https://doi.org/10.1002/cyto.a.10009.

(23) Chandler, W. L. Measurement of Microvesicle Levels in Human Blood Using Flow Cytometry. *Cytom. Part B Clin. Cytom.* **2016**, *90* (4), 326–336. https://doi.org/10.1002/cyto.b.21343.

(24) van der Pol, E.; Hoekstra, A. G.; Sturk, A.; Otto, C.; van Leeuwen, T. G.; Nieuwland, R. Optical and Non-Optical Methods for Detection and Characterization of Microparticles and Exosomes. *J. Thromb. Haemost.* **2010**, *8* (12), 2596–2607. https://doi.org/10.1111/j.1538-7836.2010.04074.x.

(25) Lippé, R. Flow Virometry: A Powerful Tool To Functionally Characterize Viruses. *J. Virol.* **2018**, *92* (3).

(26) Lacroix, R.; Robert, S.; Poncelet, P.; Dignat-George, F. Overcoming Limitations of Microparticle Measurement by Flow Cytometry. *Semin. Thromb. Hemost.* **2010**, *36* (8), 807–818. https://doi.org/10.1055/s-0030-1267034.

(27) Van Der POL, E.; Van GEMERT, M. J. C.; STURK, A.; NIEUWLAND, R.; Van LEEUWEN, T. G. Single vs. Swarm Detection of Microparticles and Exosomes by Flow Cytometry. *J. Thromb. Haemost.* **2012**, *10* (5), 919–930. https://doi.org/10.1111/j.1538-7836.2012.04683.x.

(28) Marie, D.; Brussaard, C. P. D.; Thyrhaug, R.; Bratbak, G.; Vaulot, D. Enumeration of Marine Viruses in Culture and Natural Samples by Flow Cytometry. *Appl. Environ. Microbiol.* **1999**, *65* (1), 45–52.

(29) Zamora, J. L. R.; Aguilar, H. C. Flow Virometry as a Tool to Study Viruses. *Methods* **2018**, *134–135*, 87–97. https://doi.org/https://doi.org/10.1016/j.ymeth.2017.12.011.

(30) Arakelyan, A.; Fitzgerald, W.; Margolis, L.; Grivel, J.-C. Nanoparticle-Based Flow Virometry for the Analysis of Individual Virions. *J. Clin. Invest.* **2013**, *123* (9), 3716–3727. https://doi.org/10.1172/JCI67042.

(31) Bonar, M. M.; Tilton, J. C. High Sensitivity Detection and Sorting of Infectious Human Immunodeficiency Virus (HIV-1) Particles by Flow Virometry. *Virology* **2017**, *505*, 80–90. https://doi.org/10.1016/j.virol.2017.02.016.

(32) Allen, L. Z.; Ishoey, T.; Novotny, M. A.; McLean, J. S.; Lasken, R. S.; Williamson, S. J. Single Virus Genomics: A New Tool for Virus Discovery. *PLoS One* **2011**, *6* (3), e17722.

(33) El Bilali, N.; Duron, J.; Gingras, D.; Lippé, R. Quantitative Evaluation of Protein Heterogeneity within Herpes Simplex Virus 1 Particles. *J. Virol.* **2017**, *91* (10).

(34) Gaudin, R.; Barteneva, N. S. Sorting of Small Infectious Virus Particles by Flow Virometry Reveals Distinct Infectivity Profiles. *Nat Commun* **2015**, *6*.

(35) Rossi, C. A.; Kearney, B. J.; Olschner, S. P.; Williams, P. L.; Robinson, C. G.; Heinrich, M. L.; Zovanyi, A. M.; Ingram, M. F.; Norwood, D. A.; Schoepp, R. J. Evaluation of ViroCyt(®) Virus Counter for Rapid Filovirus Quantitation. *Viruses* **2015**, *7* (3), 857–872. https://doi.org/10.3390/v7030857.

(36) Brussaard, C. P. D. Optimization of Procedures for Counting Viruses by Flow Cytometry.

Appl. Environ. Microbiol. **2004**, *70* (3), 1506–1513. https://doi.org/10.1128/AEM.70.3.1506-1513.2004.

(37) Chen, F.; Lu, J.; Binder, B. J.; Liu, Y.; Hodson, R. E. Application of Digital Image Analysis and Flow Cytometry To Enumerate Marine Viruses Stained with SYBR Gold. *Appl. Environ. Microbiol.* **2001**, *67* (2), 539–545.

(38) Maat, D. S.; van Bleijswijk, J. D. L.; Witte, H. J.; Brussaard, C. P. D. Virus Production in Phosphorus-Limited Micromonas Pusilla Stimulated by a Supply of Naturally Low Concentrations of Different Phosphorus Sources, Far into the Lytic Cycle. *FEMS Microbiol. Ecol.* **2016**, *92* (9), fiw136–fiw136.

(39) Marie, D.; Vaulot, D.; Partensky, F. Application of the Novel Nucleic Acid Dyes YOYO-1, YO-PRO-1, and PicoGreen for Flow Cytometric Analysis of Marine Prokaryotes. *Appl. Environ. Microbiol.* **1996**, *62* (5), 1649 LP – 1655.

(40) Lebaron, P.; Parthuisot, N.; Catala, P. Comparison of Blue Nucleic Acid Dyes for Flow Cytometric Enumeration of Bacteria in Aquatic Systems. *Appl. Environ. Microbiol.* **1998**, *64* (5), 1725 LP – 1730.

(41) Brown, M. R.; Camézuli, S.; Davenport, R. J.; Petelenz-Kurdziel, E.; Øvreås, L.; Curtis, T. P. Flow Cytometric Quantification of Viruses in Activated Sludge. *Water Res.* **2015**, *68*, 414–422. https://doi.org/10.1016/j.watres.2014.10.018.

(42) Huang, X.; Min, J. H.; Lu, W.; Jaktar, K.; Yu, C.; Jiang, S. C. Evaluation of Methods for Reverse Osmosis Membrane Integrity Monitoring for Wastewater Reuse. *J. Water Process Eng.* **2015**, *7*, 161–168. https://doi.org/http://dx.doi.org/10.1016/j.jwpe.2015.05.001.

(43) Abzazou, T.; Salvadó, H.; Bruguera-Casamada, C.; Simón, P.; Lardín, C.; Araujo, M. R.

Assessment of Total Bacterial Cells in Extended Aeration Activated Sludge Plants Using Flow Cytometry as a Microbial Monitoring Tool. *Environ. Sci. Pollut. Res.* **2015**, *22* (15), 11446–11455. https://doi.org/10.1007/s11356-015-4372-3.

(44) Forterre, P.; Soler, N.; Krupovic, M.; Marguet, E.; Ackermann, H.-W. Fake Virus Particles Generated by Fluorescence Microscopy. *Trends Microbiol.* **2013**, *21* (1), 1–5. https://doi.org/http://dx.doi.org/10.1016/j.tim.2012.10.005.

(45) Francy, D. S.; Stelzer, E. A.; Bushon, R. N.; Brady, A. M. G.; Williston, A. G.; Riddell, K. R.; Borchardt, M. A.; Spencer, S. K.; Gellner, T. M. Comparative Effectiveness of Membrane Bioreactors, Conventional Secondary Treatment, and Chlorine and UV Disinfection to Remove Microorganisms from Municipal Wastewaters. *Water Res.* **2012**, *46* (13), 4164–4178. https://doi.org/https://doi.org/10.1016/j.watres.2012.04.044.

(46) Antony, A.; Blackbeard, J.; Leslie, G. Removal Efficiency and Integrity Monitoring Techniques for Virus Removal by Membrane Processes. *Crit. Rev. Environ. Sci. Technol.* **2012**, *42* (9), 891–933. https://doi.org/10.1080/10643389.2011.556539.

(47) Gerba, C. P.; Betancourt, W. Q. Viral Aggregation: Impact on Virus Behavior in the Environment. *Environ. Sci. Technol.* **2017**, *51* (13), 7318–7325. https://doi.org/10.1021/acs.est.6b05835.

(48) Aumiller, W. M.; Uchida, M.; Douglas, T. Protein Cage Assembly across Multiple Length Scales. *Chem. Soc. Rev.* **2018**, *47* (10), 3433–3469. https://doi.org/10.1039/C7CS00818J.

(49) Nuanualsuwan, S.; Cliver, D. O. Pretreatment to Avoid Positive RT-PCR Results with Inactivated Viruses. *J. Virol. Methods* **2002**, *104* (2), 217–225. https://doi.org/https://doi.org/10.1016/S0166-0934(02)00089-7.

(50) Hammes, F.; Berney, M.; Wang, Y.; Vital, M.; Köster, O.; Egli, T. Flow-Cytometric Total Bacterial Cell Counts as a Descriptive Microbiological Parameter for Drinking Water Treatment Processes. *Water Res.* **2008**, *42* (1–2), 269–277. https://doi.org/10.1016/j.watres.2007.07.009.

(51) Lautenschlager, K.; Hwang, C.; Ling, F.; Liu, W.-T.; Boon, N.; Köster, O.; Egli, T.; Hammes, F. Abundance and Composition of Indigenous Bacterial Communities in a Multi-Step Biofiltration-Based Drinking Water Treatment Plant. *Water Res.* **2014**, *62*, 40–52. https://doi.org/http://dx.doi.org/10.1016/j.watres.2014.05.035.

(52) Sinreich, M.; Pronk, M.; Kozel, R. Microbiological Monitoring and Classification of Karst Springs. *Environ. Earth Sci.* **2014**, *71* (2), 563–572. https://doi.org/10.1007/s12665-013-2508-7.

(53) Wang, Y.; Hammes, F.; Egli, T. The Impact of Industrial-Scale Cartridge Filtration on the Native Microbial Communities from Groundwater. *Water Res.* **2008**, *42* (16), 4319–4326. https://doi.org/https://doi.org/10.1016/j.watres.2008.07.027.

(54) Nescerecka, A.; Juhna, T.; Hammes, F. Identifying the Underlying Causes of Biological Instability in a Full-Scale Drinking Water Supply System. *Water Res.* **2018**, *135*, 11–21. https://doi.org/https://doi.org/10.1016/j.watres.2018.02.006.

(55) Ziglio, G.; Andreottola, G.; Barbesti, S.; Boschetti, G.; Bruni, L.; Foladori, P.; Villa, R. Assessment of Activated Sludge Viability with Flow Cytometry. *Water Res.* **2002**, *36* (2), 460–468. https://doi.org/10.1016/S0043-1354(01)00228-7.

(56) Prest, E. I.; Hammes, F.; Kötzsch, S.; van Loosdrecht, M. C. M.; Vrouwenvelder, J. S. Monitoring Microbiological Changes in Drinking Water Systems Using a Fast and

Reproducible Flow Cytometric Method. *Water Res.* **2013**, *47* (19), 7131–7142. https://doi.org/10.1016/j.watres.2013.07.051.

(57) Le Pecq, J.-B. Use of Ethidium Bromide for Separation and Determination of Nucleic Acids of Various Conformational Forms and Measurement of Their Associated Enzymes. *Methods of Biochemical Analysis*. October 31, 2006. https://doi.org/doi:10.1002/9780470110393.ch2.

(58) Sabnis, R. W. *Handbook of Fluorescent Dyes and Probes*; John Wiley & Sons, Inc.: Hoboken, N.J., 2015.

(59) Jernaes, M. W.; Steen, H. B. Staining of Escherichia Coli for Flow Cytometry: Influx and Efflux of Ethidium Bromide. *Cytometry* **1994**, *17* (4), 302–309. https://doi.org/10.1002/cyto.990170405.

(60) Monger, B. C.; Landry, M. R. Flow Cytometric Analysis of Marine Bacteria with Hoechst 33342. *Appl. Environ. Microbiol.* **1993**, *59* (3), 905 LP – 911.

(61) Singer, V. L.; Jones, L. J.; Yue, S. T.; Haugland, R. P. Characterization of PicoGreen Reagent and Development of a Fluorescence-Based Solution Assay for Double-Stranded DNA Quantitation. *Anal. Biochem.* **1997**, *249* (2), 228–238. https://doi.org/https://doi.org/10.1006/abio.1997.2177.

(62) Tuma, R. S.; Beaudet, M. P.; Jin, X.; Jones, L. J.; Cheung, C.-Y.; Yue, S.; Singer, V. L. Characterization of SYBR Gold Nucleic Acid Gel Stain: A Dye Optimized for Use with 300-Nm Ultraviolet Transilluminators. *Anal. Biochem.* **1999**, *268* (2), 278–288. https://doi.org/https://doi.org/10.1006/abio.1998.3067.

(63) Brussaard, C. P. D.; Payet, J. P.; Winter, C.; Weinbauer, M. G. Quantification of Aquatic

Viruses by Flow Cytometry. *Man. Aquat. Mar. Ecol.* **2010**, 102–109.

(64) Nescerecka, A.; Hammes, F.; Juhna, T. A Pipeline for Developing and Testing Staining Protocols for Flow Cytometry, Demonstrated with SYBR Green I and Propidium Iodide Viability Staining. *J. Microbiol. Methods* **2016**, *131*, 172–180. https://doi.org/http://dx.doi.org/10.1016/j.mimet.2016.10.022.

(65) Ben-Amor, K.; Heilig, H.; Smidt, H.; Vaughan, E. E.; Abee, T.; de Vos, W. M. Genetic Diversity of Viable, Injured, and Dead Fecal Bacteria Assessed by Fluorescence-Activated Cell Sorting and 16S RRNA Gene Analysis. *Appl. Environ. Microbiol.* **2005**, *71* (8), 4679–4689. https://doi.org/10.1128/AEM.71.8.4679-4689.2005.

(66) Allegra, S.; Berger, F.; Berthelot, P.; Grattard, F.; Pozzetto, B.; Riffard, S. Use of Flow Cytometry to Monitor Legionella Viability. *Appl. Environ. Microbiol.* **2008**, *74* (24), 7813–7816. https://doi.org/10.1128/AEM.01364-08.

(67) Servais, P.; Courties, C.; Lebaron, P.; Troussellier, M. Coupling Bacterial Activity Measurements with Cell Sorting by Flow Cytometry. *Microb. Ecol.* **1999**, *38* (2), 180–189.

(68) Loret, S.; El Bilali, N.; Lippe, R. Analysis of Herpes Simplex Virus Type I Nuclear Particles by Flow Cytometry. *Cytometry. A* **2012**, *81* (11), 950–959. https://doi.org/10.1002/cyto.a.22107.

(69) Li, W. K. W.; Jellett, J. F.; Dickie, P. M. DNA Distributions in Planktonic Bacteria Stained with TOTO or TO-PRO. *Limnol. Oceanogr.* **1995**, *40* (8), 1485–1495. https://doi.org/10.4319/lo.1995.40.8.1485.

Chapter 6

Flow Virometry in Environmental Matrices: Instrument Detection Capabilities Limit Our Ability to Accurately Enumerate Viruses with Small Genomes

Nicole Rockey,[1] Kate Harrison,[1] Kaitlyn Chin,[1] Lutgarde Raskin,[1] Krista R. Wigginton[*,1]

[1]Department of Civil & Environmental Engineering, University of Michigan, Ann Arbor, MI

6.1 Abstract

To validate the effective removal of viruses through water reuse treatment systems, real-time monitoring of each treatment process is required. Surrogates that are easy to measure before and after a treatment, such as turbidity, are used for this purpose. However, the lack of sensitivity in currently applied real-time virus monitoring approaches means that water reuse treatment trains are likely overengineered for virus removal. Flow cytometric detection of viruses, termed flow virometry (FVM), is gaining popularity as a rapid approach for quantifying or characterizing virus particles in the microbiology, medical, marine biology, and environmental engineering fields. While FVM is a promising method for use in water treatment virus monitoring, virus detection capabilities of high sensitivity flow cytometers are not well-characterized. In this study, we evaluate the ability of a high sensitivity flow cytometer to detect viruses with different genome types (e.g., large dsDNA genomes, small (+) ssRNA genomes) and conduct proof-of-concept experiments to evaluate FVM's ability to accurately measure virus reductions through bench-scale physical treatment processes. Our findings establish that only bacteriophage T4, a dsDNA virus

with a large genome, was detected with the cytometer after nucleic acid staining. All other viruses were below or within the background noise of the instrument. FVM was able to accurately measure up to ~ 4.5-$\log_{10}$ T4 reductions through ultrafiltration, while turbidity was only reduced by 0.5-$\log_{10}$. However, FVM measurement of native virus populations in secondary wastewater effluent yielded no significant improvement in monitoring sensitivity over turbidity measurements. These findings indicate that in its current form, FVM cannot accurately detect virus reductions for the virus populations native to relevant water matrices and is therefore not a practical real-time monitoring approach. Improvements in cytometer technologies will eventually allow for detection of viruses with smaller genomes, and as this happens, FVM should be re-assessed as a real-time monitoring option.

6.2 Introduction

Waterborne viruses pose an acute risk to human health.[1] To mitigate the risk of exposure to these viruses in water supplies, a multi-barrier approach to water treatment is used, in which numerous unit processes are placed in series to cumulatively reduce infectious virus levels to an acceptable level. The low concentrations of viral pathogens allowed in finished water (i.e., $< 1 \times 10^{-7}$ viruses/L [2]) makes ascertaining treatment performance by direct pathogen quantification infeasible. Real-time monitoring of unit processes in the water treatment field is therefore used to ensure that unit processes are performing as expected.[2] This approach is particularly important in the direct potable reuse (DPR) field, where the source water for treatment is wastewater and may contain elevated enteric virus concentrations.

Many currently used monitoring strategies in water reuse scenarios underestimate virus removal, particularly through physical treatment processes (e.g., ultrafiltration, reverse osmosis). This is because the surrogate parameters used for real-time monitoring through physical treatments are

not sensitive enough to demonstrate the full extent of log_{10} virus reductions that occur. As a result, even when a treatment is known to achieve a certain amount of log_{10} virus reduction, it will only be allotted the reductions observed by the surrogate parameter. For example, ultrafiltration research at the bench-scale has established > 5-log_{10} virus removal through treatment,[3,4] however commonly used unit process surrogates (e.g., turbidity, pressure decay test) cannot detect virus-sized membrane breaches in the treatment process.[5,6] This means that typically no virus removal is allotted for ultrafiltration. The lack of sensitive surrogate parameters for real-time monitoring leads to overengineered treatment trains for virus removal. Innovative new monitoring methods have the capability of transforming how virus removal is allotted through physical treatment processes. One promising approach is flow virometry (FVM), a high-throughput method that uses flow cytometers for virus detection.[7]

Cytometers employ powerful lasers and state-of-the-art fluidics to rapidly and sensitively analyze particles.[8] Advances in cytometer instrumentation have allowed for the detection of smaller biological particles, including some viruses.[9–17] FVM is an invaluable tool in the virology field, where it is used to rapidly analyze virus particles for various purposes, including vaccine development, virus isolation, and virus structure characterization.[14,18,19] Virology studies using FVM often employ antibodies specific to a viral protein[12,19–21] or fluorescently labeled proteins[22] to increase the virus signal and accurately detect a particular virus. In contrast, FVM research in the marine and environmental microbiology fields generally seeks to enumerate total virus populations in water samples.[11,23–28] In these studies, water samples are usually stained with a nucleic acid dye to boost the virus signal prior to FVM analysis.

FVM offers various advantages over traditional virus enumeration techniques (e.g., transmission electron microscopy, fluorescence microscopy), which are hindered by slow throughput and

quantification biases. Yet many current FVM methods push the limits of cytometer capabilities. Approaches to FVM in the environmental microbiology field are inconsistent, and questions remain regarding the feasibility of reliably detecting virus particles.[29,30] While many environmental studies have attempted to optimize FVM sample preparation and analysis, results from these experiments often identified different optimized protocols.[11,24,26] This is likely due to dissimilarities in sample types, cytometer capabilities, and measurement strategies. These distinctions, although important to address, are not typically highlighted. To more consistently monitor virus concentrations in complex environmental matrices, the limitations and capabilities of FVM methods must first be clearly characterized and better understood. For instance, while some studies use highly sensitive flow cytometers (e.g., LSR Fortessa, BioRad ZE5) with powerful lasers (> 100 mW), others use standard benchtop cytometers (e.g., BD Accuri C6) with much reduced laser wattage (~ 20 mW) and no voltage adjustment capabilities. These cytometer differences can manifest in detection disparities, allowing sensitive cytometers to successfully detect more of the virus signal, while less sensitive instruments may not be able to discriminate viruses from the instrument background. Even when using a highly sensitive flow cytometer for analysis, the voltage and threshold settings used can significantly impact the instrument's detection abilities.

Another important consideration with FVM is which virus classes can effectively be detected. In environmental matrices, a wide range of viruses have been identified.[31,32] Flow cytometric analysis of biological particles is typically conducted by using controls, including stained and unstained samples, to determine which regions of a cytometer plot confidently characterize particles of interest. In bacterial and mammalian cell FCM, the cell populations of interest generally have a sufficiently large signal so that the background noise is excluded from analysis. As shown in past

work,[10,17,33] viruses with large genomes stained with nucleic acid dyes have a sufficient fluorescence signal to be separated from the background signal, and in this scenario the traditional approach of gating the population of interest is possible to determine accurate virus concentrations. When biological particles are much smaller, however, the particle signal may be within the signal of the background noise or possibly even below the background noise signal. This is likely the case for many viruses, which range in size from ~ 5 – 300 nm and can have genomes as small as ~ 1.9 kilobases.[34] Some custom-built cytometers can separate the light scattering signal of many smaller viruses[9,35] from the background signal due to improved fluidics and laser power. However, this is likely not feasible for the high sensitivity cytometers currently on the market, which may not be able to separate all or even most viruses from the instrument background noise.

Most environmental FVM studies to date have taken the traditional approach of eliminating background noise from sample analysis, but this may result in a significant underestimation of total virus concentrations. Given the limited detection capabilities of cytometers at present, additional approaches for improving virus detection should be considered. Regardless of whether FVM is capable of detecting natural virus populations present in water matrices, FVM may still prove a useful real-time surrogate parameter for virus removal. Past work has observed 1 – 4-$\log_{10}$ reduction in the FVM signal through microfiltration,[24,25] but more information about how well FVM signal reductions correlate with simultaneous infectious virus removal through the same treatment is needed.

In this study, we undertook experiments to identify the combination of fluorescent dye, dilution solution, and flow cytometer settings that would result in accurate virus counts while maintaining low background noise levels using a large dsDNA virus, T4 bacteriophage. We also assessed the FVM signatures of a range of different bacteriophages, including T4, T3, phi6, phiX174, and MS2

(Table 6.1), to confirm which virus types are likely to be enumerated using a high sensitivity flow cytometer.

Table 6.1 The structural and molecular characteristics of the bacteriophages used in this study.

Bacteriophage	Family	Nucleic acid type	Nucleic acid size (kb or kbp)	Capsid (nm)
T4	*Myoviridae*	dsDNA, linear	~ 169	~ 90 x 200
T3	*Autographiviridae*	dsDNA, linear	~ 38	~ 60
phi6	*Cystoviridae*	dsRNA, segmented	~ 13.4	~ 85
phiX174	*Microviridae*	ssDNA, circular	~ 5.4	~ 30
MS2	*Leviviridae*	(+) ssRNA, linear	~ 3.6	27

kb = kilobases; kbp = kilobase pairs.

Ultimately, we assessed how well FVM counts correlate with viruses in water treatment scenarios compared to already established real-time monitoring approaches (e.g., turbidity). This work sheds light on the capabilities of high sensitivity flow cytometers for virus detection and enumeration. Our proof-of-concept analysis has implications for the application of FVM as a real-time monitoring tool in water treatment settings.

6.3 Materials and Methods

6.3.1 Virus propagation and purification.

Bacteriophages T4, T3, phi6, phiX174, and MS2 were included in this work to provide a range of different virus types (Table 6.1). Viruses were purified to allow for the reliable designation of FVM counts as virus particles. All purified virus stocks were kept at 4°C for short-term storage

and -80°C for long-term storage. Infectious bacteriophages were enumerated by plaque assay using the double agar overlay method.[36]

6.3.1.1 Bacteriophage T4.

E. coli ATCC strain 11303 was the host for bacteriophage T4. T4 was propagated using the soft agar overlay method. Propagated virus was purified on a sucrose gradient, which was generated by allowing five layers of 10 – 50% sucrose to linearize overnight at 4°C. 3 mL of T4 stock was overlaid on the linearized gradient and centrifuged at 28,000 rpm for 40 mins at 4°C. The resulting virus band was pulled from the gradient and buffer exchanged > 12x with 1X phosphate buffered saline (PBS) solution (Cat. No. 10010023, Invitrogen) using a 100 kDa ultrafilter (Cat. No. UFC910008, Amicon).

6.3.1.2 Bacteriophage T3.

E. coli ATCC strain 11303 was the host for bacteriophage T3. T3 was propagated using liquid propagation and concentrated by polyethylene glycol (PEG) 8000 (Cat. No. BP2331, Fisher Scientific).[37] The virus stock was purified on a linear sucrose gradient using the same approach as described for T4.

6.3.1.3 Bacteriophage phi6.

Bacteriophage phi6 and its host *P. syringae* pv phaseolicola were kindly provided by Dr. L. Marr (Virginia Tech). phi6 was propagated as previously described.[38] Following liquid propagation and filtration through a 0.22 μm polyethersulfone (PES) membrane (Cat. No. 229747, CELLTreat) to remove cell debris, the propagated virus stock was enriched and purified using a sucrose cushion. Specifically, 28 mL of propagated virus lysate was overlaid on 5 mL of 30% sucrose and run at 24,000 rpm for 1.5 hr at 4°C. The pellet was washed one time with 1X PBS and suspended in ~ 4

mL 1X PBS. The virus stock was further purified using a sucrose gradient. 3 mL of sucrose cushion purified phi6 was overlaid on a sucrose gradient generated by allowing five layers of 10 – 50% sucrose to linearize overnight at 4°C. The gradient was centrifuged at 22,000 rpm for 1.5 hr at 4°C, and the resulting band was extracted. The phi6 stock was buffer exchanged with > 12 volumes of 1X PBS through a 100 kDa Amicon ultrafiltration unit.

6.3.1.4 Bacteriophage phiX174.

Bacteriophage phiX174 and its host *E. coli* ATCC 13706 were kindly provided by Dr. C. Gerba (University of Arizona). phiX174 propagation was conducted by the soft agar overlay method, as previously described.[39] phiX174 was enriched and purified using a sucrose cushion, according to the same conditions described for bacteriophage phi6.

6.3.1.5 Bacteriophage MS2.

E. coli ATCC strain 15597 was the host for bacteriophage MS2. MS2 was propagated by liquid propagation and concentrated through PEG as previously described.[40] Propagated MS2 stocks were further purified by sucrose gradient (linear gradient resulting from five layers of 10 – 30% sucrose). 3 mL of propagated MS2 was laid over the linear gradient and centrifuged for 3 hours at 30,000 rpm at 4°C. The resulting band was collected and buffer exchanged with > 12 volumes 1X PBS by ultrafiltration through a 100 kDa Amicon filter.

6.3.2 FVM sample preparation.

Purified viruses were spiked into dilution solutions in 4 mL polyethylene sterile tubes (Cat. No. 352063, Corning) for FVM analysis. All samples were subjected to 0.5% glutaraldehyde fixation, vortexed, and incubated at 4°C for 15 min in the dark. Samples were then stained with fluorescent dyes, vortexed, and incubated at 80°C for 10 min in the dark. Following sample preparation,

samples were immediately placed on ice and kept in the dark until FVM analysis. Various dilution solutions and fluorescent dyes were used for sample preparation optimization.

6.3.2.1 Dilution solutions.

1X PBS, 0.2 µm filtered 1X PBS using a PES membrane, autoclaved 1X PBS, and 0.2 µm filtered and autoclaved 1X PBS were used to determine which dilution solution provides the clearest virus populations while not increasing background noise significantly.

6.3.2.2 Fluorescent dyes.

Samples were stained with the nucleic acid stains SYBR Green I (SGI), SYBR Green II (SGII), and SYBR Gold (SG) to final concentrations of 0.5x or 1x and with SYTO 11 to final concentrations of 1 or 2 µM.

6.3.3 FVM analysis.

We used the BioRad ZE5 flow cytometer for all FVM work. The cytometer was equipped with 100 mW 488 and 405 nm argon lasers. Voltages on the 488 nm laser were set to 600, 500, 530, 700, 700, and 700 nm for the FSC, SSC, 529 nm, 549 nm, 615 nm, and 692 nm filters, respectively. The FSC detector with small particle detector on the 405 nm laser was set to a voltage of 600. Events were set to trigger on 529 nm fluorescence channel, with a threshold of 0.03%. Sheath fluid was distilled water filtered in-line through a 0.04 µm membrane. 10 µL of each sample was run using volumetric intake at a medium flow rate (i.e., 1 µL s^{-1}). Samples were prepared so that viruses passed through the cytometer at < 1000 events s^{-1} to avoid coincident events. During analysis, the BioRad ZE5 sample chamber was kept at 4°C.

When excess background noise was detected prior to sample analysis, 30 µL of 10% bleach was run at high flow, followed by 1X PBS samples to ensure that counts were consistent from sample

to sample. This process was repeated until five consecutive 1X PBS samples displayed similar counts. In between each sample, 10 µL of a detergent (Contrad) was run at high flow, followed by 30 µL of sterile 1X PBS run at high flow. Counts from the 1X PBS were continuously monitored to ensure no unexpected spike in counts from background noise. When a spike in counts from background noise was detected, the sample results were not used in analysis. All FVM results were analyzed using FCS Express (De Novo Software).

6.3.4 Evaluation of enumeration methods through membrane filtration.

Secondary wastewater effluent from the Ann Arbor Wastewater Treatment Plant was collected and stored at 4°C until use in experiments. Purified viruses were spiked into 0.45 µm PES (Cat. No. 229771, CELLTreat) filtered secondary wastewater effluent samples to a 10% final concentration, mixed gently by inversion, and kept at 4°C for 10 minutes before filtration experiments. Spiked secondary wastewater effluent samples were passed through 0.2 µm PVDF membranes (Cat. No. 09-720-3, FisherBrand) and 0.02 µm inorganic membranes (Cat. No. WHA68091002, Whatman) to assess the correlation of FVM data with virus removal through microfiltration and ultrafiltration, respectively. The filters were wetted with virus spiked solution before filtrate collection to avoid introduction of filter-associated particles in FVM measurements.

6.3.4.1 Other surrogate measurements.

Turbidity was measured before and after treatment of 0.45 µm filtered secondary wastewater effluent through ultrafiltration and microfiltration. A 2100N Hach turbidimeter (Hach) was used for turbidity measurements.

6.3.5 Statistical analyses.

All statistical analyses were conducted in R version 4.0.0.[41] Figures were generated in Prism version 8.4.2 and in FCS Express.

6.4 Results and Discussion

6.4.1 Dilution solutions.

We determined whether one type of dilution solution was significantly better or worse than another. To this end, we evaluated several variations of buffer solution stained with SGI at a 0.5x final concentration. No significant differences were found between the counts obtained with different dilution solutions (paired t-test, all $p > 0.05$), suggesting that no components of certain solutions contributed more or less to background noise.

The limit of detection of the instrument when analyzing 10 μL of sample at a flow rate of 1 μL/second was estimated to be ~ 6 x 10^4 counts/mL (additional details provided in Appendix D).

6.4.2 SGI stain provides optimal virus fluorescence in the 529 nm channel, but SG provides elevated signal in 549 nm channel.

We stained T4 bacteriophage with four different nucleic acid stains (i.e., SG, SGI, SGII, and S11) at variable concentrations to determine which stain was best for improving the virus fluorescence signal while not adding so much background that the virus signal was overtaken. The T4 bacteriophage signal in the 529 nm fluorescence channel was distinguishable from the background noise for all nucleic acid stains and concentrations tested, however the fluorescence intensity of the T4 signal differed (Figure 6.1 and Table 6.2). We also tested the 549 nm fluorescence channel, because the nucleic acid stains used exhibit a range of peak emission wavelengths,[30] and use of

this channel could result in improved virus fluorescence signal. Indeed, the 549 nm fluorescence channel offered an increased T4 signal for several of the dyes, particularly for SG. This is not surprising, because SG has a right skewed emission spectrum with peak emission at 537 nm, which lies between the 529 nm and 549 nm bandpass filters on our BioRad ZE5 instrument. While the 529 nm fluorescence channel is commonly used in FVM work using nucleic acid stains,[29,42,43] our findings indicate the importance of evaluating detection in several channels when possible to ensure the optimal settings are used for sensitive virus detection.

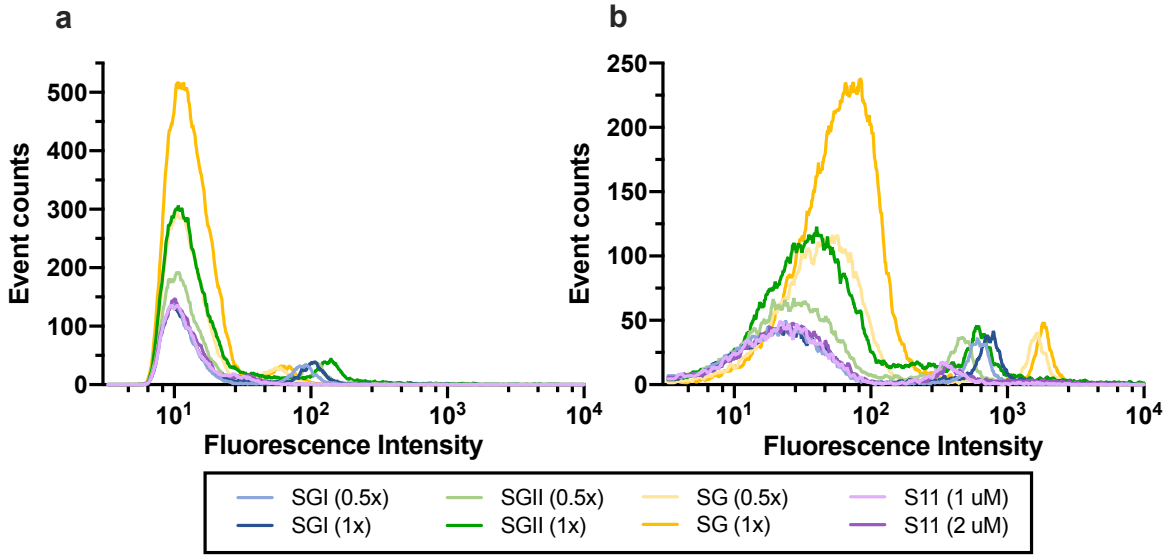

Figure 6.1 Event counts and fluorescence intensity resulting from FVM analysis of T4 bacteriophage in 1X PBS solution stained with SGI, SGII, SG, and SYTO 1, where events were captured using (a) the 529 nm fluorescence channel or (b) the 549 nm fluorescence channel.

The total T4 bacteriophage population enumerated via FVM yielded statistically similar counts for most stains, with only the SYTO 11 dye at a 2 μM concentration resulting in significantly less counts than the SGI, SGII, and SG stains at all concentrations (Table 6.2 and Table D.1). This reduction in counts is likely due to the minimal separation between the background and T4 signal with SYTO 11 dye that may result in uncounted T4 viruses.

Table 6.2 Summary of T4 stain experiments, including the T4 concentration, signal-to-noise ratio, and stain index for each stain evaluated in the 529 nm and 549 nm fluorescence channels during FVM analysis.

Stain (concentration)	T4 concentration (pfu/mL)[a]	529 nm fluorescence channel			549 nm fluorescence channel		
		T4 concentration (counts/mL)[a]	Signal-to-noise Ratio[b]	Stain Index[c]	T4 concentration (counts/mL)[a]	Signal-to-noise Ratio[b]	Stain Index[c]
SGI (0.5x)	$2.8 \times 10^4 \pm 8.8 \times 10^3$	$1.5 \times 10^5 \pm 4.7 \times 10^3$	7.87	11.7	$1.5 \times 10^5 \pm 3.6 \times 10^3$	25.0	17.3
SGI (1x)	$2.8 \times 10^4 \pm 8.8 \times 10^3$	$1.5 \times 10^5 \pm 2.7 \times 10^3$	9.42	15.5	$1.5 \times 10^5 \pm 7.9 \times 10^3$	33.5	24.1
SGII (0.5x)	$2.8 \times 10^4 \pm 8.8 \times 10^3$	$1.8 \times 10^5 \pm 1.9 \times 10^4$	8.32	12.5	$2.0 \times 10^5 \pm 3.1 \times 10^4$	17.4	12.3
SGII (1x)	$2.8 \times 10^4 \pm 8.8 \times 10^3$	$1.9 \times 10^5 \pm 2.4 \times 10^4$	10.5	15.1	$2.2 \times 10^5 \pm 3.5 \times 10^4$	17.8	12.8
SG (0.5x)	$2.8 \times 10^4 \pm 8.8 \times 10^3$	$1.5 \times 10^5 \pm 1.1 \times 10^4$	4.84	6.34	$1.6 \times 10^5 \pm 6.5 \times 10^3$	41.3	32.2
SG (1x)	$2.8 \times 10^4 \pm 8.8 \times 10^3$	$1.6 \times 10^5 \pm 8.7 \times 10^3$	4.48	5.20	$1.7 \times 10^5 \pm 4.7 \times 10^3$	27.1	22.6
SYTO 11 (1 uM)	$2.8 \times 10^4 \pm 8.8 \times 10^3$	$1.0 \times 10^5 \pm 2.8 \times 10^4$	3.30	3.71	$1.2 \times 10^5 \pm 2.6 \times 10^4$	24.7	17.9
SYTO 11 (2 uM)	$2.8 \times 10^4 \pm 8.8 \times 10^3$	$4.8 \times 10^4 \pm 5.9 \times 10^3$	3.21	3.77	$6.1 \times 10^4 \pm 6.0 \times 10^3$	17.9	12.9

[a]Concentrations shown are arithmetic mean ± standard error of three independent replicate FVM samples.

[b]Calculated as the ratio of the median fluorescence intensity of the T4 signal to the median fluorescence intensity of the background signal.

[c]Calculated as the difference between the median fluorescene intensity of the T4 signal and th median fluorescence intensity of the background signal, divided by the spread of the background signal (i.e., 2 x the robust standard deviation).

The signal-to-noise ratio, calculated as the difference in median fluorescence intensity between the T4 population signal and the background signal, was significantly greater for SGI and SGII stains in the 529 nm fluorescence channel compared to the SYTO 11 and SG stains (Table 6.2 and Table D.2). However, when analyzing events in the 549 nm fluorescence channel, SG and SGI had the best signal-to-noise ratios. Past FVM work has identified SGI and SGII as optimal stains, citing increased fluorescence signal compared to SG, although no significant differences in signal were observed.[26,44] Here, we also saw increased signal from T4 stained with SGI compared with SG in the 529 nm fluorescence channel, however when evaluating fluorescence in the 549 nm fluorescence channel SG offered elevated fluorescence.

We also considered the stain index, defined as the difference in T4 signal to background signal divided by the spread of the background noise, to identify which stains provided optimal fluorescence signal with minimal background. The two stains with the highest signal-to-noise ratios and best stain indices, SG and SGI, were used in subsequent analyses.

6.4.3 dsDNA viruses are detectable with FVM but not RNA viruses.

Five bacteriophages were analyzed to evaluate the class of viruses detectable by a sensitive cytometer. Using traditional FVM analysis approaches, no virus signals except that of T4 were completely distinguishable from the background noise signal (Table 6.2 and Figure D.1). Analysis of the viruses stained with SG at 0.5x final concentration revealed that a portion of the T3 signal was separated from the background signal in the 549 nm fluorescence channel, although the counts are much reduced from the total expected count (Figure 6.2). This could be because a portion of the T3 signal is in the background noise. Our results are in line with other studies that have not been able to separate small DNA or RNA viruses from instrument background.[29,44] However, work using a BD Accuri C6 cytometer indicated that MS2 bacteriophage was effectively enumerated via FVM.[24] Here, we were unable to detect an MS2 signal from the background signal of the instrument, despite using a more powerful laser. This discrepancy could be due to the fact that unclean samples were used in that work, so although infectious MS2 concentrations correlated with FVM counts, it is possible that those FVM counts were not in fact enumerated MS2 viral particles.

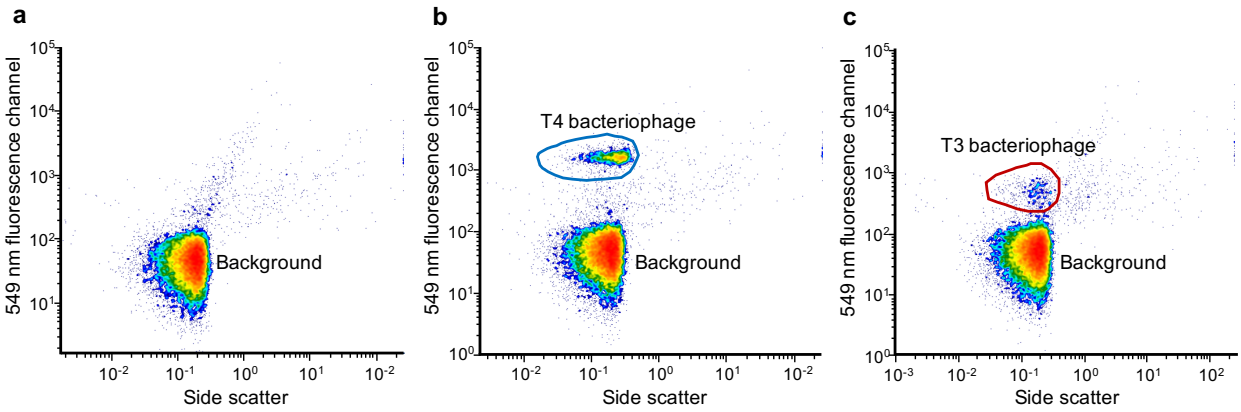

Figure 6.2 FVM analysis of (a) 1X PBS stained with 0.5x SG, (b) T4 in 1X PBS stained with 0.5x SG, and (c) T3 in 1X PBS stained with 0.5x SG in the 549 nm fluorescence channel. Side scatter area and 549 nm

fluorescence channel area are used on the axes. Heat map indicates highest event concentrations in red and lowest concentrations in blue.

The inability to quantify most virus types using the traditional approach to FVM analysis led us to evaluate an alternative approach in which we allowed a portion of the background noise in our analysis. The stained blank sample was run with the stained virus sample, and the counts from the blank samples were subtracted from the virus sample to determine the total virus particle counts in the sample. This approach requires that instrument background signal be consistent from sample to sample. We evaluated whether this was true for our purified virus solutions by enumerating T4 using both of the described approaches to FVM analysis. Our results using SGI and SG at 0.5x final concentrations demonstrate that the total counts subtraction approach over and underestimated true T4 virus counts in the sample, depending on the replicate (Table D.3). On average, the subtraction approach for samples stained with SGI or SG at 0.5x concentration resulted in ~ 0.1% or ~ 32% error from true counts, respectively. These findings suggest that SGI may provide the most accurate counts when using the subtraction approach to FVM analysis.

Ultimately, we evaluated if smaller viruses with less of a fluorescence signal could reliably be enumerated using the alternative approach to FVM analysis. The fluorescent signatures of all five bacteriophages (Table 6.1) were assessed using SGI and SG at 0.5x final concentrations. SGI stained samples revealed accurate counts for the T4 population but counts below detection for T3, phi6, phiX174, and MS2 (Table D.4). SG, in contrast, resulted in increased counts in the virus samples for all five bacteriophages (Table D.4). However, T4 counts in these samples using the total counts subtraction approach were overestimated compared to using the traditional FVM analysis approach (average percent error ~ 94%, n = 2), suggesting that increased FVM counts in the other virus samples may not be enumerating true virus particles. In addition, standard error of

two independent replicates was nearly as large as FVM counts themselves, suggesting a significant degree of variability in FVM counts when analyzing SG stained samples using the FVM subtraction approach. Additional replicates should be conducted with SG-stained virus samples to ensure that the elevated counts observed were indeed virus counts.

6.4.4 Proof-of-concept application of real-time FVM monitoring.

While our results suggest only large dsDNA viruses are separable from FVM background noise, FVM still provides potential as a sensitive real-time monitoring approach to verify $\log_{10}$ virus reduction through water treatment processes. We spiked bacteriophages T4 and T3 into secondary wastewater effluent and filtered samples through microfiltration and ultrafiltration. Our results show that FVM counts of the T4 population correlate better with infectious T4 removal through microfiltration and ultrafiltration than do turbidity measurements (Figure 6.3). Specifically, infectious T4 levels through ultrafiltration were reduced by greater than 5-$\log_{10}$, and FVM demonstrated ~ 4.5-$\log_{10}$ reduction, while turbidity was reduced by less than 1-$\log_{10}$. Reductions in infectious T4 titers were minimal through microfiltration, and this is reflected with both FVM and turbidity.

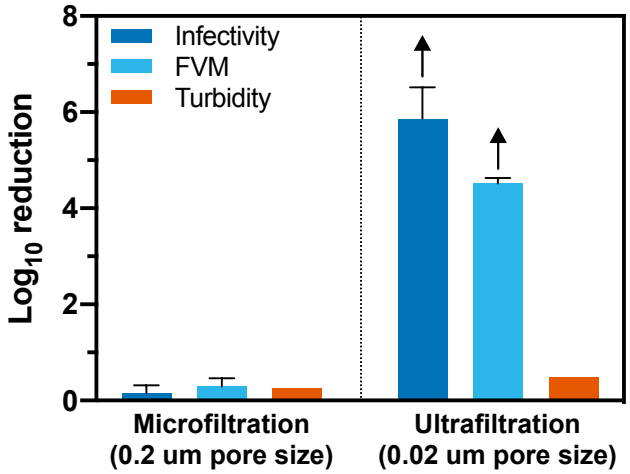

Figure 6.3 Log_{10} reduction of bacteriophage T4 infectivity, bacteriophage T4 FVM counts, and turbidity through microfiltration and ultrafiltration membranes. The samples subjected to microfiltration and ultrafiltration consisted of bacteriophage T4 spiked into secondary wastewater effluent at a 1:10 final concentration (~5 x 10^9 pfu/mL). Error bars represent the standard error of two independent replicates. Arrows above bars indicate log_{10} reductions beyond detection limits.

We also evaluated removal of T3 bacteriophage suspended in secondary wastewater effluent through membrane treatments using the subtraction approach to FVM analysis. While infectious T3 levels were reduced by over 7-log_{10}, only 2.5-log_{10} reductions could be detected via FVM (Figure D.2). A similar trend was observed using secondary wastewater effluent; only 0.5-log_{10} reduction of FVM counts resulted through ultrafiltration. In both T3-spiked samples and secondary effluent samples, increased FVM background noise was observed, which likely overwhelmed the true reduction in signal resulting from virus particles. Future analyses should raise the fluorescence threshold to decrease the background signal and in turn increase the signal of the virus population.

6.4.5 Conclusions.

This research focuses on the capabilities of FVM analysis using a high sensitivity flow cytometer. Here, we identify that while most stains evaluated provide similar counts of a large dsDNA virus, bacteriophage T4, SG provided an increased fluorescence signal when FVM analysis was conducted using the 549 nm fluorescence channel. However, this increased sensitivity from staining with SG also resulted in increased counts in background noise. The increased noise led to greater variability in counts from sample to sample, making it difficult to obtain consistently accurate virus counts. As a result, preliminary work using five different bacteriophages stained with SG at 0.5x final concentration suggested that small DNA and RNA viruses were measurable with this approach, however large variability in counts meant that additional replicates are needed before concluding which viruses were truly detected.

The proof-of-concept work using bench-scale physical removal processes demonstrated that FVM was capable of accurately monitoring virus removal of T4, a dsDNA virus with a large genome. Unfortunately, the FVM approach was unable to accurately measure virus removal for viruses with smaller genomes. In fact, FVM showed no improvement over turbidity in measuring reductions of native virus populations in wastewater effluent through ultrafiltration or microfiltration. This indicates that in its current form, FVM is not a practical option for real-time monitoring of virus removal through water treatment systems. Despite our current findings for viruses with small genomes, the fact that FVM could accurately detect T4 populations indicates that this monitoring approach could be applied in the future as cytometer technologies improve for detection of smaller particles. In addition, staining technologies and other advances in this area can work to make the detection of viruses with small RNA or DNA genomes a reality. It is important to note that our work was conducted at the bench-scale using spiked solutions of viruses. Future work in this area should focus on assessing FVM as a monitoring tool through more realistic bench-scale or pilot-scale systems.

6.5 References

(1) World Heatlh Organization. *Guidelines for Drinking-Water Quality*; Geneva, 2017.

(2) Trussell, R. R.; Salveson, A.; Snyder, S. A.; Trussell, R. S.; Gerrity, D.; Pecson, B. *Potable Reuse: State of the Science Report and Equivalency Criteria for Treatment Trains*; Alexandria, VA, 2013.

(3) Jacangelo, J. G.; Madec, A.; Schwab, K. J.; Huffman, D. E.; Mysore, C. S. Advances in the Use of Low-Pressure, Hollow Fiber Membranes for the Disinfection of Water. *Water Supply* **2005**, *5* (5), 109–115. https://doi.org/10.2166/ws.2005.0045.

(4) Antony, A.; Blackbeard, J.; Leslie, G. Removal Efficiency and Integrity Monitoring Techniques for Virus Removal by Membrane Processes. *Crit. Rev. Environ. Sci. Technol.* **2012**, *42* (9), 891–933. https://doi.org/10.1080/10643389.2011.556539.

(5) U.S. Environmental Protection Agency. *Membrane Filtration Guidance Manual*; 2005.

(6) World Health Organization. Potable Reuse: Guidance for Producing Safe Drinking-Water. **2017**.

(7) Lippé, R. Flow Virometry: A Powerful Tool To Functionally Characterize Viruses. *J. Virol.* **2018**, *92* (3).

(8) Shapiro, H. M. *Practical Flow Cytometry*, Fourth Edi.; Joh Wiley & Sons, Inc.: Hoboken, New Jersey, 2003.

(9) Hercher, M.; Mueller, W.; Shapiro, H. M. Detection and Discrimination of Individual Viruses by Flow Cytometry. *J. Histochem. Cytochem.* **1979**, *27* (1), 350–352. https://doi.org/10.1177/27.1.374599.

(10) Steen, H. B. Flow Cytometer for Measurement of the Light Scattering of Viral and Other Submicroscopic Particles. *Cytometry. A* **2004**, *57* (2), 94–99. https://doi.org/10.1002/cyto.a.10115.

(11) Brussaard, C. P. D.; Payet, J. P.; Winter, C.; Weinbauer, M. G. Quantification of Aquatic Viruses by Flow Cytometry. *Man. Aquat. Mar. Ecol.* **2010**, 102–109.

(12) Gaudin, R.; Barteneva, N. S. Sorting of Small Infectious Virus Particles by Flow Virometry Reveals Distinct Infectivity Profiles. *Nat Commun* **2015**, *6*.

(13) Bonar, M. M.; Tilton, J. C. High Sensitivity Detection and Sorting of Infectious Human Immunodeficiency Virus (HIV-1) Particles by Flow Virometry. *Virology* **2017**, *505*, 80–90. https://doi.org/10.1016/j.virol.2017.02.016.

(14) Loret, S.; El Bilali, N.; Lippe, R. Analysis of Herpes Simplex Virus Type I Nuclear Particles by Flow Cytometry. *Cytometry. A* **2012**, *81* (11), 950–959. https://doi.org/10.1002/cyto.a.22107.

(15) El Bilali, N.; Duron, J.; Gingras, D.; Lippé, R. Quantitative Evaluation of Protein Heterogeneity within Herpes Simplex Virus 1 Particles. *J. Virol.* **2017**, *91* (10).

(16) Martinez-Hernandez, F.; Fornas, O.; Lluesma Gomez, M.; Bolduc, B.; de la Cruz Peña, M. J.; Martínez, J. M.; Anton, J.; Gasol, J. M.; Rosselli, R.; Rodriguez-Valera, F.; Sullivan, M. B.; Acinas, S. G.; Martinez-Garcia, M. Single-Virus Genomics Reveals Hidden Cosmopolitan and Abundant Viruses. *Nat. Commun.* **2017**, *8*, 15892.

(17) Khalil, J. Y. B.; Langlois, T.; Andreani, J.; Sorraing, J.-M.; Raoult, D.; Camoin, L.; La Scola, B. Flow Cytometry Sorting to Separate Viable Giant Viruses from Amoeba Co-Culture Supernatants. *Front. Cell. Infect. Microbiol.* **2016**, *6*, 202.

https://doi.org/10.3389/fcimb.2016.00202.

(18) Tang, V. A.; Renner, T. M.; Varette, O.; Le Boeuf, F.; Wang, J.; Diallo, J.-S.; Bell, J. C.; Langlois, M.-A. Single-Particle Characterization of Oncolytic Vaccinia Virus by Flow Virometry. *Vaccine* **2016**, *34* (42), 5082–5089. https://doi.org/https://doi.org/10.1016/j.vaccine.2016.08.074.

(19) Zicari, S.; Arakelyan, A.; Fitzgerald, W.; Zaitseva, E.; Chernomordik, L. V; Margolis, L.; Grivel, J.-C. Evaluation of the Maturation of Individual Dengue Virions with Flow Virometry. *Virology* **2016**, *488*, 20–27. https://doi.org/http://dx.doi.org/10.1016/j.virol.2015.10.021.

(20) Arakelyan, A.; Fitzgerald, W.; Margolis, L.; Grivel, J.-C. Nanoparticle-Based Flow Virometry for the Analysis of Individual Virions. *J. Clin. Invest.* **2013**, *123* (9), 3716–3727. https://doi.org/10.1172/JCI67042.

(21) Landowski, M.; Dabundo, J.; Liu, Q.; Nicola, A. V; Aguilar, H. C. Nipah Virion Entry Kinetics, Composition, and Conformational Changes Determined by Enzymatic Virus-Like Particles and New Flow Virometry Tools. *J. Virol.* **2014**, *88* (24), 14197–14206. https://doi.org/10.1128/JVI.01632-14.

(22) Renner, T. M.; Tang, V. A.; Burger, D.; Langlois, M.-A. Intact Viral Particle Counts Measured by Flow Virometry Provide Insight into the Infectivity and Genome Packaging Efficiency of Moloney Murine Leukemia Virus. *J. Virol.* **2020**, *94* (2), e01600-19. https://doi.org/10.1128/JVI.01600-19.

(23) Marie, D.; Partensky, F.; Vaulot, D.; Brussaard, C. Enumeration of Phytoplankton, Bacteria, and Viruses in Marine Samples. *Curr. Protoc. Cytom.* **2001**, *10* (1), 11.11.1-11.11.15.

https://doi.org/10.1002/0471142956.cy1111s10.

(24) Huang, X.; Min, J. H.; Lu, W.; Jaktar, K.; Yu, C.; Jiang, S. C. Evaluation of Methods for Reverse Osmosis Membrane Integrity Monitoring for Wastewater Reuse. *J. Water Process Eng.* **2015**, *7*, 161–168. https://doi.org/http://dx.doi.org/10.1016/j.jwpe.2015.05.001.

(25) Huang, X.; Zhao, Z.; Hernandez, D.; Jiang, C. S. Near Real-Time Flow Cytometry Monitoring of Bacterial and Viral Removal Efficiencies during Water Reclamation Processes. *Water*. 2016. https://doi.org/10.3390/w8100464.

(26) Brown, M. R.; Camézuli, S.; Davenport, R. J.; Petelenz-Kurdziel, E.; Øvreås, L.; Curtis, T. P. Flow Cytometric Quantification of Viruses in Activated Sludge. *Water Res.* **2015**, *68*, 414–422. https://doi.org/10.1016/j.watres.2014.10.018.

(27) Brown, M. R.; Baptista, J. C.; Lunn, M.; Swan, D. L.; Smith, S. J.; Davenport, R. J.; Allen, B. D.; Sloan, W. T.; Curtis, T. P. Coupled Virus - Bacteria Interactions and Ecosystem Function in an Engineered Microbial System. *Water Res.* **2019**, *152*, 264–273. https://doi.org/https://doi.org/10.1016/j.watres.2019.01.003.

(28) Ma, L.; Mao, G.; Liu, J.; Yu, H.; Gao, G.; Wang, Y. Rapid Quantification of Bacteria and Viruses in Influent, Settled Water, Activated Sludge and Effluent from a Wastewater Treatment Plant Using Flow Cytometry. *Water Sci. Technol.* **2013**, *68* (8), 1763 LP – 1769.

(29) Dlusskaya, E. A.; Atrazhev, A. M.; Ashbolt, N. J. Colloid Chemistry Pitfall for Flow Cytometric Enumeration of Viruses in Water. *Water Res. X* **2019**, *2*, 100025. https://doi.org/https://doi.org/10.1016/j.wroa.2019.100025.

(30) Rockey, N.; Bischel, H. N.; Kohn, T.; Pecson, B.; Wigginton, K. R. The Utility of Flow Cytometry for Potable Reuse. *Curr. Opin. Biotechnol.* **2019**, *57*, 42–49.

https://doi.org/https://doi.org/10.1016/j.copbio.2018.12.009.

(31) Adriaenssens, E. M.; Farkas, K.; Harrison, C.; Jones, D. L.; Allison, H. E.; McCarthy, A. J. Viromic Analysis of Wastewater Input to a River Catchment Reveals a Diverse Assemblage of RNA Viruses. *mSystems* **2018**, *3* (3), e00025-18. https://doi.org/10.1128/mSystems.00025-18.

(32) Cantalupo, P. G.; Calgua, B.; Zhao, G.; Hundesa, A.; Wier, A. D.; Katz, J. P.; Grabe, M.; Hendrix, R. W.; Girones, R.; Wang, D.; Pipas, J. M. Raw Sewage Harbors Diverse Viral Populations. *MBio* **2011**, *2* (5).

(33) Brussaard, C. P. D.; Marie, D.; Bratbak, G. Flow Cytometric Detection of Viruses. *J. Virol. Methods* **2000**, *85* (1–2), 175–182. https://doi.org/10.1016/S0166-0934(99)00167-6.

(34) Flint, S. J.; Racaniello, V. R.; Rall, G.; Skalka, A. M.; Enquist, L. W. Foundations. In *Principles of Virology, Volume 1: Molecular Biology*; ASM Press: Washington, D.C., 2015; pp 2–23.

(35) Lian, H.; He, S.; Chen, C.; Yan, X. Flow Cytometric Analysis of Nanoscale Biological Particles and Organelles. *Annu. Rev. Anal. Chem.* **2019**, *12* (1), 389–409. https://doi.org/10.1146/annurev-anchem-061318-115042.

(36) Adams, M. H. *Bacteriophages*; Interscience Publishers: New York, 1959.

(37) Pecson, B. M.; Martin, L. V.; Kohn, T. Quantitative PCR for Determining the Infectivity of Bacteriophage MS2 upon Inactivation by Heat, UV-B Radiation, and Singlet Oxygen: Advantages and Limitations of an Enzymatic Treatment To Reduce False-Positive Results. *Appl. Environ. Microbiol.* **2009**, *75* (17), 5544–5554. https://doi.org/10.1128/AEM.00425-09.

(38) Ye, Y.; Chang, P. H.; Hartert, J.; Wigginton, K. R. Reactivity of Enveloped Virus Genome, Proteins, and Lipids with Free Chlorine and UV254. *Environ. Sci. Technol.* **2018**, *52* (14), 7698–7708. https://doi.org/10.1021/acs.est.8b00824.

(39) Qiao, Z.; Ye, Y.; Chang, P. H.; Thirunarayanan, D.; Wigginton, K. R. Nucleic Acid Photolysis by UV254 and the Impact of Virus Encapsidation. *Environ. Sci. Technol.* **2018**. https://doi.org/10.1021/acs.est.8b02308.

(40) Pecson, B. M.; Martin, L. V.; Kohn, T. Quantitative PCR for Determining the Infectivity of Bacteriophage MS2 upon Inactivation by Heat, UV-B Radiation, and Singlet Oxygen: Advantages and Limitations of an Enzymatic Treatment to Reduce False-Positive Results. *Appl. Environ. Microbiol.* **2009**, *75* (17), 5544–5554. https://doi.org/10.1128/AEM.00425-09.

(41) R Core Team. R: A Language and Environment for Statistical Computing. Vienna, Austria 2020.

(42) Marie, D.; Partensky, F.; Jacquet, S.; Vaulot, D. Enumeration and Cell Cycle Analysis of Natural Populations of Marine Picoplankton by Flow Cytometry Using the Nucleic Acid Stain SYBR Green I. *Appl. Environ. Microbiol.* **1997**, *63* (1), 186–193.

(43) De Corte, D.; Martínez, J. M.; Cretoiu, M. S.; Takaki, Y.; Nunoura, T.; Sintes, E.; Herndl, G. J.; Yokokawa, T. Viral Communities in the Global Deep Ocean Conveyor Belt Assessed by Targeted Viromics. *Front. Microbiol.* **2019**, *10*, 1801. https://doi.org/10.3389/fmicb.2019.01801.

(44) Brussaard, C. P. D. Optimization of Procedures for Counting Viruses by Flow Cytometry. *Appl. Environ. Microbiol.* **2004**, *70* (3), 1506–1513.

https://doi.org/10.1128/AEM.70.3.1506-1513.2004.

Chapter 7

Significance and Future Research Directions

7.1 Overview

The threat of virus persistence in our water supplies must be balanced with concerns of overengineering water treatment systems. These matters are difficult to reconcile when the microbial hazards associated with important enteric viral pathogens are unknown or when their mitigation through treatment cannot be validated. This dissertation was conducted to better understand infectious virus fate through water treatment processes and to improve viral monitoring methods in the water treatment setting. The broad objective of this work is to inform water treatment regulations that will ultimately support the design and implementation of treatment schemes that are cost-effective and sustainable while still protecting public health.

A primary focus of this research was on the use of novel approaches to assess the inactivation of an important enteric viral pathogen, HuNoV, through UV_{254}, a commonly applied disinfection treatment (Chapters 2, 3, and 4). While HuNoV is of principal concern in water settings because of its large burden of gastrointestinal illness,[1] little is known about its fate through treatment processes because of the lack of a readily available culture system. Estimation of HuNoV inactivation using novel computational and molecular approaches demonstrated that HuNoV has similar UV_{254} susceptibility compared to many other enteric (+) ssRNA viruses, such as enteroviruses (Chapters 2 and 3). In contrast, HuNoV was found to be nearly an order of magnitude more sensitive to UV_{254} treatment than enteric viruses within the *Adenoviridae* family. Work using

a culture-based HuNoV infectivity assay (Chapter 4) confirmed the UV_{254} susceptibilities determined via predictive modeling and genome extrapolation approaches. Beyond elucidating the UV_{254} susceptibility of HuNoV, this research developed and validated the use of alternative tools for accurately assessing virus behavior through UV_{254} treatment when traditional approaches are not feasible.

This body of work also centered on developing approaches to accurately and rapidly monitor virus levels through water treatment processes. Many of the surrogate parameters monitored in real-time to confirm adequate performance of treatment are not sufficiently sensitive to validate the true amount of log_{10} virus reduction occurring through a unit process. As highlighted in Chapter 5, flow virometry (FVM) is a promising alternative for real-time validation of virus removal through unit processes. However, many aspects of the technology are not yet standardized and questions remain about detection capabilities. FVM methods development in Chapter 6 indicated that only large dsDNA viruses are entirely separable from the background noise of a high sensitivity flow cytometer, while smaller dsDNA viruses are partially separable using SYBR Gold staining, and small RNA and DNA viruses are within or below the noise of the cytometer. Proof-of-concept experiments (Chapter 6) evaluating bacteriophage T4 removal through microfiltration and ultrafiltration showed that infectious T4 reductions through treatments were much more similar to reductions in FVM counts than turbidity, a common process surrogate. This suggests that FVM shows increased sensitivity over current surrogates in monitoring virus removal through physical removal processes. However, FVM measurements of secondary wastewater effluent through ultrafiltration did not show significant improvements in monitoring native virus concentration reductions as compared to turbidity.

7.2 Implications

This research demonstrated that computational and molecular methods for evaluating infectious virus fate are capable of accurately estimating virus persistence. These tools can be applied when the use of traditional culture-based methods is not feasible. The value of these methods is highlighted by the ongoing COVID-19 pandemic, in which infectious SARS-CoV-2 work has been limited due to biosafety concerns. Application of the predictive model developed in this dissertation indicated the heightened sensitivity of SARS-CoV-2 to UV_{254} and suggested the suitability of UV_{254} as an effective mitigation strategy.

The improved understanding of HuNoV fate through UV_{254} treatment gained through this work is beneficial for evaluating the risk of HuNoV infection in various food and water sources. In particular, the results are useful for the potable reuse field, as the lack of information about HuNoV infectivity through water treatment has resulted in uncertainties about whether treatment schemes are under or overengineered for HuNoV inactivation.[2,3] The findings in this dissertation indicated that UV_{254} is an effective treatment for HuNoV, and that at the 186 mJ cm^{-2} dose required to ensure 4-log_{10} adenovirus removal[4] through UV_{254}, HuNoV is inactivated by well over 20-log_{10}. While this work provides confidence that HuNoV does not exhibit any unique attributes that make it less susceptible to UV_{254} than other enteric (+) ssRNA viruses, future work should evaluate the fate of HuNoV in other disinfection processes to ensure that this trend holds true for other treatment systems.

The FVM work in this dissertation demonstrated that some large DNA viruses can be detected using state-of-the-art flow cytometers. On the other hand, the quantification of smaller RNA and DNA viruses with FVM is not yet a reality. In addition, FVM analysis revealed that tuning of the fluorescence channels, voltages, and thresholds used in detection is critical to obtain optimal

results. Proof-of-concept experiments with physical removal processes for virus removal demonstrated FVM was a more sensitive monitoring approach than traditional surrogates when large dsDNA viruses were being monitored. This finding has significant implications for the water treatment field: if methods like FVM are eventually permitted as real-time monitoring approaches for validating virus removal, treatment schemes could be completely redesigned for virus removal. This could in turn lead to far less conservative treatment systems that are better optimized to protect public health while also more economically treating water supplies. However, the fact that virus reductions in secondary wastewater effluent treated by ultrafiltration could not be measured with FVM indicates that native virus populations in secondary wastewater effluent likely have smaller genomes that are not currently detectable using a high sensitivity flow cytometer. FVM is therefore not a practical approach for real-time monitoring in water reuse at present, although cytometer technology advances may change this.

7.3 Future research directions

This dissertation work resulted in useful approaches to assess virus fate through UV_{254} disinfection. However, the fate of many important pathogens, including HuNoV, is not well-understood through other water treatment processes. To characterize the persistence of emerging or difficult-to-culture viruses through other treatment strategies, future work should expand on the computational and molecular approaches developed here for UV_{254}. One major limitation for the accuracy of these approaches is the need to understand the mechanisms by which viruses are inactivated by these different treatment strategies. For example, predictive models were feasible for UV_{254} disinfection because we understand UV_{254} inactivation mechanisms (i.e., UV_{254} primarily targets the viral genome, and genome repair is possible for dsDNA viruses once inside

the host cell). To this end, more research on the mechanisms driving virus inactivation is needed, and larger data sets incorporating a broad range of viruses are required to inform modeling efforts.

This research demonstrated that the novel enteroid culture system can be used to characterize HuNoV infectivity through treatment processes. Future work using this approach to investigate HuNoV fate in other environmental processes, including in additional water treatment systems and in different water types, will be beneficial for better understanding risks of HuNoV in these settings. However, several limitations of this cell culture system, including its inability to support productive infection of HuNoV from certain stool samples, limit its widespread use in studies of environmental fate. Continued efforts to identify the role of various cofactors and strain-specific determinants in viral pathogenesis will be invaluable for ultimately developing a HuNoV culture system that can selectively grow HuNoV so that the concentration and behavior of native HuNoV populations in environmental matrices can be explored.

FVM monitoring of virus reductions through microfiltration and ultrafiltration was evaluated using hand-held syringe filter membranes. These experiments must be scaled up to bench- or pilot-scale to ensure that the proof-of-concept results presented in this dissertation will hold in more realistic systems. As improvements in flow cytometer capabilities become available, virus detection of smaller DNA and potentially RNA viruses will result. These technologies should continue to be a focus of future research, because once cytometers are sensitive enough to detect the signal of most viruses, monitoring through treatment processes is likely to be significantly improved. While FVM shows promise to measure virus reductions through physical removal processes, FVM monitoring of biological treatment processes may not be preferred, because the growth of certain microorganisms, including bacteriophages, in these processes could result in negligible reductions of FVM counts. Instead, spiking and measurement of fluorescent virus-like particles that can be

detected using FVM analysis but do not grow in biological systems should be investigated for potential use to evaluate the effectiveness of virus removal these processes.

7.4 References

(1) Scallan, E.; Hoekstra, R. M.; Angulo, F. J.; Tauxe, R. V; Widdowson, M.-A.; Roy, S. L.; Jones, J. L.; Griffin, P. M. Foodborne Illness Acquired in the United States—Major Pathogens. *Emerg. Infect. Dis.* **2011**, *17* (1), 7–15. https://doi.org/10.3201/eid1701.P11101.

(2) Soller, J. A.; Eftim, S. E.; Warren, I.; Nappier, S. P. Evaluation of Microbiological Risks Associated with Direct Potable Reuse. *Microb. Risk Anal.* **2016**. https://doi.org/http://dx.doi.org/10.1016/j.mran.2016.08.003.

(3) Gerba, C. P.; Betancourt, W. Q.; Kitajima, M. How Much Reduction of Virus Is Needed for Recycled Water: A Continuous Changing Need for Assessment? *Water Res.* **2017**, *108*, 25–31. https://doi.org/http://dx.doi.org/10.1016/j.watres.2016.11.020.

(4) Hijnen, W. A. M.; Beerendonk, E. F.; Medema, G. J. Inactivation Credit of UV Radiation for Viruses, Bacteria and Protozoan (Oo)Cysts in Water: A Review. *Water Res.* **2006**, *40* (1), 3–22. https://doi.org/https://doi.org/10.1016/j.watres.2005.10.030.

Appendix A

Supplementary Information for Chapter 2

A.1 Supplementary Text

A.1.1 RNase experiments.

RNase experiments were conducted to determine whether extraviral RNA was a component of the HuNoV/MS2 suspensions used for inactivation experiments. RNase experiments were conducted using the same matrix of HuNoV stool suspension and MS2 stock as during UV_{254} inactivation experiments. Triplicate samples with a total volume of 110 μL were treated with RNase ONE Ribonuclease (Promega, Madison, WI) by adding 10 units RNase ONE. This amount of RNase ONE was recommended by the manufacturer to ensure an excess of RNase ONE. Specifically, 10 units of RNase ONE degrade 900,000 ng of total RNA when left in the shaking experimental solution for 15 minutes at 37°C, per the manufacturer's specifications. Quantification of the RNA in the HuNoV/MS2 suspensions using Nanodrop indicates approximately 2,772 ng of ssRNA in the RNase experiment samples, which is over two orders of magnitude less than what could be degraded with the RNase present. While we conducted these checks to ensure no significant amount of extraviral RNA was in experimental solutions, recent research with UV_{254} shows that extraviral and intraviral RNA degrades at the same rate;[1] these results suggest that the presence of extraviral RNA in a sample would not change the observed rate of genome degradation. Untreated triplicate samples were conducted in parallel. Treated and untreated samples were shaken at 37°C for 15 minutes. 1 μL RNasin Inhibitor (Promega) was added to RNase treated samples to inhibit

downstream RNase activity and all samples were subsequently shaken at room temperature for 15 minutes.

Downstream RNA extraction and cDNA synthesis were carried out as described for the HuNoV UV inactivation samples. qPCR was conducted in triplicate (n=3) with the same thermocycling instrument as for HuNoV UV inactivation experiments. A 94 base pair region of cDNA was amplified using the NV107a forward primer (AGCCAATGTTCAGATGGATG)[2] and COG2R reverse primer (TCGACGCCATCTTCATTCACA).[3] 10 µL reactions consisted of 1 µL cDNA template, 1X Fast EvaGreen qPCR Master Mix (Biotium, Inc., Fremont, CA), 0.5 µM forward and reverse primers, and 0.625 mg/ml bovine serum albumin (BSA). Thermocycling conditions included an initial denaturation at 95°C for 10 min, 40 cycles of denaturation (95°C for 20 s), annealing (60°C for 20 s), and extension (72°C for 25 s), and then a final extension step (72°C for 1 min). gBlocks (Integrated DNA Technologies, Coralville, IA) were used as qPCR standards. Each assay contained a standard curve with seven serially diluted standards measured in triplicate and a no-template control. The slope, efficiency, and R^2 of the standard curve were -4.04, 77%, and 0.997, respectively. The sequence of the gBlock standard used is as follows:

> 5’ – CTG ACC GAT ACC TGC TTC GTT GAG AAC TCA AGC CAA TGT TCA GAT GGA TGA GAT TCT CAG ATC TGA GCA CGT GGG AGG GCG ATC GCA ATC TGG CTC CCA GTT TTG TGA ATG AAG ATG GCG TCG ATT TTT CGC TGG ATG CGC TTC CAT GAC CTC GGA TTG TGG ACA GGA GAT CGC GAT CTT CTG CCC GAA TTC GTA AAT GAT GAT GGC GTC TAA GGG CCC ATC ATC TAC TCG CGT CCC TGT GGC TC – 3’

A.1.2 G2SK qPCR sensitivity analysis.

Using the G2SK amplicon to assess HuNoV concentrations through UV_{254} treatment means that amplicon degradation must be sufficient for qPCR to reliably detect a reduction in signal. To establish this level of degradation, sensitivity analyses were conducted with G2SK. Three separate dilution series of G2SK standards (starting at a concentration of ~2 x 10^8 gene copies/mL) were made, in which dilutions were 89%, 78%, 67%, 56%, and 44% of the original concentration. These dilutions were selected to capture the minimum reduction in the target concentration that was statistically significant with the qPCR assay. Each set of dilutions was quantified using qPCR as described for UV_{254} experiments. The initial qPCR concentration was compared to qPCR concentration of dilutions in the series using a paired t-test to establish which dilution resulted in a significant loss of signal (Figure A.7). The starting concentration was significantly different from the 89% dilution ($p = 0.032$). This reduction is a 0.05-log loss in the G2SK amplicon signal, which corresponds to detecting approximately a 1-log reduction of HuNoV calculated using Equation 5.

A.2 Tables

Table A.1 Forward and reverse primer sequences, positions, and amplicon lengths of seven different regions of the coxsackievirus B5 Faulkner genome assessed using qPCR.

Amplicon	Forward Primer (5' to 3')	Reverse Primer (5' to 3')	Position[a]	Size (# bases)	Pyrimidine content	LOQ[b]	Mean slope[c] (min to max)	Mean efficiency[c,d] (min to max)
1	ATGGAAATTGCGGAGTGTT	TCTTGCCTATTTGCGGAATT	272	605	302	35.7	-4.04 (-4.11 to -3.97)	77 (75 to 79)
2	CTACTTGAGGGACGATGAA	TGTCACTGTGATCGGTACAT	1069	613	283	33.8	-3.99 (-4.08 to -3.90)	78 (76 to 81)
3	AGATTGCGGAGGTGGAT	TGACACAAAGCACAAAATCT	1866	512	246	35.5	-4.69 (-4.88 to -4.51)	63 (60 to 67)
4	AGATCCGCATGTGTTTACTACA	TCAAATCTAGCCCATCCATCAT	2654	398	196	33.1	-3.62 (-3.73 to -3.51)	89 (86 to 93)
5	ACTACCGGAGTGTATTTCTGT	TGATTTCTTACCACAATAACCAGT	3470	455	214	35.7	-4.26 (-4.52 to -4.01)	72 (66 to 78)
6	AGAAAGGCATCTTGTTCACTT	AGTTGACCTCAGGAACCAA	4665	513	230	33.7	-4.20 (-4.37 to -4.04)	73 (69 to 77)
7	TTGAGGAGGCCATATTCTCAA	ATCACCGGTATTTTACTCCAAA	6072	511	224	33.1	-4.40 (-4.65 to -4.14)	69 (64 to 74)

[a]Corresponds to nucleotide position of Coxsackievirus B5 Faulkner strain (accession number AF114383.1). [b]Values are given as cycle threshold. [c]Mean slope and efficiency values are the arithmetic mean of all standard curves generated for an assay. The minimum (min) and maximum (max) values of the slope and efficiency are the minimum and maximum values taken from all standard curves generated for an assay. [d]Efficiency is given as a percentage and was calculated according to the following equation: $E = (10^{(-1/slope)} - 1) \times 100\%$. LOQ = Limit of quantification.

Table A.2 Forward and reverse primer sequences, positions, and amplicon lengths of eight different regions of the human norovirus GII.4 Sydney genome assessed using qPCR.

Amplicon	Forward Primer (5' to 3')	Reverse Primer (5' to 3')	Position[a]	Size (# bases)	Pyrimidine content	LOQ[b]	Mean slope[c] (min to max)	Mean efficiency[c,d] (min to max)
1	TTATTGAAATGTGGGATGGAG	CTGCGAAGGTCCAATCAC	390	498	257	28.0	-3.78 (-4.04 to -3.54)	84 (77 to 92)
2	TGCTTCACCCGATATTGTGGGC	AGGGGCTTCTGCGTACACGAG	1360	505	244	29.9	-3.64 (-3.79 to -3.51)	88 (84 to 93)
3	CCGAGCATCAGGGTTACT	GGTCATCTCTTCTGTGTCTTCC	2044	514	228	29.0	-3.69 (-3.79 to -3.64)	87 (84 to 88)
4	TGGCCACACTGCTCATCAAG	TGGTTTTAGCTGGTCCCTCATA	3273	506	222	28.3	-3.73 (-3.89 to -3.58)	86 (81 to 90)
5	ATGGTAAGATCAAGAAGAGGCT	TAGAAGGAGAAAAGGGAGTTGG	4098	496	261	30.1	-3.66 (-3.77 to -3.57)	88 (84 to 91)
6	TCGAGTGACGCCAACCCATCT	CATCGGGTAAGGGAATCAACACAG	5097	469	238	29.5	-3.68 (-3.8 to -3.6)	87 (83 to 89)
7	CCAGCAGTGCCTTTGTTGTCC	GGGGCCAGATGCACATTATGAG	5842	502	245	30.7	-3.66 (-3.79 to -3.56)	88 (84 to 91)
8	GTTACAACAGGAAATGATGAAA	CTTTAGGCACGGTTGAGAC	6925	500	249	32.5	-4.06 (-4.25 to -3.93)	77 (72 to 80)

G2SK[e]	CNTGGGAGGGCGATCGCAA	CCRCCNGCATRHCCRTTRTACAT	5048	344	168	31.0	-4.07 (-4.2 to -3.98)	76 (73 to 78)

[a]Corresponds to nucleotide position of GII.4 Sydney virus used in this study (accession number MN703761). [b]Values are given as cycle threshold (Ct). [c]Mean slope and efficiency values are the arithmetic mean of all standard curves generated for an assay. The minimum (min) and maximum (max) values of the slope and efficiency are the minimum and maximum values taken from all standard curves generated for an assay. [d] Efficiency is given as a percentage and was calculated according to the following equation: $E = (10^{(-1/slope)} - 1) \times 100\%$. [e]Conserved GII HuNoV amplicon. LOQ = Limit of quantification.

Table A.3 Reaction rate constants and the source of those constants for all (+) ssRNA viruses included in Figure 2.3.

Virus	NCBI accession number	Length	Purine content	Pyrimidine content	Reaction rate constant, k (cm^2 mJ^{-1})	Normalized reaction rate constant, k (cm^2 mJ^{-1} $base^{-1}$)
Human norovirus GII.4 Sydney	JX459908.1	7564	3952	3612	0.27[a]	3.6×10^{-5}
MS2	NC_001417.2	3569	1762	1807	0.14[a]	3.9×10^{-5}
Feline calicivirus	NC_001481.2	7683	3844	3839	0.37[b]	4.8×10^{-5}
Murine norovirus	EF014462.1	7382	3608	3774	0.32[b]	4.3×10^{-5}
Echovirus 12	X77708.1	7501	4014	3487	0.31[b]	4.1×10^{-5}
Coxsackievirus B5	AF114383.1	7400	3931	3469	0.35[a]	4.7×10^{-5}

[a]This study

[b]Park et al. (2011)[4]

A.3 Figures

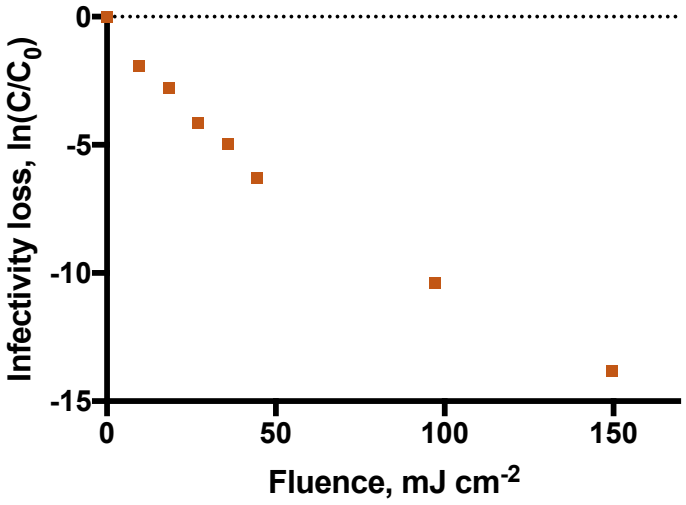

Figure A.1 Loss of MS2 infectivity following UV_{254} exposure during CVB5 experiments. Error bars depict standard error of the mean of three independent replicates (N=3). MS2 was spiked into VDB at a final concentration of 10^9 pfu/mL. Error bars are present for each symbol but in all cases are smaller than the symbol. The data resulted in an inactivation rate constant of 0.14 ± 0.01 cm^2 mJ^{-1} (mean ± 95% CI).

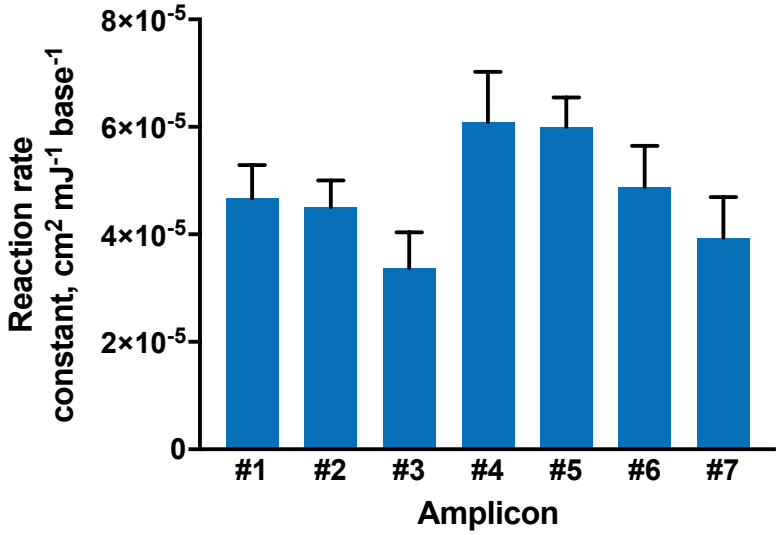

Figure A.2 UV_{254} reaction rate constants for CVB5 amplicons, normalized by number of bases in each amplicon. Error bars depict standard error of the mean of three independent replicates (N = 3).

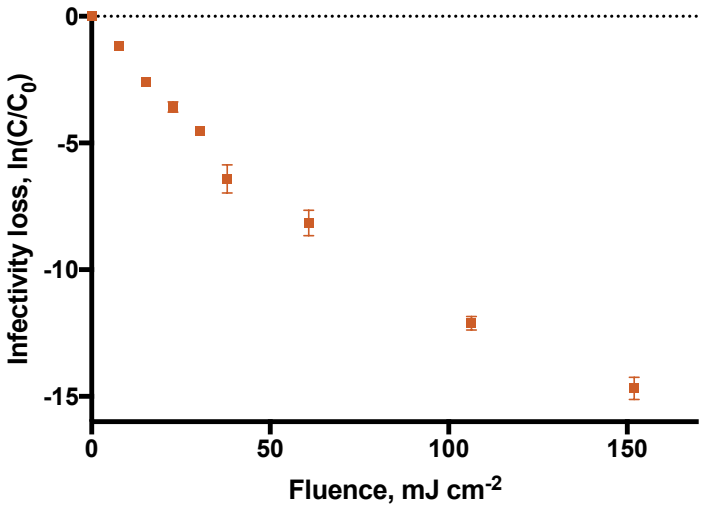

Figure A.3 Loss of MS2 infectivity following UV_{254} exposure during HuNoV experiments. Error bars depict standard error of the mean of four independent replicates (N=4). MS2 was spiked into the stool suspensions at a final concentration of 10^9 pfu/mL. Error bars are present for each symbol but in some cases are smaller than the symbol. The data resulted in an inactivation rate constant of 0.14 ± 0.02 cm^2 mJ^{-1} (mean ± 95% CI).

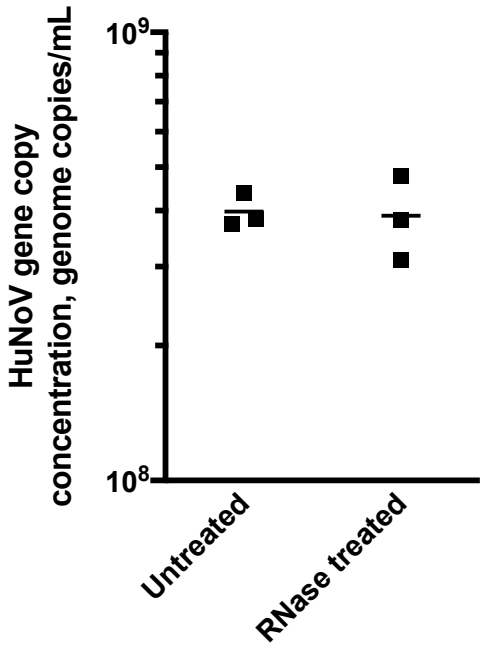

Figure A.4 HuNoV gene copy concentrations of RNase-treated and untreated HuNoV stool suspension used for inactivation experiments. The lines depict the mean of three independent replicates (N=3).

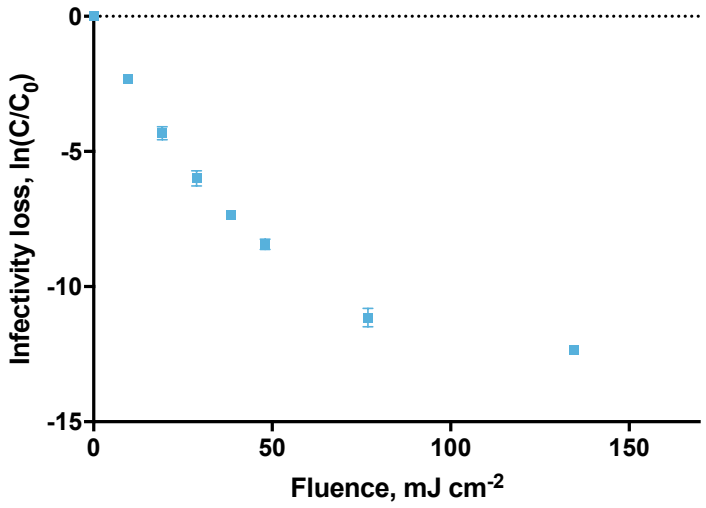

Figure A.5 Loss of MS2 infectivity following UV_{254} exposure in buffer solution. Error bars depict standard error of the mean of three independent replicates (N=3). MS2 was spiked into PBS at a final concentration of 10^9 pfu/mL. Error bars are present for each symbol but in some cases are smaller than the symbol. The data resulted in an inactivation rate constant of 0.14 ± 0.02 cm^2 mJ^{-1} (mean ± 95% CI).

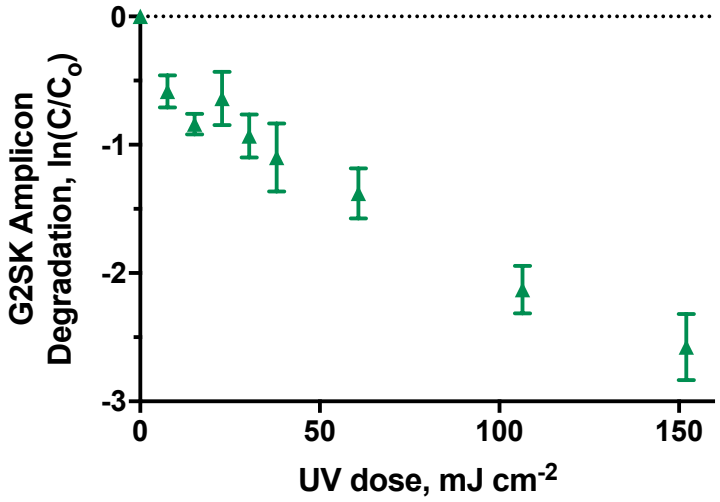

Figure A.6 Loss of G2SK amplicon signal following UV_{254} exposure. Error bars depict standard error of the mean of four independent replicates (N=4).

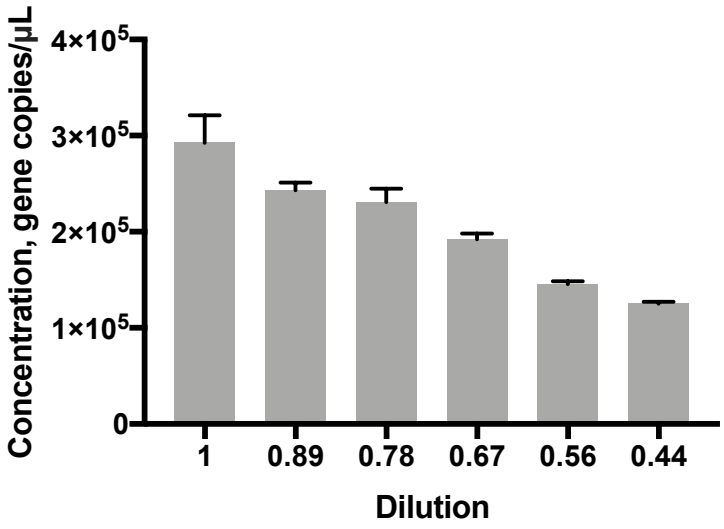

Figure A.7 Sensitivity analysis of G2SK amplicon signal reduction with qPCR. Error bars depict standard error of the mean of three independent replicates (N=3).

A.4 References

(1) Qiao, Z.; Ye, Y.; Chang, P. H.; Thirunarayanan, D.; Wigginton, K. R. Nucleic Acid Photolysis by UV254 and the Impact of Virus Encapsidation. *Environ. Sci. Technol.* **2018**, *52* (18), 10408–10415.

(2) Hoehne, M.; Schreier, E. Detection of Norovirus Genogroup I and II by Multiplex Real-Time RT- PCR Using a 3'-Minor Groove Binder-DNA Probe. *BMC Infect. Dis.* **2006**, *6* (1), 69.

(3) Kageyama, T.; Kojima, S.; Shinohara, M.; Uchida, K.; Fukushi, S.; Hoshino, F. B.; Takeda, N.; Katayama, K. Broadly Reactive and Highly Sensitive Assay for Norwalk-Like Viruses Based on Real-Time Quantitative Reverse Transcription-PCR. *J. Clin. Microbiol.* **2003**, *41* (4), 1548–1557.

(4) Park, G. W.; Linden, K. G.; Sobsey, M. D. Inactivation of Murine Norovirus, Feline Calicivirus and Echovirus 12 as Surrogates for Human Norovirus (NoV) and Coliphage (F+) MS2 by Ultraviolet Light (254 Nm) and the Effect of Cell Association on UV Inactivation. *Lett. Appl. Microbiol.* **2011**, *52* (2), 162–167.

Appendix B

Supplementary Information for Chapter 3

B.1 Supplementary Text

B.1.1 Systematic literature review. The goal of the systematic literature review was to collect UV_{254} inactivation rate constants for viruses in aqueous suspensions so that these data could be used to develop models for predicting virus inactivation by UV_{254}. The Web of Science Core Collection database was used to obtain records for the systematic literature review. Specifically, the database was searched by "Topic" (i.e., search for terms in the title, abstract, author keywords, or Keywords Plus) using the following search term: ((UV OR ultraviolet OR UVC) AND (inactivat* OR disinfect* OR degradat*) AND (virus OR viral OR phage OR bacteriophage)) in August 2019. All records, including conference proceedings and peer-reviewed publications, were output for consideration. Any records containing duplicate content (i.e., duplicate publications, conference proceedings with information also published in a peer-reviewed journal) were removed, and only records in the English language were considered. In addition, any review and microbial risk assessment publications were removed; all references of these papers, however, were screened and relevant references were included in the full-text review (Figure B.1).

During the first round of screening, the title and abstract of each result were evaluated and all records whose details indicated possible inclusion of UV_{254} virus inactivation data were kept. The text of all records passing the initial screening were then reviewed in full. Any records meeting the inclusion criteria were added to the final study set and UV_{254} virus inactivation data were

extracted. For publications that did not allow evaluation of all criteria were not explicitly stated, corresponding authors were contacted when possible to confirm whether remaining criteria were met. Screening and full-text review were carried out by one reviewer.

UV_{254} inactivation rate constants (k), in cm^2 mJ^{-1}, defined as the natural logarithm transformed reduction in infectious virus concentration per UV_{254} dose, were extracted from the publications. This relationship is described by Chick-Watson kinetics:

$$\ln\left(\frac{C}{C_0}\right) = -k \cdot D_{UV_{254}}$$

where C_0 and C are the infectious virus concentrations before and after UV exposure, respectively, and D_{UV254} is the UV_{254} dose, in mJ cm^{-2}. When available, inactivation plots from the study showing the reduction in infectious virus concentrations for varying UV doses were digitized using DigitizeIt.[1] A linear regression of the digitized data, plotted as the natural logarithm transformed reduction in infectious virus concentrations versus UV_{254} dose, was then conducted using Prism version 8.4.2 (GraphPad, La Jolla, CA). The inactivation rate constant was defined as the slope resulting from the linear regression analysis. Only data following first-order kinetics were included in the linear regression analysis. If multiple different inactivation plots with the same virus were conducted in the same study, the extracted data were combined and analyzed in a single linear regression. When no inactivation plot was available or was too blurry to digitize accurately, but the publication reported some form of the inactivation rate constant, this value was extracted and unit conversions were applied as needed. When only the dose required to achieve a specific log-reduction in infectious virus concentrations was reported (e.g., D_{90} or D_{99} values), this value was converted into the inactivation rate constant using Equation 1.

Standard errors were also collected from studies when possible. For digitized data, the standard error of the slope was obtained from the linear regression. When data could not be digitized, but a rate constant and an associated error estimate were reported, the error estimate was extracted and converted to a standard error. Specifically, if a 95% confidence interval for a rate constant was provided, the confidence interval was divided by four to obtain an estimate of the standard error. Data extraction was conducted by one reviewer. To ensure the quality of extracted data, a second reviewer re-extracted all data from the selected studies. Extracted data were then compared among the two reviewers to confirm consistency.

B.1.2 Genome sequence selection. Genome sequences were determined by searching in NCBI for the virus specified in a study. When no details of the exact virus strain or genotype were provided in the methods of a study, the corresponding author was contacted when possible to determine additional details. Ultimately, the NCBI complete genome sequence with a virus description most closely aligned with the virus description from a study was used. We did not include viruses for which we could not find a complete genome sequence as close to or more specific than the species level described in the study. For example, no full-length genome sequence of the bovine calicivirus serotype used by Malley et al.[2] was found on NCBI, so the inactivation rate constant data for this vesivirus work was not included in model development. Environmental virus isolates without available genome information were not used.

B.1.3 Predictor selection.

B.1.3.1 Virus nucleic acid type.

The form of virus nucleic acid, either double-stranded or single-stranded, was included as a categorical predictor in the combined models because research has shown that there are significant differences in the rate of photoproduct formation with UV_{254} irradiation.[3] For RNA in particular,

photoproduct formation with UV_{254} exposure appears to be suppressed significantly in double-stranded nucleic acid compared to single-stranded nucleic acid.[3,4]

B.1.3.2 Length.

The length of the viral genome has frequently been associated with UV_{254} virus inactivation.[5,6] While length is not directly a factor in UV_{254} inactivation, longer regions of the genome have more possible reaction sites for UV_{254} photoproduct formation, and so longer genomes indirectly lead to higher reaction rates. Length was determined using virus genome sequences available in NCBI databases.

B.1.3.3 Virus genome composition.

Certain components of a virus' primary genomic structure are directly impacted by UV_{254} irradiation. Nucleobases in the genome can be altered through direct photolysis, transforming the nucleic acids into photoproducts that may halt or inhibit translation, transcription, or replication of the viral genome and render the virus noninfectious. In particular, pyrimidine bases are about an order of magnitude more reactive with UV_{254} than purine bases.[7] The predictors included in modeling that related to nucleobase composition were therefore exclusively focused on pyrimidine content. Pyrimidine dimers and photohydrates are widely considered the most common products resulting from UV irradiation of nucleic acid. Studies indicate pyrimidine dimers cause a large portion of the UV-induced damage to DNA,[8–10] and the formation of thymine dimers, in particular, has been extensively studied.[7,11–13] Research focused on RNA photolysis suggests pyrimidine hydrates are the primary lesions inducing UV damage,[14] although the presence of pyrimidine dimers in UV-irradiated RNA has been observed.[14,15] Research has also shown hydrate formation in DNA through UV exposure.[16] Presence of flanking pyrimidines next to other pyrimidines is suggested to increase reactivity.[9,10,13,17] Considering these findings related to nucleic acid

photoreactivity, we selected certain predictors related to the number of specific pyrimidine-based sequence combinations in the virus genome. Specifically, the number of uracil bases (U), cytosine bases (C), uracil doublets (UU), uracil triplets (UUU), uracil quadruplets (UUUU), uracil quintuplets (UUUUU), uracil-cytosine pairs (UC), and cytosine-uracil pairs (CU) were included as predictors for RNA viruses. DNA virus predictors included the number of thymine bases (T), cytosine bases (C), thymine doublets (TT), thymine triplets (TTT), thymine quadruplets (TTTT), thymine quintuplets (TTTTT), thymine-cytosine pairs (TC), and cytosine-thymine pairs (CT). We did not incorporate pyrimidine information including the number of CC, CCC, or CCCC in the genome, because past work indicates photoproducts resulting from these nucleobase combinations are not as prevalent as the other base sequences included in the model.[18] Additionally, combinations of bases with purines flanking pyrimidines were not included because of the sparsity of data indicating which precise combinations may lead to photoproducts as well as for simplicity in genomic variable combinations.

All nucleic acid composition values were determined using the same genome sequences used to assess viral genome length. For double-stranded genomes, these variables were counted on both the template and complement strands.

B.1.3.4 Genome repair mode.

Genome repair is a process by which genomic lesions in nucleic acid can be repaired through enzymatic activity. To our knowledge, dsDNA viruses are the only class of viruses that can undergo dark genome repair following UV_{254} treatment. Genome repair can be host-mediated or virus-gene controlled. Host cell mediated genome repair occurs for many dsDNA viruses. This is because genome repair enzymes in the host cell, meant to repair host dsDNA, can repair viral dsDNA once the virus genome is in the host cell. In contrast, certain viruses encode one or more

repair enzymes in their own virus genome (e.g., T-even and T5 phages); in these cases, genome repair is considered to be virus-gene controlled.[19,20] Theoretically, it would be possible that host cell-mediated repair and virus-gene controlled repair occur simultaneously; in T-even phages known to encode genome repair genes, however, studies have shown that the virus destroys host cell repair mechanisms upon viral entry.[20] No viruses are known to undergo simultaneous repair by these distinct genome repair modes, and therefore this combined repair mode was not considered in our models. It is also important to note that no genome photoreactivation was considered in modeling, because these processes only occur when samples are exposed to a nonionizing radiation source following the irradiation treatment.[20] In all studies included in our data set, none of the samples were subject to photoreactivation steps.

Based on knowledge of genome repair among viruses from the literature, a categorical predictor, namely genome repair mode, was developed for each virus. The four levels for this predictor were: 0 = 'host cell mediated,' 1 = 'virus-gene controlled using one repair system,' 2 = 'no repair,' or 3 = 'virus-gene controlled using multiple repair systems.'

All viruses outside of the dsDNA virus Baltimore classification were designated as having no repair; to our knowledge, no evidence of genome repair in the (+) ssRNA, (-) ssRNA, dsRNA, or ssDNA virus classes has been observed. Many dsDNA viruses in our collected data set are known to undergo host cell mediated genome repair, including members of the *Adenoviridae* family, polyomavirus, and lambda phage. Unless past research had reported that a dsDNA virus undergoes virus-gene controlled repair, host cell mediated repair was assumed. This is because eukaryotic and prokaryotic hosts have dsDNA genome repair mechanisms, and there is no reason to believe a dsDNA virus genome would not benefit from these repair systems, unless other virus-mediated activities occur; only T-even phages are known to undergo virus-gene controlled genome repair.

As a result, only the T-even bacteriophages T2, T5, and T6 were categorized with 'virus-gene controlled repair using one repair system.' One virus, T4 bacteriophage, is known to undergo virus-gene controlled repair with multiple repair systems. Beyond repair mode affecting genome repair capabilities, differences among host cell mediated repair do exist, and we evaluated these differences using another categorical predictor, host cell type.

B.1.3.5 Host cell type.

Virus diversity results in significant variability in viral hosts. These hosts differ considerably in several respects; in relation to evaluating UV_{254} inactivation of viruses, we are particularly concerned with the host cell's ability to repair viral genome damage once the UV_{254}-damaged virus has entered the host cell. The efficiency of repair depends on the host cell's ability to repair genomic material. Eukaryotic and prokaryotic cells contain distinct sets of genes for encoding and producing repair enzymes. Among other dissimilarities, the number, function, and regulation of these repair genes differ.[21] Even within the same host type, repair capabilities may differ. For example, studies have shown that in human cells from xeroderma pigmentosum patients, virus UV_{254} sensitivity is significantly increased (e.g., > 3x increase in measured rate constants) compared to in wild-type (i.e., normal) host cells for the same inactivated virus; this is because the cells are deficient in one or more of the common repair genes needed to effectively repair dsDNA inside the host.[19,22–25] In addition, work has shown that genome repair systems in the cells of longer-lived mammals (e.g., human) are significantly upregulated compared to those in shorter-lived mammals (i.e., mice).[26] To incorporate these differences in host cell type that impact genome repair, we developed a categorical predictor for host cell type. Three different categories were used, including 0 = 'prokaryotic cells', 1= 'eukaryotic cells with reduced repair', and 2 = 'eukaryotic cells with wild-type repair.'

All bacteriophages were assigned the category for 'prokaryotic cells.' Some experiments with human viruses were assayed in cell lines known to have reduced repair capabilities compared to wild-type human cell lines; these virus experiments were assessed as having 'eukaryotic cells with reduced repair.' The only virus in the modeling data set with this form of repair was human polyomavirus, assayed in SVG-A cells. A previous study showed reduced repair of DNA damage in SV-derived cells but not in other cells evaluated.[25] While two adenoviruses in the data set were also evaluated in cell lines with reduced repair,[22] these rate constants did not have associated errors and were therefore not included in modeling work. All other dsDNA human viruses were given the host cell type 'eukaryotic cells with wild-type repair.'

$$w_v = \frac{\frac{\bar{k}_v^{\,2}}{SE_v^2}}{\sum_{v=1}^{n_v} \frac{\bar{k}_v^{\,2}}{SE_v^2}}$$

where n_v is the number of viruses in the data set, $\bar{k}_v$ is the inverse variance weighted mean inactivation rate constant for virus v, and SE_v is the standard error of the inverse variance weighted mean inactivation rate constant for virus v.

We employed weighted root mean squared relative prediction error (RMSrPE) to assess model prediction efficacy. Leave-one-virus-out cross-validation was used to determine each model's RMSrPE. Specifically, data from the final curated data set were split into a training set and a validation set for each round of cross-validation so each virus was left out of the training set exactly one time. Weights for viruses in the training set were rescaled to sum to the number of viruses – 1. The squared predicted error was determined for the held-out virus inactivation rate constant in each fold. The resulting relative errors for each virus were weighted by the inverse relative variance

weights and the weighted mean computed. The root of these values was then taken to obtain the RMSrPE for a particular model, as shown in the follow equation:

$$RMSrPE = \sqrt{\sum_{v=1}^{n_v} \left[\left(\bar{k}_v - \hat{k}_v \right)^2 \cdot w_v \right]}$$

where $\hat{k}_v$ is the predicted inactivation rate constant for virus v. The RMSrPE for each model was compared and top performing models were selected based on minimum RMSrPE values. The standard error associated with the relative RMSrPE was determined as the bias corrected weighted sample variance:

$$Standard\ error\ (RMSrPE) = \frac{\sum_{v=1}^{n_v} \left[\left(\bar{k}_v - \hat{k}_v \right)^2 \cdot w_v \right]}{\left(1 - \sum_{v=1}^{n_v} w_v^2 \right)}$$

Pairwise comparisons of model performance were conducted using weighted least squares regression to compare the expected log ratio of the squared prediction errors. Specifically, for each virus the squared prediction error determined during cross-validation were transformed to the natural logarithm scale and differenced. A logarithm transform was used to stabilize the variance estimates of large individual prediction errors in some models. A weighted regression was then conducted using only an intercept as the predictor and the transformed squared error ratios as the dependent variable (i.e., a weighted one-sample t-test of the logarithm squared error ratios). The average squared error ratio (ASER) was determined by exponentiating the estimated intercept from this regression. Differences in model performance were considered significant if the exponentiated 95% confidence interval of the ASER did not include 1.

B.1.4 Virus propagation and enumeration.

B.1.4.1 MHV.

MHV strain A59 was propagated and quantified in delayed brain tumor (DBT) cells (kindly provided by Dr. Julian Leibowitz at Texas A&M Health Science Center College of Medicine) according to published protocols with slight modifications.[27,28] Briefly, DBT cells were grown in medium comprised of Dulbecco's modified Eagle's medium (DMEM) with 4.5 g/L glucose without L-glutamine (Cat. No. 12614F, Lonza), 10% horse serum (Cat. No. 26050088, Life Technologies), 1% penicillin streptomycin (Cat. No. 15140122, Invitrogen), and 1% L-glutamine (100X; Cat. No. 25030081, Invitrogen) at 37°C and 5% CO_2. The medium was replaced every 48 to 72 hours.

MHV stocks were generated in 80% confluent DBT cell monolayers at a multiplicity of infection of approximately 0.01. Following 18 to 24 hours of incubation, infected DBT cells were centrifuged at 3,000 x g for 15 minutes at 4ºC and the supernatant was collected. MHV A59 stocks (~10^6 pfu/mL) were filter-sterilized with a 0.22 μm sterile polyethersulfone (PES) membrane (Cat. No. 229747, CELLTREAT Scientific) and stored in single-use aliquots at -80ºC.

MHV was enumerated via plaque assay. Specifically, DBT cell monolayers were seeded in 12-well plates (Cat. No. 353043, Corning) and incubated at 37°C and 5% CO_2 prior to infection with MHV samples. Plaque assays were performed by inoculating 90% confluent cells with MHV samples diluted in DMEM2 (DMEM with 2% horse serum, 1% penicillin streptomycin, and 1% L-glutamine) for one hour. After inoculation, virus suspensions were removed and replaced with a 1:1 solution of 1.6% agarose (Cat. No. BP160-100, ThermoFisher) and 2xMEM (2x E-MEM (Cat No. 115073101, Quality Biological, Inc.), 5% horse serum, 10 mM HEPES (Cat. No. 17737E, Lonza), 1X MEM non-essential amino acids (Cat. No. 11140050, Invitrogen), 2% L-glutamine, and 2% penicillin streptomycin). Infected DBT cell monolayers were incubated for 48 hours. Plaques were enumerated using neutral red staining (Cat. No. N2889, Sigma-Aldrich) at a final

0.01% concentration in 1X phosphate buffered saline (PBS; Cat. No. 10010023, Invitrogen). Samples were enumerated in triplicate and negative media controls were plated with samples.

B.1.4.2 HS2 bacteriophage.

HS2 marine bacteriophage and its host *Pseudoalteromonas* 13-15 (kindly provided by Dr. Melissa Duhaime at the University of Michigan Department of Ecology and Evolutionary Biology) were propagated and enumerated using established methods with modifications.[29] Briefly, HS2 bacteriophage stock was generated using the soft agar overlay method. Specifically, soft seawater agar (5 g/L peptone, 1 g/L yeast extract, 10% Widdel salt solution, 0.6% agar) containing HS2 bacteriophage and host bacteria was overlaid on hard seawater agar plates (1 g/L peptone, 0.2 g/L yeast extract, 10% Widdel salt solution, 1.2% agar) and incubated overnight at 25ºC. The soft seawater agar with virus was then scraped off and diluted with SM buffer (100 mM NaCl, 81.2 mM $MgSO_4 \bullet 7H_2O$, 50mM Tris-HCl (pH 7.5)). Chloroform was added to the agar solution (5 mL chloroform per 50 mL solution) and centrifuged at 3000 x g for 10 minutes. The supernatant was aerated to remove residual chloroform and filtered through a 0.45 μm PES membrane. The resulting HS2 bacteriophage stock (~ 10^{11} pfu/mL) was stored at 4ºC until use. HS2 infectivity was quantified by plaque assay.

B.2 Figures

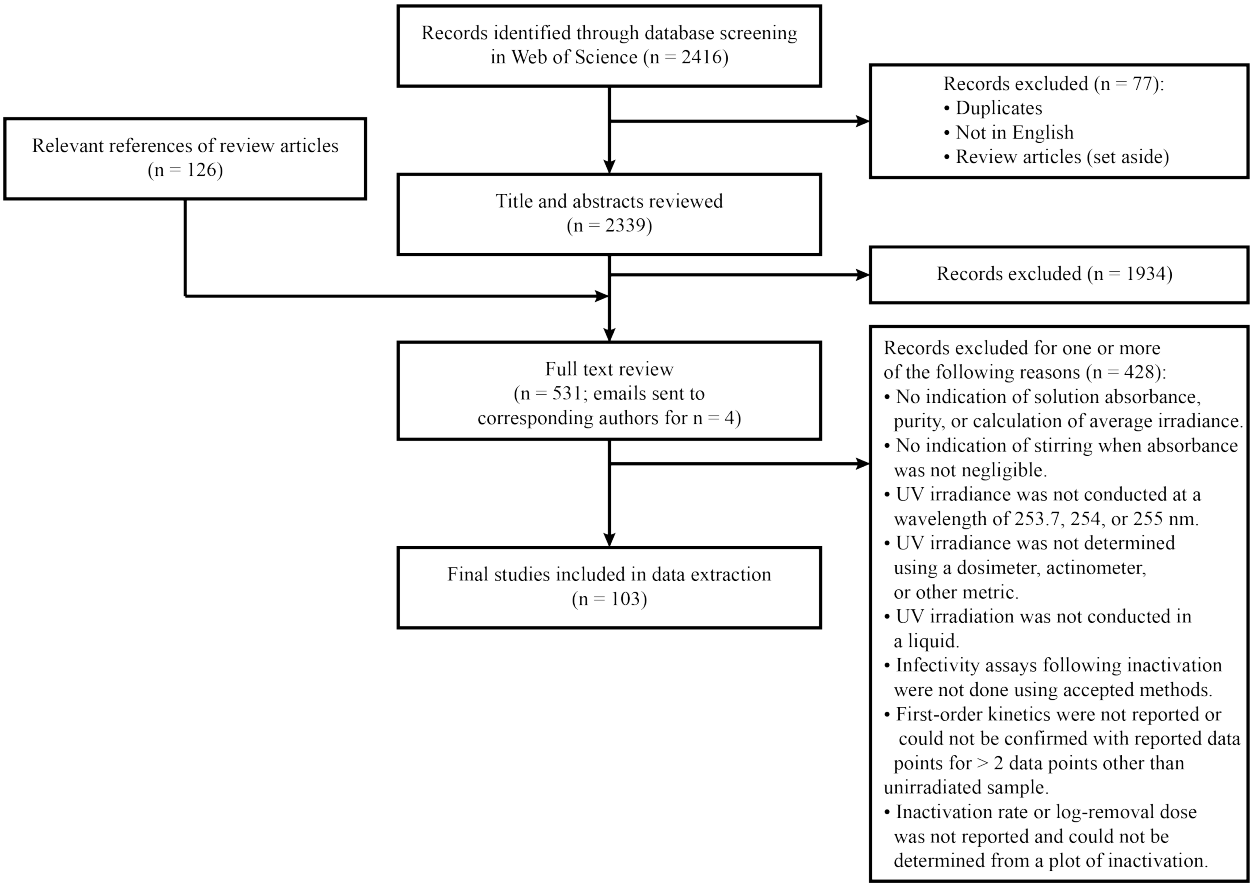

Figure B.1 Flow chart of systematic literature review conducted to collect high-quality UV_{254} virus inactivation rate constants.

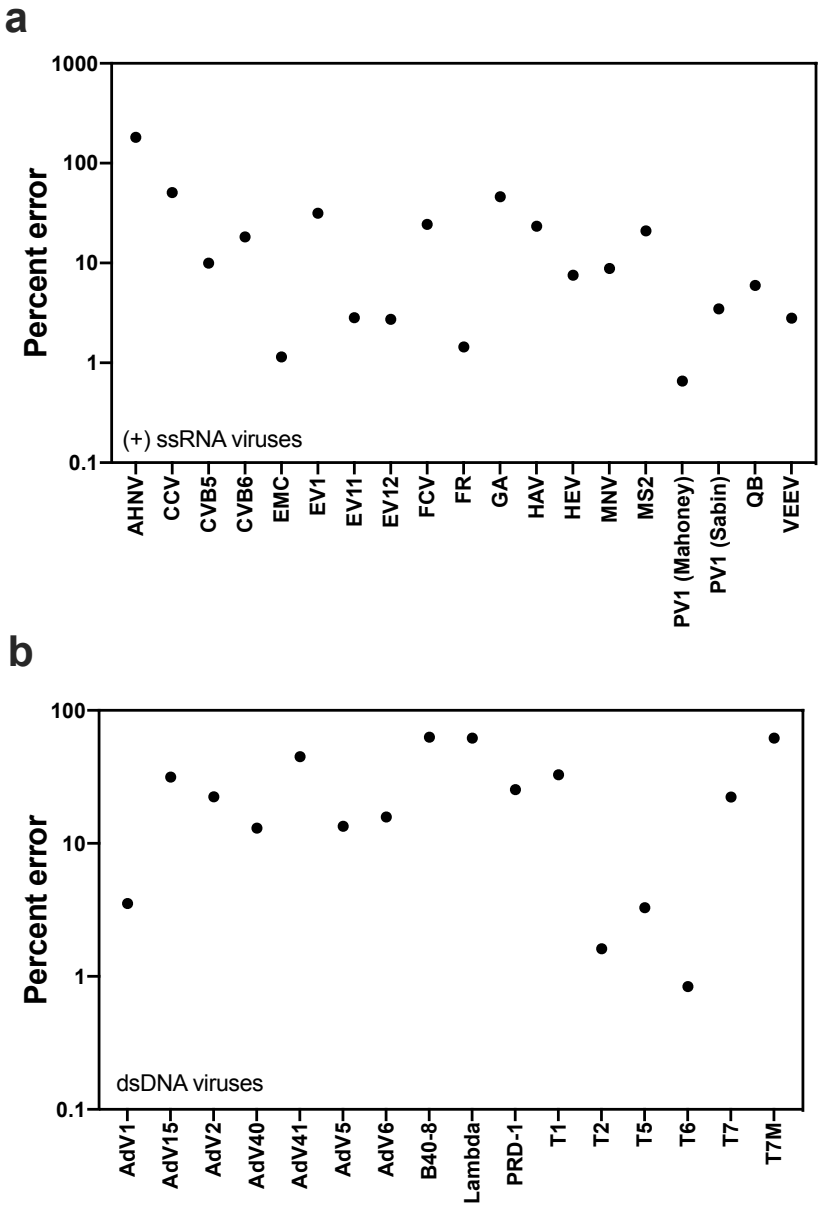

Figure B.2 Percent error of the predicted inactivation rate constant from the mean experimental rate constant for each virus where the predicted constants were determined using the top performing (+) ssRNA virus model (a) and dsDNA virus model (b).

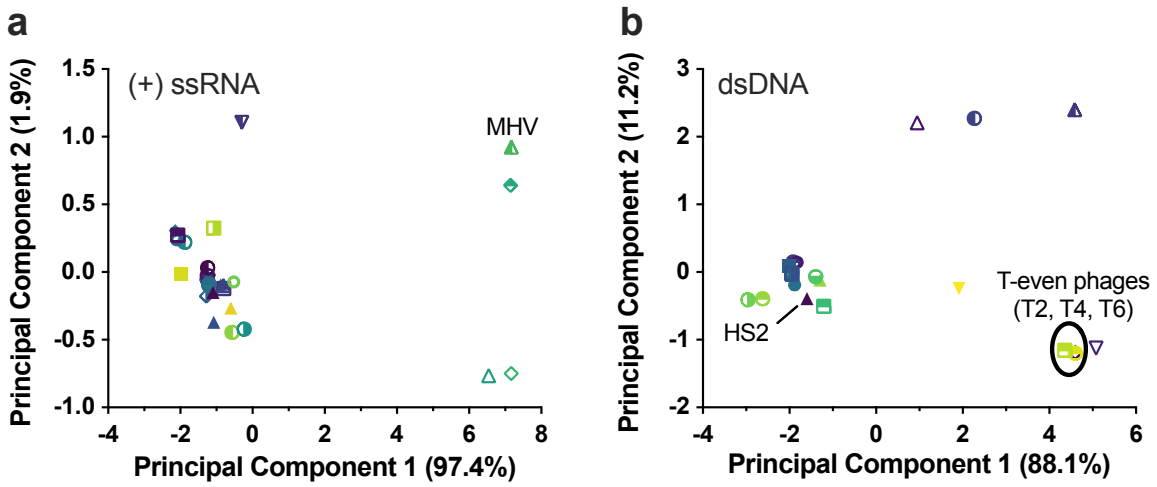

Figure B.3 Principal component analyses of virus genome attributes for (+) ssRNA viruses (a) and dsDNA viruses (b). Viruses included all viruses from the systematic review with full genome sequence information, and viruses used in predictions. Principal component analyses were conducted on standardized genome attributes, as described in methods.

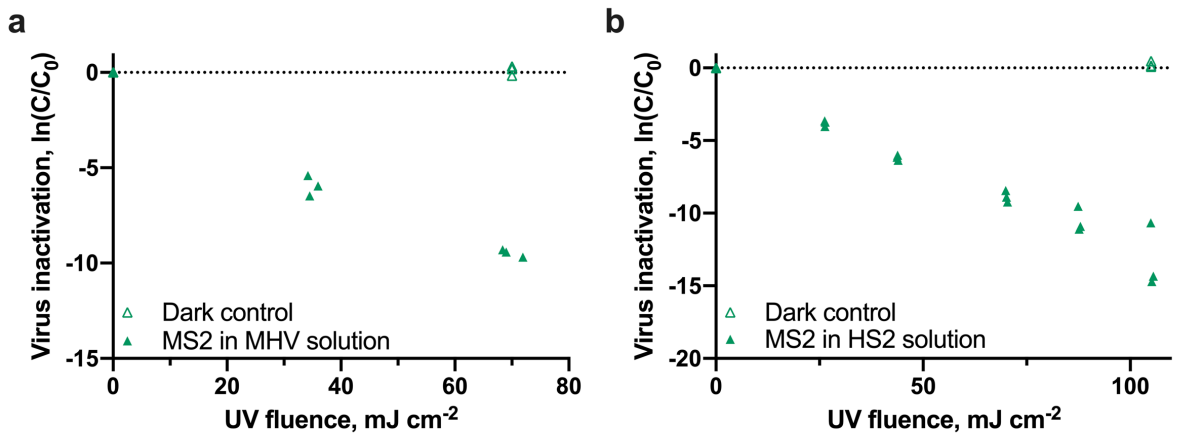

Figure B.4 Inactivation of MS2 following UV_{254} irradiation when MS2 was in the MHV experimental solution (a) and the HS2 experimental solution (b). Independent replicates (N = 3) are shown for each fluence. MS2 was spiked into the experimental solution at a final concentration of 10^9 pfu/mL.

B.3 Tables

Table B.1 Experimental UV_{254} inactivation rate constants extracted from the systematic literature review and virus rate constants and weights used in modeling work. *This table is provided as an external data file.*

Table B.2 Virus genome sequence sources and predictor information for all viruses used in training/validation and prediction. *This table is provided as an external data file.*

Table B.3 Model performance metrics for top-performing models of each class for each subset of viruses used in the training and validation set. *This table is provided as an external data file.*

Table B.4 Results of pairwise multiple linear regression model comparisons. *This table is provided as an external data file.*

Table B.5 Results of pairwise model comparisons. *This table is provided as an external data file.*

Table B.6 Predicted virus inactivation rate constants from the top performing dsDNA virus model and top performing (+) ssRNA virus model. *This table is provided as an external data file.*

B.4 References

(1) DigitizeIt - Digitizer Software https://www.digitizeit.de.

(2) Malley, J.; Linden, K.; Mofidi, A.; Bolton, J.; Crozes, G.; Cushing, B.; Mackey, E.; Laine, J. M.; Janex, M.-L. *Inactivation of Pathogens with Innovative UV Technologies*; American Water Works Association Research Foundation, 2004; Vol. 1.

(3) Pearson, M.; Johns, H. E. Suppression of Hydrate and Dimer Formation in Ultraviolet-Irradiated Poly (A + U) Relative to Poly U. *J. Mol. Biol.* **1966**, *20* (2), 215–229. https://doi.org/https://doi.org/10.1016/0022-2836(66)90061-1.

(4) Qiao, Z.; Ye, Y.; Chang, P. H.; Thirunarayanan, D.; Wigginton, K. R. Nucleic Acid Photolysis by UV254 and the Impact of Virus Encapsidation. *Environ. Sci. Technol.* **2018**. https://doi.org/10.1021/acs.est.8b02308.

(5) Simonet, J.; Gantzer, C. Inactivation of Poliovirus 1 and F-Specific RNA Phages and Degradation of Their Genomes by UV Irradiation at 254 Nanometers. *Appl. Environ. Microbiol.* **2006**, *72* (12), 7671 LP – 7677. https://doi.org/10.1128/AEM.01106-06.

(6) Lytle, C. D.; Sagripanti, J.-L. Predicted Inactivation of Viruses of Relevance to Biodefense by Solar Radiation. *J. Virol.* **2005**, *79* (22), 14244–14252. https://doi.org/10.1128/JVI.79.22.14244-14252.2005.

(7) Smith, K. C. Physical and Chemical Changes Induced in Nucleic Acids by Ultraviolet Light. *Radiat. Res. Suppl.* **1966**, *6*, 54–79. https://doi.org/10.2307/3583551.

(8) Setlow, R. B.; Carrier, W. L. The Disappearance of Thymine Dimers from DNA: An Error-Correcting Mechanism. *Proc. Natl. Acad. Sci. U. S. A.* **1964**, *51* (2), 226–231. https://doi.org/10.1073/pnas.51.2.226.

(9) Becker, M. M.; Wang, Z. Origin of Ultraviolet Damage in DNA. *J. Mol. Biol.* **1989**, *210* (3), 429–438. https://doi.org/https://doi.org/10.1016/0022-2836(89)90120-4.

(10) Kundu, L. M.; Linne, U.; Marahiel, M.; Carell, T. RNA Is More UV Resistant than DNA: The Formation of UV-Induced DNA Lesions Is Strongly Sequence and Conformation Dependent. *Chem. – A Eur. J.* **2004**, *10* (22), 5697–5705. https://doi.org/10.1002/chem.200305731.

(11) Schreier, W. J.; Schrader, T. E.; Koller, F. O.; Gilch, P.; Crespo-Hernández, C. E.; Swaminathan, V. N.; Carell, T.; Zinth, W.; Kohler, B. Thymine Dimerization in DNA Is an Ultrafast Photoreaction. *Science (80-.).* **2007**, *315* (5812), 625 LP – 629. https://doi.org/10.1126/science.1135428.

(12) Meistrich, M. L. Contribution of Thymine Dimers to the Ultraviolet Light Inactivation of Mutants of Bacteriophage T4. *J. Mol. Biol.* **1972**, *66* (1), 97–106. https://doi.org/https://doi.org/10.1016/S0022-2836(72)80008-1.

(13) Law, Y. K.; Forties, R. A.; Liu, X.; Poirier, M. G.; Kohler, B. Sequence-Dependent Thymine Dimer Formation and Photoreversal Rates in Double-Stranded DNA. *Photochem. Photobiol. Sci.* **2013**, *12* (8), 1431–1439. https://doi.org/10.1039/C3PP50078K.

(14) Small, G. D.; Tao, M.; Gordon, M. P. Pyrimidine Hydrates and Dimers in Ultraviolet-Irradiated Tobacco Mosaic Virus Ribonucleic Acid. *J. Mol. Biol.* **1968**, *38* (1), 75–87. https://doi.org/https://doi.org/10.1016/0022-2836(68)90129-0.

(15) Freeman, K. B.; Hariharan, P. V; Johns, H. E. The Ultraviolet Photochemistry of Cytidylyl-(3′-5′)-Cytidine. *J. Mol. Biol.* **1965**, *13* (3), 833-IN16. https://doi.org/https://doi.org/10.1016/S0022-2836(65)80148-6.

(16) Fisher, G. J.; Johns, H. E. 4 - Pyrimidine Photohydrates; Wang, S. Y. B. T.-P. and P. of N. A., Ed.; Academic Press, 1976; pp 169–224. https://doi.org/https://doi.org/10.1016/B978-0-12-734601-4.50010-0.

(17) Owada, M.; Ihara, S.; Toyoshima, K.; Kozai, Y.; Sugino, Y. Ultraviolet Inactivation of Avian Sarcoma Viruses: Biological and Biochemical Analysis. *Virology* **1976**, *69* (2), 710–718. https://doi.org/https://doi.org/10.1016/0042-6822(76)90499-2.

(18) Douki, T.; Cadet, J. Individual Determination of the Yield of the Main UV-Induced Dimeric Pyrimidine Photoproducts in DNA Suggests a High Mutagenicity of CC Photolesions. *Biochemistry* **2001**, *40* (8), 2495–2501. https://doi.org/10.1021/bi0022543.

(19) Rupert, C. S.; Harm, W. Reactivation After Photobiological Damage. In *Advances in Radiation Biology*; AUGENSTEIN, L. G., MASON, R., ZELLE, M. A. X. B. T.-A. in R. B., Eds.; Elsevier, 1966; Vol. 2, pp 1–81. https://doi.org/https://doi.org/10.1016/B978-1-4832-3121-1.50006-2.

(20) Harm, W. *Biological Effects of Ultraviolet Radiation*; IUPAB biophysics series. 1; Cambridge University Press: Cambridge, Eng. ; New York :, 1980.

(21) Cooper, G. M.; Hausman 1947-2015., R. E. *The Cell : A Molecular Approach*, 5th ed.; ASM Press ; Sinauer Associates: Washington, D.C. : Sunderland, Mass. :, 2009.

(22) Guo, H.; Chu, X.; Hu, J. Effect of Host Cells on Low- and Medium-Pressure UV Inactivation of Adenoviruses. *Appl. Environ. Microbiol.* **2010**, *76* (21), 7068 LP – 7075. https://doi.org/10.1128/AEM.00185-10.

(23) Day III, R. S. Cellular Reactivation of Ultraviolet-Irradiated Human Adenovirus 2 in Normal and Xeroderma Pigmentosum Fibroblasts. *Photochem. Photobiol.* **1974**, *19* (1), 9–

13. https://doi.org/10.1111/j.1751-1097.1974.tb06467.x.

(24) Rainbow, A. J. Reduced Capacity to Repair Irradiated Adenovirus in Fibroblasts from Xeroderma Pigmentosum Heterozygotes. *Cancer Res.* **1980**, *40* (11), 3945 LP – 3949.

(25) Rainbow, A. J. Defective Repair of UV-Damaged DNA in Human Tumor and SV40-Transformed Human Cells but Not in Adenovirus-Transformed Human Cells. *Carcinogenesis* **1989**, *10* (6), 1073–1077. https://doi.org/10.1093/carcin/10.6.1073.

(26) MacRae, S. L.; Croken, M. M.; Calder, R. B.; Aliper, A.; Milholland, B.; White, R. R.; Zhavoronkov, A.; Gladyshev, V. N.; Seluanov, A.; Gorbunova, V.; Zhang, Z. D.; Vijg, J. DNA Repair in Species with Extreme Lifespan Differences. *Aging (Albany. NY).* **2015**, *7* (12), 1171–1184. https://doi.org/10.18632/aging.100866.

(27) Leibowitz, J.; Kaufman, G.; Liu, P. Coronaviruses: Propagation, Quantification, Storage, and Construction of Recombinant Mouse Hepatitis Virus. *Curr. Protoc. Microbiol.* **2011**, *Chapter 15*, Unit-15E.1. https://doi.org/10.1002/9780471729259.mc15e01s21.

(28) Ye, Y.; Ellenberg, R. M.; Graham, K. E.; Wigginton, K. R. Survivability, Partitioning, and Recovery of Enveloped Viruses in Untreated Municipal Wastewater. *Environ. Sci. Technol.* **2016**, *50* (10), 5077–5085. https://doi.org/10.1021/acs.est.6b00876.

(29) Duhaime, M. B.; Solonenko, N.; Roux, S.; Verberkmoes, N. C.; Wichels, A.; Sullivan, M. B. Comparative Omics and Trait Analyses of Marine Pseudoalteromonas Phages Advance the Phage OTU Concept. *Front. Microbiol.* **2017**, *8*. https://doi.org/10.3389/fmicb.2017.01241.

(30) Nwachuku, N.; Gerba, C. P.; Oswald, A.; Mashadi, F. D. Comparative Inactivation of Adenovirus Serotypes by UV Light Disinfection. *Appl. Environ. Microbiol.* **2005**, *71* (9),

5633–5636. https://doi.org/10.1128/AEM.71.9.5633.

(31) Ballesster, N. A.; Malley, J. P. J. Sequential Disinfection of Adenovirus Type 2 with UV-Chlorine-Chloramine. *J. Am. Water Work. Assoc.* **2004**, *96* (8).

(32) Baxter, C. S.; Hofmann, R.; Templeton, M. R.; Brown, M.; Andrews, R. C. Inactivation of Adenovirus Types 2, 5, and 41 in Drinking Water by UV Light, Free Chlorine, and Monochloramine. *J. Environ. Eng.* **2007**, *133* (1), 95–103. https://doi.org/10.1061/(ASCE)0733-9372(2007)133:1(95).

(33) Beck, S. E.; Rodriguez, R. A.; Linden, K. G.; Hargy, T. M.; Larason, T. C.; Wright, H. B. Wavelength Dependent UV Inactivation and DNA Damage of Adenovirus as Measured by Cell Culture Infectivity and Long Range Quantitative PCR. *Environ. Sci. Technol.* **2014**, *48* (1), 591–598. https://doi.org/10.1021/es403850b.

(34) Bosshard, F.; Armand, F.; Hamelin, R.; Kohn, T. Mechanisms of Human Adenovirus Inactivation by Sunlight and UVC Light as Examined by Quantitative PCR and Quantitative Proteomics. *Appl. Environ. Microbiol.* **2013**, *79* (4), 1325 LP – 1332. https://doi.org/10.1128/AEM.03457-12.

(35) Bounty, S.; Rodriguez, R. A.; Linden, K. G. Inactivation of Adenovirus Using Low-Dose UV/H2O2 Advanced Oxidation. *Water Res.* **2012**, *46* (19), 6273–6278. https://doi.org/https://doi.org/10.1016/j.watres.2012.08.036.

(36) Calgua, B.; Carratalà, A.; Guerrero-Latorre, L.; de Abreu Corrêa, A.; Kohn, T.; Sommer, R.; Girones, R. UVC Inactivation of DsDNA and SsRNA Viruses in Water: UV Fluences and a QPCR-Based Approach to Evaluate Decay on Viral Infectivity. *Food Environ. Virol.* **2014**, *6* (4), 260–268. https://doi.org/10.1007/s12560-014-9157-1.

(37) Eischeid, A. C.; Meyer, J. N.; Linden, K. G. UV Disinfection of Adenoviruses: Molecular Indications of DNA Damage Efficiency. *Appl. Environ. Microbiol.* **2009**, *75* (1), 23 LP – 28. https://doi.org/10.1128/AEM.02199-08.

(38) Gerba, C. P.; Gramos, D. M.; Nwachuku, N. Comparative Inactivation of Enteroviruses and Adenovirus 2 by UV Light. *Appl. Environ. Microbiol.* **2002**, *68* (10), 5167 LP – 5169. https://doi.org/10.1128/AEM.68.10.5167-5169.2002.

(39) Linden, K. G.; Thurston, J.; Schaefer, R.; Malley, J. P. Enhanced UV Inactivation of Adenoviruses under Polychromatic UV Lamps. *Appl. Environ. Microbiol.* **2007**, *73* (23), 7571 LP – 7574. https://doi.org/10.1128/AEM.01587-07.

(40) Rodríguez, R. A.; Bounty, S.; Linden, K. G. Long-Range Quantitative PCR for Determining Inactivation of Adenovirus 2 by Ultraviolet Light. *J. Appl. Microbiol.* **2013**, *114* (6), 1854–1865. https://doi.org/10.1111/jam.12169.

(41) Ryu, H.; Cashdollar, J. L.; Fout, G. S.; Schrantz, K. A.; Hayes, S. Applicability of Integrated Cell Culture Quantitative PCR (ICC-QPCR) for the Detection of Infectious Adenovirus Type 2 in UV Disinfection Studies. *J. Environ. Sci. Heal. Part A* **2015**, *50* (8), 777–787. https://doi.org/10.1080/10934529.2015.1019795.

(42) Shin, G.-A.; Linden, K. G.; Sobsey, M. D. Low Pressure Ultraviolet Inactivation of Pathogenic Enteric Viruses and Bacteriophages. *J. Environ. Eng. Sci.* **2005**, *4* (Supplement 1), S7–S11. https://doi.org/10.1139/s04-036.

(43) Thompson, S. S.; Jackson, J. L.; Suva-Castillo, M.; Yanko, W. A.; El Jack, Z.; Kuo, J.; Chen, C.-L.; Williams, F. P.; Schnurr, D. P. Detection of Infectious Human Adenoviruses in Tertiary-Treated and Ultraviolet-Disinfected Wastewater. *Water Environ. Res.* **2003**, *75*

(2), 163–170. https://doi.org/10.2175/106143003X140944.

(44) Vazquez-Bravo, B.; Gonçalves, K.; Shisler, J. L.; Mariñas, B. J. Adenovirus Replication Cycle Disruption from Exposure to Polychromatic Ultraviolet Irradiation. *Environ. Sci. Technol.* **2018**, *52* (6), 3652–3659. https://doi.org/10.1021/acs.est.7b06082.

(45) Rattanakul, S.; Oguma, K.; Sakai, H.; Takizawa, S. Inactivation of Viruses by Combination Processes of UV and Chlorine. *J. Water Environ. Technol.* **2014**, *12* (6), 511–523. https://doi.org/10.2965/jwet.2014.511.

(46) Rattanakul, S.; Oguma, K.; Takizawa, S. Sequential and Simultaneous Applications of UV and Chlorine for Adenovirus Inactivation. *Food Environ. Virol.* **2015**, *7* (3), 295–304. https://doi.org/10.1007/s12560-015-9202-8.

(47) Sangsanont, J.; Katayama, H.; Kurisu, F.; Furumai, H. Capsid-Damaging Effects of UV Irradiation as Measured by Quantitative PCR Coupled with Ethidium Monoazide Treatment. *Food Environ. Virol.* **2014**, *6* (4), 269–275. https://doi.org/10.1007/s12560-014-9162-4.

(48) Jacangelo, J. G.; Patania, N. L.; Trussell, R. R.; Haas, C. N.; Gerba, C. *Inactivation of Waterborne Emerging Pathogens by Selected Disinfectants*; Denver, CO, 2002.

(49) Meng, Q. S.; Gerba, C. P. Comparative Inactivation of Enteric Adenoviruses, Poliovirus and Coliphages by Ultraviolet Irradiation. *Water Res.* **1996**, *30* (11), 2665–2668. https://doi.org/https://doi.org/10.1016/S0043-1354(96)00179-0.

(50) Thurston-Enriquez, J. A.; Haas, C. N.; Jacangelo, J.; Riley, K.; Gerba, C. P. Inactivation of Feline Calicivirus and Adenovirus Type 40 by UV Radiation. *Appl. Environ. Microbiol.* **2003**, *69* (1), 577–582.

(51) Ding, N.; Craik, S. A.; Pang, X.; Lee, B.; Neumann, N. F. Assessing UV Inactivation of Adenovirus 41 Using Integrated Cell Culture Real-Time QPCR/RT-QPCR. *Water Environ. Res.* **2017**, *89* (4), 323–329. https://doi.org/10.2175/106143017X14839994523028.

(52) Ko, G.; Cromeans, T. L.; Sobsey, M. D. UV Inactivation of Adenovirus Type 41 Measured by Cell Culture MRNA RT-PCR. *Water Res.* **2005**, *39* (15), 3643–3649. https://doi.org/https://doi.org/10.1016/j.watres.2005.06.013.

(53) Diston, D.; Ebdon, J. E.; Taylor, H. D. The Effect of UV-C Radiation (254 Nm) on Candidate Microbial Source Tracking Phages Infecting a Human-Specific Strain of Bacteroides Fragilis (GB-124). *J. Water Health* **2012**, *10* (2), 262–270. https://doi.org/10.2166/wh.2012.173.

(54) Sommer, R.; Haider, T.; Cabaj, A.; Pribil, W.; Lhotsky, M. Time Dose Reciprocity in UV Disinfection of Water. *Water Sci. Technol.* **1998**, *38* (12), 145–150. https://doi.org/10.2166/wst.1998.0526.

(55) Sommer, R.; Pribil, W.; Appelt, S.; Gehringer, P.; Eschweiler, H.; Leth, H.; Cabaj, A.; Haider, T. Inactivation of Bacteriophages in Water by Means of Non-Ionizing (Uv-253.7nm) and Ionizing (Gamma) Radiation: A Comparative Approach. *Water Res.* **2001**, *35* (13), 3109–3116. https://doi.org/https://doi.org/10.1016/S0043-1354(01)00030-6.

(56) Lee, H. S.; Sobsey, M. D. Survival of Prototype Strains of Somatic Coliphage Families in Environmental Waters and When Exposed to UV Low-Pressure Monochromatic Radiation or Heat. *Water Res.* **2011**, *45* (12), 3723–3734. https://doi.org/https://doi.org/10.1016/j.watres.2011.04.024.

(57) Martignoni, K. D.; Haselbacher, I. Inactivation of Bacteriophage Lambda by Combined X-

Ray and U.V.-Light Exposure. *Int. J. Radiat. Biol. Relat. Stud. Physics, Chem. Med.* **1979**, *35* (5), 441–447. https://doi.org/10.1080/rab.35.5.441.447.

(58) Rauth, A. M. The Physical State of Viral Nucleic Acid and the Sensitivity of Viruses to Ultraviolet Light. *Biophys. J.* **1965**, *5* (3), 257–273.

(59) Latarjet, R.; Cramer, R.; Montagnier, L. Inactivation, by UV-, X-, and γ-Radiations, of the Infecting and Transforming Capacities of Polyoma Virus. *Virology* **1967**, *33* (1), 104–111. https://doi.org/10.1016/0042-6822(67)90098-0.

(60) Bae, K. S.; Shin, G.-A. Inactivation of Various Bacteriophages by Different Ultraviolet Technologies: Development of a Reliable Virus Indicator System for Water Reuse. *Environ. Eng. Res.* **2016**, *21* (4), 350–354. https://doi.org/10.4491/eer.2016.032.

(61) Gerrity, D.; Ryu, H.; Crittenden, J.; Abbaszadegan, M. Photocatalytic Inactivation of Viruses Using Titanium Dioxide Nanoparticles and Low-Pressure UV Light. *J. Environ. Sci. Heal. Part A* **2008**, *43* (11), 1261–1270. https://doi.org/10.1080/10934520802177813.

(62) Kashinkunti, R. D.; Linden, K. G.; Shin, G.-A.; Metz, D. H.; Sobsey, M. D.; Moran, M. C.; Samuelson, A. M. Investigating Multibarrier Inactivation for Cincinnati—UV, By-Products, and Biostability. *J. - AWWA* **2004**, *96* (6), 114–127. https://doi.org/10.1002/j.1551-8833.2004.tb10785.x.

(63) Rodriguez, R. A.; Bounty, S.; Beck, S.; Chan, C.; Mcguire, C.; Linden, K. G. Photoreactivation of Bacteriophages after UV Disinfection : Role of Genome Structure and Impacts of UV Source. *Water Res.* **2014**, *55*, 143–149. https://doi.org/10.1016/j.watres.2014.01.065.

(64) Sommer, R.; Haider, T.; Cabaj, A.; Heidenreich, E.; Kundi, M. Increased Inactivation of

Saccharomyces Cerevisiae by Protraction of UV Irradiation. *Appl. Environ. Microbiol.* **1996**, *62* (6), 1977 LP – 1983.

(65) Fallon, K. S.; Hargy, T. M.; Mackey, E. D.; Wright, H. B.; Clancy, J. L. Development and Characterization of Nonpathogenic Surrogates for UV Reactor Validation. *J. - AWWA* **2007**, *99* (3), 73–82. https://doi.org/10.1002/j.1551-8833.2007.tb07890.x.

(66) Luria, S. E.; Dulbecco, R. Genetic Recombinations Leading to Production of Active Bacteriophage from Ultraviolet Inactivated Bacteriophage Particles. *Genetics* **1949**, *34* (2), 93–125.

(67) Beck, S. E.; Wright, H. B.; Hargy, T. M.; Larason, T. C.; Linden, K. G. Action Spectra for Validation of Pathogen Disinfection in Medium-Pressure Ultraviolet (UV) Systems. *Water Res.* **2015**, *70*, 27–37. https://doi.org/https://doi.org/10.1016/j.watres.2014.11.028.

(68) Gunter-Ward, D. M.; Patras, A.; S. Bhullar, M.; Kilonzo-Nthenge, A.; Pokharel, B.; Sasges, M. Efficacy of Ultraviolet (UV-C) Light in Reducing Foodborne Pathogens and Model Viruses in Skim Milk. *J. Food Process. Preserv.* **2018**, *42* (2), e13485. https://doi.org/10.1111/jfpp.13485.

(69) Bohrerova, Z.; Shemer, H.; Lantis, R.; Impellitteri, C. A.; Linden, K. G. Comparative Disinfection Efficiency of Pulsed and Continuous-Wave UV Irradiation Technologies. *Water Res.* **2008**, *42* (12), 2975–2982. https://doi.org/https://doi.org/10.1016/j.watres.2008.04.001.

(70) Otaki, M.; Okuda, A.; Tajima, K.; Iwasaki, T.; Kinoshita, S.; Ohgaki, S. Inactivation Differences of Microorganisms by Low Pressure UV and Pulsed Xenon Lamps. *Water Sci. Technol.* **2003**, *47* (3), 185–190.

(71) Templeton, M. R.; Andrews, R. C.; Hofmann, R. Impact of Iron Particles in Groundwater on the UV Inactivation of Bacteriophages MS2 and T4. *J. Appl. Microbiol.* **2006**, *101* (3), 732–741. https://doi.org/10.1111/j.1365-2672.2006.02980.x.

(72) Templeton, M. R.; Hofmann, R.; Andrews, R. C. UV Inactivation of Humic-Coated Bacteriophages MS2 and T4 in Water. *J. Environ. Eng. Sci.* **2006**, *5* (6), 537–543.

(73) Timchak, E.; Gitis, V. A Combined Degradation of Dyes and Inactivation of Viruses by UV and UV/H2O2. *Chem. Eng. J.* **2012**, *192*, 164–170. https://doi.org/https://doi.org/10.1016/j.cej.2012.03.054.

(74) Bowker, C.; Sain, A.; Shatalov, M.; Ducoste, J. Microbial UV Fluence-Response Assessment Using a Novel UV-LED Collimated Beam System. *Water Res.* **2011**, *45* (5), 2011–2019. https://doi.org/https://doi.org/10.1016/j.watres.2010.12.005.

(75) Cornelis, J. J.; Su, Z. Z.; Rommelaere, J. Direct and Indirect Effects of Ultraviolet Light on the Mutagenesis of Parvovirus H-1 in Human Cells. *EMBO J.* **1982**, *1* (6), 693–699. https://doi.org/10.1002/j.1460-2075.1982.tb01232.x.

(76) Battigelli, D. A.; Sobsey, M. D.; Lobe, D. C. The Inactivation of Hepatitis a Virus and Other Model Viruses by UV Irradiation. *Water Sci. Technol.* **1993**, *27* (3–4), 339–342.

(77) Giese, N.; Darby, J. Sensitivity of Microorganisms to Different Wavelengths of UV Light: Implications on Modeling of Medium Pressure UV Systems. *Water Res.* **2000**, *34* (16), 4007–4013. https://doi.org/10.1016/S0043-1354(00)00172-X.

(78) Ho, J.; Seidel, M.; Niessner, R.; Eggers, J.; Tiehm, A. Long Amplicon (LA)-QPCR for the Discrimination of Infectious and Noninfectious Phix174 Bacteriophages after UV Inactivation. *Water Res.* **2016**, *103*, 141–148.

https://doi.org/https://doi.org/10.1016/j.watres.2016.07.032.

(79) Liltved, H.; Hektoen, H.; Efraimsen, H. Inactivation of Bacterial and Viral Fish Pathogens by Ozonation or UV Irradiation in Water of Different Salinity. *Aquac. Eng.* **1995**, *14* (2), 107–122. https://doi.org/https://doi.org/10.1016/0144-8609(94)P4430-J.

(80) Liltved, H.; Vogelsang, C.; Modahl, I.; Dannevig, B. H. High Resistance of Fish Pathogenic Viruses to UV Irradiation and Ozonated Seawater. *Aquac. Eng.* **2006**, *34* (2), 72–82. https://doi.org/https://doi.org/10.1016/j.aquaeng.2005.05.002.

(81) Øye, A. K.; Rimstad, E. Inactivation of Infectious Salmon Anaemia Virus, Viral Haemorrhagic Septicaemia Virus and Infectious Pancreatic Necrosis Virus in Water Using UVC Irradiation. *Dis. Aquat. Organ.* **2001**, *48* (1), 1–5.

(82) Ye, Y.; Chang, P. H.; Hartert, J.; Wigginton, K. R. Reactivity of Enveloped Virus Genome, Proteins, and Lipids with Free Chlorine and UV254. *Environ. Sci. Technol.* **2018**, *52* (14), 7698–7708. https://doi.org/10.1021/acs.est.8b00824.

(83) Harris, G. D.; Adams, V. D.; Sorensen, D. L.; Curtis, M. S. Ultraviolet Inactivation of Selected Bacteria and Viruses with Photoreactivation of the Bacteria. *Water Res.* **1987**, *21* (6), 687–692. https://doi.org/https://doi.org/10.1016/0043-1354(87)90080-7.

(84) Chang, J. C.; Ossoff, S. F.; Lobe, D. C.; Dorfman, M. H.; Dumais, C. M.; Qualls, R. G.; Johnson, J. D. UV Inactivation of Pathogenic and Indicator Microorganisms. *Appl. Environ. Microbiol.* **1985**, *49* (6), 1361–1365.

(85) Li, D.; Gu, A. Z.; He, M.; Shi, H.-C.; Yang, W. UV Inactivation and Resistance of Rotavirus Evaluated by Integrated Cell Culture and Real-Time RT-PCR Assay. *Water Res.* **2009**, *43* (13), 3261–3269. https://doi.org/https://doi.org/10.1016/j.watres.2009.03.044.

(86) Smirnov, Y. A.; Kapitulets, S. P.; Amitna, N. N.; Ginevskaya, V. A.; Kaverin, N. V. Effect of UV-Irradiation on Rotavirus. *Acta Virol.* **1991**, *35* (1), 1–6.

(87) Wilson, B. R.; Roessler, P. F.; Vandellen, E.; Abbaszadegan, M.; Gerba, C. P. Coliphage-MS-2 as a UV Water Disinfection Efficacy Test Surrogate for Bacterial and Viral Pathogens. In *Water Quality Technology Conference 1992, Parts I and II*; American Water Works association: Denver, CO, 1993; pp 219–235.

(88) Huber, P.; Petri, B.; Allen, S.; Lumsden, J. S. Viral Haemorrhagic Septicaemia Virus IVb Inactivation by Ultraviolet Light, and Storage Viability at 4 and −20 °C. *J. Fish Dis.* **2010**, *33* (4), 377–380. https://doi.org/10.1111/j.1365-2761.2009.01134.x.

(89) de Roda Husman, A. M.; Bijkerk, P.; Lodder, W.; van den Berg, H.; Pribil, W.; Cabaj, A.; Gehringer, P.; Sommer, R.; Duizer, E. Calicivirus Inactivation by Nonionizing (253.7-Nanometer-Wavelength [UV]) and Ionizing (Gamma) Radiation. *Appl. Environ. Microbiol.* **2004**, *70* (9), 5089 LP – 5093. https://doi.org/10.1128/AEM.70.9.5089-5093.2004.

(90) Mayer, B. K.; Ryu, H.; Gerrity, D.; Abbaszadegan, M. Development and Validation of an Integrated Cell Culture-QRTPCR Assay for Simultaneous Quantification of Coxsackieviruses, Echoviruses, and Polioviruses in Disinfection Studies. *Water Sci. Technol.* **2010**, *61* (2), 375–387. https://doi.org/10.2166/wst.2010.818.

(91) Zavadova, Z.; Gresland, L.; Rosenbergova, M. Inactivation of Single- and Double-Stranded Ribonucleic Acid of Enchephalomycarditis Virus by Ultraviolet Light. *Acta Virol.* **1968**, *12* (6), 515+.

(92) Zhong, Q.; Carratala, A.; Ossola, R.; Bachmann, V.; Kohn, T. Cross-Resistance of UV- or Chlorine Dioxide-Resistant Echovirus 11 to Other Disinfectants. *Front. Microbiol.* **2017**, *8*.

https://doi.org/10.3389/fmicb.2017.01928.

(93) Park, G. W.; Linden, K. G.; Sobsey, M. D. Inactivation of Murine Norovirus, Feline Calicivirus and Echovirus 12 as Surrogates for Human Norovirus (NoV) and Coliphage (F+) MS2 by Ultraviolet Light (254 Nm) and the Effect of Cell Association on UV Inactivation. *Lett. Appl. Microbiol.* **2011**, *52* (2), 162–167. https://doi.org/10.1111/j.1472-765X.2010.02982.x.

(94) Werbin, H.; Valentine, R. C.; McLaren, A. D. Photobiology of RNA Bacteriophages — I. Ultraviolet Inactivation and Photoreactivation Studies. *Photochem. Photobiol.* **1967**, *6* (3), 205–213. https://doi.org/10.1111/j.1751-1097.1967.tb08805.x.

(95) Tanaka, T.; Nogariya, O.; Shionoiri, N.; Maeda, Y.; Arakaki, A. Integrated Molecular Analysis of the Inactivation of a Non-Enveloped Virus, Feline Calicivirus, by UV-C Radiation. *J. Biosci. Bioeng.* **2018**, *126* (1), 63–68. https://doi.org/https://doi.org/10.1016/j.jbiosc.2018.01.018.

(96) Tree, J. A.; Adams, M. R.; Lees, D. N. Disinfection of Feline Calicivirus (a Surrogate for Norovirus) in Wastewaters. *J. Appl. Microbiol.* **2005**, *98* (1), 155–162. https://doi.org/10.1111/j.1365-2672.2004.02442.x.

(97) Sigstam, T.; Gannon, G.; Cascella, M.; Pecson, B. M.; Wigginton, K. R.; Kohn, T. Subtle Differences in Virus Composition Affect Disinfection Kinetics and Mechanisms. *Appl. Environ. Microbiol.* **2013**, *79* (11), 3455–3467. https://doi.org/10.1128/AEM.00663-13.

(98) Guerrero-Latorre, L.; Gonzales-Gustavson, E.; Hundesa, A.; Sommer, R.; Rosina, G. UV Disinfection and Flocculation-Chlorination Sachets to Reduce Hepatitis E Virus in Drinking Water. *Int. J. Hyg. Environ. Health* **2016**, *219* (4), 405–411.

https://doi.org/https://doi.org/10.1016/j.ijheh.2016.04.002.

(99) Lee, J.; Zoh, K.; Ko, G. Inactivation and UV Disinfection of Murine Norovirus with TiO(2) under Various Environmental Conditions. *Appl. Environ. Microbiol.* **2008**, *74* (7), 2111–2117. https://doi.org/10.1128/AEM.02442-07.

(100) Weng, S.; Dunkin, N.; Schwab, K. J.; McQuarrie, J.; Bell, K.; Jacangelo, J. G. Infectivity Reduction Efficacy of UV Irradiation and Peracetic Acid-UV Combined Treatment on MS2 Bacteriophage and Murine Norovirus in Secondary Wastewater Effluent. *J. Environ. Manage.* **2018**, *221*, 1–9. https://doi.org/https://doi.org/10.1016/j.jenvman.2018.04.064.

(101) Batch, L. F.; Schulz, C. R.; Linden, K. G. Evaluating Water Quality Effects on UV Disinfection of MS2 Coliphage. *J. - AWWA* **2004**, *96* (7), 75–87. https://doi.org/10.1002/j.1551-8833.2004.tb10651.x.

(102) Beck, S. E.; Rodríguez, R. A.; Salveson, A.; Goel, N.; Rhodes, S.; Kehoe, P.; Linden, K. G. Disinfection Methods for Treating Low TOC, Light Graywater to California Title 22 Water Reuse Standards. *J. Environ. Eng.* **2013**, *139* (9), 1137–1145. https://doi.org/10.1061/(ASCE)EE.1943-7870.0000738.

(103) Beck, S. E.; Rodriguez, R. A.; Hawkins, M. A.; Hargy, T. M.; Larason, T. C.; Linden, K. G. Comparison of UV-Induced Inactivation and RNA Damage in MS2 Phage across the Germicidal UV Spectrum. *Appl. Environ. Microbiol.* **2016**, *82* (5), 1468–1474.

(104) Beck, S. E.; Ryu, H.; Boczek, L. A.; Cashdollar, J. L.; Jeanis, K. M.; Rosenblum, J. S.; Lawal, O. R.; Linden, K. G. Evaluating UV-C LED Disinfection Performance and Investigating Potential Dual-Wavelength Synergy. *Water Res.* **2017**, *109*, 207–216. https://doi.org/https://doi.org/10.1016/j.watres.2016.11.024.

(105) Bohrerova, Z.; Mamane, H.; Ducoste, J. J.; Linden, K. G. Comparative Inactivation of Bacillus Subtilis Spores and MS-2 Coliphage in a UV Reactor: Implications for Validation. *J. Environ. Eng.* **2006**, *132* (12), 1554–1561. https://doi.org/10.1061/(ASCE)0733-9372(2006)132:12(1554).

(106) Braunstein, J. L.; Loge, F. J.; Tchobanoglous, G.; Darby, J. L. Ultraviolet Disinfection of Filtered Activated Sludge Effluent for Reuse Applications. *Water Environ. Res.* **1996**, *68* (2), 152–161. https://doi.org/10.2175/106143096X127334.

(107) Budowsky, E. I.; Kostyuk, G. V; Kost, A. A.; Savin, F. A. Principles of Selective Inactivation of Viral Genome. 2. Influence of Stirring and Optical-Density of the Layer to Be Irradiated upon Uv-Induced Inactivation of Viruses. *Arch. Virol.* **1981**, *68* (3–4), 249–256. https://doi.org/10.1007/BF01314578.

(108) Butkus, M. A.; Labare, M. P.; Starke, J. A.; Moon, K.; Talbot, M. Use of Aqueous Silver to Enhance Inactivation of Coliphage MS-2 by UV Disinfection. *Appl. Environ. Microbiol.* **2004**, *70* (5), 2848–2853. https://doi.org/10.1128/aem.70.5.2848-2853.2004.

(109) Cho, M.; Gandhi, V.; Hwang, T.-M.; Lee, S.; Kim, J.-H. Investigating Synergism during Sequential Inactivation of MS-2 Phage and Bacillus Subtilis Spores with UV/H2O2 Followed by Free Chlorine. *Water Res.* **2011**, *45* (3), 1063–1070. https://doi.org/https://doi.org/10.1016/j.watres.2010.10.014.

(110) Guo, H.; Hu, J. Effect of Hybrid Coagulation–Membrane Filtration on Downstream UV Disinfection. *Desalination* **2012**, *290*, 115–124. https://doi.org/https://doi.org/10.1016/j.desal.2012.01.015.

(111) Havelaar, A. H.; Meulemans, C. C. E.; Pothogeboom, W. M.; Koster, J. Inactivation of

Bacteriophage-MS2 in Waste-Water Effluent with Monochromatic and Polychromatic Ultraviolet-Light. *Water Res.* **1990**, *24* (11), 1387–1393. https://doi.org/10.1016/0043-1354(90)90158-3.

(112) Hull, N. M.; Linden, K. G. Synergy of MS2 Disinfection by Sequential Exposure to Tailored UV Wavelengths. *Water Res.* **2018**, *143*, 292–300. https://doi.org/https://doi.org/10.1016/j.watres.2018.06.017.

(113) Jenny, R. M.; Simmons, O. D.; Shatalov, M.; Ducoste, J. J. Modeling a Continuous Flow Ultraviolet Light Emitting Diode Reactor Using Computational Fluid Dynamics. *Chem. Eng. Sci.* **2014**, *116*, 524–535. https://doi.org/https://doi.org/10.1016/j.ces.2014.05.020.

(114) Jolis, D. The Effect of Storage and Lag Time on MS2 Bacteriophage Susceptibility to Ultraviolet Radiation. *Water Environ. Res.* **2002**, *74* (6), 516–520. https://doi.org/10.2175/106143002X140305.

(115) Lénès, D.; Deboosere, N.; Ménard-Szczebara, F.; Jossent, J.; Alexandre, V.; Machinal, C.; Vialette, M. Assessment of the Removal and Inactivation of Influenza Viruses H5N1 and H1N1 by Drinking Water Treatment. *Water Res.* **2010**, *44* (8), 2473–2486. https://doi.org/https://doi.org/10.1016/j.watres.2010.01.013.

(116) Lodder, W. J.; van den Berg, H. H. J. L.; Rutjes, S. A.; Bouwknegt, M.; Schijven, J. F.; de Roda Husman, A. M. Reduction of Bacteriophage MS2 by Filtration and Irradiation Determined by Culture and Quantitative Real-Time RT–PCR. *J. Water Health* **2013**, *11* (2), 256–266. https://doi.org/10.2166/wh.2013.204.

(117) Mamane-Gravetz, H.; Linden, K. G.; Cabaj, A.; Sommer, R. Spectral Sensitivity of Bacillus Subtilis Spores and MS2 Coliphage for Validation Testing of Ultraviolet Reactors for Water

Disinfection. *Environ. Sci. Technol.* **2005**, *39* (20), 7845–7852. https://doi.org/10.1021/es048446t.

(118) Mattle, M. J.; Kohn, T. Inactivation and Tailing during UV254 Disinfection of Viruses: Contributions of Viral Aggregation, Light Shielding within Viral Aggregates, and Recombination. *Environ. Sci. Technol.* **2012**, *46* (18), 10022–10030. https://doi.org/10.1021/es302058v.

(119) Mbonimpa, E. G.; Blatchley III, E. R.; Applegate, B.; Harper Jr, W. F. Ultraviolet A and B Wavelength-Dependent Inactivation of Viruses and Bacteria in the Water. *J. Water Health* **2018**, *16* (5), 796–806. https://doi.org/10.2166/wh.2018.071.

(120) Nieuwstad, T. J.; Havelaar, A. H. The Kinetics of Batch Ultraviolet Inactivation of Bacteriophage-MS2 and Microbiological Calibration of an Ultraviolet Pilot Plant. *J. Environ. Sci. Heal. Part A* **1994**, *29* (9), 1993–2007. https://doi.org/10.1080/10934529409376160.

(121) Sholtes, K. A.; Lowe, K.; Walters, G. W.; Sobsey, M. D.; Linden, K. G.; Casanova, L. M. Comparison of Ultraviolet Light-Emitting Diodes and Low-Pressure Mercury-Arc Lamps for Disinfection of Water. *Environ. Technol.* **2016**, *37* (17), 2183–2188. https://doi.org/10.1080/09593330.2016.1144798.

(122) Shoults, D. C.; Ashbolt, N. J. Total Staphylococci as Performance Surrogate for Greywater Treatment. *Environ. Sci. Pollut. Res.* **2018**, *25* (33), 32894–32900. https://doi.org/10.1007/s11356-017-9050-1.

(123) Sobsey, M. D.; Battigelli, D. A.; G-A, S.; Newland, S. RT-PCR Amplification Detects Inactivated Viruses in Water and Wastewater. *Water Sci. Technol.* **1998**, *38* (12), 91–94.

(124) Tree, J. A.; Adams, M. R.; Lees, D. N. Virus Inactivation during Disinfection of Wastewater by Chlorination and UV Irradiation and the Efficacy of F+ Bacteriophage as a "Viral Indicator." *Water Sci. Technol.* **1997**, *35* (11–12), 227–232. https://doi.org/10.1016/S0273-1223(97)00263-1.

(125) Wang, Z.; Xing, X.; Ma, L. The Inactivation Effect of Ultraviolet Disinfection Reactor on the High Concentration of Bacteriophage MS2. *J. Food Agric. Environ.* **2013**, *11* (1), 1042–1044.

(126) Wang, Y.; Araud, E.; Shisler, J. L.; Nguyen, T. H.; Yuan, B. Influence of Algal Organic Matter on MS2 Bacteriophage Inactivation by Ultraviolet Irradiation at 220 Nm and 254 Nm. *Chemosphere* **2019**, *214*, 195–202. https://doi.org/https://doi.org/10.1016/j.chemosphere.2018.09.065.

(127) Wigginton, K. R.; Pecson, B. M.; Sigstam, T.; Bosshard, F.; Kohn, T. Virus Inactivation Mechanisms: Impact of Disinfectants on Virus Function and Structural Integrity. *Environ. Sci. Technol.* **2012**, *46* (21), 12069–12078. https://doi.org/10.1021/es3029473.

(128) Rattanakul, S.; Oguma, K. Inactivation Kinetics and Efficiencies of UV-LEDs against Pseudomonas Aeruginosa, Legionella Pneumophila, and Surrogate Microorganisms. *Water Res.* **2018**, *130*, 31–37. https://doi.org/https://doi.org/10.1016/j.watres.2017.11.047.

(129) Smirnov, Y. A.; Kapitulez, S. P.; Kaverin, N. V. Effects of UV-Irradiation upon Venezuelan Equine Encephalomyelitis Virus. *Virus Res.* **1992**, *22* (2), 151–158. https://doi.org/https://doi.org/10.1016/0168-1702(92)90041-7.

Appendix C

Supplementary Information for Chapter 4

C.1 Supplementary Text

C.1.1 Preliminary work with the B cell culture system.

Initial work to find an *in vitro* HuNoV culture system focused on evaluating HuNoV infectivity using a previously described B cell culture system.[1] Various experiments were conducted with different HuNoV positive stool samples, and while some yielded moderate increased levels of RNA gene copies from 0 to 3 dpi (~ 6x to 15x increases in 3 to 0 dpi RNA gene copy levels), others did not. In many infections, bile was added to cells in an effort to increase virus replication. Unfortunately, no consistently successful infections resulted from the addition of bile, and the increases in RNA levels were not as great as desired.

After two years of difficulties in establishing productive or consistent HuNoV infection of the B cells, we started working with the HIE cell culture system, which had recently been described.[2]

C.1.2 Difficulties with the HIE cell culture system.

Although the HIE system was ultimately used for our infectious HuNoV MPN assay and in preliminary UV_{254} inactivation experiments, work was delayed due to initial difficulties in identifying a stool sample that productively replicated in HIEs. Specifically, de-identified stool samples were frequently screened, however infection did not result in any of the initial samples tested (infection was defined by a > 3x increase in RNA gene copies from 0 to 3 dpi). These stool

samples ranged in genotype and age, and in certain cases the genotype or age was unknown (Table C.3). Similar to the B cell work, bile was added to infections in an attempt to promote viral replication, however no successful infections were observed. The inability of HIEs to support replication of certain HuNoV stool samples has been demonstrated by other laboratories, most prominently in a study that found only 20% of HuNoV positive stool samples could replicate in HIEs.[3]

One prominent confounding factor in these initial HIE experiments was the lack of a positive control – that is, a HuNoV positive stool sample known to result in measurable 3 dpi RNA gene copy levels after HIE infection. This means it is also possible that the HIEs were not healthy enough to support replication of HuNoV. In this case, false negatives may have resulted, in which even stool samples that could have replicated in healthy HIEs would have appeared unable to infect cells. As a result, we cannot say with complete certainty that the HIEs did not support replication with these stool samples. After obtaining sufficient volume of HuNoV positive stool sample known to infect HIEs, a positive control infection was included in subsequent experiments.

Yet another obstacle afflicting successful HuNoV infections with the HIE cell culture system is the difficulty in maintaining healthy HIEs. We experienced a visual change in cell health and a lack of successful HuNoV replication in HIEs at elevated passages in this study (i.e., > P37). Studies reporting HuNoV infection of HIEs often do not report the cell passage number used for infections.[2,4,5] However, members in the Wobus laboratory have also noted a visual degradation of HIEs in both 3D culture and monolayers at around 35 or more passages. At this time, it is unclear what changes in HIEs occur at increased passages that would result in poor HuNoV replication. More research is needed to better understand the changes in these cell types through passage.

An additional hurdle in sustaining the growth of healthy HIE cells is that HIEs grow best with certain types of media that may be commercially made and extremely expensive. We often noted significant variability in HIE health from passage to passage when applying the laboratory made HIE growth media originally used for HuNoV culture system work. Improved HuNoV infection of HIEs has recently been reported by using commercial media, including the expensive cell culture media Intesticult.[4] This means any slight change in media may result in poor growth of HIEs and decreased replication of HuNoV in HIEs during infection. In this work, these difficulties frequently manifested in the inability to obtain a confluent monolayer after passaging 3D cells into 2D. To improve HIE health, the laboratory made media could be supplemented with Intesticult media.

These complications aside, when the HIEs are growing well and a HuNoV sample of high titer has been identified that replicates well in the HIEs, HuNoV infections of HIEs proceeds smoothly and productively. As work continues to better understand the best conditions for optimal HIE growth and for susceptibility to HuNoV infection, the system will undoubtedly become more straightforward.

C.2 Tables

Table C.1 Composition of media used in 2d and 3d HIE maintenance.

Component	Final Concentration
Complete media without growth factors (CMGF$^-$)	
Advanced DMDM/F12 (Invitrogen)	-
GlutaMax-100x (Invitrogen)	2 mM
HEPES (Invitrogen)	10 mM
Penicillin/Streptomycin (Invitrogen)	100 U/mL
Complete media with growth factors (CMGF$^+$)	
CMGF$^-$	-
L-WNT3A-conditioned media (ATCC)	50%
R-Spondin-conditioned media (Trevigen)	20%
Noggin-conditioned media	10%
B27 (Invitrogen)	1x
N2 (Invitrogen)	1x
N-acetylcysteine (Sigma-Aldrich)	1 mM
Mouse recombinant EGF (Invitrogen)	50 ng/mL
[Leu15]-Gastrin 1 (Sigma-Aldrich)	10 nM
Nicotinamide (Sigma-Aldrich)	10 mM
A-83-01 (Tocris)	500 nM
SB202190 (Sigma-Aldrich)	10 **μ**M
Differentiation media	
CMGF$^-$	-
Noggin-conditioned media	5%
B27 (Invitrogen)	1x
N2 (Invitrogen)	1x
N-acetylcysteine (Sigma-Aldrich)	1 mM
Mouse recombinant EGF (Invitrogen)	50 ng/mL
[Leu15]-Gastrin 1 (Sigma-Aldrich)	10 nM
A-83-01 (Tocris)	500 nM

Table C.2 Primers and probes used for the quantification of HuNoV RNA in one-step RT-qPCR.

Primer or probe	Sequence (5' to 3')[a]	Reference
QNIF2d	ATGTTCAGRTGGATGAGRTTCTCWGA	(Loisy et al. 2005)
COG2R	TCGACGCCATCTTCATTCACA	(Kageyama et al. 2003)
QNIFS	FAM-AGCACGTGGGAGGGCGATCG-TAMRA[b]	(Loisy et al. 2005)

[a]Degenerate sequences include the following mixed nucleobases: R = A or G; W = A or T

[b]6-FAM (6-Carboxyfluorescein) and TAMRA were used as reporter dye and quencher, respectively, for probe-based qPCR.

Table C.3. HuNoV positive stool samples used in screening for HIE infections.

Stool Sample Identifier	Genotype	Source	Year obtained
GII.4 Sydney #1	GII.4 Sydney	MI DHHS	Unknown
GII.4 Sydney #2	GII.4 Sydney	MI DHHS	Unknown
GII.4 Sydney #3	GII.4 Sydney	MI DHHS	Unknown
GII.4 Sydney #4	GII.4 Sydney	MI DHHS	Unknown
GII.4 Sydney #5	GII.4 Sydney	MI DHHS	Unknown
GII.6	GII.6	Unknown	Unknown
GII.4 #14	GII.4	CDC	Unknown
St. Judes	Unknown	St. Judes Hospital	Unknown
Cincinnati	Unknown	Cincinnati	Unknown
NIH A	GII.4	NIH	2015
NIH C	GII.17B	NIH	2015
CL17 - 32	GII.4	MI DHHS	2017
CL17 - 46	GII.4	MI DHHS	2017

MI DHHS = Michigan Department of Health and Human Services; NIH = National Institutes of Health; CDC = Centers for Disease Control

C.4 References

(1) Jones, M. K.; Watanabe, M.; Zhu, S.; Graves, C. L.; Keyes, L. R.; Grau, K. R.; Gonzalez-Hernandez, M. B.; Iovine, N. M.; Wobus, C. E.; Vinjé, J.; Tibbetts, S. A.; Wallet, S. M.; Karst, S. M. Enteric Bacteria Promote Human and Mouse Norovirus Infection of B Cells. *Science* **2014**, *346* (6210), 755–759. https://doi.org/10.1126/science.1257147.

(2) Ettayebi, K.; Crawford, S. E.; Murakami, K.; Broughman, J. R.; Karandikar, U.; Tenge, V. R.; Neill, F. H.; Blutt, S. E.; Zeng, X.-L.; Qu, L.; Kou, B.; Opekun, A. R.; Burrin, D.; Graham, D. Y.; Ramani, S.; Atmar, R. L.; Estes, M. K. Replication of Human Noroviruses in Stem Cell–Derived Human Enteroids. *Science (80-.).* **2016**.

(3) Costantini, V.; Morantz, E. K.; Browne, H.; Ettayebi, K.; Zeng, X.-L.; Atmar, R. L.; Estes, M. K.; Vinjé, J. Human Norovirus Replication in Human Intestinal Enteroids as Model to Evaluate Virus Inactivation. *Emerg. Infect. Dis. J.* **2018**, *24* (8). https://doi.org/10.3201/eid2408.180126.

(4) Ettayebi, K.; Tenge, V. R.; Cortes-Penfield, N. W.; Crawford, S. E.; Neill, F. H.; Zeng, X.-L.; Yu, X.; Ayyar, B. V.; Burrin, D.; Ramani, S.; Atmar, R. L.; Estes, M. K. New Insights and Enhanced Human Norovirus Cultivation in Human Intestinal Enteroids. *mSphere* **2021**, *6* (1), e01136-20. https://doi.org/10.1128/mSphere.01136-20.

(5) Zou, W. Y.; Blutt, S. E.; Crawford, S. E.; Ettayebi, K.; Zeng, X.-L.; Saxena, K.; Ramani, S.; Karandikar, U. C.; Zachos, N. C.; Estes, M. K. Human Intestinal Enteroids: New Models to Study Gastrointestinal Virus Infections; Humana Press: Totowa, NJ, 2017; pp 1–19. https://doi.org/10.1007/7651_2017_1.

(6) Loisy, F.; Atmar, R. L.; Guillon, P.; Le Cann, P.; Pommepuy, M.; Le Guyader, F. S. Real-Time RT-PCR for Norovirus Screening in Shellfish. *J. Virol. Methods* **2005**, *123* (1), 1–7. https://doi.org/https://doi.org/10.1016/j.jviromet.2004.08.023.

(7) Kageyama, T.; Kojima, S.; Shinohara, M.; Uchida, K.; Fukushi, S.; Hoshino, F. B.; Takeda, N.; Katayama, K. Broadly Reactive and Highly Sensitive Assay for Norwalk-Like Viruses Based on Real-Time Quantitative Reverse Transcription-PCR. *J. Clin. Microbiol.* **2003**, *41* (4), 1548–1557. https://doi.org/10.1128/JCM.41.4.1548-1557.2003.

Appendix D

Supplementary Information for Chapter 6

D.1 Supplementary text

D.1.1 FVM limit of detection.

In this work, the limit of detection (LOD) of the FVM approach was defined as the lowest concentration of events in a sample that could be reliably detected above the background noise of the instrument. We established the LOD for a standard FVM protocol of analyzing 10 μL of sample at a flow rate of 1 μL s^{-1}. To obtain the LOD, we determined the number of counts generated for replicate blank samples, and we calculated the standard deviation of those counts to capture the variability in the signal from the instrument background noise (standard deviation ~ 600 counts). We then computed the concentration of this standard deviation for a sample run with the standard protocol, which takes a total volume of 10 μL (concentration ~ 6 x 10^4 counts/mL). This can be taken as the number of counts needed to be confident that FVM analysis is detecting particles above the background noise of the instrument. This LOD can be improved by capturing events for a longer duration and by increasing the threshold to reduce background signal.

D.2 Figures

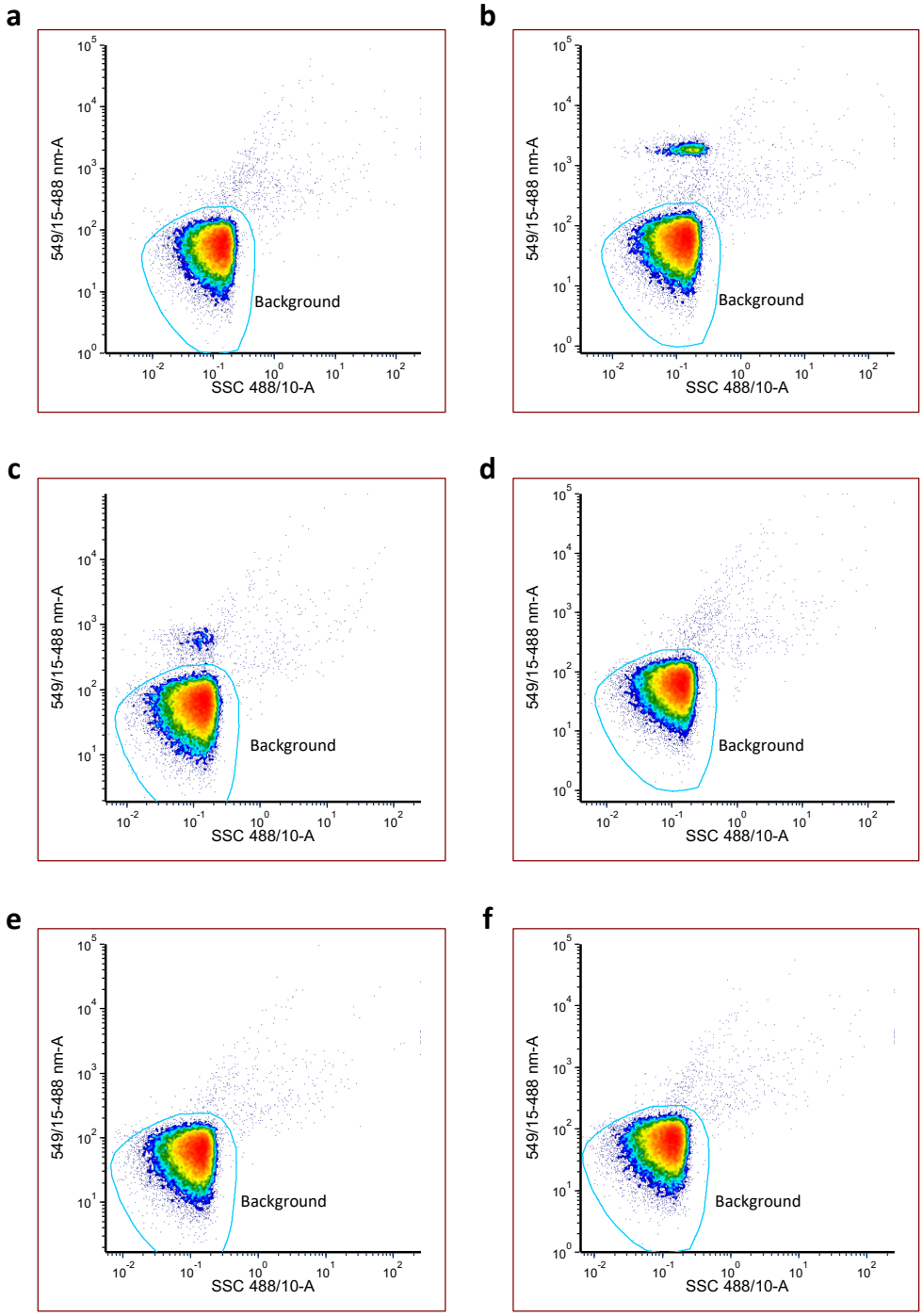

Figure D.1 Heat map FVM dot plots of the signal from SG (0.5x final concentration) stained PBS (a), bacteriophage T4 (b), bacteriophage T3 (c), bacteriophage phi6 (d), bacteriophage phiX174 (e), and bacteriophages MS2 (f). Light blue gating denotes background noise of instrument.

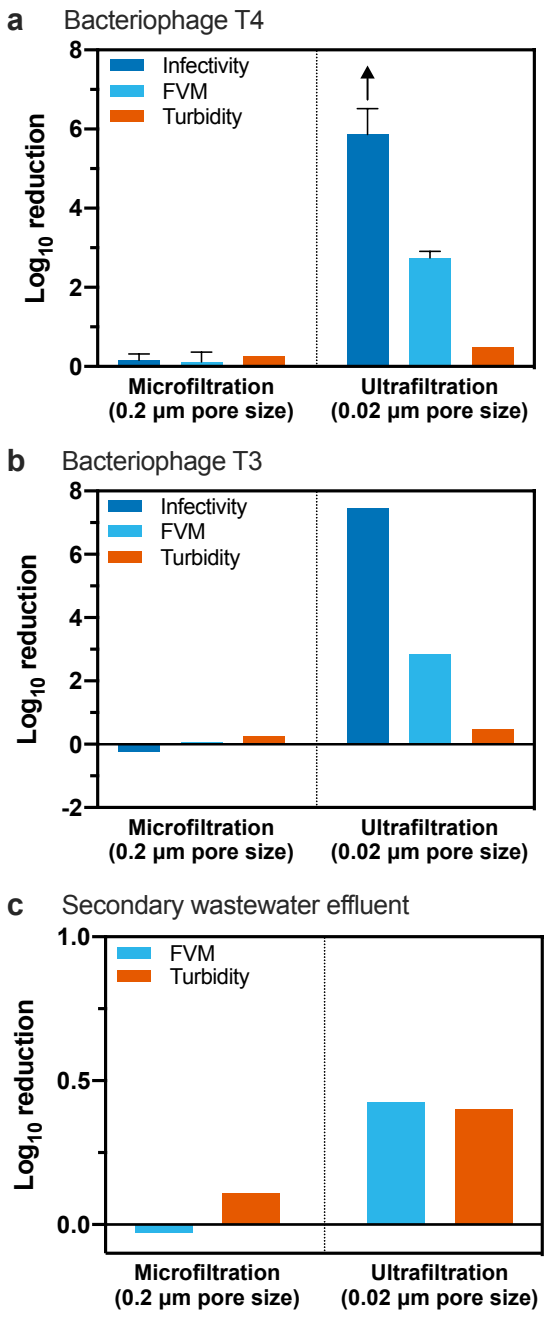

Figure D.2 Log_{10} reductions of FVM signal for samples containing bacteriophage T4 (a), bacteriophage T3 (b), or secondary wastewater effluent (c), determined using the total FVM counts subtraction approach to FVM analysis. Turbidity and FVM counts were obtained for all samples, and infectivity was determined for T3 and T4-spiked samples. Samples in (a) and (b) consisted of bacteriophage spiked into secondary wastewater effluent at a 1:10 final concentration (~5 x 10^9 pfu/mL). The sample in (c) consisted of

secondary wastewater effluent. Error bars represent the standard error of two independent replicates. Arrows above bars indicate $\log_{10}$ reductions beyond detection limits.

D.2 Tables

Table D.1 P-values from paired t-tests of the T4 counts enumerated via FVM using different stains, stain concentrations, and fluorescence channels. P-values resulting from significantly different comparisons are indicated in bold.

529 nm fluorescence channel	SGI (0.5x)	-															
	SGI (1x)	0.78	-														
	SGII (0.5x)	0.39	0.30	-													
	SGII (1x)	0.22	0.24	0.72	-												
	SG (0.5x)	0.73	0.46	0.064	0.27	-											
	SG (1x)	0.51	0.54	0.49	0.17	0.47	-										
	SYTO 11 (1 uM)	0.23	0.20	0.083	0.22	0.17	0.24	-									
	SYTO 11 (2 uM)	**0.010**	**0.0013**	**0.010**	**0.031**	**0.0036**	**0.0085**	0.18	-								
549 nm fluorescence channel	SGI (0.5x)	0.12	0.47	0.33	0.20	0.84	0.36	0.25	**0.0087**	-							
	SGI (1x)	0.86	0.48	0.22	0.17	0.75	0.22	0.26	**0.0034**	0.96	-						
	SGII (0.5x)	0.34	0.29	0.28	0.96	0.13	0.39	0.081	**0.027**	0.31	0.23	-					
	SGII (1x)	0.21	0.22	0.51	0.19	0.25	0.18	0.21	**0.046**	0.20	0.17	0.76	-				
	SG (0.5x)	0.50	0.33	0.31	0.38	0.08	0.94	0.13	**0.00039**	0.35	0.30	0.30	0.31	-			
	SG (1x)	0.20	0.093	0.57	0.30	0.26	0.33	0.18	**0.0034**	0.12	0.077	0.43	0.25	0.67	-		
	SYTO 11 (1 uM)	0.43	0.37	0.14	0.30	0.39	0.40	**0.008**	**0.085**	0.47	0.49	0.13	0.28	0.23	0.30	-	
	SYTO 11 (2 uM)	**0.014**	**0.0016**	**0.013**	**0.037**	**0.0051**	**0.010**	0.27	**0.00077**	**0.012**	**0.0040**	**0.033**	0.053	**0.00068**	**0.0042**	0.12	-
		SGI (0.5x)	SGI (1x)	SGII (0.5x)	SGII (1x)	SG (0.5x)	SG (1x)	SYTO 11 (1 uM)	SYTO 11 (2 uM)	SGI (0.5x)	SGI (1x)	SGII (0.5x)	SGII (1x)	SG (0.5x)	SG (1x)	SYTO 11 (1 uM)	SYTO 11 (2 uM)
		529 nm fluorescence channel								549 nm fluorescence channel							

Table D.2 P-values from paired t-tests of the signal-to-noise-ratios obtained via FVM using different stains, stain concentrations, and fluorescence channels. P-values resulting from significantly different comparisons are indicated in bold.

529 nm fluorescence channel	SGI (0.5x)	-															
	SGI (1x)	**0.022**	-														
	SGII (0.5x)	0.23	0.15	-													
	SGII (1x)	**0.017**	**0.020**	0.055	-												
	SG (0.5x)	**0.019**	**0.0017**	**0.031**	**0.00034**	-											
	SG (1x)	**0.025**	**0.004**	**0.040**	**0.0025**	0.21	-										
	SYTO 11 (1 uM)	**0.011**	**0.0017**	**0.020**	**0.0010**	**0.0074**	**0.0035**	-									
	SYTO 11 (2 uM)	**0.0065**	**0.00056**	**0.013**	**0.00015**	**0.00069**	**0.028**	0.59	-								
549 nm fluorescence channel	SGI (0.5x)	**0.026**	**0.036**	**0.025**	**0.045**	**0.025**	**0.025**	**0.022**	**0.0208**	-							
	SGI (1x)	**0.0056**	**0.0050**	**0.0067**	**0.0047**	**0.0028**	**0.0026**	**0.0025**	**0.0026**	0.22	-						
	SGII (0.5x)	**0.012**	**0.011**	**0.018**	**0.011**	**0.0028**	**0.0024**	**0.0021**	**0.002**	0.19	**0.0028**	-					
	SGII (1x)	**0.015**	**0.014**	**0.023**	**0.016**	**0.0042**	**0.0028**	**0.0028**	**0.004**	0.21	**0.0037**	0.53	-				
	SG (0.5x)	0.0043	**0.0040**	**0.0056**	**0.0044**	**0.0029**	**0.0023**	**0.0023**	**0.00266**	0.066	0.064	**0.0059**	**0.0034**	-			
	SG (1x)	**0.035**	**0.038**	**0.041**	**0.043**	**0.023**	**0.020**	**0.019**	**0.0206**	0.74	0.210	0.10	0.086	**0.012**	-		
	SYTO 11 (1 uM)	0.068	0.075	0.078	0.086	**0.045**	**0.040**	**0.037**	**0.039**	0.97	0.16	0.22	0.20	**0.021**	0.17	-	
	SYTO 11 (2 uM)	**0.017**	**0.0171**	**0.026**	**0.022**	**0.0060**	**0.0037**	**0.0037**	**0.00497**	**0.213**	**0.0082**	**0.633**	0.766	**0.00166**	0.0673	0.18	-
		SGI (0.5x)	SGI (1x)	SGII (0.5x)	SGII (1x)	SG (0.5x)	SG (1x)	SYTO 11 (1 uM)	SYTO 11 (2 uM)	SGI (0.5x)	SGI (1x)	SGII (0.5x)	SGII (1x)	SG (0.5x)	SG (1x)	SYTO 11 (1 uM)	SYTO 11 (2 uM)
		529 nm fluorescence channel								549 nm fluorescence channel							

Table D.3 Comparison of T4 counts obtained using the traditional FVM analysis approach and T4 counts obtained using the total FVM counts subtraction approach.

Stain	Average percent error[a,b] (standard error)
SGI (0.5x)	-0.0012 (0.083)
SGI (1x)	-0.23 (0.31)
SGII (0.5x)	0.049 (0.12)
SGII (1x)	0.047 (0.40)
SG (0.5x)	0.32 (0.46)
SG (1x)	-0.20 (1.3)
SYTO 11 (1 uM)	0.0075 (0.13)
SYTO 11 (2 uM)	1.0 (0.26)

[a]Percent error = (T4 counts using traditional FVM approach - T4 counts using total FVM count subtraction approach) / T4 counts using traditional FVM approach

[b]Counts and resulting percent errors were determined using 549 nm fluorescence signal. Results were comparable between the 529 nm fluorescence channel and the 549 nm fluorescence channel.

Table D.4 FVM counts obtained for five bacteriophages using the total FVM counts subtraction method for SG and SGI stains. Infectious virus concentrations in the same samples are also shown.

Bacteriophage	Infectious virus (pfu/mL)	Average FVM virus counts ± standard error[a]	
		SGI (0.5x)	SG (0.5x)
T4	4.5×10^4	$1.4 \times 10^5 \pm 3.3 \times 10^4$	$2.8 \times 10^5 \pm 9.2 \times 10^4$
T3	5.0×10^4	BD	$3.4 \times 10^5 \pm 2.6 \times 10^5$
phi6	1.1×10^4	BD	$3.7 \times 10^5 \pm 1.6 \times 10^5$
phiX174	1.4×10^5	BD	$4.4 \times 10^5 \pm 1.7 \times 10^5$
MS2	1.2×10^5	BD	$2.8 \times 10^5 \pm 1.5 \times 10^5$

[a]FVM counts were obtained using the total FVM counts subtraction method, which takes the total stained virus signal and subtracting the stained blank signal.

pfu = plaque forming unit; BD = below detection; SGI = SYBR Green I; SG = SYBR Gold